HARVARD UNIVERSITY
Graduate School of Arts and Sciences



DISSERTATION ACCEPTANCE CERTIFICATE

The undersigned, appointed by the

Department of Earth and Planetary Sciences

have examined a dissertation entitled
"Paleomagnetic and Geochronologic constraints on the Neoproterozoic Tectonics and Climate of the Western Margin of Laurentia"

presented by Athena E. Eyster

candidate for the degree of Doctor of Philosophy and hereby certify that it is worthy of acceptance.

Signature _____

Typed name: Assoc. Prof. Francis Macdonald

Signature _____

Typed name: Prof. Andrew Knoll

Signature _____

Typed name: Prof. Jerry Mitrovica

Signature _____

Typed name: Prof. Benjamin Weiss, MIT

Date: April 27, 2017

Paleomagnetic and Geochronologic constraints on the Neoproterozoic Tectonics and Climate of the Western Margin of Laurentia

A DISSERTATION PRESENTED
BY
ATHENA E. EYSTER
TO
THE DEPARTMENT OF EARTH AND PLANETARY SCIENCES

IN PARTIAL FULFILLMENT OF THE REQUIREMENTS
FOR THE DEGREE OF
DOCTOR OF PHILOSOPHY
IN THE SUBJECT OF
EARTH AND PLANETARY SCIENCES

HARVARD UNIVERSITY
CAMBRIDGE, MASSACHUSETTS
APRIL 2017

©2017 – Athena E. Eyster
all rights reserved.

Thesis advisor: Professor Francis A. Macdonald Athena E. Eyster

Paleomagnetic and Geochronologic constraints on the Neoproterozoic Tectonics and Climate of the Western Margin of Laurentia

Abstract

This dissertation focuses on three unique but complementary projects related to Neoproterozoic (1000-542 Ma) tectonics and climate of western North America (Laurentia). I have 1) isolated paleomagnetic evidence for crustal block rotations during rifting along the western margin of Laurentia, 2) refined Neoproterozoic magmatic zircon ages to constrain the age of rifting and onset of global glaciation, and finally 3) created an improved model for the paleogeography of Laurentia in the period leading up to the initial extension of its western margin and the first Cryogenian glaciation.

I studied the Mount Harper Volcanics in Canada to understand the rift history of Laurentia and associated crustal rotations. Through mapping and measured sections, I created a robust geological framework for paleomagnetic data. By isolating a primary paleomagnetic pole 50° away from the expected pole, I suggest that the Yukon block rotated counterclockwise relative to Laurentia. My reconstruction facilitates future studies that relate sedimentary and structural patterns to Rodinian rifting and my low latitude pole supports the Snowball Earth interpretation of the related glacial deposits. Next, by studying the strata exposed at Gataga Mountain in Canada, I improved constraints on the nature and timing of Laurentian rifting and the Sturtian Snowball Earth glaciation. I documented three informal sequences: a basal quartzite, the Gataga Volcanics (interpreted to record sub-glacial sedimentation and volcanism), and overlying mixed carbonate-siliciclastics. Using U-Pb chemical abrasion isotope dilution thermal ionization mass spectrometry zircon geochronology, I generated five precise magmatic ages from Gataga Volcanics and a detrital zircon maximum age

from underlying non-glacial quartzite that constrains the onset of glaciation. In this research I documented new evidence for the Sturtian glaciation and identified two rift stages: the first indicated by the Gataga Volcanics, and the second by the overlying mixed carbonate-siliciclastics. Finally, my studies took me to the Grand Canyon, where I integrated new paleomagnetic data from the Chuar Group with existing paleomagnetic and geochronological datasets from Laurentia to constrain Neoproterozoic paleogeography and tectonics. In this work I showed that there is paleomagnetic evidence contradicting each of the proposed candidates for the conjugate Laurentian margin. I thus suggest that there may not be a conjugate margin craton for western Laurentia. Instead I posit that the 780-750 Ma southern crustal extension was triggered by strike slip motion along the southwestern Laurentian promontory. Furthermore, post-720 Ma northern crustal extension may have been triggered by the Franklin Large Igneous Province and then propagated down the margin. I speculate that eventual rift event that initiated the Laurentian rift-drift transition may have involved the later rifting of a ribbon continent.

Contents

Abstract v

Acknowledgements ix

1 Introduction 1
- 1.1 Glaciation . . . 1
- 1.2 Tectonics . . . 2
- 1.3 More data needed to test hypothesized connections between tectonics and climate 4
- 1.4 Overview . . . 5
  - 1.4.1 Chapter 1- Mount Harper paleomagnetic data elucidating tectonic rotations and latitude of glaciation. . . . 5
  - 1.4.2 Chapter 2- Geochronology of the Gataga Volcanics of British Columbia and implications for Neoproterozoic glaciation and rifting. . . . 6
  - 1.4.3 Chapter 3-Geochronologically calibrated 780-720Ma Laurentian paleomagnetic path and reconciliation of global craton locations and Laurentian geological rift constraints. . . . 7
- 1.5 Summary . . . 8

2 Paleomagnetic evidence for a large rotation of the Yukon Block relative to Laurentia: Implications for a low-latitude Sturtian Glaciation and the break-up of Rodinia 10
- 2.1 Abstract . . . 10
- 2.2 Introduction . . . 11
- 2.3 Geological Setting . . . 14
- 2.4 Diagenetic Considerations . . . 22
- 2.5 Methods . . . 22
- 2.6 Results . . . 25
- 2.7 Magnetic Carriers For High-Temperature Component Directions . . . 30
  - 2.7.1 Rock Magnetism Results . . . 33
- 2.8 Discussion . . . 36
  - 2.8.1 Timing of Magnetizations Determined by Fold Tests . . . 36
  - 2.8.2 Discussion of Primary Nature of HT1 . . . 37
  - 2.8.3 Interpretations of Directions and Comparison to the Laurentian Apparent Polar Wander Path . . . 39

2.8.4 Geological Context of Rotation . . . 45
2.8.5 Neoproterozoic Paleogeographic Implications . . . 51
2.8.6 Low Latitude Glaciation . . . 54
2.9 Conclusions . . . 55

3 One Diamictite and Two Rifts: Stratigraphy and Geochronology of the Gataga Mountain of Northern British Columbia 57
3.1 Abstract . . . 57
3.2 Introduction . . . 59
3.3 Methods . . . 64
3.3.1 Mapping and Stratigraphy . . . 64
3.3.2 Geochronology Sample Preparation . . . 64
3.3.3 U-Pb LA-ICP-MS Geochronology and Zircon Geochemistry . . . 67
3.3.4 U-Pb ID-TIMS Geochronology . . . 67
3.3.5 Carbon Isotope Chemostratigraphy . . . 68
3.4 Results . . . 69
3.4.1 Metamorphism and structure . . . 69
3.4.2 Stratigraphy . . . 69
3.4.3 U-Pb Geochronology . . . 76
3.4.4 Chemostratigraphy . . . 83
3.5 Discussion . . . 85
3.5.1 Geochronology . . . 85
3.5.2 Igneous Geochemistry . . . 88
3.5.3 Depositional Setting . . . 90
3.5.4 Regional Correlations . . . 97
3.5.5 Rift History . . . 105
3.5.6 Cryogenian Glaciation . . . 107
3.6 Conclusions . . . 108

4 Paleomagnetism of the Chuar Group and evaluation of the 780-720 Ma Laurentian apparent polar wander path: implications for the makeup and breakup of Rodinia 109
4.1 Abstract . . . 109
4.2 Introduction . . . 111
4.2.1 Previous Rodinia Reconstructions . . . 114
4.3 Geologic Overview . . . 116
4.4 Methods . . . 123
4.5 Results . . . 125
4.5.1 Results and Fold tests by Member . . . 130
4.5.2 Combined directions and fold tests . . . 132
4.6 Discussion . . . 134

4.6.1 Comparison of with previous work . . . 134
4.6.2 Inclination Flattening . . . 139
4.6.3 Proposed New Paleomagnetic Poles . . . 141
4.6.4 Interpretation of the shallow directions . . . 143
4.6.5 Interpretation of the steep directions . . . 143
4.6.6 Rotation of the Colorado Plateau . . . 144
4.7 Interpretations of Directions and Comparison to the Laurentian Apparent Polar Wander Path . . . 146
4.7.1 Gunbarrel event . . . 147
4.7.2 Nankoweap Formation . . . 148
4.7.3 Uinta Mountain Group (UMG) . . . 148
4.7.4 Franklin Large Igneous Province (LIP) . . . 151
4.8 Neoproterozoic Paleogeography . . . 154
4.8.1 Australia . . . 155
4.8.2 South China . . . 160
4.8.3 North China . . . 161
4.8.4 Tarim . . . 162
4.8.5 North Australia . . . 163
4.8.6 Congo . . . 164
4.8.7 India . . . 165
4.8.8 Siberia . . . 166
4.8.9 Antarctica, Baltica, Amazonia, Kalahari, Rio de La Plata, Sao Francisco, West Africa . . . 168
4.9 Paleogeographic reconstructions ca. 780, 750 and 720 Ma . . . 170
4.9.1 Remark on the longevity of AUSMEX . . . 175
4.10 Conclusions . . . 176

Appendix A Supplementary Information, figures and Tables for Chapter 2 178
A.1 Sample Analysis . . . 178

References 186

To the fields and woods of Chelsea, Michigan–where I got my start exploring the natural world.

Acknowledgments

So many people have assisted me in this endeavor. I first want to thank my co-authors for their assistance and the wealth of knowledge they bestowed on me: Roger Fu, Justin Strauss, Ben Weiss, Charlie Roots, Galen Halverson, Dave Evans, Filippo Ferri, Mark Schmitz, Karl Karlstrom. In addition to Ben Weiss, I am also very grateful to my Harvard committee members who have always made time to help me improve my research: Jerry Mitrovica, Dave Johnston, Andy Knoll and Brendan Meade.

During this work I had some wonderful folks assisting me in the field. In the Yukon, Erik Sperling, Esther Kennedy, Grant Cox and Eric Bellefroid all help with the sample collection, while Mark Holland and Brandon Salisbury were especially helpful carrying samples in the Grand Canyon. My paleomagnetic education was vastly contributed to by Joe Panzik, Taylor Killian, Eduardo Lima and Sonia Tikoo-Schantz. Jacob Kremers was particularly invaluable in running samples at the MIT lab. I also thank Astera S. Tang for her assistance in getting me started measuring magnetic hysteresis curves. On the geochronology side, I was mentored and helped by Jim Crowley, Vince Isakson and Marion Lytle, and Debbie Pierce at the Boise State University Isotope Geology Laboratory. I also am very grateful to Sarah Dendy, Sasha Brues and Camille Dwyer for providing assistance and training in the geochronology sample preparation process.

I have had many mentors over the years, and I am very grateful for the following science teachers and mentors: Eric Swager at Chelsea High School, and Rob van der Voo, Jeroen Ritsema, Mat Domeier, and David Gerdes at the University of Michigan.

Here at Harvard, I have had a wonderful group to work with, and I have learned so much and had so many wonderful conversations with Alan Rooney, Justin Strauss, Emmy Smith, Blake Hodgin, Uyanga Bold, and Judy Pu. I am particularly thankful to Emmy for always making time to help me and for being such a support during my postdoc search.

The Harvard EPS department staff have all been so helpful and supportive, and I want to that Marisa Reilly, Paul Kelley, Maryorie Grande, Chenoweth Moffatt, and especially Sarah Colgan. Lisa McCaig graced the first floor with her friendship, counsel and support.

On a more personal note, I want to thank my friends and fellow graduate students, past and present, for enriching this experience, especially Hannah Horowitz, Jocelyn Fuentes, Emma Bertran, Anna Waldeck, Tamara Pico, Jenny Middleton, Shannon Kopliz, Katie Dagon, Katie Travis, Jenny Middleton, Rachel Silvern, Jonathan Tucker, Alex Robel, Joseph Fitzgerald, Jacky Austermann, Rita Parai, Mary Moore, Harriet Lau, Alex Turner, Karen Yu, and Chris O'Grady.

My family has helped and supported me every step of the way. My siblings, Artemis, Theodore, and Harold, as well as my parents, Diana and Jason, have read countless drafts of abstracts, papers and posters and I am constantly in awe and inspired by them. Special thanks to my father who has always pushed all of us to ask questions and examine the world around us. I am so grateful to my fiance, Richard Moran, for helping me grow outside the lab and for all our adventures, in Boston and beyond.

Most especially, I want to thank Francis Macdonald and Rick O'Connell. Without them, I wouldn't be where I am now. To Francis I am thankful for his tireless mentoring and boundless enthusiasm, and from him I learned about being a card carrying geologist, running like a goat up mountains to scope out new outcrops, and how to find a diamictite I could hang my hat on. Rick always had an open door, always ready discuss science, as well as books, music, and hobbies. From him I learned about propagator matrices, the joys that owning a sailboat can bring, and the importance of making things simple, but not *too* simple. To both, I am eternally grateful.

1

Introduction

During the Neoproterozoic, the supercontinent Rodinia is suggested to have amalgamated and broken apart (Li et al. 2008) and two long-lasting Cryogenian Snowball Earth glaciations took place (Kirschvink, 1992; Hoffman and Schrag, 2002; Rooney et al., 2015). Tectonics and continental configurations associated with supercontinent cycles may drive climate and evolutionary change on geologic timescales. In particular, previous studies have linked the low-latitude break-up of Rodinia with the onset of Cryogenian glaciation (for example Hoffman and Schrag, 2002; Godderis et al., 2003; Cox et al., 2016; Li et al., 2008); however, the age and kinematics of Rodinia's fragmentation, and the timing of its relationship to environmental change remains poorly constrained.

1.1 Glaciation

Although Neoproterozoic glacial successions are recognized worldwide, the nature, timing, and duration of glacial episodes have remained controversial (Spence et al., 2016). Nonetheless, paleomag-

netic data suggests that some of the Cryogenian glacial diamictites were deposited at low latitudes, consistent with the Snowball Earth hypothesis (Kirschvink, 1992; Evans and Raub, 2011). Moreover, recent geochronology confirms that there were two discrete, long-lived Cryogenian glaciations, the Sturtian and the Marinoan (Rooney et al., 2015; Prave et al., 2016). The onset of the Sturtian glaciation can be dated by chemical abrasion isotope dilution thermal ionization mass spectrometry (CA-ID-TIMS). The closest constraint to the onset is U-Pb zircon age of 716.47 $\pm$ 0.24 Ma from diamictites of the Mount Harper Group in Yukon, Canada (Macdonald et al., 2010a). The end of the same glaciation is marked by a postglacial Re-Os date of 662.4 $\pm$ 3.9 Ma on the basal Twitya Formation in Northwest Territories, Canada (Rooney et al., 2014). The age of the Marinoan glacial epoch is bracketed between 655 Ma (Zhang et al., 2008) and 635 Ma (Condon et al., 2005; Calver et al., 2013; Rooney et al., 2015), with the later marking the age of the Marinoan cap carbonate. These data, along with the most robust geochronological constraints globally, suggest a $>$55 Myr duration for the Sturtian glaciation (Rooney et al., 2014; 2015), and $>$ 5 Myr duration for the Marinoan glaciation (Prave et al., 2016). Although, some suggest that there were multiple glaciations between ca. 716-660 Ma, with a possible interglacial period (Le Heron, 2011; Keeley et al., 2012), only one Sturtian cap carbonate has been identified.

Records of these Cryogenian glaciations are preserved along the western Laurentian margin (for example Crittenden et al., 1983; Gabrielse, 1972; Stewart, 1972; Eisbacher, 1978; Christie-Blick and Levy, 1989; Aitken, 1991; Link et al., 1994; Miller, 1994; Prave, 1999; Lund et al., 2003; Macdonald et al., 2010a).

1.2 Tectonics

There is general agreement that Earth's continental crust assembled to form the supercontinent Rodinia in the late Mesoproterozoic and early Neoproterozoic. Rodinia is thought to have been

produced by collisional events of broadly Grenvillian (late Mesoproterozoic) age, and to have been relatively long-lived (c. 1100-750Ma) (McMenamin and McMenamin, 1990; Hoffman, 1991). Despite various differences, most of the models depict Laurentia as the core of Rodinia because Laurentia was surrounded by Cambrian passive margins suggested to have formed during the supercontinent's breakup in the late Neoproterozoic (Bond et at. 1984; Hoffman et al., 1991).

A plethora of different reconstructions, many of them with a strong focus on paleomagnetic data, have been published and most conclude that crustal blocks rifted apart from western Laurentia by 750 Ma (Meert and Torsvik, 2003; Cawood, 2005; Li et al., 2008; Sears and Price, 1978; Moores, 1991; Hoffman, 1991; Dalziel, 1997; Sears and Price, 2003; Pisarevsky et al., 2003; Li et al., 2008; Evans, 2009; Fu et al., 2015). These models increasingly suggest that breakup occurred on the western margin ca. 800-750 Ma.

The age of rifting predicted from paleogeographic models can be compared with the age predicted from geological work on western Laurentia. The rift history of the western margin of Laurentia is recorded in the Windermere Supergroup of the U.S. and Canadian Cordillera (Ross 1991; Link et al. 1993). The Windermere Supergroup is commonly divided into three main stratigraphic ensembles: 1) narrow fault-bounded extensional basins referred to as the ChUMP basins (Dehler et al., 2007; Dehler et al., 2017; Macdonald, et al., 2013; Strauss, et al., 2014; Smith, et al., 2015); 2) Cryogenian siliciclastic and volcanic successions often interbedded with glacial diamictites that have been interpreted as representing rift basins; and 3) a more widespread succession of Ediacaran carbonate and siliciclastic strata, composed largely of turbidites, that are widely interpreted to be related to subsidence and the initiation of passive margin sedimentation (Stewart, 1972; Ross, 1991; Jefferson & Parish, 1989; Eisbacher, 1979).

Earlier geochronology work on rift-related magmatism suggested that the age of rifting and volcanism could have been ca 750-780 Ma, which would be consistent with the paleogeographic reconstructions (Armstrong et al., 1982; Jefferson and Parrish, 1989; Devlin et al., 1988; Roots and Parrish

1988). However, with recent advances in geochronology these ages are now being refined. Increasingly, there appears to be evidence for isolated magmatism on the western margin ca. 780 Ma (the Gunbarrel event), and large spread magmatism on the northern margin ca 720 Ma (the Franklin LIP). This extensional volcanism is also found in the central and southern Canadian Cordillera and in Washington and Idaho (Miller, 1994; Brown, 1995; Keeley et al., 2012; Lund et al., 2010). This volcanism has been dated at 717 Ma in the Yukon (Macdonald et al., 2010), 690 Ma in northern British Columbia (Eyster et al., accepted) and ca. 685 Ma in Idaho (Keeley et al., 2012; Lund et al., 2010).

An additional complication is that subsidence curves of Paleozoic strata on the western margin of Laurentia (Armin and Mayer, 1983; Bond and Kominz, 1984; Bond et al., 1985) suggest that the rift-drift transition and development of the passive margin did not occur until the Precambrian-Cambrian boundary (now 541 Ma). Thus, basal Windermere magmatism may be too old to be tied to the thermal subsidence and development of the Paleozoic passive margin. This discrepancy in ages could suggest multiple rift events or protracted rifting (Prave et al., 1999; Colpron et al. 2001). Indeed, a third episode of Late Ediacaran rift-related volcanism has also been identified in British Columbia (Colpron et al. 2001).

1.3 More data needed to test hypothesized connections between tectonics and climate

It has been suggested that tectonic forcings may have helped trigger these events as the supercontinent Rodinia achieved amalgamation and breakup (Li et al. 2008). The rifting of a supercontinent may have affected the length of continental margins and led to sharp increases in riverine runoff and silicate weathering. In addition it is argued that the spike in Rift volcanics and flood basalts may have enhanced CO_2 drawdown and helped trigger glaciation (ex. Godderis et al., 2003; Donnadieu, et al., 2004). However, previous modeling has suggested that there may be a 50 Ma lag between rifting

and glaciation (Godderis et al., 2003). Thus, understanding the paleogeography of Rodinia and the timing of its break-up is key for understanding and testing proposed links between Neoproterozoic tectonics and climate, as well as informing our understanding of supercontinent cycles. In order to better inform hypothesis related to the rifting of the Supercontinent Rodinia and global glaciation as well as supercontinent dynamics, I have isolated paleomagnetic evidence for crustal block rotations during rifting along the western margin of Laurentia, I have refined Neoproterozoic magmatic zircon ages to constrain the age of rifting and onset of global glaciation, and finally I have created an improved model of the paleogeography of Laurentia in the period leading up to the initial extension of its western margin and the first Cryogenian glaciation.

1.4 Overview

1.4.1 Chapter 1- Mount Harper paleomagnetic data elucidating tectonic rotations and latitude of glaciation.

To better understand the rift history of Laurentia and tectonic rotations, I have completed an intensive paleomagnetic study of The Mount Harper volcanics of Yukon, Canada (Mustard and Roots, 1997; Macdonald et al., 2010). I completed fieldwork there, mapping and measuring volcanic sections to better understand the geologic context of the area and to provide a framework for analyzing paleomagnetic data. I then prepared paleomagnetic samples and conducted thermal, AF and liquid nitrogen demagnetization to isolate magnetic components and directions. I also conducted a suite of rock magnetism experiments to understand the magnetic carriers. In this work, I isolated four paleomagnetic directions: a low-temperature direction recording the present geomagnetic field, a mid-temperature direction consistent with a Cretaceous overprint, and two high-temperature directions. Of the two high-temperature directions, one likely represents a chemical overprint, while the other direction is interpreted to be primary. The primary nature of this direction is supported

by 6 of the 7 van der Voo reliability criteria, including a conglomerate test; fold test, and reversal test. This primary pole is 50 degrees away from the expected ca. 720 Ma Laurentian pole derived from the Franklin large igneous province (Denyszyn et al. 2009). The two poles can be aligned via an approximately 50 degree counterclockwise rotation of the Yukon block relative to Laurentia. The pre-rotation reconstruction of the Yukon Block relative to Laurentia aligns Neoproterozoic fault orientations and facies belts between the Wernecke and Mackenzie Mountains, rectifies paleo-flow measurements in Mesoproterozoic and Paleoproterozoic strata, and realigns the orientation of the ca. 1260 Ma Bear River Dikes with the Mackenzie Dike Swarm of northern Canada (Aitken and McMechan 1992, Abbot 1997). This reconstruction also facilitates future studies that relate Neoproterozoic sedimentary and structural patterns to the fragmentation of Rodinia. Finally, this low-latitude pole supports the Snowball Earth interpretation of the ca. 717 Ma Sturtian glacial deposits (Macdonald et al., 2010).

1.4.2 Chapter 2- Geochronology of the Gataga Volcanics of British Columbia and implications for Neoproterozoic glaciation and rifting.

To further investigate the timing of Laurentian rifting and the extent of the Neoproterozoic snowball Earth glaciation I have studied the Gataga Volcanics in British Columbia, Canada (Ferri et al., 1999).I conducted field mapping, measured volcanic and sedimentary sections and collected samples for U-Pb chemical abrasion isotope dilution thermal ionization mass spectromentry zircon geochronology and carbon isotope chemostratigraphy. I documented three informal sequences exposed at Gataga Mountain: a basal quartzite, the Gataga Volcanics, and an overlying mixed carbonate-siliciclastic succession. The basal quartzite is dominated by cross-bedded sandstone with an intertidal facies assemblage including herringbone cross-stratification and mud-cracks, indicative of non-glacial deposition. The overlying Gataga Volcanics are over one kilometer thick, comprising both mafic and felsic units, with volcaniclastic breccia and interbedded sedimentary units includ-

ing iron formation and matrix-supported diamictite with cosmopolitan clasts. Magmatic ages in the upper Gataga Volcanics span 696.2 ± 0.2 to 690.1 ±0.2 Ma, and detrital zircon from the underlying non-glacial quartzite provide a maximum age constraint on the onset of glaciation <735.8 ± 0.6 Ma.The interfingering beds of matrix-supported diamictite with cosmopolitan clasts within the Gataga Volcanics are interpreted to record sub-ice shelf sedimentation and volcanism during the Sturtian Glaciation. Although volcanic facies are consistent with eruption in a sub-ice to sub-aqueous (below ice shelf) environment, I acknowledge the difficulty of distinguishing sub-glacial from sub-aqueous explosive volcanic facies. Overlying the Gataga Volcanics, a mixed carbonate-siliciclastic succession contains minor basalt flows that are geochemically distinct from the underlying volcanic rocks. Based on chemostratigraphic and lithostratigraphic similarities, I suggest that this sequence is correlative with Ediacaran strata to the north. Together, I suggest that the stratigraphy and geochemical signature of volcanic rocks at Gataga Mountain records two distinct episodes of Neoproterozoic extension-related sedimentation and volcanism, the first indicated by the Cryogenian Gataga Volcanics and interbedded sedimentary strata and the second by the overlying Ediacaran carbonate-siliciclastic succession with interfingering basalt.

1.4.3 Chapter 3-Geochronologically calibrated 780-720Ma Laurentian paleomagnetic path and reconciliation of global craton locations and Laurentian geological rift constraints.

To better understand Neoproterozoic paleogeography and identify the conjugate craton margin for western Laurentia, I obtained new paleomagnetic results from the Chuar Group exposed in the Grand Canyon and incorporated this new data with existing paleomagnetic and geochronologic data. I report a new paleomagnetic pole for the Awatabi and Carbon Butte members within the Chuar group. This direction is preserved in hematite and magnetite the primary nature of this

paleomagnetic direction is supported by five of the seven Van der Voo (1990) reliability criteria. In addition to this direction that I interpret as primary, I also identified pervasive overprints both mid-temperature demagnetized between 400-560°C and a high-temperature component that is unblocked by 680°C and seems to be carried by hematite. Unlike previous work, I identified these steep overprints in multiple members and demonstrated the widespread nature of this event. I incorporated this updated paleomagnetic pole with recent geochronological data and existing paleomagnetic data to present a new and revised ca. 780-720 Ma Laurentian APWP. Having examined the 780-720 Ma databases of other cratons and concluded that there is evidence for an AUSMEX configuration at both 780 Ma and 750 Ma (as well as 1070 Ma), but there is paleomagnetic evidence against all the other models for various cratons as conjugate margins to Laurentia. I thus suggest that there may not be a conjugate margin for western Laurentia and that, instead, ca. 780-750 Ma, southern crustal extension was triggered by strike-slip motion along the southwestern Laurentian promontory. Furthermore, post-720 Ma northern crustal extension may have been triggered by the Franklin LIP and then propagated down the margin. The eventual rift event that triggered the rift-drift transition may have involved a ribbon continent with Laurentia affinity.

1.5 Summary

To conclude, the Mount Harper Volcanics demonstrate ca. 717 Ma rift-related volcanism, and, although the tectonics are complicated by counterclockwise tectonic block rotation, by identifying this rotation I can correct for it and interpret the Coal Creek strata as recording E-W directed extension and faulting, perhaps triggered by extension on the northern margin. The paleomagnetic data also indicates low latitude (<30°) for the earliest deposits of the ca. 717 Ma Sturtian glaciation. Further south, the Gataga mountain strata suggest two rift events, one ca. 700-685 Ma, similar to ages to the south, and a later event, as evidenced by geochemically distinct rift volcanism. In addition,

there is evidence for glaciation ca. 690 Ma. In both of these sequences, the rift-related volcanism slightly predates the glaciogenic deposits. Although this may be preservation bias, it is also possible that this is a real signal, suggesting that extensional magmatism just barely predates the start of glaciation, thus requiring a short lead-up time for rift magmatism to trigger glaciation. In addition, my study of the Chuar Group suggests that the rift magmatism itself may be triggered not by the rifting of a different continental craton, but by ca. 780 Ma strike-slip motion to the south, and to the north by far field effects of the Franklin LIP. With no conjugate craton, the configuration of the supercontinent Rodinia may not have been as tightly-packed as previous models have suggested. Therefore, the associated rifting along the western margin may not have dramatically increased the length of continental margins, and may not have led to sharp increases in riverine runoff and silicate weathering. Thus, the explanation that increased silicate-weathering of newly created continental rift margins initiated the Sturtian glaciation might bear reevaluation. Finally, when considering supercontinents, it is tempting to use our knowledge of Pangea as the key to understanding Rodinia. However, the rifting of Rodinia may involve overlooked features that were not as important for the rifting of Pangea, namely, strike-slip motions, block rotations, and rifting of ribbon continents.

2

Paleomagnetic evidence for a large rotation of the Yukon Block relative to Laurentia: Implications for a low-latitude Sturtian Glaciation and the break-up of Rodinia

2.1 Abstract

Understanding the tectonic history of the supercontinent Rodinia is crucial for testing proposed links between Neoproterozoic tectonics, supercontinent cycles, climate, and biogeochemistry. The

A version of this chapter was published: Eyster, A. E., Fu, R. F., Strauss, J. V., Weiss, B. P., Roots, C.F., Halverson, G.P., Evans, D.A.D., Macdonald, F.A., 2016. Geological Society of America Bulletin.

Neoproterozoic Mount Harper volcanics of the Ogilvie Mountains, Yukon, Canada, interfinger with Sturtian-age (ca. 717–660 Ma) glacial deposits that were deposited in narrow, fault-bounded basins related to the break-up of Rodinia. Here, I present new paleomagnetic data from the Mount Harper volcanics and isolate four paleomagnetic directions: a low-temperature direction recording the present geomagnetic field, a mid-temperature direction consistent with a Cretaceous overprint, and two high-temperature directions, one of which is carried by hematite and likely represents a chemical overprint, and the other, which is carried by magnetite, is likely a primary direction. This primary pole passes the fold and conglomerate tests, and includes a reversal but is 50° away from the coeval 721-712 Ma Laurentian Franklin large igneous province pole. This difference can be reconciled using a 50° counterclockwise rotation of the Yukon Block relative to Laurentia. The pre-rotation reconstruction of the Yukon Block relative to Laurentia aligns Neoproterozoic fault orientations and facies belts between the Wernecke and Mackenzie Mountains, rectifies paleo-flow measurements in Mesoproterozoic and Paleoproterozoic strata, and realigns the orientation of the ca. 1260 Ma Bear River Dikes with the Mackenzie Dike Swarm of northern Canada. This reconstruction also facilitates future studies that relate Neoproterozoic sedimentary and structural patterns to the fragmentation of Rodinia. Finally, this low-latitude pole supports the Snowball Earth interpretation of the ca. 717 Ma Sturtian glacial deposits.

2.2 Introduction

The protracted breakup of the supercontinent Rodinia has long been associated with Neoproterozoic environmental and biological change (Kirschvink, 1992; Hoffman and Schrag, 2002; Goddéris et al., 2003). However, the age, geometry, configuration and kinematics of Rodinia's fragmentation remain poorly constrained. Because Laurentia is surrounded by Neoproterozoic passive margins (Hoffman, 1991), many paleogeographic reconstructions place it at the core of Rodinia (e.g., Li et

al., 2008). Due to this central location, studies of Laurentian basins can assist in understanding the break-up of Rodinia (e.g., Ross, 1991; Macdonald et al., 2012; Strauss et al., 2015). Several discrete extensional events on the western margin of Laurentia have been attributed to the rifting of Rodinia, implying a prolonged and complex break-up history. Early Neoproterozoic (~1.2-0.78 Ga Sequence B of Young et al., 1979) sedimentary successions were interpreted as recording basin-forming events consistent with a NNW-facing margin in present coordinates (Aitken, 1981). Alternatively, Turner and Long (2008) argued for NE-SW extension on the western margin of Laurentia based on the interpretation of multiple NE–SW-oriented structures in the Mackenzie Mountains as transfer faults. In addition to these older structures, which can be interpreted as recording early Neoproterozoic rifting, late Neoproterozoic rifting (Sequence C of Young et al., 1979, Windermere Supergroup) is thought to have occurred during two separate intervals: ~780-660 Ma (Jefferson and Parrish, 1989; Mustard, 1991) and ~580–560 Ma in the southern Cordillera (Colpron et al., 2002; Lund, 2008; Lund et al., 2010; Yonkee et al., 2014).

There are numerous candidates for the continents that rifted away from Laurentia's northern and western margins, including Antarctica, Australia, South China, North China, Siberia and West Africa (Sears and Price, 1978; Moores, 1991; Hoffman, 1991; Dalziel, 1997; Sears and Price, 2003; Pisarevsky et al., 2003; Li et al., 2008; Evans, 2009; Fu et al., 2015; Ernst et al., 2016). Irrespective of the identity of its former conjugate partners in Rodinia, Yukon records the Neoproterozoic tectonic evolution of both the northern and western margins of Laurentia (e.g., Thorkelson et al., 2005; Macdonald et al., 2012; Strauss et al., 2015), and is a keystone for future attempts to elucidate the extensional history in this part of Rodinia.

Recent geochronological data from Neoproterozoic sedimentary successions in Yukon enable more accurate constraints on basin-forming events in Laurentia during the early fragmentation of Rodinia. In the Coal Creek inlier of west-central Yukon (Figs. 1 and 2), early Neoproterozoic synsedimentary faulting and subsidence have been linked to extension on the northern margin of Lauren-

tia (Macdonald et al., 2012). In contrast, the later Neoproterozoic Mount Harper Group was deposited in a volcanically active half-graben previously attributed to extension or transtension along the western margin of Laurentia (Mustard, 1991; Mustard and Roots, 1997; Strauss et al., 2015). Recent geochronological and geochemical data from the Mount Harper volcanics (MHV) of the upper Mount Harper Group (Macdonald et al., 2010; Cox et al., 2013) highlight connections with igneous activity associated with the Franklin large igneous province (LIP) (Heaman et al., 1992; Denyszyn et al., 2009a; Denyszyn et al., 2009b), which has yielded a robust, low-latitude grand-mean paleomagnetic pole (Fahrig et al., 1971; Robertson and Baragar, 1972; Fahrig and Schwarz, 1973; Palmer and Hayatsu, 1975; Park, 1981; Christie and Fahrig, 1983; Palmer et al., 1983; Heaman et al., 1992; Pehrsson and Buchan, 1999, Buchan et al., 2000; Denyszyn et al., 2009a; Denyszyn et al., 2009b). Taken at f I ace value, these data connect extension or transtension recorded in Yukon with the paleogeography of Laurentia relative to the other cratons in Rodinia. Moreover, the link between the ca. 717 Ma onset of the Sturtian glaciation in Yukon and the low-latitude paleomagnetic pole on the Franklin LIP is a key line of evidence for Snowball Earth (Macdonald et al., 2010). The similarity in ages and robust Franklin paleomagnetic pole provides a unique opportunity to better understand the Sturtian glaciation and identify tectonic movements of the Yukon Block relative to the Laurentian craton using paleomagnetism.

A previous reconnaissance-level paleomagnetic study of the MHV suggested a pole distinct from the Franklin grand mean pole (Park et al., 1992); however, it was unclear if this difference was due to large true polar wander, anomalous magnetic field behavior, or a tectonic rotation of Cretaceous, Paleozoic, or Neoproterozoic age. In addition, Park et al. (1992) acknowledged that their results were inconclusive due to limited sampling, and that additional sampling and examination were needed to validate or refute them. Here I present new paleomagnetic results from the MHV that resolve these uncertainties, allowing us to infer the geometry of Neoproterozoic synsedimentary structures relative to the Laurentian craton and relative motions during the breakup of Rodinia, and

additionally, to explore the paleomagnetic constraints on the ca. 717 Ma Yukon glacial deposits that may record the initiation of Snowball Earth glaciation on Laurentia.

2.3 Geological Setting

The Yukon Block (Jeletsky, 1962) is a crustal fragment separated from contiguous Laurentia to the east by the Richardson trough and the Richardson fault array (Fig. 1). The Richardson trough represents a Cambrian–Devonian deep-water basin formed above a failed rift arm between the Yukon Block and Mackenzie platform (Gabrielse, 1967; Pugh, 1983; Norris, 1985; Cecile et al., 1997; Morrow, 1999; Rohr et al., 2011). The Richardson fault array is a regional scale fault system with a history of reactivation that has controlled sedimentation and deformation in the area since its inception in the Proterozoic (Eisbacher, 1981; Eisbacher, 1983; Norris, 1985; Aitken and McMechan, 1992; Aitken, 1993; Abbott, 1996; Norris, 1997; Abbott, 1997; Crawford et al., 2010; Rohr et al., 2011). Proterozoic strata in the Yukon Block consist of three major successions (Young et al., 1979) exposed in four inliers: the Tatonduk, Coal Creek, Hart River and Wernecke inliers (Fig. 1). The oldest rocks consist of Sequence A, a poly-deformed succession of mixed carbonate and siliciclastic strata of the late Paleoproterozoic–early Mesoproterozoic Wernecke Supergroup (Delaney, 1981; Thorkelson et al., 2005; Furlanetto et al., 2013). Sequence B includes the Pinguicula, Hematite Creek, and Fifteenmile groups in the Yukon Block inliers. These groups are correlative with the Mackenzie Mountains Supergroup, which compose the oldest strata found in the Mackenzie Mountains to the east. A tuff in the Fifteenmile Group of the Coal Creek inlier has been dated at 811.51 $\pm$ 0.25 Ma (U-Pb ID-TIMS on zircon, Macdonald et al., 2010). Sequence C includes the Cryogenian–Ediacaran-aged strata of the Windermere Supergroup.

The focus of this study is the Coal Creek inlier, in the south-central Ogilvie Mountains (Figs. 1 and 2). In this area, the Mount Harper Group forms the base of the Windermere Supergroup and

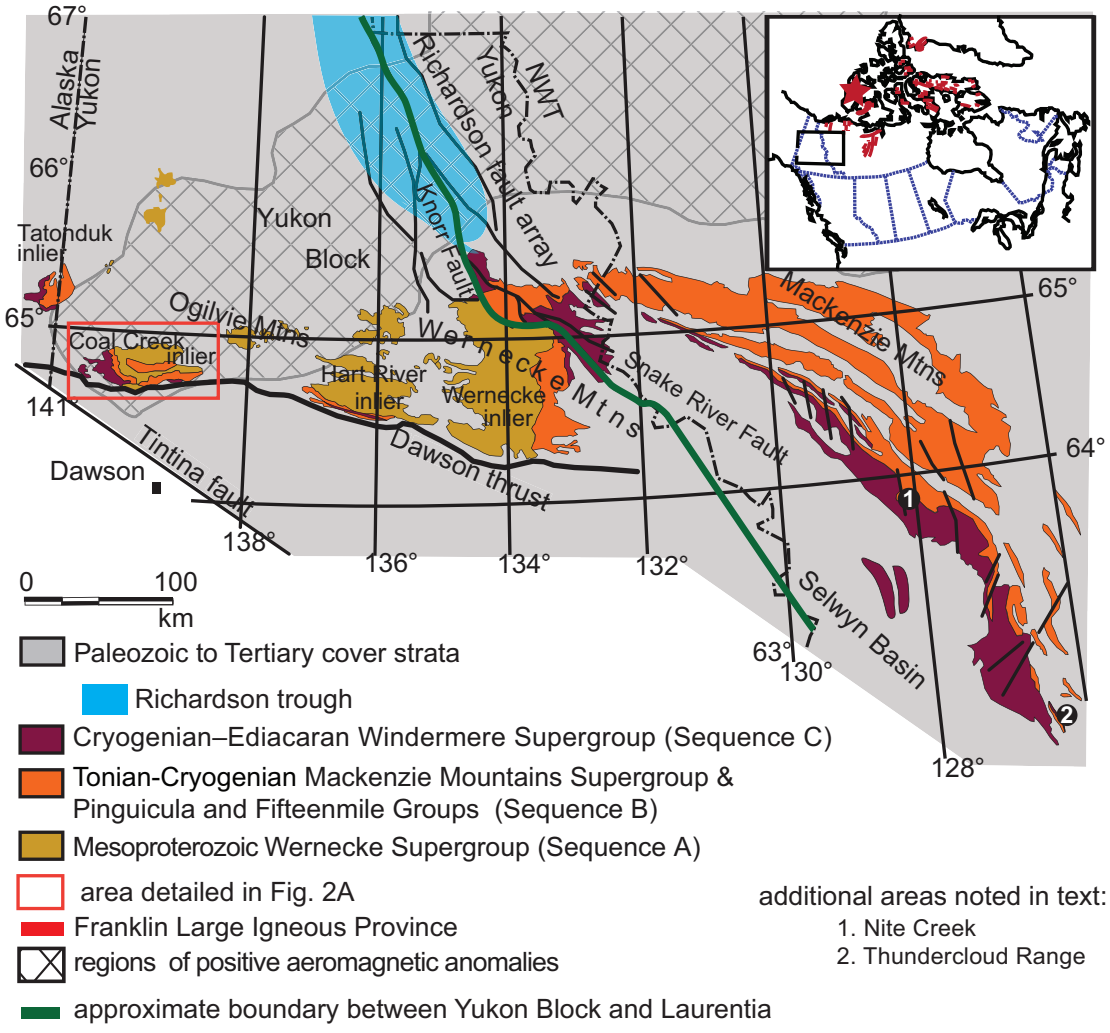


Figure 2.1: Note Richardson trough (after Morrow, 1999) and Richardson fault array separates the Tatonduk, Coal Creek, Hart River and Wernecke inliers from the Mackenzie Mountains. The cross-hatched areas indicate aeromagnetic highs following Aspler et al. (2003) and Pilkington and Saltus (2009). The solid green line depicts approximate boundary between the Yukon Block and Laurentia. Inset depicts the extent of the Franklin large igneous province (red) (Buchan and Ernst, 2004; Buchan et al., 2010; Buchan and Ernst, 2013).

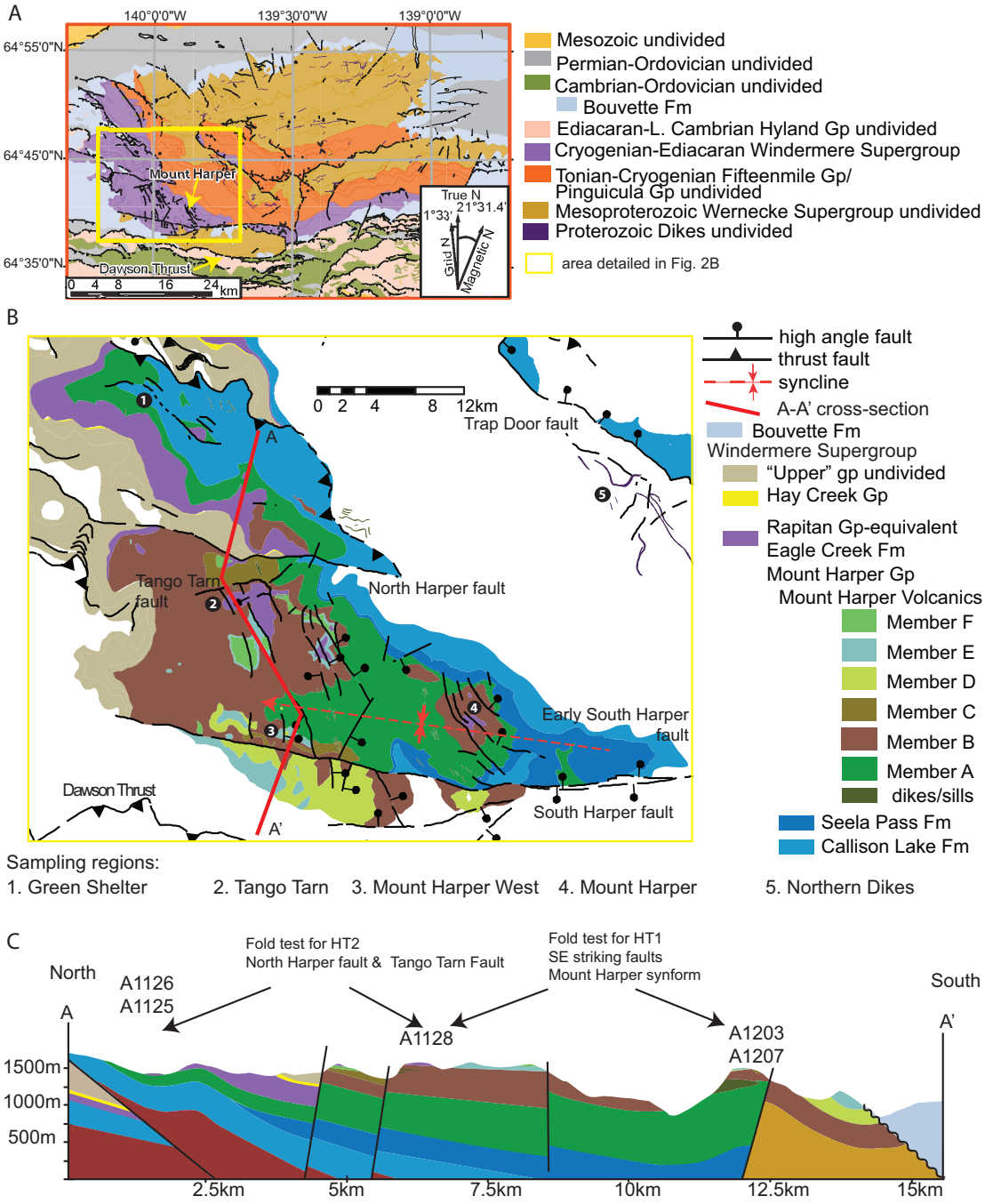


Figure 2.2: A. Map of the Coal Creek inlier (Modified from Strauss et al., 2014b). B. Focus on the Mount Harper Group with the Mount Harper volcanics divided into informal members. Important sample areas and cross section line A-A' indicated on map. C. Cross section A-A' across the MHV.

includes, in stratigraphically-ascending order, the ~755–735 Ma Callison Lake Formation (Strauss et al., 2014a; 2015; Rooney et al., 2015), the Seela Pass Formation, and the Mount Harper volcanics (Mustard, 1991; Mustard and Roots, 1997; Macdonald et al., 2010; 2011; Strauss et al., 2014b; 2015). The Callison Lake and Seela Pass formations record fault-related carbonate and siliciclastic sedimentation associated with early phases of Neoproterozoic extension in NW Canada (Mustard, 1991; Mustard and Roots, 1997; Strauss et al., 2015).

The Mount Harper Volcanics consist of a bimodal magmatic suite that is divided into six informal members along with intrusive domes and dikes (Figs. 2 and 3; Mustard and Roots, 1997). Geochemically, the total alkali-FeO-MgO (AFM) projection shows samples on both sides of the tholeiitic/calc-alkaline divide (Mustard and Roots, 1997; Cox, 2015). This is unusual, as at the same time, the close association of the volcanics with normal faulting and extensional activity, indicates a relationship between extension and volcanism (Mustard and Roots, 1997). The existence of magmas with calc-alkaline affinities but connected to lithospheric extension rather than subduction has been documented in the North American Pacific Northwest and Basin and Range (Robyn, 1979; Gans et al., 1989; Smith et al., 1990; Hooper et al., 1995; Hawkesworth et al., 1995; Morris et al., 2000, Camp et al., 2003) as well as in eastern Queensland, Australia (Ewart et al., 1992) and northeastern China (Fan et al., 2003). In such cases, it is suggested that the rift related calc-alkaline magmatism can be explained by extension related decompression melting of subcontinental crust or mantle that was previously hydrated and enriched by earlier subduction events, rather than by contemporaneous subduction. The basaltic lower suite consists of members A, B and C, and the more felsic upper suite comprises members D, E and F (Mustard and Roots, 1997). Local evidence of soft sediment deformation in the Seela Pass units beneath the basal pillow basalt flows of member A (Fig. 3) suggest these units were unlithified during emplacement of the volcanics (Mustard and Roots, 1997). Member A consists of pillowed and minor massive flows and member B comprises basaltic flows of two facies: a pillow-dominated chloritic facies and an overlying hematitic and highly vesiculated

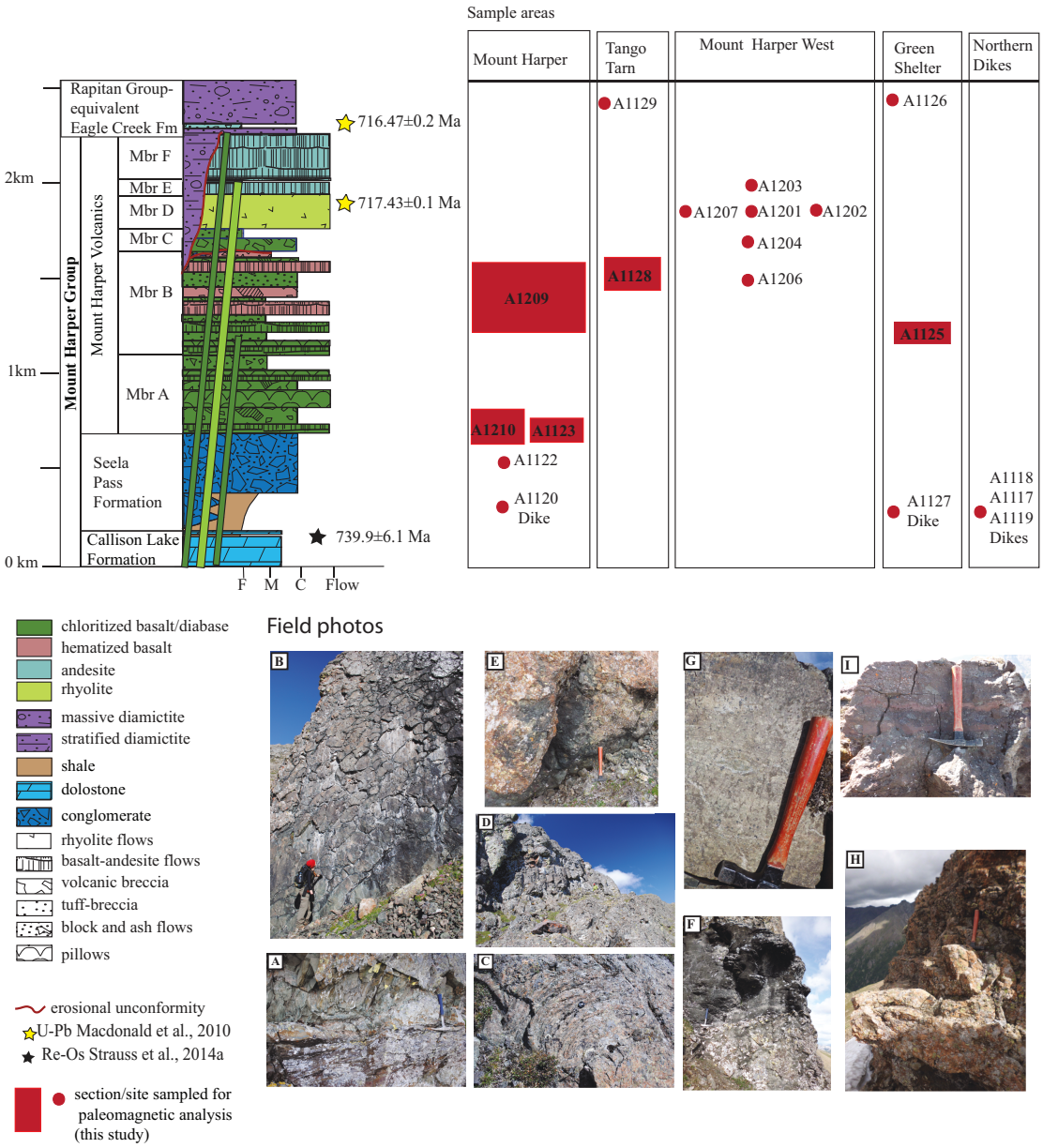


Figure 2.3: Composite stratigraphic section of the Mount Harper volcanics with the approximate stratigraphic position of sampled units along with field photos of the lower members (A and B) from Mount Harper and of the upper members (C, D and E) from Mount Harper West (photos by J. Strauss and A. Eyster). A. Contact between the Seela Pass Formation and member A. B. Member A pillows. C. Member B pahoehoe flow top. D. Member B columnar joints. E. Member C breccia. F. Member C mafic tuff. G. Member D flow banding. H. Member E flows. I. Basal Eagle Creek formation with volcanic clasts.

unit with pahoehoe flow tops (Fig. 3). The transition between these members was originally defined in reference sections based on chemical analysis (Mustard and Roots, 1997). For the hematitic facies, it is likely that iron oxidation of subaerially erupted basalts resulted in the growth of syn-volcanic hematite (Mustard and Roots, 1997; Roots, 1988). Fine- to medium-grained chloritic and SE-trending diabase dikes and sills are associated with members A and B (Mustard and Roots, 1997), and the dikes may have fed the extrusive member B volcanics. Member B is disconformably overlain by various members of the upper MHV and Rapitan Group-equivalent strata of the Eagle Creek formation (Mustard and Roots, 1997; Strauss et al., 2014b). Member C consists predominantly of basaltic pyroclastic to epiclastic breccias, whereas member D is rhyolitic in composition and locally dominated by massive columnar jointed flows that weather light pink to grey-green (Fig. 3). A thin crystal tuff layer marks the upper contact of member D in two places. Member E is composed primarily of dark blue chlorite-bearing andesitic flows, tuffs and breccias (Mustard and Roots, 1997). Pillowed flows up to 20 m thick are found in member E, as well as local subaerial pahoehoe textures (Fig. 3). Three mounds of silicic rubble, thought to be ancient rhyolite domes, are locally centered on feeder dikes and appear to be younger than the rest of member D because they intrude member E (Mustard and Roots, 1997). These rhyolite domes were dated with U-Pb CA-ID-TIMS on zircon at 717.43 $\pm$ 0.14 Ma (Macdonald et al., 2010). Member F is the youngest of the rocks in the MHV and includes intermediate to mafic flows, sills, dikes, breccias and tuffs that weather orange to brown (Mustard and Roots, 1997). Flows from member F are locally interstratified with the overlying glaciogenic deposits of the Rapitan Group-equivalent Eagle Creek formation (Mustard and Roots, 1997; Macdonald et al., 2010; Strauss et al., 2014b).

The Rapitan Group-equivalent Eagle Creek formation is locally in erosional contact with members A-E and it interfingers with member F. A tuff near the base of the Eagle Creek formation yielded a U-Pb zircon age of 716.47 $\pm$ 0.24 Ma (CA-ID-TIMS; Macdonald et al., 2010). These glacial strata are locally overlain by various strata equivalent to the Cryogenian Hay Creek Group and the Edi-

acaran to Early Cambrian informal "Upper" group (Macdonald et al., 2011; Strauss et al., 2014b). The Bouvette Formation, a thick sequence of Cambrian to Devonian dolostone, regionally rests with angular unconformity on the Windermere Supergroup and older strata (Thompson et al., 1994; Mustard and Roots, 1997; Macdonald et al., 2011; Strauss et al., 2014b).

Synsedimentary tectonism during deposition of basal Windermere rocks has been investigated in the northern Canadian Cordillera (for example, Eisbacher, 1981, 1985; Jefferson and Parrish, 1989), in British Columbia (Root, 1987), and in the United States (Stewart, 1972; Miller, 1985; Yonkee et al., 2014). In the Coal Creek inlier, for the Mount Harper Group, the oldest Neoproterozoic extensional structures in the area include the Trap Door and Early South Harper faults, both of which governed the depositional patterns of the Callison Lake and Seela Pass formations (Fig. 2; Mustard, 1991; Mustard and Roots, 1997; Strauss et al., 2014b; 2015). The MHV, Seela Pass and Callison Lake formations occur north of the Early South Harper fault within the broad, informally-termed Mount Harper synform (Fig. 2; Roots, 1987; Strauss et al., 2015). The Callison Lake synrift strata show evidence of thickening in the trough of the synform, which indicates that the folding is related to fault initiation at depth, with the development of growth stratigraphy above a fault tip (Schlische, 1995; Sharp et al., 2000). This type of hanging wall synformal basin is well documented in extensional settings associated with normal fault systems (Schlische, 1995; Sharp et al., 2000; Gawthorpe and Leeder, 2000; Schlische, 2003). The synform likely developed during the late stages of Callison Lake sedimentation and Mount Harper volcanism, as the broad synformal geometry is still apparent in the MHV (Fig. 2C; Strauss et al., 2015). The synform plunges gently westward, preserving the younger volcanic members of the MHV in the western Coal Creek inlier.

There are also a number of syn-MHV brittle extensional structures. The north-side-down Tango Tarn fault was inferred from the distribution of members B and C of the MHV and the Eagle Creek formation (Fig. 2, Roots, 1987; Mustard and Roots, 1997). The Early South Harper fault was also active during MHV volcanism, but during most of the volcanic activity, the southern margin of the

half graben remained high as indicated by a transition from subaqueous hydroclastic breccia in the north to subaerial volcanism to the south (Roots, 1987). Following the eruption of the MHV, the Early South Harper fault was reactivated as the partially reverse South Harper fault, and numerous SSE-striking faults and the North Harper fault were active (Fig. 2). The dominantly parallel SSE-striking faults do not cut the South Harper or North Harper faults but they do cut the strata of the Rapitan Group-equivalent Eagle Creek formation (Fig. 2). The North Harper fault near the northern edge of the volcanics displays as much as 350 m of north side down displacement indicated by the juxtaposition of the stratigraphically higher beds of the Eagle Creek formation and "Upper" group strata on the north side, with the volcanics on the south side (Roots, 1987).

Observations of the regional outcrop extent of the Seela Pass and Eagle Creek formations highlight the potential development of two distinct and slightly diachronous sub-basins with opposed but offset footwall scarps (Mustard, 1991). The emplacement of the MHV could be related to the development of an accommodation zone between the two offset grabens (Mustard, 1991; Mustard and Roots, 1997; Strauss et al., 2015). The angle between the SSE-striking faults and the North and South Harper faults could represent minor counterclockwise block rotations in a sinistral strike-slip system (Roots, 1987).

The modern expression of the Ogilvie Mountains is a result of late Mesozoic northward-directed shortening associated with the Cordilleran orogeny (Norris, 1997; Mair et al., 2006; Martel et al., 2011). Despite this regionally significant tectonic activity, map relationships in west-central Yukon suggest that the Coal Creek inlier acted as an orogenic welt, with wrench faults on the west side and counterclockwise faulting on the east side, but with minimal faulting or reactivation of faults observed within the inlier itself. In the MHV, some primary structures in the area experienced minor reactivation, such as the Early South Harper fault (Roots, 1987).

2.4 Diagenetic Considerations

The MHV experienced prehnite-pumpellyite to lower greenschist facies metamorphism resulting from burial and fluid alteration during Mesozoic–Paleogene shortening associated with the Cordilleran orogeny (Roots, 1987; Greenwood et al., 1991; Mustard and Roots, 1997). The volcanics are highly hydrated and display abundant chlorite and sericite alteration (Cox et al., 2013). During alteration, volcanic glass was altered to quartz and feldspar, olivine phenocrysts were pseudomorphed into quartz and hematite, and plagioclase phenocrysts were replaced by clay minerals (Mustard and Roots, 1997). Primary paleomagnetic signals carried by magnetite can survive heating to the greenschist metamorphic range (300°–500°C) but not to the amphibolite range (600°–750°C) (Pullaiah et al., 1975; Dunlop and Buchan, 1977). Furthermore, metamorphic changes that alter the ferromagnetic minerals can destroy the primary natural remanent magnetization and result in chemical remagnetization. Consequently, understanding the occurrence and nature of the magnetic minerals (hematite, magnetite and titanomagnetite) is of particular interest for paleomagnetism studies. Alteration in members A and B involved hematite replacing olivine and albitization of plagioclase that was later filled in with hematite. Primary iron oxidation likely occurred during the eruption of the hematized facies, in addition to later iron oxidation that occurred during secondary mobilization for both the chloritized and hematized volcanics. It is likely that synvolcanic hematite formed in some of the subaerially erupted basalts (Mustard and Roots, 1997; Roots, 1987)

2.5 Methods

Paleomagnetic samples were collected via drilling of small cores and hand sampling with orientations measured by a combination of Brunton and sun compass. The orientations of flow-tops, along with any nearby sedimentary or water-lain units, were measured to correct for any tectonic tilting. Although the original volcanic units were likely tilted (gentle paleoslopes), the areal and

stratigraphic sampling was large enough to hopefully average any paleoslope effects. The parallel orientation of flow banding and flow tops to sedimentary bedding suggests paleoslopes of less than 10°. Even so, errors in bedding corrections due to paleoslopes cannot be unambiguously quantified and may affect paleohorizontal corrections (Irving and Thorkelson, 1990).

We collected a total of two hundred and fifty-five samples from twenty different rock units or localities, including two conglomerate tests and five measured sections. I sampled the upper and lower members of the MHV, the MHV dikes, and sedimentary deposits within the Seela Pass Formation and the Eagle Creek formation, with sampling concentrated at five main regions that ranged over 14 km across regional strike: Mount Harper, Mount Harper West, Tango Tarn and Green shelter and Northern dikes (Figs. 2 and 3). The lower suite members were sampled at four of the regions, while the upper suite members were sampled only at Mount Harper West. At Tango Tarn and Green shelter I collected both clasts and matrix samples for conglomerate tests from the base of the Eagle Creek formation. For the stratigraphic sections that spanned multiple flows/sites, I normally collected at least 6 samples total, with 1-3 samples per flow or stratigraphic horizon. I collected at least 3 samples from dikes ranging between $\sim$ 2-12.5 m thick, focusing on sampling at the chilled margins that are more likely to contain primary magnetization due to the smaller sizes expected for the magnetite carriers.

Individual samples were drilled and cut to specimens 2.5 cm in diameter and 2 cm long. One to two specimens were measured for each sample. Magnetization measurements were made with a 2G Enterprises 755 Superconducting Rock Magnetometer (SRM) in the Massachusetts Institute of Technology Paleomagnetism Laboratory using an automated sample handling system (Kirschvink et al., 2008). This instrument has a sensitivity of 10^{-9} Am^2 and is located in a magnetically shielded room (DC field $<$150 nT). The natural remanent magnetism (NRM) was measured for all specimens. Then, I immersed a portion of the specimens in a liquid nitrogen bath to preferentially remove the magnetization carried by multidomain magnetite and hematite grains. This procedure

was followed by AF demagnetization up to 15 mT on most of the specimens, and finally thermal demagnetization on all the specimens. The thermal demagnetization was conducted using an ASC Scientific Thermal Demagnetizer with peak DC fields inside $<$ 10 nT. Specimens were thermally demagnetized in steps of 2.5-50°C until completely demagnetized. Similar demagnetization behaviors were observed in specimens that were subject to both thermal and AF demagnetization and those that were only thermally demagnetized.

Because lightning strikes can cause remagnetization, care was taken in the field to use both a sun compass and a Brunton to identify locations that may have experienced strong remagnetization. AF demagnetization up to 10-15 mT was able to remove randomly oriented minor secondary NRM components that may represent lightning-induced IRM in 31 out of 220 specimens. A1128 was the only section from which specimens did not undergo AF demagnetization. However, specimens from A1128 did not demonstrate strong single-component magnetizations and high NRM intensities that would suggest lightning remagnetization. Lightning remagnetized specimens were identified in about 2% of analyzed specimens. Most of the specimens ($\sim$84%) from sites and measured sections yielded resolvable components of magnetization. Magnetic components were determined using principal component analysis of both best-fitting lines and, for 15% of the specimens, great circles (Kirschvink, 1980). When analyzing the data, I used a maximum angle of deviation (*MAD*) cutoff of 15° following the recommendation of Butler (1992), but in most cases the *MAD* angle was $<$10°. Specimen analysis was completed using the PaleoMag OS X program (Jones, 2002). If multiple specimens were prepared from a sample, then the specimen directions were averaged. In this and every other case, I applied Fisher statistics to calculate mean directions.

For our sites (single flows or cooling units), it was straightforward to calculate mean component directions using all the samples from the site. For our sections, I typically had 1-2 samples for each flow and calculated mean component directions three different ways. In our first approach I calculated section means using all the samples. For our second approach I calculated section means,

but using flow mean directions when possible. Here, when I collected multiple samples from a single flow I calculated a mean flow direction. If this mean flow direction had $a_{95}<20°$ (for number of samples, $n>2$) or angular standard deviation $<20°$ (for $n=2$), then it was combined with data from single sampled flows to obtain a section mean. In the third approach, I focused on directions from the individual flows within a section and only used data from flows with $n\geq 3$ and $a_{95}<20°$. I then calculated flow or site-mean component directions. The first two methods are more relevant to post-emplacement magnetic acquisition (i.e., chemical-remanent magnetization) that is expected to cut across depositional flow boundaries; whereas the third method is most applicable to primary thermal-remanent magnetization with eruptive events separated by brief hiatuses and non-negligible geomagnetic secular variation.

2.6 Results

We classified the magnetizations based on their unblocking temperature range and directionality into a low-temperature (LT), a mid-temperature (MT) and two high-temperature (HT) component directions (Fig. 4). Although both conglomerate tests (A1126 and A1129) yielded random clast directions, only one of them yielded a coherent high-temperature component matrix direction (A1126).

The three approaches that I used to calculate mean directions for the sections yielded essentially the same results (see Appendix 1). In the following discussions, I use our first approach, except when discussing HT1, where I also mention our results from the third approach (only using individual flows/sites) because I interpret that component to be a primary thermal remanence. The within-section/site precision parameters normally ranged between 10 and 50. The sections or sites that did not yield useful data include those with $\alpha_{95}>25°$ and two or fewer samples with resolvable directions (A1119, A1122, A1127), sites dominated by samples with no obvious decay to the origin that required great circle fits (A1118, A1201), and those with strong (moment $>10^{-6}$ A m^2) random di-

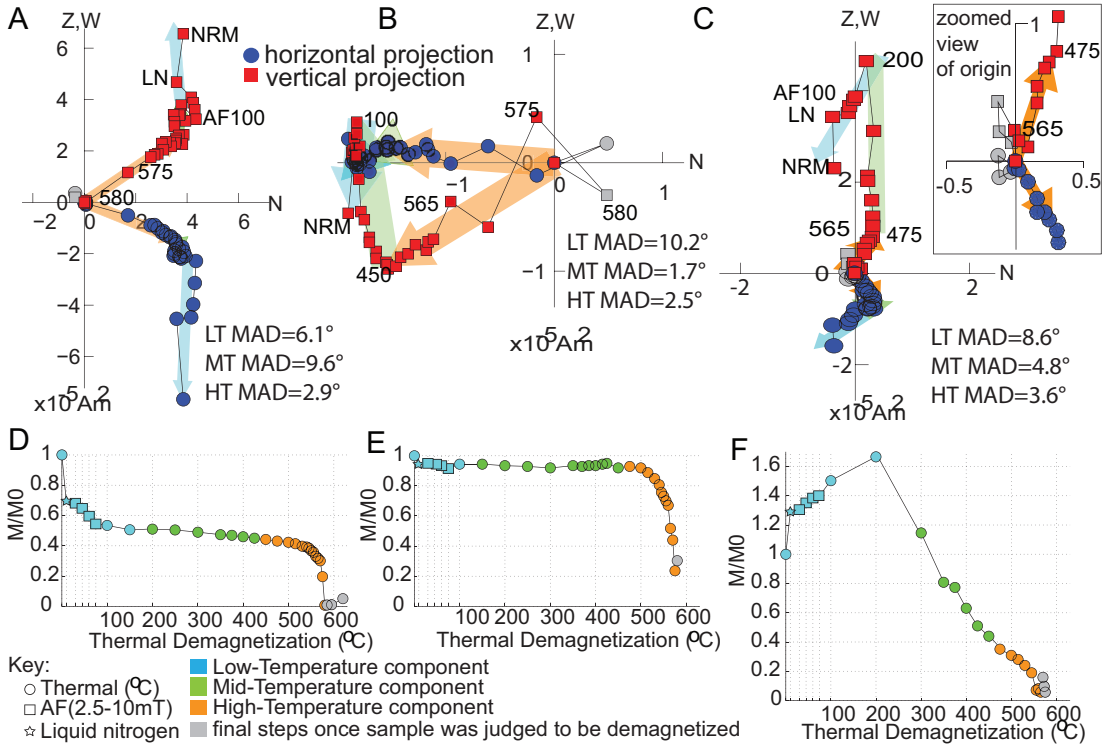


Figure 2.4: A. Representative orthogonal projection diagrams showing the demagnetization of sample A1207-5 that carries HT1. B. Representative orthogonal projection diagrams showing the demagnetization of sample A1203-3 that carries HT1. C. Representative orthogonal projection diagrams showing the demagnetization of sample A1123-17 that carries HT2. The corresponding *M/M0* plots are shown in D, E and F. The stars represent the liquid nitrogen demagnetization step, the squares represent the AF demagnetization steps, and the circles represent thermal demagnetization. The representative orthogonal projections are shown using in situ coordinates.

rections that responded strongly to AF demagnetization and were interpreted to be the result of lightning (A1202, A1121). Additionally, two sites (A1117 and A1120) had three samples with resolvable directions and α_{95}>20°. The Tauxe and Watson (1994) fold test was applied and uncertainty was quantified by utilizing bootstrapped data sets and repetition of the fold test for various percentages of unfolding.

The LT component direction is found in two sections (39 samples), representing members A and B (Figs. 5A and 5B). This component is removed during thermal demagnetization between 100 and 150°C. The LT direction failed the Tauxe and Watson (1994) fold test. The maximum eigenvalue of the orientation matrices (τ_1) occurs at -10% unfolding and the 95% confidence interval of bootstrapped samples is between -10% and 28% unfolding.

The MT component direction is found in eight sections encompassing 128 samples (Figs. 5C and 5D). These sites include member A, member B, member C, member E and the Eagle Creek formation. This component is demagnetized upon heating to 425-500°C. In 50% of the measured samples this direction is tightly clustered (α_{95}<10°). The mid-temperature direction is also a post-tilting direction, as the maximum τ_1 occurs at -10% untilting and the 95% confidence interval spans -10% to 8% unfolding.

Finally, the high-temperature directions from the individual samples were observed to fall into two groupings, one with moderate positive inclinations towards the south and one with low negative inclinations towards the northeast. I label these the HT1 (Figs. 5E and 5F) and HT2 (Figs. 5G and 5H) components respectively. Two sections (A1128) yielded both HT1 and HT2 components with α_{95}<20°. Section A1128 was 191.5 meters thick and samples carrying HT1 were identified throughout the section, while samples carrying HT2 were scattered near the top of the section. Section A1209 was 273 meters thick and 3 samples carrying HT2 with unblocking temperatures expected for hematite were collected from near the top as well as one sample near the base. Additionally, 1 sample carrying HT1 was analyzed from the top of A1210. In most cases where I collected mul-

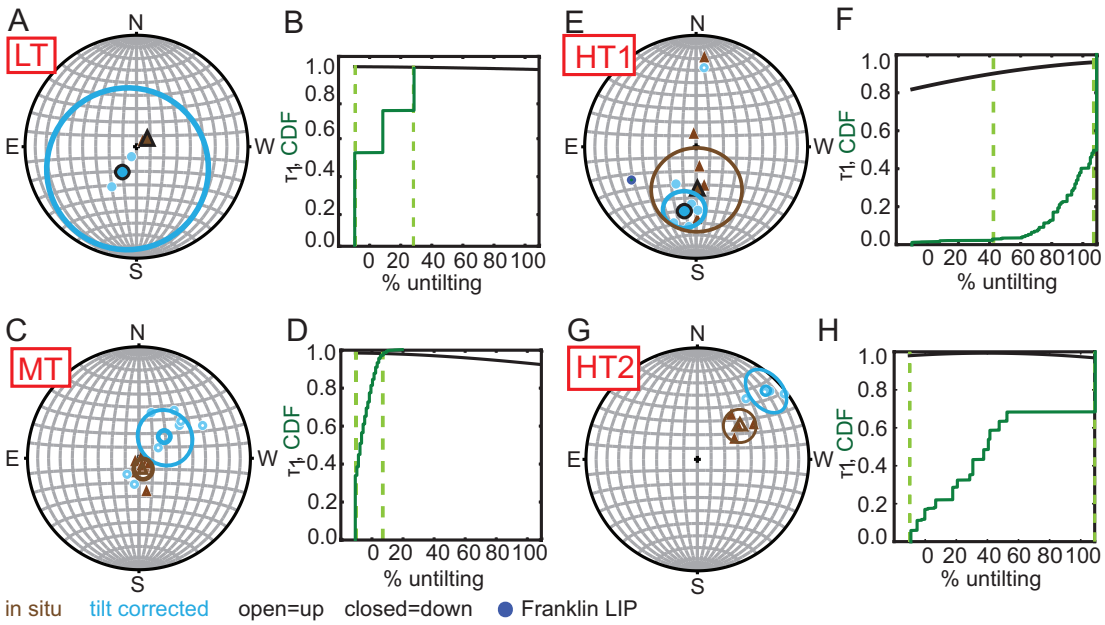


Figure 2.5: A. Sections with a LT direction. B. Results from the Tauxe and Watson (1994) fold test. C. Sections with a MT direction. D. Results from the Tauxe and Watson (1994) fold test. E. Section results for HT1 direction. Note that section A1207 has a high stability HT1 direction reversed from the rest. The direction expected from the Franklin LIP (Denyszyn et al., 2009a) is also indicated. F. Results for HT1 from the Tauxe and Watson (1994) fold test. G. section results for HT2 direction. H. Results for HT2 from the Tauxe and Watson (1994) fold test. For the plots of the section-mean directions, the in situ directions are indicated with brown triangles and the tilt corrected directions with blue circles, with negative directions represented by open symbols and positive directions represented by closed symbols. For the Tauxe and Watson (1994) fold tests, the black curves indicate maximum eigenvalue (τ_1) as a function of untilting. The green line is the cumulative distribution of the percent untilting required to maximize τ_1 for all the bootstrapped data sets. The dashed vertical lines are 95% confidence bounds on the % untilting that yield the most clustered result (maximum τ_1). If the 95% confidence bounds include 0, then a pre-tilt magnetization is indicated. If the 95% confidence bounds include 100, then a post-tilt magnetization is indicated. If the 95% confidence bounds exclude both 0 and 100, syn-tilt magnetization is possible.

tiple samples from a single flow, HT1 and HT2 were found in different flows. However, in section A1128, one flow had one sample with HT2 (A1128-50), while the other samples from that flow were carrying HT1. In two cases, a sample displayed both HT1 and HT2 directions: both specimens from sample A1209-17 displayed a HT1 component direction unblocked by 575°C and HT2 unblocked at 680°C and sample A1209-4 displayed a HT1 direction unblocked at 565°C and a higher temperature circle fit to HT2.

In total, using approach 1, I resolved HT1 site/section mean directions with $\alpha_{95}<20$ in one site and four sections (60 samples), including members B, D, and E along with the matrix from the Rapitan Group-equivalent strata of the Eagle Creek formation. Using approach 3, I identified HT1 site mean directions with $\alpha_{95}<20$ in 7 flows/sites (34 samples) from members B, D and E. In most samples this component was fully demagnetized between 565 and 575°C, indicating magnetite as the principal ferromagnetic carrier. Among all the samples, some were demagnetized much earlier than 565°C, starting at 400°C. There were four samples where the HT1 direction had unblocking temperatures between 605-680°C. Under further examination, it was observed that these samples carrying a HT1 with high unblocking temperatures also displayed a substantial decay of the intensity of the magnetization at 580°C in the direction of HT1. From this I conclude in these samples the HT1 direction is carried by both magnetite and hematite.

The HT1 component passes the Tauxe and Watson (1994) fold test as the maximum τ_1 occurs at 109% unfolding and the 95% confidence bounds are from 42-109% unfolding, suggesting that the magnetization was acquired pre-folding. Using approach 3, the HT1 direction also passed the fold test, this time with maximum τ_1 at 92% unfolding with confidence bounds from 89 – 109% unfolding.

One sampled unit (A1207-member D) displays a reversed HT1 direction (Fig. 5E). This represents a double reversal, as this direction is reversed from those stratigraphically both above and below. In tilt corrected coordinates, the reversal test (for the isolated reversed section) results in an observed

angle between the mean directions of 16.8° and a critical angle calculated for the two sets of observations at which the null hypothesis of a common mean direction would be rejected with 95% confidence of 38.7°. However, due to the limited number of observations, the high value of the critical angle places the reversal test in the "indeterminate" classification of McFadden and McElhinny (1990). For the HT1 directions from approach 3, the observed angle is 18.0° and the critical angle is 18.7°, thus these directions pass the reversal test with a C classification (McFadden and McElhinny, 1990). Finally, the primary nature of this direction is also supported by one of the conglomerate tests. A high-temperature component was isolated in five clasts and four matrix samples from one of the conglomerate tests (A1126). For the clasts, the critical value of the resultant vector (R_o) is 3.50 at the 95% confidence level, while the value of the resultant vector (R) is 2.2, which is less than the critical value and indicates that a uniform distribution can be rejected at the 95% confidence level (Watson, 1956). This contrasts with the four matrix samples with HT components that display the HT1 direction.

The HT2 direction was found in 4 sections (35 samples total) only from members A and B. The HT2 direction was more likely to be isolated using great circle fits in the principal component analysis than the HT1 direction. Depending on the sample, the HT2 component could be removed after heating to 350-680°C, but in most samples was removed by heating up to 570°C or 680°C. These unblocking temperatures are consistent with the temperatures expected from magnetite and hematite. The Tauxe and Watson (1994) fold test for the HT2 direction is ambiguous, the maximum τ_1 occurs at 40% untilting but the 95% confidence interval spans -10% to 109% unfolding.

2.7 Magnetic Carriers For High-Temperature Component Directions

Thin sections were made from select samples that carried the HT1 (A1203, A1207) and HT2 (A1128, A1210) component directions. The samples carrying the HT1 component were observed to include

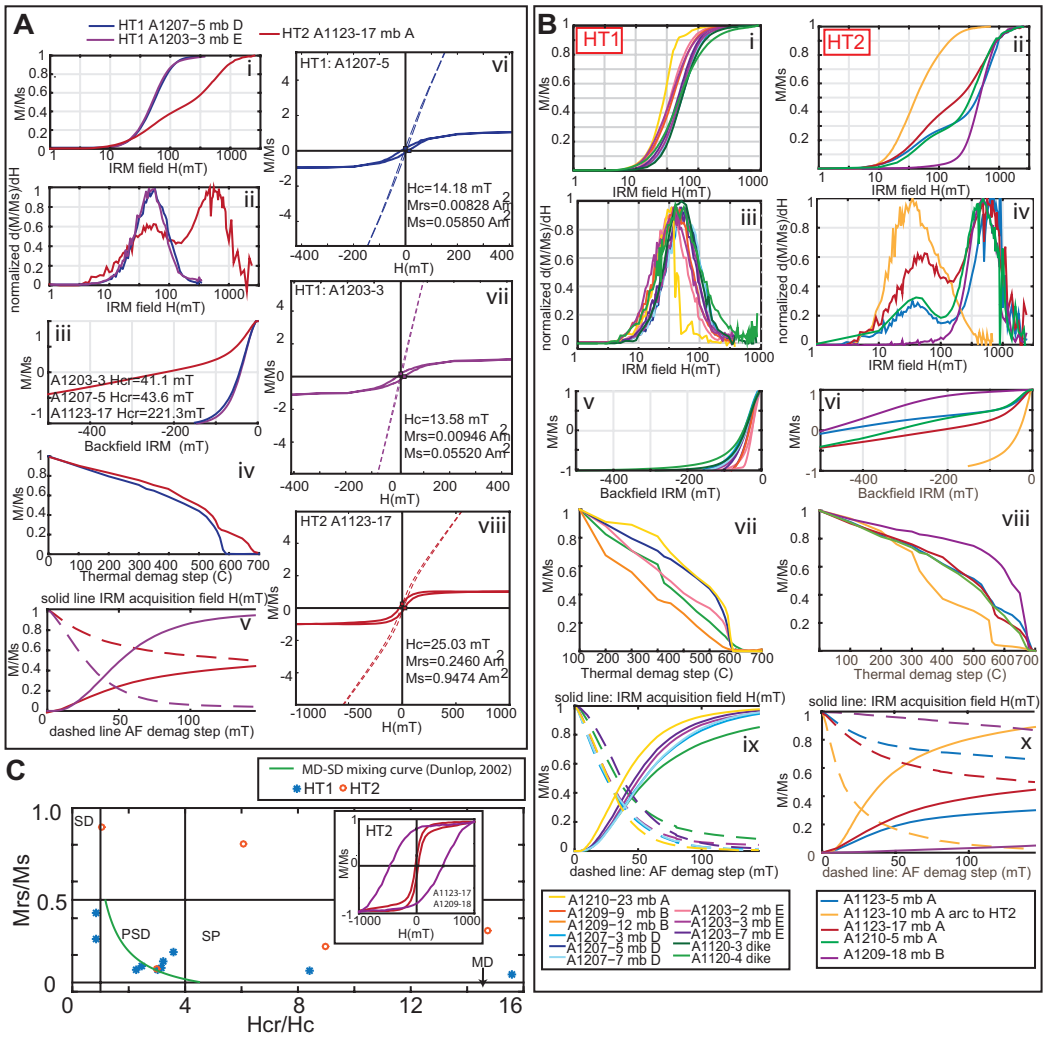


Figure 2.6: Results of rock magnetic experiments. A. Comparison of rock magnetic results for representative samples shown above (Fig. 3) carrying HT1 and HT2. Sample A1207-5 from member D carries reversed HT1, sample A1203-3 from member E carries normal HT1, while sample A1123-17 from member A carries HT2. i. Linear acquisition plot. ii. Gradient curve of IRM acquisition, iii. Backfield IRM data. iv. Thermal demagnetization of sIRM. v. AF demagnetization of sIRM. vi. Hysteresis curves for A1207-5 carrying HT1, dashed line is raw data, solid line is data corrected for paramagnetic slope. vii. Hysteresis curves for A1203-3 carrying HT1, dashed line is raw data, solid line is data corrected for paramagnetic slope. viii. Hysteresis curves for A1123-17, dashed line is raw data, solid line is data corrected for paramagnetic slope. B. Comprehensive plot of all rock magnetic results for selected samples carrying HT1 (left side) and HT2 (right side). i, ii. Linear acquisition plots. iii, iv. Gradient curves of IRM acquisition. v, vi. Backfield IRM data. vii, viii. Thermal demagnetization of sIRM. ix,x. AF demagnetization of sIRM. C. Day plot of results from hysteresis experiments. Blue asterisks mark results for samples carrying HT1, while red circles mark those for samples carrying HT2. Also shown are boxes marking SD, PSD, MD and SP regimes as well as in green is the MD-SD mixing curve of Dunlop (2002). Inset shows behavior of samples carrying HT2, specifically, the wasp-waisted behavior of A1123-17, likely due to dual-population ferromagnetic mineralogy and the SD hematite behavior of A1209-18.

small interlocking opaque minerals, likely magnetite and titanomagnetite, in the matrix. The vesicles in these samples tended to be filled with calcite. The samples that displayed the HT2 direction were found to have some smaller opaque minerals in the matrix, with some larger likely magnetite crystals, as well as vesicles filled with quartz and titanomagnetite. Finally, I observed some fine hematite staining that preferentially filled cracks and veins. Because multidomain (MD) sized grains visible in the microscope do not necessarily carry the bulk of the stable magnetization (Jackson, 1990), I relied on rock magnetism experiments to characterize the bulk properties of the magnetic carriers. The magnetic mineralogy of sixteen different samples was analyzed with IRM acquisition and IRM backfield experiments, thermal demagnetization of saturation IRM (sIRM), AF demagnetization of sIRM, and hysteresis experiments. I applied stepwise IRM acquisition in a field up to 2.5 T to determine the coercivity spectra and saturation fields and thereby resolve distinct populations of ferromagnetic minerals. Following the IRM acquisition, backfield IRM was applied in order to determine the coercivity of remanence (H_{cr}). I obtained hysteresis experiments with maximum fields of 1 T using the vibrating sample magnetometer (VSM) in the Massachusetts Institute of Technology laboratory of C. Ross to determine the values of saturation magnetization ($\mathcal{M}_s$), saturation remanence ($\mathcal{M}_{rs}$) and coercivity (H_c). I used these parameters to constrain the domain states of the magnetic carriers. Next, for five samples carrying the HT1 component and five samples carrying the HT2 component, I investigated the thermal demagnetization of sIRM to identify the magnetic carriers based on their unblocking behavior. Finally, on six samples carrying the HT component and four carrying the HT2 component I conducted AF demagnetization of the sIRM to determine the crossover values and the strength of the interactions between the ferromagnetic grains (Cisowski, 1981).

2.7.1 Rock Magnetism Results

IRM acquisition and backfield IRM experiments

Following Kruiver et al. (2001), I display the IRM acquisition data on the linear acquisition plot (LAP) and the gradient of acquisition plot (GAP) (Fig. 6). I decomposed the measured IRM data into cumulative log-Gaussian (CLG) curves, each of which is characterized by the sIRM, mean coercivity ($H_{1/2}$) and dispersion (dp). $H_{1/2}$ is a measure of the coercivity of remanence H_{cr} if a sample contains only a single population of ferromagnetic grains. The two most important magnetic phases in geological materials are magnetite and hematite, which have maximum coercivities of approximately 300 and >1000 mT, respectively (O'Reilly, 1984; Banerjee, 1971). The principal ferromagnetic phase in samples that carried origin-trending HT1 reached saturation magnetization before 300 mT, consistent with a lower coercivity mineral such as magnetite (Figs. 6A and 6B). Furthermore, samples carrying an HT1 direction displayed a single peak in the GAP plots, suggesting that they contained only one significant ferromagnetic mineral (Figs. 6A and 6B). The dike samples (A1120-4 and A1120-3) contained a minor component of a higher coercivity mineral, possibly hematite or pyrrhotite, but the peak on the GAP plot was difficult to distinguish. These samples reached 99.5% of their sIRM at 550-840 mT. For all samples carrying the HT1 component, the backfield IRM experiments indicated H_{cr}values of 26-47 mT, consistent with a low coercivity magnetic mineralogy.

All samples with an HT2 component reach 99.5% of the sIRM between 500 mT to 2000-2400 mT (Figs. 6A and 6B), which suggests these samples contain a high coercivity mineral such as hematite. In addition, most of the samples that carry the HT2 direction display two peaks, suggesting two populations of magnetic carriers (Figs. 6A and 6B), with the higher coercivity component containing 75% of the sIRM. Of the HT2 component-bearing samples, sample A1123-10 displayed only one dominant peak, with 99.5% of the saturation reached at 500 mT. This suggests that in rare cases a lower coercivity mineral, such as low coercivity magnetite, carries the HT2 direction. The backfield

IRM experiments generally indicated H_{cr} of 220-490 mT, which is higher than those of samples carrying HT1, except for that of A1123-10, which had an H_{cr} of 31 mT.

Hysteresis Experiments

I obtained hysteresis parameters after processing the uncorrected hysteresis data by closing the ascending and descending loops when needed, subtracting the high field slope and adjusting such that the y-intercepts are equal (plots and analysis were done using the PmagPy cookbook code, methods discussed in Tauxe et al., 2010). The uncorrected data for all samples displayed loops with strong positive (paramagnetic) high field slopes and potbellied shape. This paramagnetic component dominates the uncorrected data for most samples (dashed lines in the hysteresis curves in Fig. 6A), except for four samples that had an uncorrected shape closer to pseudo-single domain shape: A1210-23 (carrying HT1), A1123-5,10,17 (all carrying HT2). Potbellied behavior can result when the magnetic carriers are a mixture of SD and fine-grained SP magnetite. For samples carrying HT1, the shapes of the corrected hysteresis curves were consistent with those expected for pseudo-single domain grains reaching M_s by ~300 mT (Fig. 6A, right side).

As most samples carrying HT2 were not fully saturated by the maximum field allowed by the VSM, minor hysteresis loops were obtained. The corrected hysteresis curves displayed pseudo-single domain behavior (A1123-10), wasp-waisted (A1123-5, A1123-17, A1210-5), and single domain hematite behavior (A1209-18). The wasp-waisted curves occur when there are multiple fractions of magnetic minerals with strongly contrasting coercivity or presence of significant superparamagnetic component. As already determined from the IRM acquisition experiments, many of the samples carrying HT2 have two populations of ferromagnetic carriers with distinct coercivity ranges.

Saturation magnetization saturation remanence and coercivity, as well as backfield coercivity, were used to construct a Day plot to determine if the magnetic carriers were single domain (SD), MD, pseudo-single domain (PSD), or superparamagnetic (SP) (Fig. 6C). Samples carrying the HT1

component are either in the PSD range or a mixture of SD and MD particles, but there is no real trend in the data along any MD-SD mixing lines. Additionally, some samples carrying the HT1 component lie far to the right, likely indicative of SP-SD mixtures of magnetite grains (Dunlop, 2002). Day plots are not as informative for samples with multiple magnetic minerals, and when considering the samples carrying HT2 and there is no dominant clustering observed.

Thermal Demagnetization of sIRM

The thermal demagnetization of sIRM of samples carrying HT1 displayed a distributed range of unblocking temperatures (T_{ub}) up to 580°C, in some cases with about 70% of the remanence destroyed, followed by a steep drop at (580°C), as expected for magnetite. These data combined with the IRM acquisition curves suggest that HT1 is carried by low coercivity magnetite. In one sample from a dike (A1120-4), there is a minor decay at 100-325°C, followed by a gradual decay to 650°C, indicating a small contribution of pyrrhotite or Ti-rich titanomagnetites as well as hematite. Some magnetization carried by hematite or pyrrhotite is also suggested based on a higher coercivity component in the IRM acquisition curves.

Samples carrying the HT2 direction are observed to have only hematite or both hematite and magnetite as magnetic carriers. I observe a distributed range in unblocking temperatures for the samples with both hematite and magnetite, with steeper drops observed at 560°C, 580°C and 680°C. Sample (A1123-10), which carried a great circle fit towards HT2, displays a drop at both 560°C, as well as at 680°C, consistent with the presence of titanomagnetite and hematite.

AF demagnetization of sIRM

For samples carrying the HT1 component, AF demagnetization of sIRM resulted in the median destructive fields (MDF) of ∼25-35 mT, typical for PSD magnetite. The field at which the demagnetization and acquisition curves cross (the cross-over point Rx) is sensitive to particle interaction. As all

the cross over points for HT1 occur at normalized M_s values $<$0.5 (between 0.3 and 0.4), suggesting a moderate degree of inter-particle interaction. The shape of the AF demagnetization curves is softer than expected for non-interacting SD grains. Additionally, one of the dikes (A1120-4) was not fully demagnetized by 145 mT (the highest AF level available), suggesting the presence of a high coercivity mineral such as pyrrhotite, hematite or goethite. As seen in Fig. 6B, most samples carrying HT2 were not fully demagnetized by 145 mT, which was the AF demagnetization capability of the instrument. Most curves therefore went off the scale and thus a cross-over point was not determined. One sample, A1123-10, had a MDF of 15 mT, with low MDF more consistent with MD-dominant sample, and a cross over point at M/M_s=0.3074, suggesting the presence of negatively interacting SD minerals or MD minerals.

We conclude that the magnetic mineralogy of samples carrying HT1 can be characterized by single low-coercivity population of interacting magnetite that is likely PSD or a mixture of SD and SP states. The magnetic mineralogy of most samples carrying HT2 includes two populations of minerals with distinct ranges of coercivities. Observed unblocking temperatures suggest that the higher coercivity mineral is hematite and the lower coercivity mineral is magnetite. In some cases, the samples carrying HT2 only have high coercivity SD hematite as the magnetic carrier.

2.8 Discussion

2.8.1 Timing of Magnetizations Determined by Fold Tests

As discussed above, while the LT and MT directions are characterized by failed fold tests and the HT2 direction results in an ambiguous fold test; the HT1 direction passes this important confidence criterion. For the HT1 fold test, the most important sections were those of members A and B with dips to the SW near Tango Tarn and Mount Harper, and members D and E with shallow dips to the north near Mount Harper West (Fig. 2C). The difference in paleohorizontal orientation between

these areas is likely related to the synvolcanic Mount Harper synform, which initially developed during extensional activity on the Mount Harper fault and deposition of the Callison Lake Formation. As HT1 passes the fold test, it was likely acquired before the folding involved in the Mount Harper synform and therefore may represent a primary magnetization. It may be confusing that the MHV are characterized by a remanence that pre-dates folding while at the same time the folding was syn-eruptive; however, because the volcanics were likely erupting at the same time as the synform was developing, the primary magnetization was acquired on much shorter timescales (related to the cooling of the lavas), while the synform developed over a longer timescale–this difference in the timing results in a passage of the fold test and a pre-folding primary magnetization. For all of the flows, the magnetization was acquired before it was folded or tilted, and thus the most clustered result for the HT1 direction is when all flows are at around 100% of the untilting, i.e., restored close to paleohorizontal.

The failure of the LT direction fold test suggests that the LT direction postdates any activity on the North Harper fault, which displaces the Bouvette Formation. The failure of the MT fold test suggests that it was likely acquired after the development of the Mount Harper synform and movement on the SSE-striking faults. As the HT2 fold test is ambiguous, it is difficult to interpret the timing of the HT2 overprint.

2.8.2 Discussion of Primary Nature of HT1

Several lines of evidence suggest that the HT1 direction is primary. The HT1 direction passes a fold test defined by the Mount Harper synform, a positive conglomerate test, and also, the presence of a reversed unit adds weight to the conclusion that HT1 is primary. The rock magnetism experiments suggest that HT1 is carried by a single low-coercivity population of interacting magnetite grains that are likely PSD or a mixture of SD and SP states, which is consistent with the expected primary ferromagnetic mineralogy of volcanic rocks. In the few cases where HT1 was carried by hematite,

there is evidence that the basalt flows erupted subaerially, and I suggest that this caused some early alteration and hematization resulting in a practically primary magnetization but carried by hematite.

With respect to secular variation, based on the geochronological constraints, the MHV erupted between ~739-716 Ma (Macdonald et al., 2010; Strauss et al., 2014a), but the eruption duration was likely much shorter than that. Typically, around 5 lava flows are used to characterize paleosecular variations at a site (McElhinny and McFadden, 1997; Johnson and Constable, 1995). Here, my stratigraphic sections vary in thickness, but section A1128 spans around 200 meters and multiple flows with samples carrying the HT1 direction throughout. The time interval represented by a thick section, such as this, is likely >1 Myr and long enough to average out secular variations (McElhinny and Merrill, 1975).

Butler (1992) suggested using the scatter of virtual geomagnetic poles (VGPs) to determine whether secular variation has been averaged out or if there is excess scatter in the data. If secular variation has been adequately sampled, the observed angular dispersion of site-mean VGPs should be consistent with that predicted for the paleolatitude of the sampling sites. Assuming that the last 0-5 Ma records similar field behavior to that in the Neoproterozoic, the observed angular dispersion for 15-38° paleolatitude should be around 12.1-16.46° (Table 4; McElhinny and McFadden, 1997). For my site/flow mean VGPs determined from approach 3, the observed angular dispersion is 7.3°, less than the expected dispersion, suggesting that I may not have successfully averaged out secular variation. However, another method for investigating secular variation is to use confidence envelopes for A_{95} as a measure of secular variation (Deenen et al., 2011). Deenen et al. (2011) investigated values of A_{95}, given N, the number of paleomagnetic sites, and K, the dispersion. Comparing my VGP data (K=71.8, N=7, A_{95}=7.2°) to the A_{95} envelopes of Fig. 3 of Deenen et al. (2011), my data falls in the grey envelope, which indicates that the observed scatter is consistent with adequately averaging secular variation.

My HT1 pole passes six out of the seven reliability criteria of Van der Voo (1990), failing the struc-

tural control and tectonic coherence criterion. Specifically, the primary nature of this direction is supported by a well-determined rock age and sufficient documentation in one site and four sections (Approach 1: 1 site and 4 sections, 60 samples, α_{95},=14.3°, A_{95} =13.8° both $<$ 16°, and a k=29.5 and K=31.6, both $>$ 10; Approach 3: 7 sites, 34 samples α_{95},=7.7°, A_{95} =7.2° both $<$ 16°, and a k=61.8 and K=71.6, both $>$ 10). Additionally, I have applied adequate demagnetization with vector subtraction and benefit from a positive fold test, a positive conglomerate test, presence of reversals, and no resemblance to younger paleopoles.

When considering the key pole criteria of Buchan (2014), HT1 is related to a robust age, the primary remanence is properly isolated, and secular variation may have been averaged out. With regard to the Buchan (2014) field tests that constrain the magnetism to be primary, my fold test just establishes the relative timing of the magnetization. Although my conglomerate test is on the younger sediments of the Eagle Creek formation, the matrix in that conglomerate does carry HT1, so that indicates that the test itself still constrains the magnetization as a intraformational (MHV combined with Eagle Creek formation) conglomerate test on HT1.

2.8.3 Interpretations of Directions and Comparison to the Laurentian Apparent Polar Wander Path

Four paleomagnetic poles were distinguished in this study: a low-temperature (LT), mid-temperature (MT), and two high-temperature poles (HT1-primary and HT2-chemical overprint), (Table 1 and Fig. 7). These poles are plotted along with the Laurentian apparent polar wander path (APWP) from 510 Ma to the present (Torsvik et al., 2012), for 200 Ma to the present (Besse and Courtillot, 2002), and for 230-50 Ma (Kent and Irving, 2010), along with a schematic pole envelope that encompasses Cryogenian-Ediacaran poles from Laurentia (Park, 1995; 1997; Mitchell et al., 2011 and references therein), and the pole for the coeval Franklin LIP. For the Franklin LIP pole I used the autochthon-only mean pole (D+09can) from Denyszyn et al., (2009a), which overlaps with the

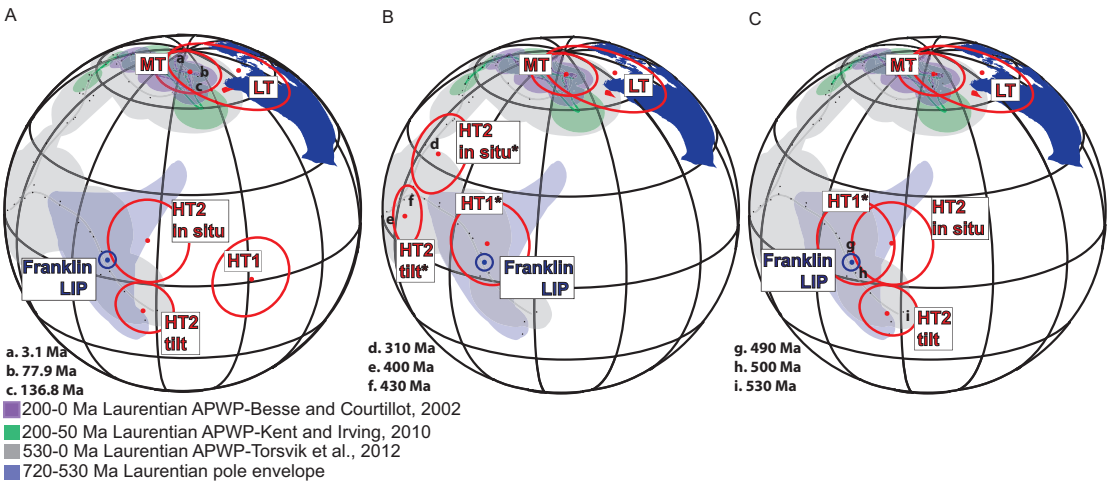


Figure 2.7: Paleomagnetic poles from this study (red, with the circle identifying the circle of A_{95} confidence). In blue is the Franklin LIP pole is the D+90can pole of Denyszyn et al. (2009a), with the circle identifying the circle of A_{95} confidence. The 200 Ma to present APWP is from Besse and Courtillot (2002), the 230-50 Ma APWP is from Kent and Irving (2010), the 530 Ma to present Laurentian APWP is from Torsvik et al. (2012), and the 720-530 Ma Laurentian Pole envelope is from data of Park (1995; 1997), and compiled by Mitchell et al. (2011). A. Poles in current positions. B. Poles plotted with expected locations if the rotation occurred between the Carboniferous-Cretaceous, after the HT2 overprint was acquired but before the MT and LT overprints. C. Poles plotted with expected location if the rotation occurred in the Cryogenian-Ediacaran, before the HT2, MT and LT overprints were acquired. The asterisks indicate a pole in a restored (pre-rotation) position and the lower case letters indicate poles of particular times of interest (a ,b, c from Besse and Courtillot, 2002, APWP, and d, e, f, g, h, i from Torsvik et al., 2012, APWP).

older mean pole of Buchan et al. (2000).

This primary pole (HT1) is located at similar longitudes as the HTA pole of Park et al. (1992), but the errors associated with the pole have been improved and the latitude has been refined. My paleomagnetic data from the coeval Neoproterozoic MHV (HT1 this study) and Franklin LIP (Denyszyn et al., 2009a) are different: the HT1 pole longitude is about 50° east of what is expected based on the Franklin pole (Fig. 7A). There are at least three options for explaining this difference: 1) secular variation of the geomagnetic field, specifically a 50° excursion during the eruption of the MHV; 2) rapid oscillatory motion of Laurentia that could be due to either plate motion or True Polar Wander (TPW); or 3) a counterclockwise tectonic block rotation relative to Laurentia subsequent to the eruption and emplacement of the MHV.

TABLE 1. PALEOMAGNETIC DIRECTIONS AND POLES

	In situ directions				Tilt corrected directions				Paleomagnetic Poles[†]				MHV paleo-latitude
Component	Declination/ Inclination (°)	k	N[*]	α_{95} (°)	Declination/ Inclination (°)	k	N[*]	α_{95} (°)	Latitude/ Longitude (°N/°E)	A_{95} (°)	N	K	(°)
LT	54.0/80.9	1886.5	2	5.8	209.2/69.7	21.6	2	56.6	69.6/265[§]	10.8	2	533.83	NA[###]
MT	161.7/-82.1	89.6	8	5.9	49.1/-65.4	9.5	8	20.1	77.7/197.4[§]	10.4	8	29.4	NA[***]
HT2	52.2/-50.3	62.3	4	11.7	45.8/-15.3	39.0	4	14.9	14.5/176.0[§]	13.4	4	49.8	NA[***]
									-9.8/174.3[#]	9.8	4	88.1	NA[***]
HT1	179.1/58.1	6.9	5	31.3	190.0/42.1	29.5	5	14.3	0.4/210.7[#]	13.8	5	31.6	24.3
Approach 1													
HT1	174.9/48.3	18.1	7	14.6	182.4/44.4	61.8	7	7.7	1.4/218.1[#]	7.2	7	71.6	26.1
Approach 3													
70 Ma[**]	NA[***]	NA[***]	NA[***]	NA[***]	NA[***]	NA[***]	NA[***]	NA[***]	75.9/204.7	4.6	7	169.8	NA[***]
77.9 Ma[††]	NA[***]	NA[***]	NA[***]	NA[***]	NA[***]	NA[***]	NA[***]	NA[***]	74.7/207.4	5.9	14	47.2	NA[***]
80 Ma[§§]	NA[***]	NA[***]	NA[***]	NA[***]	NA[***]	NA[***]	NA[***]	NA[***]	74.5/201.3	7.9	7	ND[†††]	NA[***]
Franklin LIP[###]	NA[***]	NA[***]	NA[***]	NA[***]	243.2/35.0	NA[***]	NA[***]	NA[***]	6.7/162.1	3.00	26	ND[†††]	19.3

[*]N—number of sites and/or sections
[†]Poles calculated as means from site/section poles for the Mount Harper Volcanics (64.7°N, 139.9°W) with HT1 directions from site A1207 reversed and only the matrix HT1 directions from site A1126
[§]Calculated from the in situ direction
[#]Calculated from the tilt corrected direction
[**]Pole from Kent and Irving, 2010
[††]Pole from Besse and Courtillot, 2002
[§§]Pole from Torsvik et al., 2012
[###]D+09can pole from Denyszyn et al., 2009
[***]NA= not applicable
[†††]ND= no data

Anomalous directions dissimilar from the Franklin pole were previously recovered from Borden dikes on Baffin island (Christie and Fahrig, 1983; Pehrsson and Buchan, 1999), and dikes on Ellesmere and Devon islands (Denyszyn et al., 2009a, Denyszyn et al., 2009b), as well as from the Rapitan Group in the Mackenzie Mountains (Park, 1997; Morris, 1977). Initially, the northwest trending Borden dikes were thought to be part of a much older event, due to an older ca 950 Ma age, cross-cutting relationships, and a steep paleomagnetic direction (Christie and Fahrig, 1983). Reevaluation of these dikes by Pehrsson and Buchan (1999) updated the age to Franklin times (ca 720 Ma) and suggested that the steep magnetizations resulted from the superposition of a Cretaceous–Tertiary aged chemical remanent magnetization on normal and reversed primary Franklin components. The anomalous paleomagnetic results from the Franklin-affiliated dikes on Ellesmere and Devon islands were shown to be due to chemical remagnetization (Denyszyn et al., 2009b). In contrast, at Mt. Harper I have documented a double reversal, presence of the HT1 direction throughout the MHV complex, and a robust single domain magnetite carrier, all suggestive of a primary magnetization. Moreover, calculation of the secular variation captured in the stratigraphic sections suggests that I

have adequately sampled for secular variation.

Rapid TPW could involve up to 90° rotation of the crust and mantle relative to the spin axis due to changes in the Earth's moment of inertia (e.g., Kirschvink et al., 1997). As paleomagnetic studies assume plate tectonic speeds have remained relatively constant through time, observations of large, rapid (>20 cm/yr) continental movements, particularly in the Neoproterozoic, have been attributed instead to TPW (Kirschvink et al., 1997; Li et al., 2004; Maloof et al., 2006). For example, it has been suggested that a rising superplume centered under Rodinia initiated a Neoproterozoic TPW event (800 Ma-750 Ma) as well as the breakup of Rodinia (Li et al., 2004). As noted above, the MHV are coeval with the Franklin LIP and no regular trend in the paleomagnetic data was observed stratigraphically through the MHV members. These observations suggest that it is unlikely that the rotation was caused by rapid TPW, and thus I consider the third possibility: that the rotation was due to a counterclockwise tectonic block rotation subsequent to the eruption and emplacement of the MHV and the Franklin LIP. The HT1 pole can be restored to its original position aligned with the Franklin LIP by rotating the MHV ~50° clockwise (Figs. 7B and 7C).

As for the HT2 direction, rock magnetic results and unblocking temperatures suggest that hematite is its main magnetic carrier. As high temperatures were needed to thermally demagnetize this component (680°C for many samples), this requires a very high metamorphic temperature in order to have a thermoviscous origin; therefore, I interpret this result as being a chemical remanent magnetization (CRM). CRM is acquired as a magnetic mineral nucleates and grows through a critical volume at which its magnetic direction becomes stable with respect to thermal fluctuations (Stokking and Tauxe, 1990). This can occur during mineral alteration (e.g., oxidation of magnetite to hematite) or mineral precipitation (grain growth or crystallization), which may accompany weathering, diagenesis, or low-grade metamorphism (Stokking and Tauxe, 1990). CRM remagnetization overprints via secondary precipitation/growth of hematite or conversion to hematite are generally a result of large-scale fluid flow during orogenesis (Miller and Kent, 1988), pronounced hydrother-

mal events (Witte and Kent, 1991), hydrothermal systems circulating in permeable rocks below basalts (Wynne et al., 1998), or migration of fluids along fractures and unconformities during uplift-enhanced surface meteoric fluid circulation (Geissman and Harlan, 2002; Preeden et al., 2009).

As the HT2 direction results in an ambiguous fold test, both the in situ and tilt corrected poles are plotted (Fig. 7). The HT2 pole overlaps with other Laurentian paleomagnetic poles in both pre-rotation and post-rotation positions (Figs. 7B and 7C). If the rotation occurred after HT2 was acquired (Fig. 7B), then after restoring the HT1 pole to align with the Franklin pole, the HT2 direction is similar to Carboniferous (HT2 in situ) and Silurian-Devonian poles (HT2 tilt) of the Laurentian APWP (Torsvik et al., 2012). Alternatively, if the rotation occurred before HT2 was acquired (Fig. 7C), the HT2 pole is similar to the Cryogenian to Ediacaran poles and later 500-490 Ma poles (HT2 in situ) and 530-500 Ma poles (HT2 tilt). At intermediate restoration times, the HT2 in situ pole bears similarity to Laurentian Cambrian-Ordovician poles.

Throughout the northern Cordillera, there are several periods of orogenic, hydrothermal and igneous activity that could have induced hematization that facilitated the acquisition of the HT2 overprint. These events could include Ordovician–Mississippian mineralization events that resulted in localized SEDEX or VMS deposits (the late Devonian thermal event, the Howard's Pass deposits, Tom and Jason deposits), as well as the Cambrian-late Ordovician Selwyn basin volcanism and the Neoproterozoic hematization events (e.g., Morrow, et al., 1990; Goodfellow et al., 1995; Park, 1997; Martel et al., 2011; Ootes et al., 2013; and references therein). Of these, the Neoproterozoic hematization events have produced documented paleomagnetic overprints (Park, 1997), while the effect of the other events on paleomagnetic data is currently unclear. Thus, the most straightforward explanation is that HT2 direction is Neoproterozoic to early Paleozoic in age and post-dates the rotation.

The MT direction unblocks around 450°C, and given the usual temperatures for greenschist facies metamorphism, this direction is likely a thermo-viscous remanent magnetization (TVRM) due to regional metamorphism associated with the Cordilleran Orogeny. In the Yukon, this meta-

morphism is broadly constrained to be Late Jurassic to Cretaceous in age, with widespread mid-Cretaceous metamorphism along with intrusions of granitic rocks (Greenwood et al., 1991; McMechan et al., 1992; Tempelman-Kluit et al., 1992; Murphy, 1997). In the Ogilvie Mountains and Selwyn basin, the youngest deformed strata observed are dominantly Late Cretaceous, and intrusions of the mid-Cretaceous Selwyn plutonic suites are large with minimal post-emplacement deformation (Yorath, 1992; McMechan et al., 1992). However, deformation did continue later, as suggested by folded Paleocene-Eocene stratigraphy in the northern Ogilvie and Wernecke Mountains. When considering whether the MT pole was acquired before or after a rotation, I have compared my MT section-mean poles to those predicted from the APWPs of Torsvik et al. (2012), Besse and Courtillot (2002), and Kent and Irving (2010). Specifically, I focused the comparison on those Mesozoic poles furthest east and most likely to be similar to the rotated MT pole (Table 1). I applied Watson's V statistic test for a common mean (Watson, 1983; Tauxe et al., 2010). For each APWP pole, the MT direction passes the test for a common mean if it was acquired after the rotation, but fails the test for a common mean if it was acquired before the rotation(supplementary Table S6). Statistically, the MT pole is similar to poles ranging from 136.8–3.0 Ma in age, but as I suggest that it is an overprint acquired during the Cordilleran orogeny, that constrains it to be likely older than the Late Cretaceous. Additionally, as my MT direction has a reversed polarity, it cannot have been obtained during the Cretaceous Normal Polarity Superchron (120.6–83.0 Ma) (Gee and Kent, 2007). Thus, the MT pole is due to greenschist metamorphism acquired either between 136.8-120.6 Ma, or after 83.0 Ma but before the end of Cordilleran metamorphism, and the large-scale rotation was completed by this time. Finally, the LT pole is similar to the present day field, and given its low unblocking temperature, it is likely a recent viscous remanent magnetization (VRM).

2.8.4 Geological Context of Rotation

The paleomagnetic data presented here suggests that the MHV rotated relative to the Laurentian craton sometime after the eruption of the MHV (Neoproterozoic) and before the acquisition of the MT overprint (Mesozoic). There are several possible scenarios for the scale of this rotation: 1) local block rotation of the MHV complex, 2) regional rotation of the Coal Creek inlier, and 3) a greater rotation of the Yukon Block relative to the Laurentian craton. As suggested initially by Roots (1987), the MHV and accompanying SSE-striking faults may have been rotated counterclockwise (CCW) between the North and South Harper faults during regional transtension (Fig. 2); however, the observed angles between SSE-striking faults and the North and South Harper faults, suggest that only 20° of rotation can be explained by this mechanism, and therefore it is unlikely that a 50° rotation could be accommodated locally. It is possible that the tectonic rotation involved just the greater Coal Creek inlier, but regional geological data (Eisbacher, 1981; Aitken and McMechan, 1992; Abbott, 1996) support wholesale motion between the Yukon Block and autochthonous Laurentia. Additionally, there are two scenarios for the timing of the rotation: 1) the rotation occurred between the Carboniferous-Cretaceous, after the HT2 overprint was acquired but before the MT overprint, and 2) the rotation occurred in the Cryogenian-Ediacaran, before the HT2 overprint was acquired.

Geological and Geophysical constraints on rotation of the Yukon Block

The restoration of the Yukon Block to a pre-rotation position results in alignment of the correlative Bear River dikes (e.g., Schwab et al., 2004) and Mackenzie dike swarm (LeCheminant and Heaman, 1989; Thorkelson et al., 2005), as well as paleocurrent orientations in the correlative Wernecke and Hornby Bay-Dismal Lakes groups (Aitken and McMechan, 1992). This tectonic rotation also explains the profound differences in Neoproterozoic facies belts and stratigraphy across the Snake River fault between the Wernecke Mountains and the Mackenzie Mountains (Eisbacher, 1981; Eis-

bacher, 1983; Aitken and McMechan, 1992; Abbot, 1996; Thorkelson, 2000). More specifically, distinct strata of the extensive Mackenzie Mountains Supergroup are abruptly truncated at the Snake River fault and are in part represented by strikingly different strata of the Pinguicula, Hematite Creek and Fifteenmile groups to the west in Yukon (Eisbacher, 1981; Thorkelson et al., 2005; Turner, 2011; Macdonald et al., 2012). The Windermere Supergroup also shows dramatic facies change across the Snake River fault (Eisbacher, 1981, Gabrielse and Campbell, 1992; Macdonald et al., 2013). Therefore, geologic evidence suggests that large-scale tectonic displacement may have fortuitously juxtaposed the Proterozoic strata of the Wernecke inlier adjacent to cogenetic but not originally contiguous strata of the northern Mackenzie Mountains.

Any displacement or rotation inferred from the MHV paleomagnetic data should be matched by the orientation of regional basement trends; however, the crystalline basement is not exposed in Yukon. Previous workers have used aeromagnetic data to elucidate the extent of the basement (e.g., Norris and Dyke, 1997; Aspler et al., 2003; Crawford et al., 2010; see cross-hatched area, Fig. 1). The greater Mackenzie region is dominated by a large positive curvilinear magnetic anomaly called the Fort Simpson anomaly to the south, and the Mackenzie River anomaly in the north (Aspler et al., 2003; Cook et al., 2005; Pilkington and Saltus, 2009; Crawford et al., 2010). Although it is possible that the Mackenzie River/Fort Simpson anomaly reflects continuous crystalline basement into the Yukon Block, it cannot be demonstrated that it represents a single tectonic entity along its entire length (Brunstein, 2002; Aspler et al., 2003; Cook et al., 2005). In fact, a recent aeromagnetic study of the Wernecke inlier suggests that the present geometry of the Mackenzie River anomaly is partially offset between the Yukon Block and the rest of the craton with about 100 km of sinistral displacement (Crawford et al., 2010).

Carboniferous-Cretaceous rotation, after HT2 overprint but before MT overprint

If the rotation occurred after the HT2 overprint but before the MT overprint, it could be linked to the putative Jurassic-Cretaceous opening of the Canada basin, in which it has been proposed that the Arctic Alaska terrane rotated ~66 degrees counterclockwise about a pole within the Mackenzie Delta region (Halgedahl and Jarrard, 1987). Despite the apparent similarity of this proposed large counterclockwise rotation, there are inconsistencies in kinematic models for the opening of the Canada basin (e.g., Lane, 1997). Furthermore, more recent models for the opening of the Canada Basin suggest a multi-phase extensional and rotational history involving a number of smaller tectonic blocks (e.g., Miller et al., 2008; Shephard et al., 2013) or strike-slip motion along the Arctic margin of Canada. Additionally, the collective rotation of Arctic Alaska plus the entire Yukon Block is inconsistent with the geometry of structures within northern Yukon (Norris, 1997).

Alternatively, a Mesozoic rotation could be consistent with a potential rotation related to the Ogilvie deflection (Johnston, 2008). The Ogilvie deflection refers to the 90° change in orientation of the boundary between basinal shales (Medial Basin) and platform facies (Ogilvie or Yukon Platform) as well as a change in the strike of the Cordilleran fold-thrust belt, from east-west trending to a north-south orientation in westernmost Yukon (Norris, 1972; Johnston, 2008). If the Ogilvie deflection is original, then the Cretaceous propagation of thrust sheets continuously around a preexisting bend should have resulted in strike-parallel contraction within the hinge region, which is not observed. Additionally, palinspastic restoration of the Mesozoic thrust sheets results in a ~10,000 km "hole" which has been argued as evidence of Cretaceous bending about a vertical axis of rotation of an originally more linear fold and thrust belt (Johnston, 2008). If this Cretaceous bending occurred and was involved in my rotation, the scenario requires that HT2 be related to a Silurian-Carboniferous fluid-flow hematization event capable of resulting in a paleomagnetic overprint and

that the creation of the Ogilvie deflection occurred before MT overprint was acquired.

Cryogenian-Ediacaran rotation, before HT2 overprint

Although a Mesozoic rotation of the Yukon Block is permissible, previous studies have concluded that the Cambrian-Devonian paleogeographic features are regionally continuous between the Yukon Block and North America to the east (Cecile, 1984). Despite deformation along the southern segments of the Richardson fault array, Paleozoic strata such as the mid-Cambrian Slats Creek Formation persist across the fault array with only right-lateral displacement on the order of 10 to 20 km (Fritz, 1972; Cecile, 1984; Morrow, 1999). By the late Cambrian, the Bouvette Formation was deposited across the entire Yukon Block and its equivalents are present on the Mackenzie-Peel shelf. In contrast, Proterozoic strata show large discontinuities across the Richardson fault array (e.g. Abbot, 1996). Below I discuss three intervals of tectonic activity that are post-MHV eruption and pre-Bouvette Formation deposition and could signal the development of this tectonic rotation. This rotation could have been accommodated along a structure or structures between the Yukon block and Mackenzie Mountains.

The first episode, the Cryogenian Hayhook extensional event (Young et al., 1979; Jefferson and Parrish, 1989), was marked by block faulting, uplift, and basinal subsidence during deposition of the lower Windermere Supergroup (Young et al., 1979; Eisbacher, 1981; Jefferson and Parrish, 1989). North-trending normal faults controlled the facies patterns and depositional outline of the basal Windermere Supergroup (pre- to syn-Sayunei Formation of the Rapitan Group) (Young et al., 1979; Eisbacher, 1978; 1981; 1985; Jefferson and Parrish, 1989; Norris, 1997). The NNE-trending faults also control the proximal to transitional facies of the Rapitan Group (Eisbacher, 1981; Eisbacher, 1985), and although many of the faults are inferred from thickness and facies patterns, some of the synsedimentary paleofault scarps are observed with distinct stratigraphic offsets and associated alluvial fan conglomerates (Eisbacher, 1981; Jefferson and Parrish, 1989).

The Hayhook event faults are also associated with tight folds beneath a prominent angular unconformity; for example, in the Nite Creek area (Fig. 1), folds in the Coppercap and Sayunei formations that are overturned to the west are overlain by flat-lying Shezal Formation glacial deposits (Helmstaedt et al., 1979; Eisbacher, 1981; Yeo, 1984). Further south, in the Thundercloud Range (Fig. 1), a large faulted and overturned anticline-syncline pair underlies an undeformed section of the Shezal Formation (Jefferson and Parrish, 1989). The north-trending tight folds and unconformities are interpreted to represent regional transpressional contraction during the deposition of the Sayunei Formation, followed by an intra-Sayunei unconformity (Helmstaedt et al., 1979; Eisbacher, 1981; Yeo, 1984). In the Wernecke inlier, Thorkelson (2000) observed east-trending normal faults of the Hayhook extensional event that crosscut older, west-verging thrust faults and folds in Sequence B rocks, suggesting that the compressional folds represent an earlier event referred to as the Corn Creek orogeny (1.00–0.78 Ga from Thorkelson et al., 2005). The Corn Creek structures fold the ca. 850-780 Ma Mackenzie Mountains Supergroup (Eisbacher, 1981; Jefferson and Parrish 1989) and are sealed by ca. 660–635 Ma strata (Mount Profeit dolostone of Eisbacher, 1981; Macdonald et al., 2013; Rooney et al., 2014; 2015). Thus, the Corn Creek structures likely formed between ca. 780–635 Ma and could represent transpressional activity related to motion along the Snake River fault. The syn-Rapitan Hayhook extensional event likely reached its peak shortly after the emplacement of the ca. 717 Ma MHV (Jefferson and Parrish, 1989).

Following the Hayhook extensional event, the next possible time that the Yukon Block could have rotated is during the deposition of units overlying the Rapitan Group in the upper Windermere Supergroup, such as the Keele and Ice Brook formations, and the equivalent Mount Profeit dolostone (Eisbacher, 1981; Aitken, 1991a). Near the Snake River fault in the Wernecke Mountains, sedimentary facies of the Hay Creek Group dramatically change from the massive Mount Profeit dolostone to carbonate olistoliths encased in shale and sandstone turbidites (Eisbacher, 1981; Thorkelson, 2000). The olistolith-bearing succession is overlain by a thick package of siliciclastic

turbidites (Eisbacher, 1981). Eisbacher (1981) related these dramatic facies changes to synsedimentary tectonism along the Snake River fault zone. A similar pattern is seen west of the Plateau Thrust in the central Mackenzie Mountains where platformal carbonates of the Keele Formation "breakaway" into olistoliths and overlying turbidites of the Durkan and Delthore members of the Ice Brook Formation (Aitken, 1991a; Aitken, 1991b). The Durkan and Delthore members of the Ice Brook Formation are locally overlain by glacial diamictite of the Stelfox Member (Aitken, 1991a; Aitken, 1991b) along with the overlying carbonate of the Ediacaran Ravensthroat formation, which are correlative with the Marinoan glaciation and associated cap carbonates, respectively (Young, 1995; James et al., 2001). This correlation suggests that any tectonic activity associated with the dramatic facies changes must have been initiated after 662.4 $\pm$ 3.9 Ma (base of the Twitya; Rooney et al., 2014) and completed by the deposition of the 632.6 $\pm$ 6.3 Ma Sheepbed Formation (Rooney et al., 2015).

Finally, the rotation could have occurred during the deposition of the Ediacaran to early Cambrian informal "Upper" group (divided into four major depositional sequences that include the following formations and informal units: Sheepbed, Sheepbed carbonate, June beds, Gametrail, Blueflower, and Risky) and Backbone Ranges Formation, specifically during deposition of the June beds (Aitken, 1989; Dalrymple and Narbonne, 1996; MacNaughton et al., 2000; Pyle et al., 2004; MacNaughton et al., 2008; Macdonald et al., 2013). Previously, June bed strata were interpreted as Sheepbed-equivalent slope deposits characterized by debris flows and turbidites (Dalrymple and Narbonne, 1996); however, the abrupt appearance of poorly-sorted and coarse-grained sandstone and conglomerate units within the lower June beds, as well as the regional documentation of rapid facies changes from NE to SW in the central Mackenzie Mountains and the Wernecke Mountains suggest synsedimentary tectonism during "Upper" group sedimentation (Macdonald et al., 2013; Moynihan, 2014). Ediacaran fossils in the June beds can be correlated globally with the ca. 580–560 Ma Avalon assemblage (Narbonne and Aitken, 1990; Narbonne, 1994; Gehling et al., 2000; Nar-

bonne and Gehling, 2003; Narbonne et al., 2012). This ca. 580-560 Ma age for the June beds would place the possible syn-tectonic event coincident with the ca. 570 Ma syn-rift volcanics preserved in the southern Canadian Cordillera (Colpron et al., 2002) and with thermal subsidence models (e.g., Bond and Kominz, 1984) that indicate latest Ediacaran rifting on the western margin of Laurentia.

2.8.5 Neoproterozoic Paleogeographic Implications

This rotation has implications for the interpretation of the Neoproterozoic stratigraphy and structures in the Coal Creek inlier and their bearing on the breakup of Rodinia. In its present position, with the assumption that the Yukon Block has not rotated, the pre-811 Ma WSW-ENE structures in the Fifteenmile Group suggest north-directed extension on the northern margin of Laurentia (Macdonald et al., 2012). Additionally, syn-Windermere extensional structures involve a 120° bend in orientation from the Mackenzie Mountains to the Coal Creek inlier, with SW-oriented extension in Mackenzie Mountains and N-directed extension in Yukon. With the rotation, pre-811 Ma WSW–ENE structures in the Fifteenmile Group rotate roughly parallel to the strike of the Mackenzie Arc (Aitken and Long, 1978) and could be related to E-W directed extension of an aulacogen related to the deposition of the Mackenzie Mountain Supergroup to the east. Restoration of the Yukon Block to its pre-rotation position also aligns extensional structures of the Coal Creek and Hart River inliers with those of the NW Mackenzie Mountains, as well as connecting Mount Harper Group embayments to asymmetrical extensional half-grabens in the Coates Lake Group of the Mackenzie Mountains (Strauss et al., 2015).

Here, I integrate my data from Laurentia into a recent model of Rodinia put forth by Li et al. (2013). My preferred model of counterclockwise rotation of the Yukon Block with respect to Laurentia is consistent with Neoproterozoic Laurentian tectonic events divided into three main phases. First, prior to this putative rotation, a NNW trending (present day coordinates) failed rift developed during early Neoproterozoic extension along the northern margin of Laurentia (Aitken, 1981;

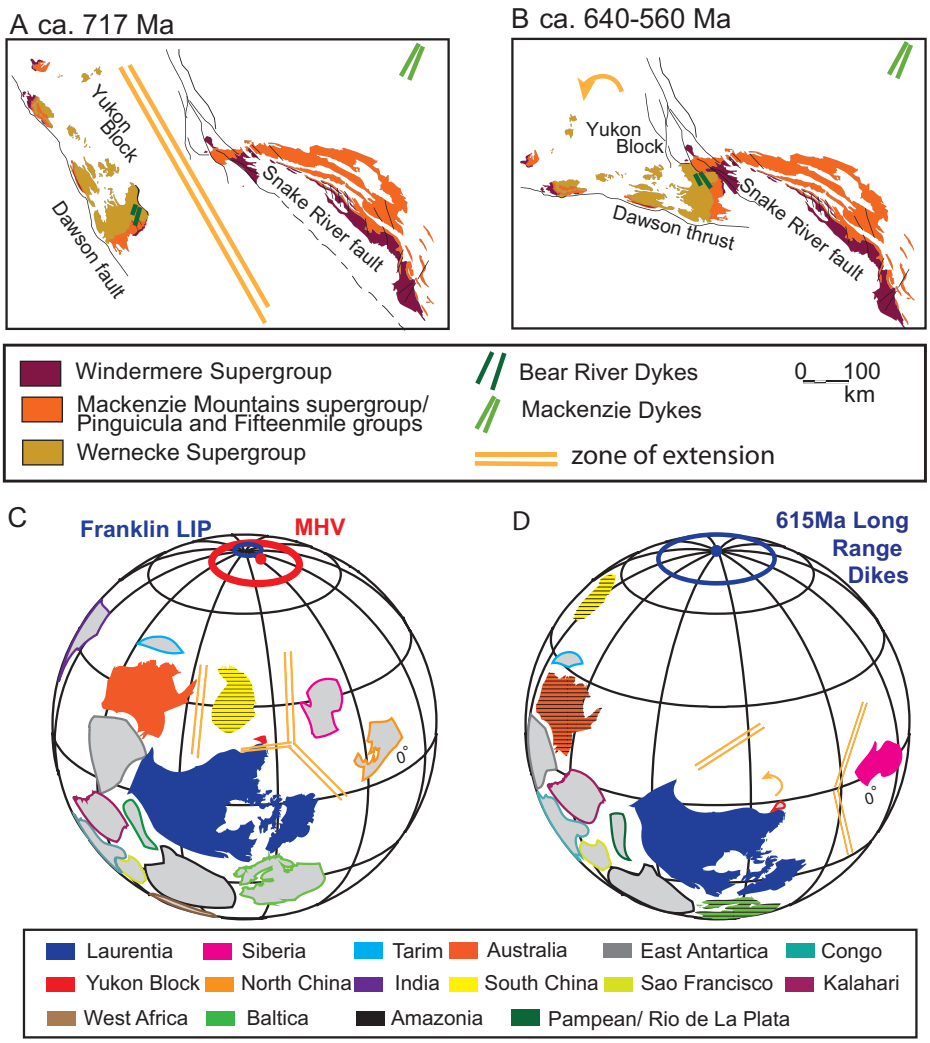


Figure 2.8: Top: change in orientation with time of the Proterozoic inliers, black boxes match the extent of the Fig. 1 map of northwest Canada with Proterozoic inliers. The orientation of the Bear River dikes in the Wernecke inlier and the correlative Mackenzie dike swarm on the Laurentian craton are represented with green lines in their approximate geographic location and orientation. A. The Yukon Block restored to its position prior to tectonic rotation. B. The Yukon Block in its present-day position. Bottom: paleogeographic reconstructions that incorporate the tectonic block rotation of the Yukon Block into the context of the rifting of Rodinia. The reconstructions are modified slightly from those Li et al. (2013). The pole for the Long Range dikes is from Buchan (2014). Brightly colored continents are those with paleomagnetic data within 5 Ma of the reconstructed time. Continents overlain with horizontal lines are those with paleomagnetic data within 30 Ma of the reconstructed time. Continents in grey with colored outlines lack paleomagnetic data within 30 Ma to support any reconstruction for that time. Steps in the reconstruction: C. Following the development of an aulacogen and rifting on the northern margin, the MHV and Franklin LIP erupt ca. 717 Ma. D. The Yukon Block rotates CCW relative to Laurentia. Subsequently, Ediacaran rifting commences on the western margin of Laurentia.

Macdonald et al., 2012). With this failed rift, the pre-811 Ma WSW- and ENE-oriented structures in the Fifteenmile Group of the Coal Creek inlier could represent conjugate structures to the extensional structures in the Mackenzie Mountain Supergroup, rather than orthogonal extension on the NW margin of Laurentia (e.g., Turner and Long, 2008). During the second phase, syn-Windermere extension resulted in opposing asymmetrical extensional half-grabens in the Coal Creek inlier and the Mackenzie Mountains (Figs. 8A and 8C) with the eruption of the Mount Harper volcanics coincident with the emplacement of the Franklin LIP. Syn-magmatic extension associated with the Franklin LIP could have been related to rifting on the northern margin of Laurentia (Pisarevsky et al., 2013; Rainbird, 1993).

The development of smaller extensional structures (e.g., the N-S trending Mount Harper fault) orthogonal to larger, margin-scale rifting is a common feature during opening of ocean basins such as in Africa during the opening of the South Atlantic, in which rifting along the future continental margins was accompanied by activity in basins trending orthogonal to that dominant rift expression (Maurin and Guiraud, 1990; Guiraud and Maurin, 1992). Finally, I suggest that the Yukon Block rotated counterclockwise during either one or more of the following events: the Cryogenian Hayhook event, deposition of the Cryogenian Keele and Ice Brook formations and equivalent Mount Profeit dolostone, or the Ediacaran to early Cambrian deposition of the informal "Upper" group and Backbone Ranges Formation (Figs. 8B and 8D).

It is possible that, in addition to this rotation, the Yukon Block may have experienced large-scale translation relative to stable Laurentia, potentially localized along the Snake River fault. Although the folding and unconformities in the Wernecke and Mackenzie Mountains have previously been interpreted to represent regional transpression during the deposition of the Sayunei formation (Helmstedt et al., 1979; Eisbacher, 1981), there are few constraints on the nature of lateral displacements. If the counterclockwise rotation was coincident with a translation, it would have occurred within a sinistral strike slip system. Eisbacher (1983) initially proposed sinistral displacement between the

Yukon Block and Laurentia, although he suggested a Devonian age for the displacement that was later called into question based on geological grounds by Cecile (1984). An analogous tectonic rotation would be the >60° clockwise rotation of the Transverse Ranges of southwestern US during early development of the San Andreas fault system (Jackson and Molnar, 1990). In addition, some amount of sinistral translation seems consistent with displacements observed in the aeromagnetic data (Pilkington and Saltus, 2009; Crawford et al., 2010).

2.8.6 Low Latitude Glaciation

The Snowball Earth hypothesis suggests that Neoproterozoic glaciations were global and synchronous at low latitudes (Hoffman et al., 1998; Hoffman and Schrag, 2002). The geochronological correlation between the MHV and the Franklin LIP suggest that the glaciogenic Rapitan Group equivalent in the Coal Creek inlier was deposited at low latitudes (Macdonald et al., 2010) and is used to argue for the highest reliability evidence for the low latitude nature of the Sturtian glaciation (Evans and Raub, 2011). However, the paleolatitude predicted for the MHV from the Franklin LIP paleomagnetic data (21° ± 3°, Evans and Raub, 2011, or 19.3± 3° using the D+90can pole of Denyszyn et al., 2009a) was higher than the previous estimates of paleolatitude for the Sturtian glaciation (Park, 1997; Evans, 2000; Evans and Raub, 2011). The paleomagnetic poles from the Rapitan Group (Morris, 1977; Park, 1997) suggest very low latitude (6° ± 4° and 4° ± 6°) glaciogenic sedimentation; however, it is uncertain if these poles are primary (e.g., Evans, 2000). As the MHV interfinger with glaciogenic Sturtian deposits, this paleomagnetic data is well suited to better understand the low latitude nature of these deposits. The paleomagnetic data from the previous study of the MHV results in very low paleolatitudes of 3° ± 12° (Park et al., 1992) and substantial overlap between the Yukon Block and Laurentia. Using my HT1 pole, the MHV restores to a paleolatitude of 24.3° ± 13.8°. This is consistent with the interpretation that the age from member D of the MHVC provides a maximum age constraint on the low-latitude Sturtian glaciation and the MHV-Rapitan Group

equivalent sequence provides a unique exposure that captures the transition into glacial conditions of the Sturtian glaciation, after which ice advanced extremely rapidly to the equator. Here, I provide a paleolatitude for volcanics that were emplaced immediately before and during deposition of the Rapitan Group that indicates low latitude (<30°) ca. 717 Ma Sturtian glaciation.

2.9 Conclusions

We confirm the presence of a Mount Harper volcanics (MHV) pole 50° away from the expected 721-712 Ma Laurentian Franklin pole of Denyszyn et al. (2009a). The paleomagnetic direction identified and used to create the reconstructions presented here does have some issues, most notably that the HT1 direction is not ubiquitous in the MHV, but is based on data from five sections. Additionally, I suggest that I have captured secular variation in my primary pole, although I lack definitive evidence. Despite these limitations, the primary nature of this paleomagnetic direction is supported by six of the seven Van der Voo (1990) reliability criteria. Finally, I acknowledge that the paleomagnetic data does not provide firm constraints on the timing of the rotation, only that the rotation occurred after the eruption of the MHV and before the MT overprint was acquired. Although a Mesozoic rotation of the Yukon Block is permissible, the abundance of potential overprint events in the Neoproterozoic and Cambrian compared to the later Paleozoic suggest that the rotation occurred during the early Cambrian or Neoproterozoic. I explain the paleomagnetic data via the following sequence of events. First, the MHV erupted and two reversals were captured during volcanism. Syn-volcanic normal displacement along the Mount Harper fault resulted the development of the Mount Harper synform. Although volcanism and the development of the synform were occurring at the same time, the magnetization was acquired on much shorter timescales, resulting in a passage of the fold test and a pre-folding, syn-volcanic, primary magnetization for HT1. Second, the Yukon Block and the MHV rotated 50° counterclockwise relative to autochthonous Laurentia. Regional geological con-

siderations suggest this rotation may have been Cryogenian to early Paleozoic in age. Either before or after this rotation, fluid flow and hematization events resulted in the HT2 chemical overprint. Next, during the Cordilleran orogeny, Cretaceous greenschist metamorphism imparted the MT thermal overprint. Finally the recently acquired LT VRM overprint records the present day geomagnetic field.

Northwest Laurentia records the complex breakup of Rodinia. Vertical axis tectonic block rotations can complicate interpretations of this geological history; however, identifying and restoring those rotations may also provide insight into earlier tectonics. With the rotation presented herein, the WSW–ENE structures of the early Neoproterozoic basin forming events (Sequence B of Young et al., 1979) on the Yukon Block represent the conjugate margin of a extensional system formed opposite of the Mackenzie Mountain Supergroup basin, rather than extension on the NW margin of Laurentia. In addition, the HT1 pole from the MHV is a low-latitude pole from volcanic units that interfinger with deposits from the Sturtian glaciation, thus adding more evidence in favor of a global snowball Earth event at ca. 717 Ma.

3

One Diamictite and Two Rifts: Stratigraphy and Geochronology of the Gataga Mountain of Northern British Columbia

3.1 Abstract

Neoproterozoic glacial diamictites and rift-related volcanics are preserved throughout the North American Cordillera, yet the nature and timing of both glaciation and rifting are poorly constrained.

A version of this chapter was accepted for publication: Eyster, A. E., Ferri, F., Schmitz, M. D., Macdonald, F. A., *accepted*, One Diamictite and Two Rifts: Stratigraphy and Geochronology of the Gataga Mountain of Northern British Columbia, American Journal of Science.

New geochronological, geochemical, and stratigraphic data from the Cryogenian Gataga Volcanics and bounding units at Gataga Mountain, in the Kechika Trough of northern British Columbia better constrains the age of these rift-related volcanics and suggests that they erupted during glaciation. At Gataga Mountain, three informal sequences are exposed; a basal quartzite, the Gataga Volcanics, and an overlying mixed carbonate-siliciclastic succession. The basal quartzite is dominated by cross-bedded sandstone with an intertidal facies assemblage including herringbone cross-stratification and mud-cracks, indicative of non-glacial deposition. The overlying Gataga Volcanics are over one kilometer thick, comprising both mafic and felsic units, with volcaniclastic breccia and interbedded sedimentary units including iron formation and matrix-supported diamictite with cosmopolitan clasts. Magmatic ages in the upper Gataga Volcanics span 696.2 $\pm$0.2 to 690.1 $\pm$ 0.2 Ma, and detrital zircon from the underlying non-glacial quartzite provide a maximum age constraint on the onset of glaciation $<$735.8 $\pm$ 0.6 Ma. We interpret interfingering beds of matrix-supported diamictite with cosmopolitan clasts within the Gataga Volcanics to record sub-ice shelf sedimentation and volcanism during the Sturtian Glaciation. Although volcanic facies are consistent with eruption in a sub-ice to sub-aqueous (below ice shelf) environment, we acknowledge the difficulty of distinguishing sub-glacial from sub-aqueous explosive volcanic facies. Overlying the Gataga Volcanics, a mixed carbonate-siliciclastic succession contains minor basalt flows that are geochemically distinct from the underlying volcanic rocks. Based on chemostratigraphic and lithostratigraphic similarities, we suggest that this sequence is correlative with Ediacaran strata to the north. Together, we suggest that the stratigraphy and geochemical signature of volcanic rocks at Gataga Mountain records two episodes of Neoproterozoic extension-related sedimentation and volcanism, the first indicated by the Cryogenian Gataga Volcanics and interbedded sedimentary strata and the second by the overlying Ediacaran carbonate-siliciclastic succession with interfingering basalt.

3.2 Introduction

During the Neoproterozoic, the supercontinent Rodinia amalgamated and broke apart (Li et al. 2008), and there were two long-lasting Cryogenian Snowball Earth glaciations (Kirschvink, 1992; Hoffman and Schrag, 2002; Rooney et al., 2015). Laurentia is central to unraveling the tectonic history of Rodinia because it was surrounded by Neoproterozoic to Cambrian rifted passive margins (Hoffman, 1991), and reconstructions place it at the core of Rodinia (Li et al., 2008, 2013; Evans, 2013). Previous studies have linked the low-latitude break-up of Rodinia with the onset of Cryogenian glaciation (for example Hoffman and Schrag, 2002; Godderis et al., 2003; Cox et al., 2016); however, the age and kinematics of Rodinia's fragmentation, and the relationship to environmental change remain poorly constrained.

The rift history of the western margin of Laurentia is recorded in strata exposed in the U.S. and Canadian Cordillera and is commonly represented by three main stratigraphic ensembles. The first is found in the narrow fault bounded extensional Chuar-Uinta Mountains-Pahrump (ChUMP) basins of the U.S., which includes the Chuar Group exposed in Arizona, the Pahrump Group of California, and the Uinta Mountains Group and the Big Cottonwood Formation in Utah (Karlstrom et al., 2001; Dehler et al., 2010; Smith et al., 2016), and the Mt. Harper (Strauss et al., 2015) and Coates Lake (Jefferson and Parrish, 1989) groups of the Yukon and Northwest Territories, Canada. These basins formed between ca. 775 and 717 Ma (Milton et al., 2014; Macdonald et al., 2010a) and are filled with mixed carbonate-siliciclastic sequences that share correlative fossil assemblages and carbon isotope chemostratigraphic profiles (Porter and Knoll, 2000; Dehler et al., 2010; Macdonald et al., 2013a; Strauss et al., 2014a; Strauss et al., 2015; Smith et al., 2016). Subsidence in these latest Tonian basins has been attributed to early rifting and subsidence (Dehler et al., 2010), initial development of intracratonic basins (Yonkee et al., 2014), oblique transtension (Strauss et al., 2015), or distinct and separate tectonothermal events (Smith et al., 2016). The second ensemble encompasses

Cryogenian to early Ediacaran siliciclastic and volcanic successions commonly interbedded with glacial diamictite and carbonate that have been interpreted as representing rifting across the entire margin (Stewart, 1972; Eisbacher, 1981; 1985; Jefferson and Parish, 1989). Finally, there is a widespread succession of Ediacaran carbonate and siliciclastic strata that are widely interpreted to be related to subsidence and the initiation of passive margin sedimentation (Ross, 1991; Ross et al., 1995; and Dalrymple and Narbonne 1996), or to a separate, later rifting event (Colpron et al., 2002; Macdonald et al., 2013b).

Previous studies have marked the onset of Neoproterozoic rifting in the Cordillera with the identification of alkalic igneous rocks and coarse sedimentation (Gabrielse, 1972; Stewart, 1972; Christie-Blick and Levy, 1989; Aitken, 1993; Link et al., 1993; Lund et al., 2003); however, because there are multiple magmatic events over a period of more than 200 Myrs, it is unclear if all of the magmatism can be attributed to one episode of rifting. Sills, dikes and basalts associated with the Gunbarrel Large Igneous Province (LIP) have been dated at ca. 775 Ma (Harlan et al., 2003; Milton et al., 2014), and have been suggested to mark rifting on the western margin of Laurentia (for example Jefferson and Parrish, 1989). Additionally, basal Windermere volcanics have been dated at 717.43 $\pm$ 0.14 Ma with U-Pb chemical abrasion-isotope dilution-thermal ionization mass spectrometry (CA-ID-TIMS) on zircon in the Yukon, and at 685.5 $\pm$ 0.4 Ma (zircon U-Pb CA-ID-TIMS) in Idaho (Macdonald et al., 2010a; Keeley et al., 2012). Finally, there are younger magmatic events, recorded by ca. 665 to 650 Ma alkaline plutons in central Idaho (Lund et al., 2010), and a 569.6 $\pm$ 5.3 Ma flow (bulk zircon U-Pb ID-TIMS) from the Hamill Group in southeastern British Columbia (Colpron et al., 2002).

An additional complication is that subsidence curves of Paleozoic strata on the western margin of Laurentia (Armin and Mayer, 1983; Bond and Kominz, 1984; Bond et al., 1985) suggest that the rift-drift transition and development of the passive margin did not occur until the ca. 541 Ma

Precambrian-Cambrian boundary [*]. Thus, the older magmatism is too old to be tied to the thermal subsidence and development of the Paleozoic passive margin. This discrepancy in ages could suggest multiple rift events or protracted rifting (Prave, 1999; Colpron et al. 2002; Macdonald et al., 2013b).

The geochronological data on rift-related volcanic rocks and the later rift-drift transition at the Precambrian-Cambrian boundary is also at odds with paleogeographic models that rely on paleomagnetic data, which depict crustal blocks that have successfully rifted off the western Laurentia by 750 Ma (e.g. Meert and Torsvik, 2003; Cawood, 2005; Li et al., 2008). However, it is still not agreed upon what continent(s) rifted away from Laurentia's western margin, with candidates including Antarctica, Australia, North China, South China, Tarim, and West Africa (Sears and Price, 1978; Moores, 1991; Hoffman, 1991; Dalziel, 1997; Sears and Price, 2003; Pisarevsky et al., 2003; Li et al., 2008; Evans, 2009; Fu et al., 2015). Considering such uncertainty in the paleomagnetic and paleogeographic models, it is also possible that the western margin experienced multiple rift events that involved the rifting of ribbon continents, rather than a separation of a large craton (Hildebrand, 2009).

Along with uncertainties and inconsistencies related to the timing of Rodinian break-up, and the identity of what rifted off, the geometry and kinematics of rifting is also poorly constrained. It has been proposed that the current zigzag-geometry of the Neoproterozoic to Cambrian margin is related to pure-shear extension with opposing upper and lower plate segments (Wernicke, 1985; Lister et al., 1986), with the lower plate experiencing extreme thinning of continental crust and subsidence across a broad continental shelf, while the upper plate is marked by limited thinning of the crust and narrow continental shelf margins (Lund et al., 2010). In this model, the broad basins of the Selwyn Basin and Mackenzie Platform in northern Canada formed on a northwest-striking lower-plate extensional margin, while in British Columbia, the narrow Kechika Trough and the MacDonald Plat-

[*] The rift-drift transition reported in these manuscripts is older because at the time the age of the Precambrian-Cambrian boundary was thought to be ca. 575 Ma.

form formed on a northwest-striking upper-plate margin (Ross, 1991; Cecile et al., 1997), with the northeast-striking Liard line representing a transfer zone that separates opposite-polarity segments (Cecile et al., 1997; Lund, et al. 2003; Lund, 2008). However, it is unclear how this model would relate to protracted rifting, translation along the margin, or changing plate geometries and plate directions. Particularly, local evidence for transpression (for example Eisbacher, 1981) and vertical axis block rotations (Eyster et al., accepted) suggest at a component of oblique motion along the margin.

In addition to the complex rift history preserved in the Windermere Supergroup, these strata also preserve evidence of Cryogenian glaciations (for example Crittenden et al., 1983; Gabrielse, 1972; Stewart, 1972; Eisbacher, 1978; Christie-Blick and Levy, 1989; Aitken, 1991; Link et al., 1994; Miller, 1994; Prave, 1999; Lund et al., 2003; Macdonald et al., 2010a). Although Neoproterozoic glacial successions are recognized worldwide, the nature, timing, and duration of glacial episodes has remained controversial (Spence et al., 2016). Nonetheless, paleomagnetic data suggests that some of the Cryogenian glacial diamictites were deposited at low latitudes, consistent with the Snowball Earth hypothesis (Kirschvink, 1992; Evans and Raub, 2011; Eyster et al., accepted). Moreover, recent geochronology confirms that there were two discrete, long-lived Cryogenian glaciations, the Sturtian and the Marinoan (Rooney et al., 2015; Prave et al., 2016). The onset of the Sturtian glaciation is dated by chemical abrasion isotope dilution thermal ionization mass spectrometry (CA-ID-TIMS) U-Pb zircon age of 716.47 $\pm$ 0.24 Ma from diamictites of the Mount Harper Group in Yukon, Canada (Macdonald et al., 2010a). The end of the glaciation is marked by a postglacial Re-Os date of 662.4 $\pm$ 3.9 Ma on the basal Twitya Formation in Northwest Territories, Canada (Rooney et al., 2014). The age of the Marinoan glacial epoch is bracketed between 655 Ma (Zhang et al., 2008) and 635 Ma (Condon et al., 2005; Calver et al., 2013; Rooney et al., 2015), with the later marking the age of the Marinoan cap carbonate. These data, along with the most robust geochronological constraints globally, suggest a $>$55 Myr duration for the Sturtian glaciation (Rooney et al., 2014; 2015), and $>$ 5 Myr duration for the Marinoan glaciation (Prave et al., 2016). Although, some suggest that there

were multiple glaciations between ca. 716-660 Ma, with a possible interglacial period (Le Heron, 2011; Keeley et al., 2012), only one Sturtian cap carbonate has been identified. Thus, during much of the interval that the western margin of Laurentia was experiencing rifting, it appears that equatorial latitudes may have been entombed by Cryogenian glaciation.

To further explore the relationships between rifting and glaciation on the western margin of Laurentia, we revisited the Gataga Mountain area in northern British Columbia. A rhyolite within the Gataga Volcanics was previously dated (five bulk zircon fractions ID-TIMS upper intercept age) at 688.9 +9.5 / -6.2 Ma (U-Pb) and 689.1 $\pm$ 4.6 Ma (Pb-Pb) (Ferri et al., 1999). This age has been cited as a constraint on rift-related Windermere magmatism (Colpron et al., 2002, Lund, 2008; Keeley et al., 2012). In addition to the volcanic rocks exposed at Gataga Mountain, Ferri et al. (1999) documented carbonate, siliciclastic rocks and additional basalt flows (Upper Gataga Volcanics) about 7 km to the north. The preferred interpretation of Ferri et al. (1999) was that the Upper Gataga Volcanics were due to a separate, younger volcanic extensional event and that there was an unconformity between the two volcanic packages; however, it was also acknowledged that it is possible that the volcanics were of a similar age, and the observed relationships had been complicated by faulting (Ferri et al., 1999). As the Gataga Volcanics were interpreted to conformably overlie carbonate and quartzite, and underlie an additional Neoproterozoic to Cambrian sedimentary succession with interbedded volcanic rocks, both without evidence for glaciation (Ferri et al., 1999), this date presents a challenge to age models for an extended Sturtian glaciation, and also potentially provides an important constraint on rifting. To place the Neoproterozoic volcano-sedimentary sequence into a tighter temporal and regional stratigraphic framework, we report new geological mapping, measured stratigraphic sections, geochronology, and carbon isotope chemostratigraphy. These data are then integrated with Neoproterozoic tectonic and climate records across the western margin of Laurentia.

3.3 Methods

3.3.1 Mapping and Stratigraphy

We report new data from two main localities, Gataga Mountain itself and a ridge 7 km to the northwest that we informally refer to as Matulka Creek Ridge (fig. 1). My updated mapping focused on three informal Precambrian units, the Frog quartzite, the Gataga Volcanics, and the Matulka group. The Gataga Volcanics were further subdivided into six mappable members, A-F. These units are exposed in north plunging folds, bounded to the east by a series of thrust faults. During the course of geological mapping, suitable sections were identified for measuring the stratigraphy (fig. 1), and these sections were staffed and described using standard lithostratigraphic terminology (fig. 2). All geochronological and geochemical samples were collected from these measured stratigraphic sections.

3.3.2 Geochronology Sample Preparation

Fourteen samples were collected for geochronology (fig. 2). Mineral separation was performed at Harvard University, using standard density and magnetic isolation techniques. The entire zircon separate was placed in a muffle furnace at 900°C for 60 hours in quartz beakers to anneal minor radiation damage; annealing enhances cathodoluminescence (CL) emission (Nasdala et al., 2002), promotes more reproducible inter-element fractionation during laser ablation inductively coupled plasma mass spectrometry (LA-ICPMS) (Allen and Campbell, 2012), and prepares the crystals for subsequent chemical abrasion (Mattinson, 2005). Following annealing, individual grains were handpicked and mounted in epoxy, polished and imaged by cathodoluminence (CL) on a JEOL T-300 scanning electron microscope fitted with a GATAN MiniCL detector. From these compiled images, grains with consistent and dominant CL patterns were selected for further isotopic analysis.

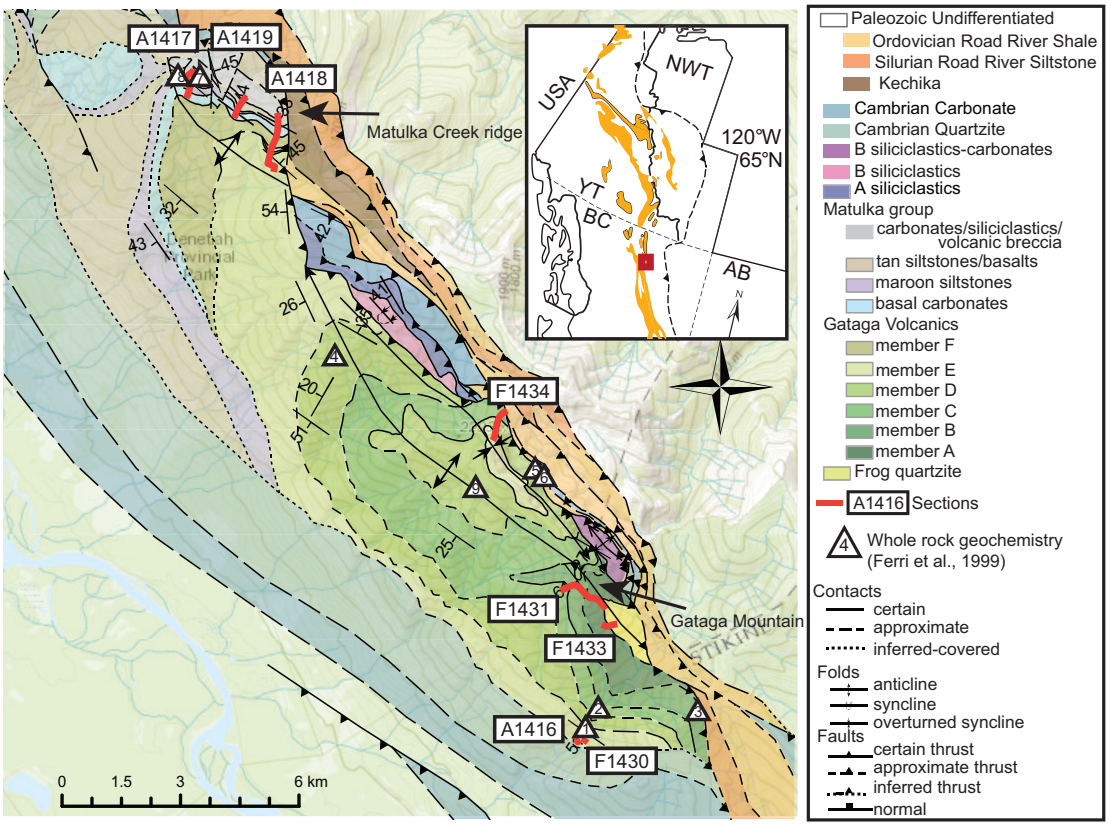


Figure 3.1: Geological map of the Gataga Mountain area with sample and section locations indicated

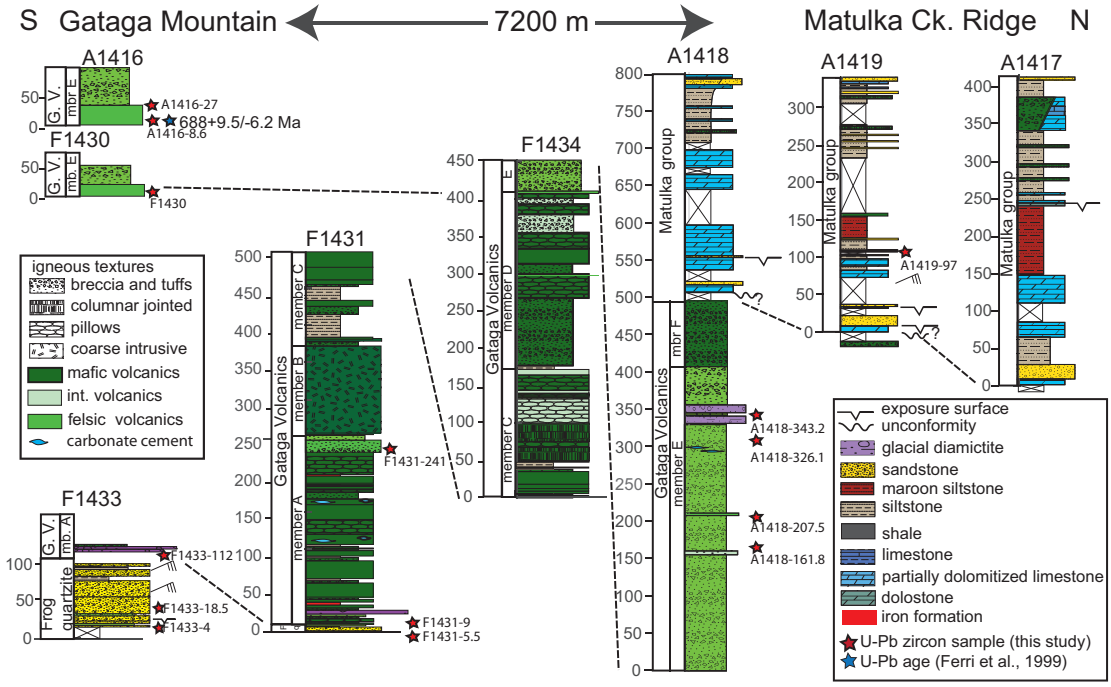


Figure 3.2: Measured stratigraphic sections from Gataga Mountain in the south to Matulka Creek ridge in the north. Stratigraphy scale is in meters and the heights of geochronology samples are indicated as well as the location of the previously sampled age from Ferri et al. (1999).

3.3.3 U-Pb LA-ICP-MS Geochronology and Zircon Geochemistry

Microbeam analysis of zircon was conducted using a ThermoElectron X-series II quadrupole inductively coupled plasma mass spectrometer (ICPMS) and New Wave Research UP-213 Nd:YAG UV (213nm) laser ablation system to obtain U-Pb ages and high field strength element (HFSE) and rare earth element (REE) data. For this, a laser diameter of 25 μ m, fluence of 5 J/cm $\wedge$ 2, and continuous pulse repetition of 10 Hz was used in a 30 second spot acquisition. Two to four U-Pb calibration (Plesovice) and quality control (Zirconia, Seiland) standards were measured every 10 samples, as well as NIST 610 and 612 glass standards for elemental concentration calibration. For the detrital samples, reported ages for zircon samples younger than 1000 Ma reflect the $^{206}Pb/^{238}U$ date, and the $^{207}Pb/^{206}Pb$ date for zircons older than 1000 Ma. Ages with $>\pm 10\%$ discordance were eliminated from subsequent detrital zircon analysis. The plots of relative age probability were made using Microsoft Excel "Isoplot" developed by the Berkeley Geochronology Center and include 2σ errors. The LA-ICP-MS work was followed by CA-ID-TIMS work on selected grains. Selected grains were those that were youngest for the DZ or mixed DZ-volcanic samples, and those that appeared representative of a single magmatic population for the volcanic samples.

3.3.4 U-Pb ID-TIMS Geochronology

U-Pb geochronology methods for ID-TIMS follow those previously published by Davydov et al. (2010) and Schmitz and Davydov (2012). Zircon crystals were subjected to a modified version of the chemical abrasion method of Mattinson (2005), whereby single crystal fragments plucked from grain mounts were individually abraded in a single step with concentrated HF at 180°C for 12 hours. All analyses were undertaken on crystals previously mounted, polished and imaged by cathodoluminescence (CL), and selected on the basis of zoning patterns. U-Pb dates and uncertainties for each analysis were calculated using the algorithms of Schmitz and Schoene (2007) and the U decay con-

stants of Jaffey et al. (1971). Uncertainties are based upon non-systematic analytical errors, including counting statistics, instrumental fractionation, tracer subtraction, and blank subtraction. These error estimates should be considered when comparing my $^{206}Pb/^{238}U$ dates with those from other laboratories that used tracer solutions calibrated against the EARTHTIME gravimetric standards. When comparing my dates with those derived from other decay schemes (for example, $^{40}Ar/^{39}Ar$, ^{187}Re-^{187}Os), the uncertainties in tracer calibration (0.03%; Condon et al., 2015; McLean et al., 2015) and U decay constants (0.108%; Jaffey et al., 1971) should be added to the internal error in quadrature. Quoted errors for calculated weighted means are thus of the form ±X(Y)[Z], where X is solely analytical uncertainty, Y is the combined analytical and tracer uncertainty, and Z is the combined analytical, tracer and ^{238}U decay constant uncertainty.

3.3.5 Carbon Isotope Chemostratigraphy

Fist- to golf ball-sized samples were collected at 1-5 m resolution in measured stratigraphic sections for carbonate carbon ($\delta^{13}C_{carb}$) and oxygen ($\delta^{18}O_{carb}$) isotope chemostratigraphy. At Harvard University, the samples were cut perpendicular to laminations and approximately 5 mg of powder was produced by drilling, taking care to avoid veins and fractures. The $\delta^{13}C_{carb}$ and $\delta^{18}O_{carb}$ data was obtained on a VG Optima dual inlet isotope ratio mass spectrometer coupled with a VG Isocarb preparation device (Micromass, Milford, MA) in the Laboratory for Geochemical Oceanography at Harvard University. Approximately 1 mg of sample powder was reacted in a common, purified phosphoric acid (H_3PO_4) bath at 90°C. The evolved CO_2 was collected cryogenically and analyzed using an in-house reference gas. Calibration to (Vienna-Pee-Dee Belemnite) VPDB was done using the Cararra marble standard (CM2). Total analytical errors (1σ) were better than ± 0.1□ for both $\delta^{13}C_{carb}$ and $\delta^{18}O_{carb}$ based on repeat analysis of standards and samples. The $\delta^{13}C_{carb}$ and $\delta^{18}O_{carb}$ isotopic results are reported in per mil notation of $^{13}C/^{12}C$ and $^{18}O/^{16}O$ relative to the standard VPDB.

3.4 Results

3.4.1 Metamorphism and structure

It must be noted that throughout the Gataga Volcanics folding and pervasive foliation obscures paleo-topographic and textural features. At its western boundary, the Gataga mountain area follows the Northern Rocky Mountain Trench fault zone, an area of deformation that separates displaced continental rocks of Laurentian affinity. Therefore, it is unremarkable that the Gataga Mountain rocks have been substantially faulted and display metamorphism and cleavage. The metamorphism and cleavage in the area is consistent with previous documentation by Ferri et al. (1999). Metamorphic mineral assemblages in mafic volcanics was of chlorite, calcite, albite(?), epidote,white mica, pumpellyite, stilpnomelane, while pelitic rocks contained white mica (illite or phengite), chlorite, quartz, calcite and dolomite (Ferri et al., 1999). Throughout the area, pervasive, slaty cleavage is preent within argillaceous units. While cleavage was rare in clean quartzite and carbonate, there was displayed a widely spaced fracture cleavage, while a pressure-solution cleavage was sometimes seen in argillaceous limestones (Ferri et al., 1999). In addition, although in some cases primary textures were observed, many of the carbonate outcrops were recrystallized, dolomitized and silicified. Stylolites were observed in many carbonate outcrops. This cleavage and alteration tended to be more pervasive nearing thrust faults. These small-scale features were related to the intense eastward compression during the late Mesozoic that produced the dominant structural fabrics and the interrelated folding and thrusting, with thrusts commonly carrying detached anticlines (Ferri et al., 1999). Despite, this deformation, primary textures were identifiable in all units.

3.4.2 Stratigraphy

The oldest map unit, which we refer to as the Frog quartzite, after nearby Frog River, is exposed in the core of the Gataga anticline. This unit is up to several hundred meters thick and dominated by

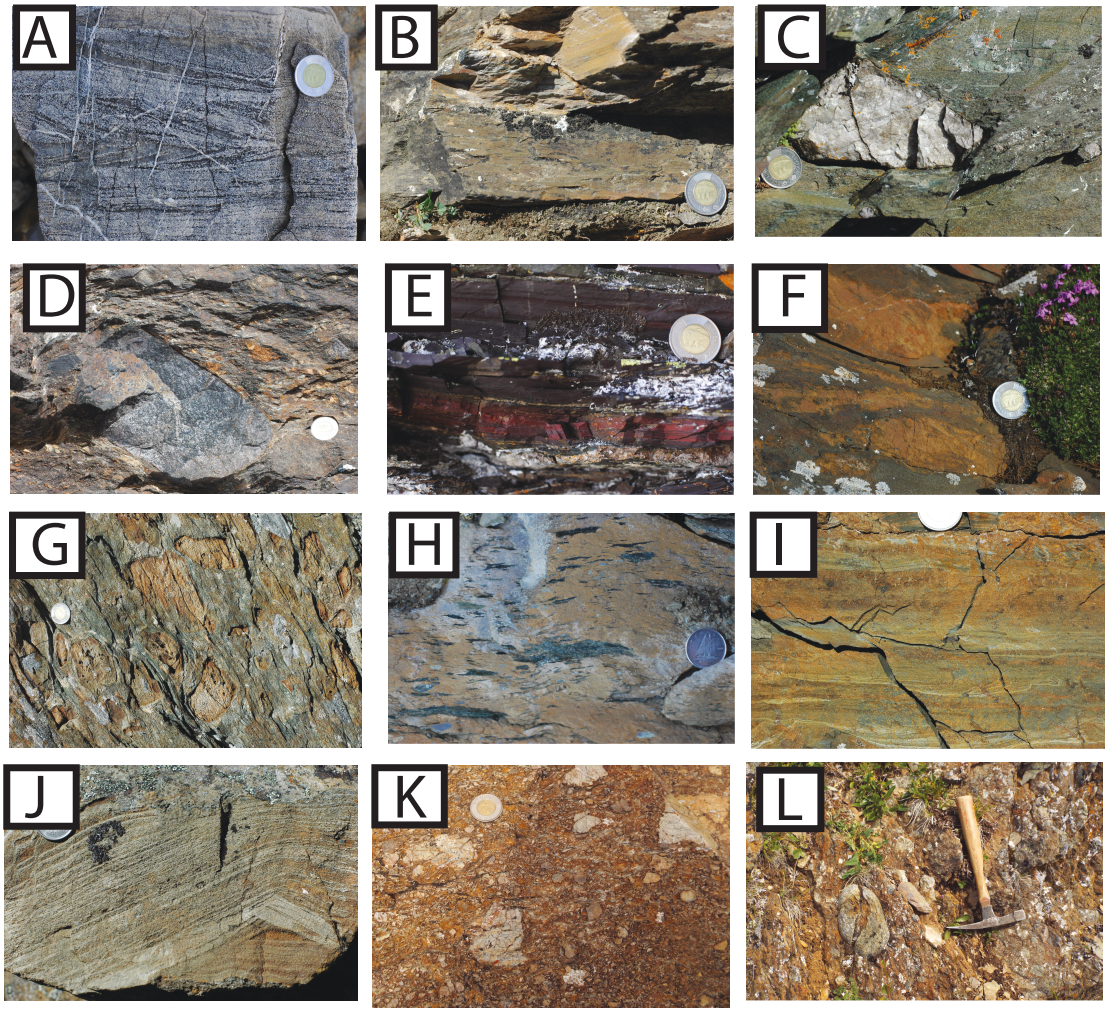


Figure 3.3: Field photos. Frog quartzite: A. F1433 bidirectional crossbeds. Gataga Volcanics member A: B. F1431-9 interbedded lithic tuff, C. F1431 diamictite, D. F1433-116 quartzite clast in diamictite, E. F1431 iron formation. Gataga Volcanics member D: F. F1431 carbonate cements in volcanics, G. F1434-340 block and ash flow, H. F1434 flattened volcanic clasts, I. F1434-310 festoon cross bedding, J. F1434-320 antidune clast in block. Gataga Volcanics member E: K. A1418 volcanic breccia, L. A1418 large sub-rounded clasts.

white-cream fresh and beige weathering massive mature quartzite with meter-scale planar cross-beds and bi-directional cross-stratification (fig. 3A). Minor interbeds of yellow- to green-brown siltstone, lithic tuffs and fine-grained sandstone are present and mud cracks were observed in scree. Above a sharp surface, the Frog quartzite is succeeded by the Gataga Volcanics, which were previously subdivided into two packages: a unit of alkalic mafic to intermediate flows and volcaniclastic rocks, followed by a sequence of felsic volcanics and volcaniclastic rocks found only along the southwestern slopes of Gataga Mountain. My new work subdivides the Gataga Volcanics into six mappable members, A-F, and observes that the felsic volcanics and volcaniclastic rocks outcrop rather expansively to the north of Gataga Mountain. Member A is approximately 350 m thick and is dominated by green to black weathering basalt flows with minor inter-tonguing sedimentary strata. Basalt flows range in thickness from tens of centimeters to tens of meters. Some flows are massive but in others features such as pillows and fine-grained volcaniclastic breccia were observed. Fine to medium-grained green tuff and lithic tuff up to 2 m thick with both graded and massive, homogeneous beds are present near the base of member A (fig. 3B). Notably, near the base is a diamictite unit (fig. 3C, D). This diamictite was documented in sections F1431 and F1433 that were about 700 meters apart. In F1433, the diamictite is 23 meters above the last outcrop of Frog Quartzite. The intervening strata is either quartzite rubble or is not exposed. The diamictite itself has two parts, the basal three meters is composed of fine sand-sized pink lithic matrix with boulder clasts of quartzite, dolostone, and limestone. This is overlain by four meters of wacke matrix with sand-sized lithic fragments and boulders of quartzite. The upper contact is conformable with mafic volcaniclastic breccia. In F1431, the diamictite is 16 meters above the last Frog Quartzite outcrop. It overlies green-black basalt, green tuff and lithic tuff, and fine-grained volcaniclastic breccia. Directly below the diamictite is fine-grained volcaniclastic breccia. The 5 meters thick diamictite has a wacke matrix with gravel-pebble clasts of limestone, dolostone, siltstone, and white and grey quartzite, and laterally has clasts up to cobble and boulder sized. The upper contact with fine-grained volcaniclastic breccia appears to be con-

formable. The rest of member A is dominated by basalt with minor interbedded black, green, and maroon siltstone. Additionally, two thin beds of iron formation were observed, one near the base of member A, above the matrix-supported diamictite, and one near the top of member A (fig. 3E). Previously, Neoproterozoic iron formation has been classified into three facies, hematitic-jaspilite, hematitic-mud/silt and ferruginous mud/silt (Halverson et al., 2011; Cox et al., 2015). Although the iron formation at Gataga Mountain is not as extensive as in the Rapitan group to the north, it displays features similar to the hematitic-mud facies, with mm-laminations that are defined by the relative concentrations of grey hematite and red siltstone. Irregular pods of secondary grey limestone and orange- brown weathering dolostone are also present within the basalt of member A (fig. 3F). Member B is composed of medium to very coarse grained amalgamated green mafic sills, up to 100 m thick. This is followed by about 200 m of member C, which is dominated by dark green basalt with interbedded maroon to green siltstone. Near the base, member C consists of thin mafic flows and siltstone. Up-section, the flows are more massive, and preserve columnar jointing. The uppermost flows of member C are dominated by pillow basalts. Member D is approximately 400 m thick and composed of light green vesicular and pillowed basalt and andesite together with volcaniclastic flows. The volcaniclastic units are generally massive and contain rounded to angular fragments in a coarse-grained chloritic matrix (fig. 3G). Additionally, weakly flattened volcanic clasts were observed in member D (fig. 3H). Some of the volcaniclastic units contained large block and ash breccia, and high-energy volcaniclastic deposits that preserve festoon cross-bedding (Fig 3I) and a clast was found within member D volcanic breccia that displayed antidune cross-bedding (fig. 3J). Member E is a felsic unit that is at least 400 m thick and dominated by volcaniclastic breccia, but also contains minor andesitic to rhyolitic flows and tuffs. Member E is preserved on dip-slopes southwest of Gataga Mountain, but is most clearly exposed at the informal Matulka Creek Ridge. Overall, the volcaniclastic rocks of member E are massive and very poorly sorted to unsorted. The bedding appears to be more prominent in exposure near the base of member E at Gataga Mountain, but more massive at

exposures along Matulka Creek Ridge. Member E is dominated by matrix supported breccia consisting of poorly sorted, angular to sub-rounded, green-white pumaceous felsic fragments ranging from several mm to 30 cm in diameter with a matrix of brown-orange weathering, poorly sorted siltstone and sandstone (fig. 3K, L). Additionally, sub-rounded quartzite clasts were documented as well as isolated carbonate and laminated siltstone clasts (fig. 4A), and large, rounded, rhyolitic and granitic clasts (fig. 4B, C). Orange-weathering carbonate cement is present within some of the volcaniclastic units.

In addition to the massive weathering volcaniclastic breccia, there are some flows as well as laminated fine-grained volcaniclastic units. The flows are isolated, lenticular pale grey, aphanitic rhyolitic flows with phenocrysts of plagioclase and quartz. The laminated fine-grained volcaniclastic units are more abundant near the top, where there are several units with laminated and graded tuffaceous beds containing some larger angular carbonate clasts and a few isolated large rhyolitic clasts. In the upper part of these units, one particularly striking pale rhyolite clast appears to be a dropstone that punctured the laminated beds below (fig. 4D), but we cannot rule out the possibility that this is a volcanic bomb. Member F succeeds member E and consists of dark brown weathering, intermediate to mafic, hornblende-bearing volcaniclastic breccia with abundant lapilli sized clasts. Overlying the Gataga Volcanics are siliciclastic rocks, carbonate and basalt of the Matulka group. The Matulka group is exposed in the anticline at Matulka Creek Ridge and undergoes dramatic facies changes across the anticline. The anticline is cut by several N-S trending high angle faults with up to 10 m of displacement. The contact between the overlying Matulka group and the volcanics is nowhere exposed and was not directly observed. Map relations suggest that the beds of member F of the Gataga volcanics are truncated by the Matulka group, suggestive of an angular unconformity (Fig 1). Alternatively, there may be erosional features associated with the volcanics themselves or structural complications. The lowermost unit of the Matulka group is a carbonate-dominated ridge former. The base consists of ooid grainstone that has been dolomitized and partially silicified (fig. 4E and

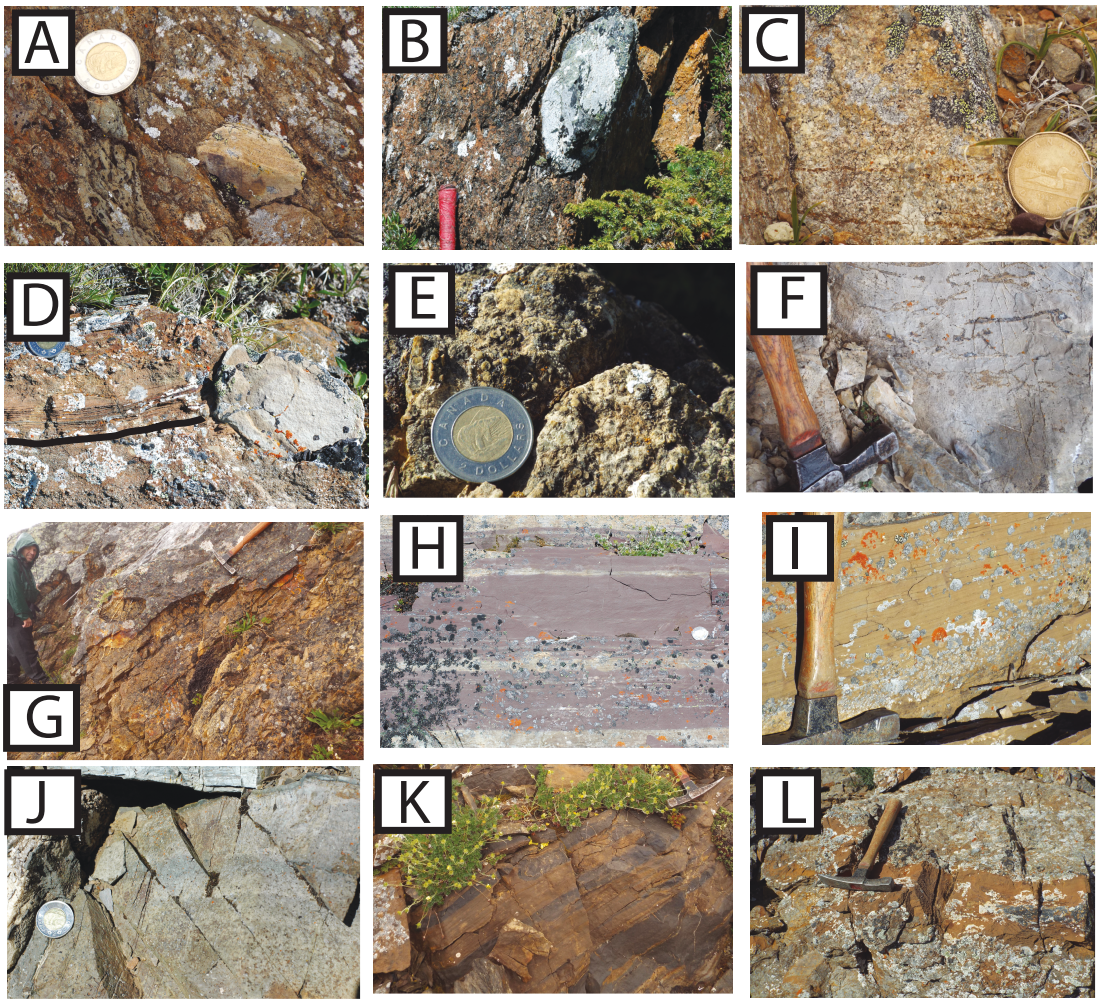


Figure 3.4: Field photos. Gataga Volcanics member E: A. A1418 laminated siltstone clasts, B. A1418 rounded granite clasts, C. A1418-343.2 ash, D. A1418-355.4 diamictite unit with rhyolite dropstone puncturing laminations-this photo has been annotated to highlight punctured laminations. Matulka group: E. A1417 lower oolitic carbonates, F. A1418 lower recrystallized carbonate, G. A1419 exposure surface, H. A1417 maroon siliciclastics, I. A1417 tan siliciclastics, J. A1417 basalt flows, K. A1419 interbedded oolitic limestone and siliciclastics, L. A1417 volcanic breccia

F). Dolomitization and silicification is more pervasive in eastern sections, closer to the thrust faults carrying the stratigraphy. In section A1419, a karst surface is present 12.3 m from the base that is filled and overlain by massive orange to grey weathering quartzite (fig. 4G). This quartzite is followed by about 10 m of cover. Overlying the basal carbonate is a recessive maroon siltstone (fig. 4H) that is a slope former and thickens to the west. To the east, the maroon siltstone grades into brown-green siltstone and thinly bedded sandy dolostone (fig. 4I). These units include interbedded basalt flows (fig. 4J), with chilled margins and joints (Upper Gataga Volcanics of Ferri et al. (1999)). These are overlain by dark oolitic limestone and siliciclastic rocks (fig. 4K) that interfinger with volcanic breccia that is dominated by cobble sized angular basalt clasts (fig. 3L). To the north of the map area, additional strata were documented by Ferri et al. (1999) that may be Cambrian in age and overlie the Matulka group. These include a quartzite unit (Csc, referred to as the Cambrian Quartzite here and in fig. 1) of grey to white quartz sandstone and calcareous or dolomitic quartz sandstone. These are overlain by grey to buff-grey limestone and lesser dolostone (Cl), that contain possible archaeocyathids, and finally, a siliciclastic unit of variable lithology (Cgm) that includes maroon and pale olive green, laminated siltstone, limestone, quartz sandstone and a maroon limestone-pebble conglomerate (Ferri et al., 1999). These strata can be traced northward where they interfinger with and are succeeded by more siliciclastic rocks of the Cambrian Quartzite unit. Additional siliciclastic dominated successions are present within thrust slivers just to the east of Gataga Mountain, as well as to the north (fig. 1), although the exact connection to other units is unclear due to numerous thrust faults that leave the sections hanging. To the east of Gataga Mountain, the B siliciclastic-carbonate unit includes interbedded light-blue-grey-pink cross-bedded carbonate interbedded with texturally and chemically mature medium bedded sandstone. To the north, the basal unit (A siliciclastic) consists of black to grey to brown siltstone and shale with red-yellow silty-dolostone near the top. This is overlain by the B siliciclastic unit that consists of siltstone interbedded with pink-yellow cross-bedded calcareous sandstone and sandy dolomite. Finally, on the west flank of the large anticline,

the Gataga Volcanics are succeeded by mature, bidirectional cross-stratified sandstone and quartzite of the Cambrian Quartzite unit, which in turn is overlain by the Cambrian Carbonate, a blue-grey to cream, white weathering recrystallized carbonate. The direct relationship of these units to the A and B siliciclastic units and the other strata on the east side of the anticline is unclear.

The main differences from previous mapping are that, first, instead of only less than 10% of the Gataga Volcanics being felsic as previously estimated by Ferri et al. (1999), by documenting the northward extent of the felsic volcaniclastic rocks of Member E, we have found that approximately 30% of the Gataga Volcanics are felsic. Second, the B siliciclastic-carbonate unit exposed to the east of Gataga Mountain is not correlative with the Frog quartzite, and does not sit stratigraphically below the Gataga Volcanics. The B siliciclastic-carbonate unit was suggested to be Late Proterozoic age after the initial dating of the volcanics (Ferri et al., 1999). We suggest that the contact between these and the Gataga Volcanics is a thrust fault and although complicated by additional thrust faults, these units are likely Late Ediacaran to Early Cambrian in age. To the northwest, similar rocks are overturned where they are in contact with the main thrust fault. Finally, instead of a single "Gataga Mountain Anticline", the Gataga Volcanics and Matulka group are exposed in two different north plunging anticlines (fig. 1).

3.4.3 U-Pb Geochronology

F1431-5.5: Frog quartzite

The sample was collected from the top of the Frog quartzite, a thick-bedded quartzite, tan to brown-red weathered and grey-tan fresh and cross-bedded, (figs. 1, 2). Throughout the quartzite there is additional iron staining and 0.5 centimeter thick quartz veins. The sample is composed of well-sorted millimeter-sized quartz grains with isolated dark lithic fragments. 146 detrital zircon grains were analyzed from sample F1431-5.5, of which 136 were $<$ 10% discordant (fig. 5, supplementary table S1).

The dominant age population is between 1246-920 Ma (62 grains), with secondary peaks at 1710-1246 Ma (39 grains), and 2008-1710 Ma (18 grains). Smaller age populations are present between ca. 731-814 Ma, 2253-2321 Ma, and 2492-2664 Ma. CA-ID-TIMS analyses of four young grains yielded dates of: 735.8 ± 0.6 Ma, 737.2 ± 0.6 Ma, 741.3 ± 0.6 Ma, and 742.3 ± 0.6 Ma (Fig 6F, table 1). This gives a maximum depositional age for the Frog quartzite of <735.8 Ma.

F1433-112; Lower Member A, Gataga Volcanics

A pink lithic volcaniclastic unit near the base of the Gataga Volcanics, in the lowermost part of Member A (figs. 1, 2). The sample is orange weathering and pink-yellow fresh, supported by fine-sand to pebble sized clasts of pale-white aphanitic rhyolite, flattened yellow and darker flattened maroon clasts and a matrix that included fine lithic clasts, aphantic pink volcaniclastic material and muscovite. 116 detrital zircon grains were analyzed from sample F1433-112, of which 97 were < 10% discordant (fig. 5, supplementary table S1). The dominant age population is between 2060-1780 Ma (41 grains). Smaller age populations at 1090-961 Ma (12 grains), and 840-655 Ma (6 grains). CA-ID-TIMS analyses of six young grains yielded dates of 707.6 ± 0.5 Ma, 711.6 ± 0.5 Ma, 726.2 ± 0.5 Ma, 726.7 ± 1.0 Ma, 729.8 ± 0.8 Ma and 734.7 ± 1.4 Ma (fig. 6F, table 1). This gives a maximum depositional age for the base of the Gataga Volcanics of <707 Ma.

F1431-241: Upper Member A, Gataga Volcanics

A green volcaniclastic sandstone near the top of Member A of the lower Gataga Volcanics (figs. 1, 2), orange weathering and dominantly blue-grey fresh with small millimeter-sized crystals of quartz, plagioclase feldspar, dark mafic fragments, as well as orange weathering iron dominated mafic fragments. The clasts were aligned parallel to foliation in a matrix that was blue-grey and aphanitic. 111 detrital zircon grains were analyzed from sample F1431-241, of which 89 were < 10% discordant (fig. 5, supplementary table S1). The dominant age population is between 830-642 Ma (30 grains).

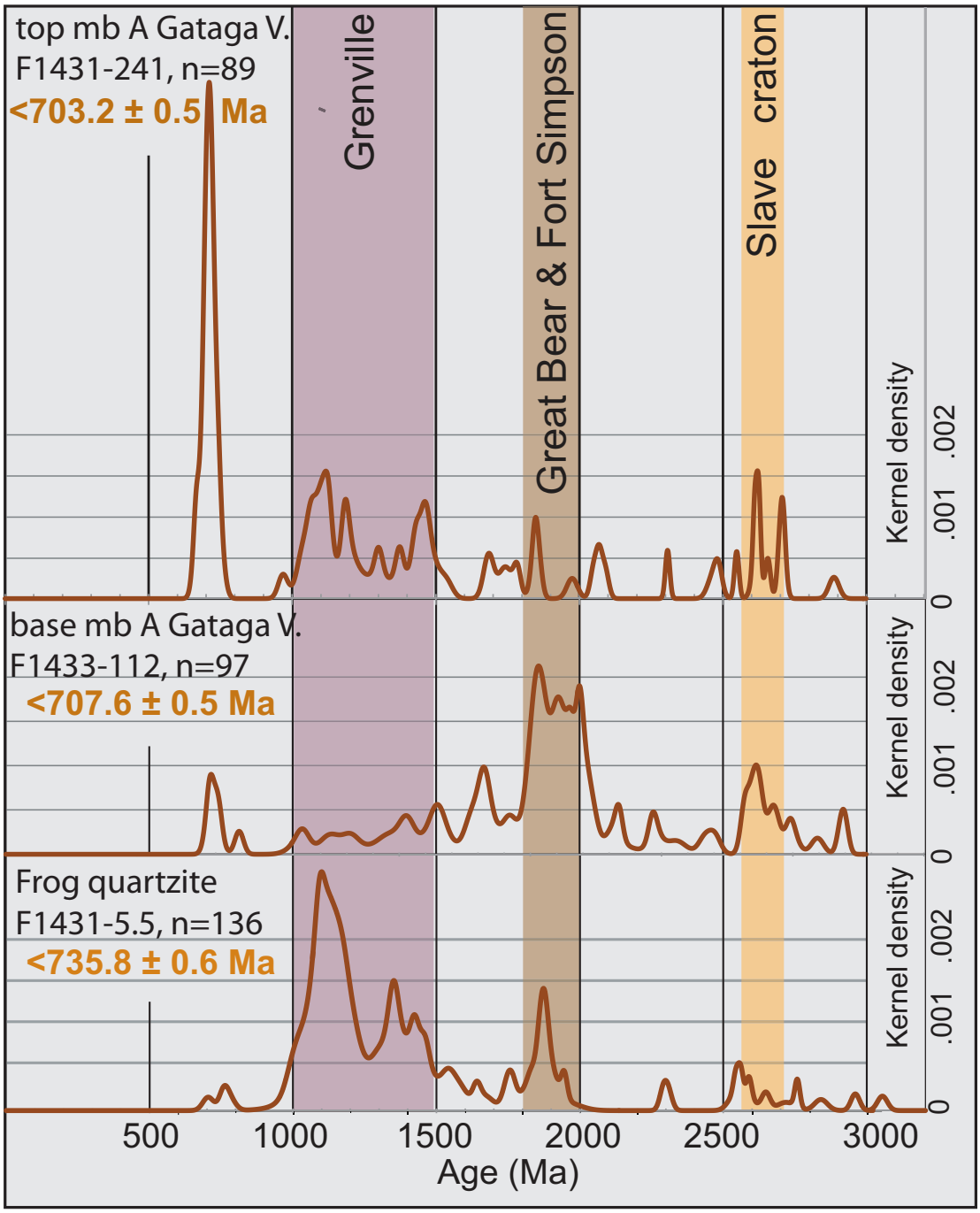


Figure 3.5: Detrital spectra normalized probability plots of U-Pb dates obtained by LA-ICP-MS on zircon collected from samples F1431-5.5, F1431-241, and F1433-241. Regional basement and orogenic events that could correspond to the data peaks are highlighted.

Table 1. CA-TIMS U-Pb isotopic data

	Compositional Parameters						Radiogenic Isotope Ratios									Isotopic Ages					
Sample	Th/U	$^{206}Pb^*$ x10^{-13} mol	mol % $^{206}Pb^*$	Pb^*/Pb_c	Pb_c (pg)	$^{206}Pb/^{204}Pb$	$^{208}Pb/^{206}Pb$	$^{207}Pb/^{206}Pb$	% err	$^{207}Pb/^{235}U$	% err	$^{206}Pb/^{238}U$	% err	corr. coef.	$^{207}Pb/^{206}Pb$	±	$^{207}Pb/^{235}U$	±	$^{206}Pb/^{238}U$	±
(a)	(b)	(c)	(c)	(c)	(c)	(d)	(e)	(e)	(f)	(e)	(f)	(e)	(f)		(g)	(f)	(g)	(f)	(g)	(f)
Gataga volcanic rocks																				
A1418-343,2																				
z7	0.534	1.4424	0.989	28.1	1.30	1667	0.165	0.06257	0.1	0.975334	0.2	0.113060	0.067	0.879	693.53	2.52	691.21	0.87	**690.50**	**0.44**
z4	0.565	2.8416	0.991	35.0	2.07	2053	0.175	0.06246	0.1	0.973136	0.2	0.112990	0.066	0.918	690.05	2.10	690.08	0.78	**690.09**	**0.43**
z2	0.635	1.4532	0.995	68	0.56	3904	0.197	0.06254	0.1	0.974245	0.2	0.112981	0.067	0.854	692.64	2.36	690.65	0.81	**690.04**	**0.44**
z1	0.588	1.5835	0.994	51.1	0.80	2984	0.182	0.06262	0.1	0.975306	0.2	0.112967	0.067	0.864	695.22	2.31	691.20	0.81	**689.96**	**0.44**
z6	0.580	1.5887	0.996	72.9	0.56	4272	0.180	0.06253	0.1	0.973845	0.2	0.112960	0.067	0.894	692.16	2.07	690.44	0.76	**689.92**	**0.44**
z5	0.587	1.8444	0.983	17.7	2.68	1039	0.182	0.06259	0.1	0.974867	0.2	0.112958	0.087	0.806	694.44	2.98	690.97	1.00	**689.90**	**0.57**
A1418-326,1																				
z1	0.509	2.0540	0.997	95.2	0.54	5694	0.158	0.06255	0.1	0.978443	0.2	0.113445	0.072	0.827	693.07	2.29	692.81	0.80	692.73	0.47
z2	0.532	1.8943	0.997	91.2	0.53	5415	0.165	0.06258	0.1	0.977730	0.1	0.113310	0.066	0.899	694.05	1.99	692.44	0.75	691.94	0.44
z6	0.469	1.2816	0.994	46.8	0.68	2846	0.145	0.06257	0.1	0.976017	0.2	0.113140	0.068	0.830	693.53	2.69	691.56	0.89	**690.96**	**0.45**
z5b	0.486	0.3797	0.984	18.9	0.50	1150	0.150	0.06257	0.3	0.975894	0.4	0.113115	0.094	0.672	693.72	6.39	691.50	1.78	**690.81**	**0.62**
z4	0.571	2.7129	0.994	53.5	1.30	3191	0.177	0.06260	0.1	0.976377	0.1	0.113112	0.066	0.915	694.84	1.97	691.75	0.75	**690.80**	**0.43**
z3	0.538	3.4563	0.998	125.8	0.70	7491	0.167	0.06257	0.1	0.975666	0.1	0.113094	0.064	0.951	693.62	1.61	691.38	0.67	**690.69**	**0.42**
z7	0.567	2.4577	0.996	74.7	0.84	4436	0.175	0.06255	0.1	0.975290	0.1	0.113085	0.069	0.914	692.96	1.87	691.19	0.73	**690.64**	**0.45**
A1418-207,5																				
z8	0.555	0.1481	0.941	4.9	0.77	309	0.172	0.06304	0.8	0.991364	0.9	0.114060	0.211	0.575	709.49	16.86	699.42	4.53	**696.28**	**1.40**
z2	0.530	0.2151	0.964	8.3	0.66	511	0.164	0.06263	0.6	0.984571	0.7	0.114012	0.149	0.612	695.75	12.59	695.95	3.38	**696.01**	**0.98**
z3	0.581	0.6900	0.994	50.9	0.35	2991	0.180	0.06274	0.1	0.986178	0.2	0.114003	0.078	0.783	699.40	2.99	696.77	0.97	**695.95**	**0.51**
z1	0.615	0.4170	0.988	26.4	0.41	1549	0.190	0.06262	0.2	0.984295	0.3	0.113999	0.088	0.690	695.40	5.31	695.80	1.52	**695.93**	**0.58**
z9	0.561	1.9397	0.998	137.0	0.36	8062	0.174	0.06266	0.1	0.984871	0.1	0.113992	0.080	0.924	696.78	1.60	696.10	0.72	**695.89**	**0.53**
z6	0.538	0.4380	0.992	39.8	0.28	2369	0.167	0.06276	0.2	0.986146	0.2	0.113960	0.091	0.747	700.14	3.64	696.75	1.15	**695.70**	**0.60**
z4	0.586	0.5826	0.982	17.1	0.87	1026	0.181	0.06273	0.2	0.985289	0.3	0.113908	0.081	0.723	699.24	4.81	696.31	1.40	**695.41**	**0.54**
A1418-161,8																				
z6	0.524	0.3493	0.990	28.9	0.31	1729	0.162	0.06262	0.2	0.985031	0.3	0.114094	0.096	0.687	695.21	4.73	696.18	1.39	**696.48**	**0.64**
z3	0.548	0.3297	0.987	24.1	0.35	1439	0.170	0.06256	0.3	0.983822	0.3	0.114056	0.097	0.673	693.31	5.69	695.56	1.62	**696.26**	**0.64**
z1	0.546	0.4450	0.988	24.3	0.46	1451	0.169	0.06271	0.2	0.986138	0.3	0.114053	0.085	0.708	698.38	5.15	696.75	1.48	**696.24**	**0.56**
z5	0.557	0.5938	0.985	20.0	0.75	1205	0.173	0.06281	0.2	0.987580	0.3	0.114039	0.083	0.750	701.74	4.32	697.48	1.30	**696.16**	**0.55**
z9	0.504	0.5236	0.985	19.7	0.67	1195	0.156	0.06268	0.2	0.979817	0.3	0.113366	0.080	0.753	697.54	4.71	693.51	1.38	692.27	0.52
z4	0.378	1.0431	0.990	30.3	0.84	1898	0.117	0.06253	0.1	0.976442	0.2	0.113250	0.070	0.810	692.38	3.16	691.78	1.00	691.59	0.46
z2	0.519	3.2240	0.999	216.4	0.38	12860	0.161	0.06265	0.1	0.978223	0.1	0.113248	0.065	0.964	696.29	1.47	692.69	0.65	691.59	0.43
z8	0.417	0.3504	0.941	4.8	1.81	313	0.129	0.06218	0.5	0.965157	0.5	0.112572	0.119	0.616	680.38	9.69	685.96	2.58	687.67	0.78
A1416-8,6																				
z8	0.678	0.7035	0.994	50.2	0.37	2878	0.210	0.06272	0.1	0.991122	0.2	0.114605	0.072	0.789	698.83	3.06	699.29	0.98	699.44	0.48
z2	0.540	0.4283	0.931	4.1	2.67	255	0.167	0.06255	0.5	0.987228	0.5	0.114470	0.116	0.570	692.95	9.66	697.30	2.57	698.65	0.77
z4	0.845	0.7190	0.988	27	0.74	1471	0.262	0.06273	0.2	0.987226	0.2	0.114132	0.073	0.770	699.25	3.78	697.30	1.15	**696.70**	**0.48**
z1	0.549	0.6855	0.985	19.6	0.89	1168	0.170	0.06267	0.2	0.985947	0.3	0.114106	0.080	0.694	696.98	4.86	696.65	1.39	**696.55**	**0.53**
z6	0.542	0.5229	0.991	34.9	0.38	2080	0.168	0.06248	0.2	0.982663	0.2	0.114067	0.081	0.718	690.58	3.91	694.97	1.17	**696.33**	**0.53**

Smaller age populations are between 1567-907,1888-1654 Ma, 2100-2010-2100 Ma, and 2773-2418 Ma. CA-ID-TIMS analyses of 12 young grains yielded dates of ca. 703-705 Ma (n=3), ca. 712 Ma (n=8), and ca. 715 Ma (n=1) (fig. 6F, table 1). The youngest crystal implies a maximum depositional age for the top of member A of the Gataga Volcanics of <703 Ma.

A1416-8.6: Middle Member E, Gataga Volcanics

A pale blue-green foliated aphanitic rock with isolated millimeter sized quartz crystals and plagioclase phenocrysts that was the resampled location of Ferri et al. (1999). There were no discernable clasts in hand sample and could be an effusive rhyolitic flow. 6 of the 8 dated zircon grains yielded concordant analyses with a weighted mean $^{206}Pb/^{238}U$ date of 696.24 ± 0.22 Ma (MSWD = 1.93), which is interpreted as the eruptive age (fig. 6A, table 1, table 2). Two crystals (Z2 and Z8) not included in this date are older (698.65 ± 0.77 Ma 699.44 ± 0.48 Ma) and interpreted as inherited grains.

A1418-161.8:Middle Member E, Gataga Volcanics

A massive blue-colored andesite with larger plagioclase feldspar crystals that is grey-brown weathering and grey fresh with an aphanitic matrix with biotite crystals, and includes 5 millimeter long angular grey quartz-rich lithic fragments and pale white plagioclase fragments that are 1 millimeter long. The biotite dominated regions formed bands parallel to foliation. This appeared to be a volcaniclastic rock resulting from explosive eruption. Four of the dated zircon grains yielded concordant and equivalent analyses with a weighted mean $^{206}Pb/^{238}U$ date of 696.28 ± 0.30 Ma (MSWD = 0.20), which is interpreted as the eruptive age (fig. 6B, table 1, table 2). The four grains that were not included have a scatter of ages of that are younger 692.27± 0.52 Ma, 691.59± 0.46 Ma, 691.59± 0.43 Ma, 687.67± 0.78 Ma, likely due to persistent lead loss in the sampled zircons, which is consistent with CL images that display dark regions damaged by radioactive decay.

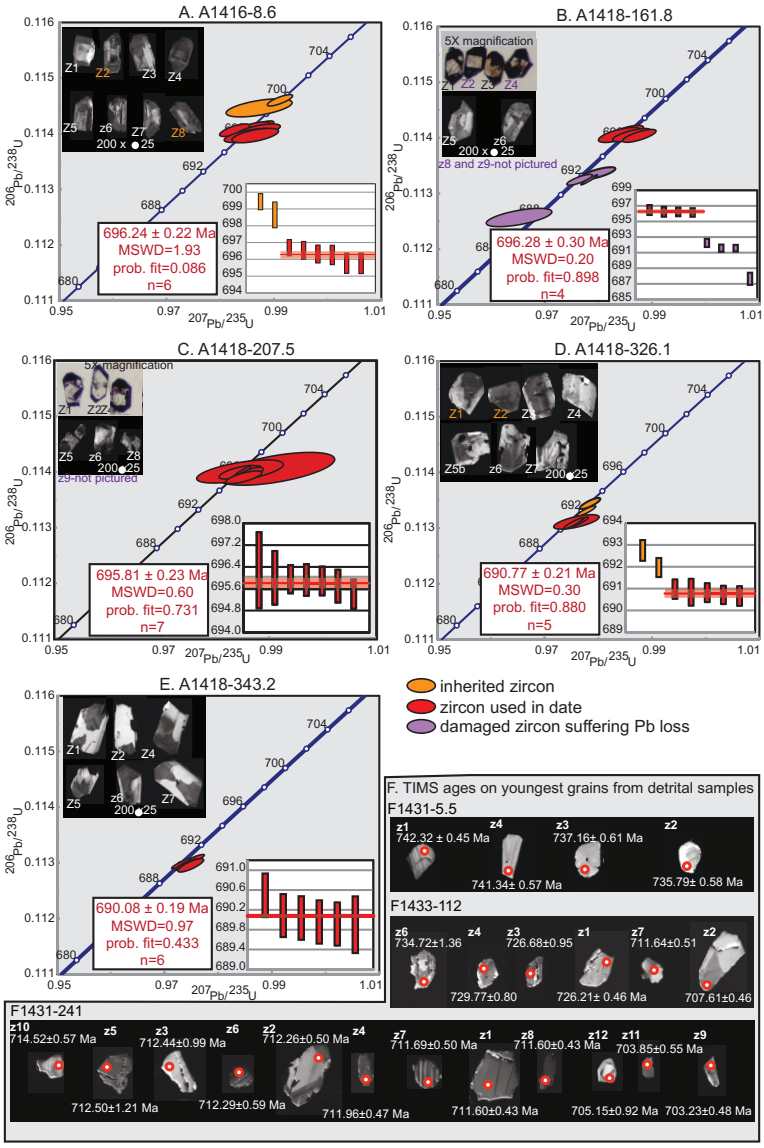


Figure 3.6: Concordia diagrams of zircon 206Pb/238U CA-ID-TIMS dates with ranked age diagrams as insets: A. A1416-8.6-rhyolite from Member E near Gataga Mountain, B. A1418-161.8- volcaniclastic andesite from member E on Matulka Creek Ridge, C. A1418-207.5-rhyolite from member E on Matulka Creek Ridge, D. A1418-326.1-felsic laminated tuff just below diamictite units, E. A1418-343.2-felsic laminated tuff between two diamictite units. The data point error ellipses are 2σ; F. CL images of youngest grains from the detrital samples F1431-5.5, F1433-112, and F1431-241 along with TIMS dates.

Table 2. Weighted Mean Age Calculations for Volcanic Samples

	Lithology	$^{206}Pb/^{238}U$ age ± 2s (Ma) analytical (+ tracer) [+ l]	n#	MSWD*	prob. fit*
A1418-343.2	rhyolite tuff	690.08 ± 0.19 (0.38) [0.80]	6	0.97	0.433
A1418-326.1	rhyolite tuff	690.77 ± 0.21 (0.39) [0.81]	5	0.30	0.880
A1418-207.5	rhyolite lava	695.81 ± 0.23 (0.4) [0.82]	7	0.60	0.731
A1418-161.8	andesite tuff	696.28 ± 0.30 (0.44) [0.84]	4	0.20	0.898
A1416-8.6	rhyolite lava	696.29 ± 0.22 (0.40) [0.82]	6	1.93	0.086

indicates number of zircons included, see bolded ages in Table 1

* MSWD = mean squared weighted deviation; prob. fit = probability of fit

Sample A1418-207.5: Middle Member E, Gataga Volcanics

This unit was green-brown weathering, pale grey to pale green fresh aphanitic matrix with interlocking mm-sized quartz phenocrysts. There were biotite dominated bands subparallel to foliation and rust-weathering iron-rich veins scattered throughout. This likely effusive rhyolite lava flow was of short lateral extent and was interbedded with felsic volcanic breccia. All seven of the dated zircon grains yielded concordant analyses with a weighted mean $^{206}Pb/^{238}U$ date of 695.81 ± 0.23 Ma (MSWD = 0.6), which is interpreted as the eruptive age (fig. 6C, table 1, table 2).

A1418-326.1: Upper Member E, Gataga Volcanics

An orange weathering, pale blue-grey fresh volcaniclastic rock, dominated by 2-6 millimeter-long fine-grained pale blue-white lithic fragments as well as dark-green to black lithic fragments. The unit spanned three meters, encompassing multiple beds up to 70 cm thick. Overlying this explosive volcaniclastic tuff was brown weathering laminated beds of orange brown siltstone and darker quartzite. Five of the seven dated zircon grains yielded concordant and equivalent analyses with a weighted mean $^{206}Pb/^{238}U$ date of 690.77 ± 0.21 Ma (MSWD = 0.30), which is interpreted as the

eruptive age (fig. 6D, table 1, table 2). The two grains that were not included (Z1 and Z2) are interpreted as inherited grains as they had slightly older dates of 692.73 ± 0.47 Ma and 691.94 ± 0.44 Ma.

Sample A1418-343.2: Upper Member E, Gataga Volcanics

An orange weathering, grey-pink fresh coarse pale volcaniclastic tuff that is clast supported and dominated by 2-4 millimeter-long pink feldspar and clear quartz crystals, 5 millimeter-long angular fragments of grey quartz. The matrix is aphantic but includes some green-brown biotite crystals. The tuff is 4 m thick, and the outcrop was traced laterally for 10 m before the exposures became poor, at the base of the unit there are centimeter-sized pale felsic volcanic clasts. This tuff overlies fine laminated beds with outsized clasts and is about 10 meters below the large felsic dropstone that penetrates the laminated beds below (fig. 4D). All six dated zircon grains yielded concordant and equivalent analyses with a weighted mean $^{206}Pb/^{238}U$ date of 690.08 ± 0.19 Ma (MSWD = 0.97), which is interpreted as the eruptive age (fig. 6E, table 1, table 2).

3.4.4 Chemostratigraphy

The basal carbonates of the Matulka group are pervasively recrystallized, with carbonate veins and fabric destructive dolomite decimating most of the primary sedimentary structures (fig. 4F). Isotope data from these units are extremely scattered (fig. 7, supplementary table S3). In one section, A1417, limestone with primary textures are preserved. Data from these samples is less scattered and preserves stratigraphic trends (fig. 7, supplementary table S3). Particularly, these samples record a negative $\delta^{13}C_{carb}$ excursion, with values trending from -4.22‰ to -5.72‰ and then returning to +3.99‰ and back to values just under 0 ‰ (Fig. 7). Carbon-oxygen cross-plots for the basal carbonates in the Matulka group display covariance, possibly resulting from meteoric diagenesis (fig. 7).

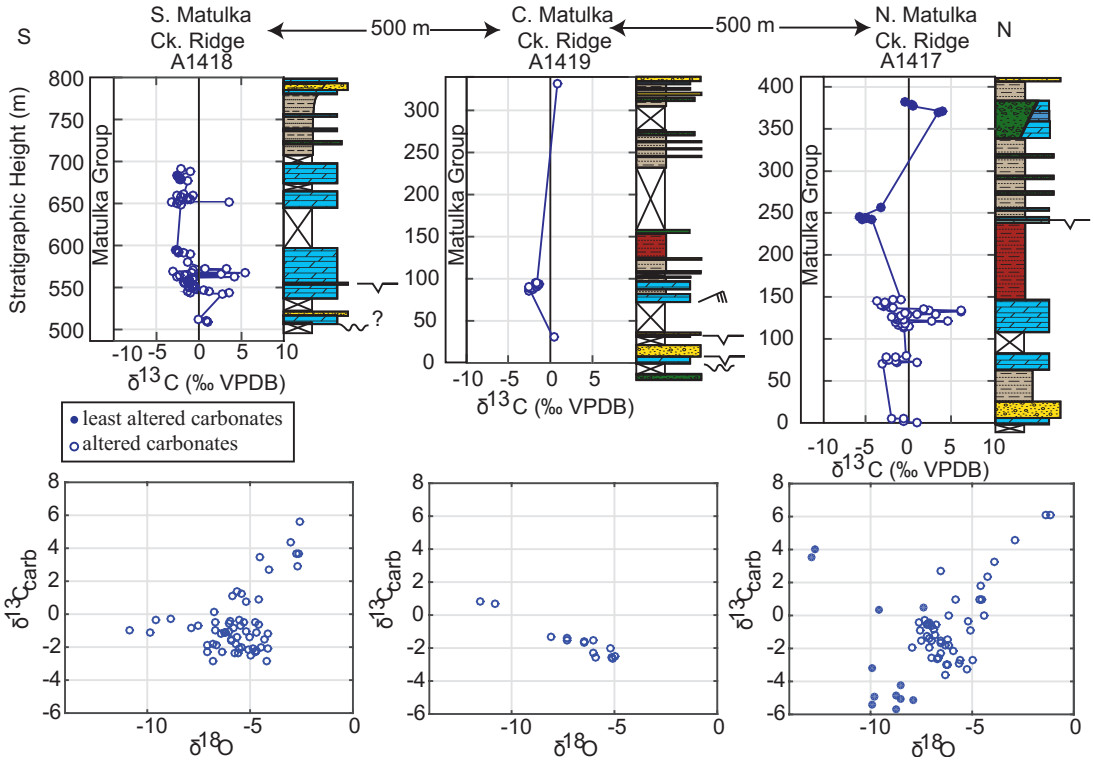


Figure 3.7: Top row: Matulka group stratigraphic sections and carbon isotope data. Bottom row: corresponding carbon-oxygen cross plots. See figure 1 for location of sections, and figure 2 for lithology key.

3.5 Discussion

3.5.1 Geochronology

Magmatic ages

Based on sections A1418 and A1416, the final reported dates and uncertainties of the Gataga Volcanics are weighted mean dates from populations of single zircons (fig. 8, table 2). This approach weights each individual analysis according to its precision, so analyses with a small uncertainty contribute more to the weighted mean than those with larger uncertainty. The mean squared weighted deviation (MSWD) measures the coherence of the dataset and the scatter of the data that can be considered due to analytical factors alone and varies according to the number of data points in the calculation (Wendt and Carl 1991; Condon and Bowring, 2011). The calculation of the weighted mean date is based on the assumption of a single population with normally distributed errors, which requires eliminating all zircons that suffer from lead loss or that are inherited (Condon and Bowring, 2011).

With regard to lead loss, the effects can be minimized by the selection of the best quality zircon grains and aggressive chemical abrasion. Lead loss may still influence some high-U zircon grains, but can be identified with high precision analyses (Bowring et al., 2006). Only in A1418-161.8, were there were four grains that we interpreted as experiencing lead loss and were excluded from the mean date (fig. 6B). Inheritance of older zircon grains can be a common occurrence in magmatic systems, through the assimilation of the host rock, including only slightly older volcanic and plutonic rocks. Older crystals or crystal with inherited cores can comprise more than 50% of the zircons recovered from an ash (Bowring et al., 2006). For the samples, A1416-8.6 and A1418-326.1 both had two grains that we interpreted as inherited (fig. 6A, 6D).

Despite the presence of a minority of zircon dates compromised by Pb-loss or inheritance, the

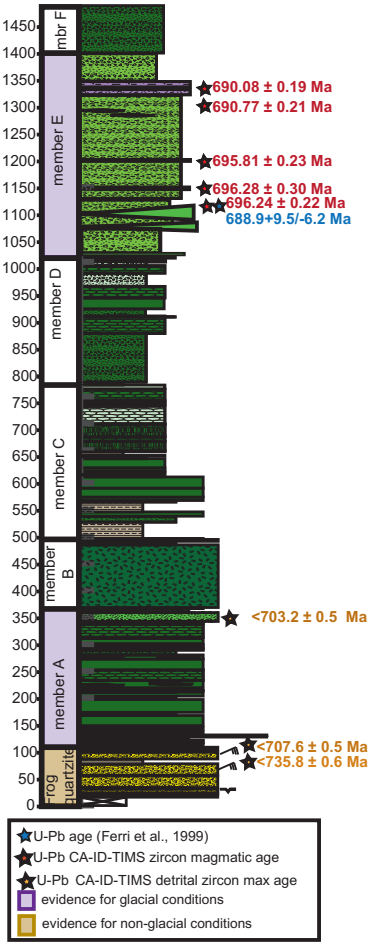


Figure 3.8: Composite stratigraphy and geochronology results with magmatic ages for samples A1416-8.6, A1418-161.8, A1418-207.5, A1418-326.1, and A1418-343.2. See figure 2 for lithology key.

majority clusters of dates from the same A1418 section of member E (fig. 8), conform to the constraints of stratigraphic superposition in their range from 696.28 ± 0.30 Ma near the base to 690.08± 0.19 Ma near the top. This ordering lends credence to the objectivity of the age assignments. The weighted mean dates for the majority clusters of zircons in samples from A1418 and A1416 are further interpreted as volcanic eruptive ages, as they are measured from stratigraphic horizons illustrating effusive and pyroclastic textures.

The efficacy of chemical over air abrasion is illustrated by sample A1416-8.6; the legacy age for this volcanic from Ferri et al. (1999) was obtained on zircons that underwent air-abrasion to assist in removing the outer portions of crystals more likely to have experienced lead loss. Five zircon fractions were analyzed and a York II best-fit regression line through these variably discordant populations gave an upper intercept $^{206}Pb/^{238}U$ of 688.9 +9.5/-6.2 Ma or a $^{207}Pb/^{206}Pb$ age of 689.1 ± 4.6 Ma. My age of 696.24 ± 0.82 Ma for the same horizon, based upon concordant and equivalent $^{206}Pb/^{238}U$ dates, is ∼7 Ma older due to the better mitigation of ancient lead loss using chemical abrasion, which accesses and removes high-U open-system domains throughout the crystal. Combined with the eruptive ages for section A1418, this new age verifies my correlation between the exposures of member E, with the 696.28 ± 0.30 Ma andesite at the base of member E at Matulka Creek ridge representing an isochronous horizon with the 696.24 ± 0.22 Ma rhyolite from member E west of Gataga Mountain (fig. 8).

Detrital spectra

The detrital zircon spectra record a shift in sources between the Frog quartzite and the basal Gataga Volcanics (fig. 5). Specifically there appears to be a more cosmopolitan source for the Frog quartzite and a more local source or a source similar to the Great Bear Lake magmatic zone or Slave craton for the basal Gataga Volcanics. The spectra from the Frog quartzite is similar to data from Tonian quartzites elsewhere in the Cordillera that are interpreted to have been transported via a transconti-

nental river system and recycling of material from the Grenville clastic wedge in northeast Laurentia (Rainbird et al., 2012; Dehler et al., 2010; Yonkee et al., 2014). The textural and compositional maturity of the Frog quartzite is also consistent with long transport. Similar lithological controls on detrital zircon spectra have been observed in other Neoproterozoic units on Laurentia where mature sandstone contains abundant grains interpreted to have been sourced from the distal provinces, whereas feldspathic quartzites tend to have more grains sourced from more local provinces (Dehler et al., 2010; Yonkee et al., 2014). The youngest grains for each of the samples, the ca. 740 Ma detrital ages in the Frog quartzite and the ca. 730 Ma detrital zircons in the basal Gataga Volcanics could be sourced from basement, such as the 736+23/-17 Ma Hugh Allan gneiss (U-Pb zircon McDonough and Parrish, 1991) and the 728+9/-7 Ma Deserters Gneiss (U-Pb zircon Evenchick, 1988). However, these are imprecise ages, and examination of the original data reveals evidence for inheritance. The ca. 740 detrital ages in the Frog quartzite also are similar to the 742 ± 6 Ma ash interpreted as the depositional age of the uppermost Chuar Group in Arizona (Karlstrom et al., 2004).

Later, during the eruption of the Gataga volcanics we suggest that tectonic activity associated with sedimentation and volcanism could have brought local sources to the surface. Thus the ca. 711-714 Ma zircon grains in the base of the Gataga Volcanics could be locally sourced. Alternatively, they could be from the 723-711 Ma Franklin LIP to the north (Heaman et al., 1992; Denyszyn et al., 2009a; Denyszyn et al., 2009b).

3.5.2 Igneous Geochemistry

No new bulk geochemical data was collected, as data was already available from both from the Gataga Volcanics and the Matulka group volcanics (Table 2 of Ferri et al., 1999). Geochemical data from mafic rocks was replotted on the Th/Hf/Nb triangular discrimination diagram (fig. 9A) of Wood (1980). Data clusters for both the Gataga Volcanics (PGm of Ferri et al., 1999) and the Matulka group (CPv of Ferri et al., 1999) fall in the alkaline within-plate basalts field.

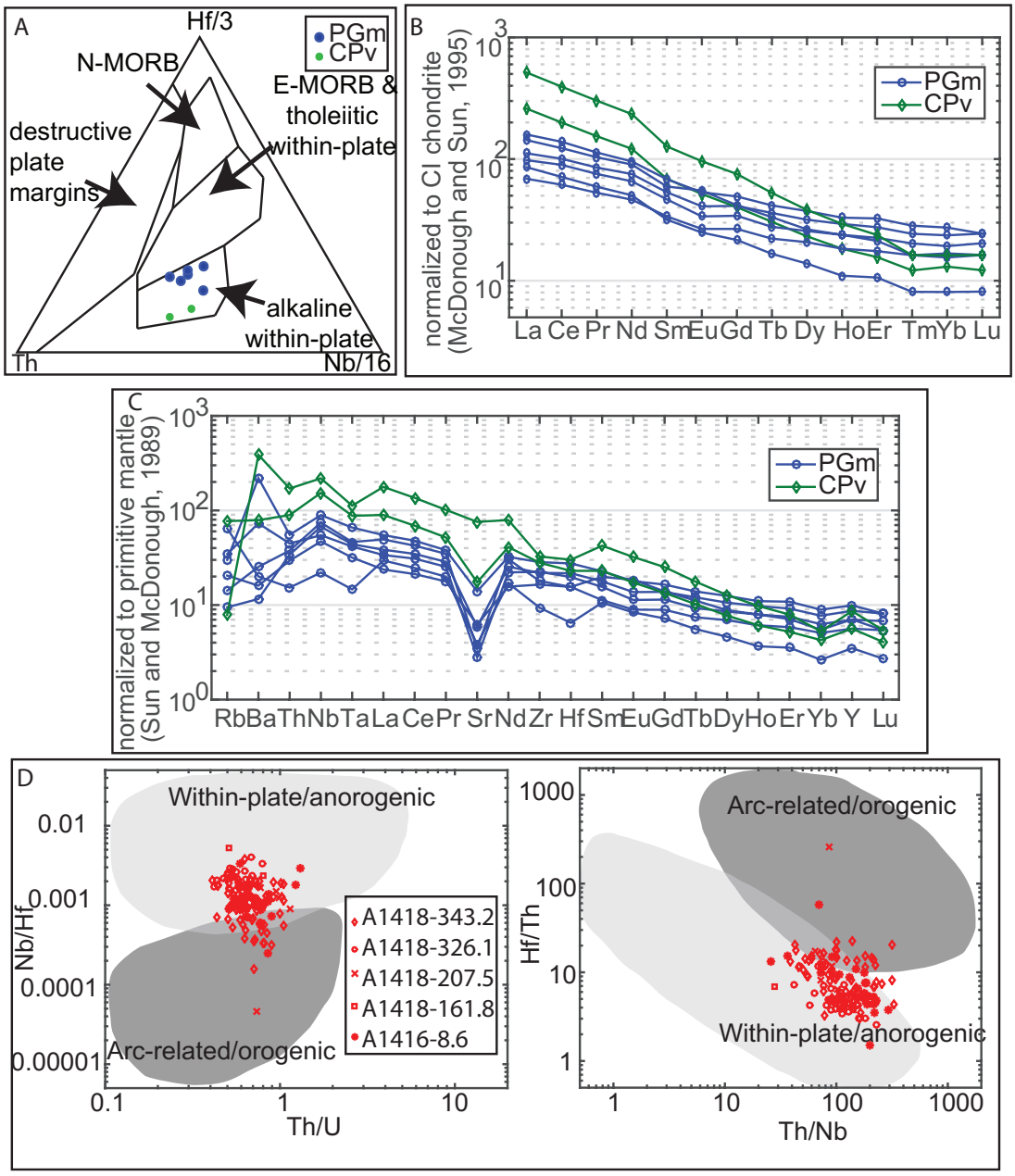


Figure 3.9: Volcanic zircon and bulk geochemistry: A. Wood diagram using geochemical data from the mafic Gataga Volcanics (PGm) and mafic Matulka group volcanics (CPv) from Ferri et al. (1999), B. CI Chondrite normalized REE spider diagram for the mafic volcanics, data from Ferri et al. (1999), C. Primitive mantle normalized spider diagram for the mafic volcanics, data from Ferri et al. (1999), D. Tectonic setting discrimination diagrams following figure 8 Yang et al. (2012), overlaid with geochemical data from member E zircons.

Additionally, when the normalized REE and trace elements are examined (trace elements normalized to primitive mantle of Sun and McDonough 1989, and REE normalized to CI chondrite of Mcdonough and Sun 1995), the data from the Matulka group volcanics display steeper signatures and depletion in heavier elements then data from the Gataga Volcanics (fig. 9B and C). These differences suggest that the Matulka group volcanics are geochemically distinct from the Gataga Volcanics.

New geochemical data (supplementary table S2) from the zircon extracted from member E and dated with LA-ICPMS were plotted on Nb/Hf versus Th/U and Th/Nb versus Hf/Th discrimination diagrams following the work of Yang et al. (2012). The data from the Member E of the Gataga Volcanics (fig. 9D) generally fall in the field of within-plate magmatism rather than the arc/orogenic field (Yang et al., 2012), consistent with volcanism related to anorogenic magmatism, such as rift-related magmatism.

3.5.3 Depositional Setting

Frog quartzite.

Cross-bedded sandstone, including tidally influenced herringbone cross-stratification, and mud-cracks, indicate that the Frog quartzite was deposited in a shallow intertidal or shoreface environment without evidence for glaciation. This is somewhat consistent with the original interpretation of Ferri et al. (1999); however, we suggest that this was a clastic dominated succession, not carbonate dominated. This is because we interpret the carbonates to the east of the Gataga Mountain Thrust as being different from the Frog quartzite and deposited much later, the carbonates within the Gataga Volcanics as being diagenetic carbonates, and the Matulka group carbonate strata is significantly younger.

Gataga Volcanics.

As the depositional environment of the Gataga Volcanics is intimately connected to the interpretation of the exotic clasts, origin of the diamictites, we will first focus broadly on the various acceptable depositional environments for members A-F, and then address the possibility of glacial influence. The interbedded mafic pillow lavas, massive flows, fine-grained volcaniclastic breccia and interbedded siltstone of member A are consistent with submarine to sub-ice shelf eruptions, as pillows are a distinct feature of basaltic lavas erupted under water, ice, or an ice shelf. The fine-grained volcaniclastic breccia could be submarine epiclastic deposits and laminated siltstone further suggests a deeper-water setting. Up-section, the deposition of interbedded mudstone, siltstone, massive mafic flows, and pillows basalts of Member C suggest relatively deep-water quiescent periods interrupted by volcanism that could be, at least in part, representative of a sub-aqueous or sub-ice shelf environment. Member C also contains massive flat-topped flows with columnar joints, which can form from rapid cooling due to post-solidification thermal contraction typical of subaerial flows, but is also found in subglacial eruptions (Tuffen et al., 2001; Edwards et al., 2002). The pillows, flows and volcaniclastic breccias of member D along with festoons and block and ash flows suggest higher energy pyroclastic deposits interbedded with effusive flows. The increased abundance of breccia in member D compared with members A and C below could reflect a slightly more evolved magma composition and increased magma viscosity, but could also be related to increased volatile content or decreased hydroclastic pressures. It is difficult to determine if the deposits are subaqueous or subglacial pyroclastic deposits or epiclastic deposits. The angular antidune clast suggests that the eruptions included fast low-density pyroclastic deposits (Cas and Wright, 1987). It may be expected that subaqueous eruptions would produce dense pumiceous quench fragmented blocky hyaloclastite fragments of silicic glass and hyaloclastite debris flow deposits. The combination of pillows and pyroclastic flows suggest that member D was deposited in a shallow subaqueous or subglacial envi-

ronment. The massive felsic volcaniclastic deposits of member E could represent subaqueous or subglacial eruptions, in the form of hydrothermal explosion breccias, hyaloclastites, lahars, and block and ash flows. Near the top of member E, the thinly laminated volcanic beds could be indicative of airfall ashes and tuffs, ground or ash-cloud surge deposits, or epiclastic reworking of volcanically derived sediment. The poorly exposed mafic gravel sized volcaniclastic deposits of member F marks a return to more primitive magma composition. These rocks are poorly bedded and could represent a hydroclastic or pyroclastic deposits. In summary, the Gataga Volcanics sharply overly the Frog quartzite and begin with subaqueous or subglacial mafic volcanism, and followed by continued mafic-intermediate subaqueous volcanism that interrupted relatively deep-water deposition of graded beds of siltstone interpreted as thin turbidites (member A). Volcanism continued with more felsic and explosive facies that were either erupted in a subaqueous or subglacial setting (members C and D). Next, the most extensive deposits were massive to crudely layered felsic volcaniclastic breccia, most likely of a subaqueous or subglacial origin consisting of hydrothermal explosion breccias or hyaloclastites, although they could also represent subaerial block and ash flows (member E). The uppermost clastic volcanics record a return to more mafic volcanism (member F). Overall, the progression of volcanism defines a magmatic system that is differentiating and becoming more felsic through time.

Discussion of glacial influence within the Gataga Volcanics

Volcaniclastic breccias, columnar jointing, as well as clasts in basal and upper matrix-supported diamictite are present in the Gataga Volcanics and interbedded units are water-lain, consistent with volcanic influenced deposition in either a sub-aqueous environment involving higher energy debris flows or in a glaciomarine environment. The key question is whether the volcanic deposits indicate subaerial, subaqueous or subglacial volcanism. Extensional tectonics can complicate interpretations, as rifting can create accommodation space and considerable relief that can aid in mass wasting and

debris flows. Alternatively rapid facies changes could be due to the heterogeneous nature of volcanic deposits and volcanic environments. Ideally, the presence of glacially striated or faceted clasts, or deposition on glacially scoured bedrock, can assist in distinguishing between glacial and non-glacial environments.

The best-documented intra-glacial and sub-glacial volcanoes are from Iceland and also Antartica. There, basaltic subglacial volcanoes display masses of pillow lavas followed by palagonitised breccias and volcaniclastic deposits (Werner et al., 1996; Skilling, 2009). Rhyolitic eruptions consist primarily of hyaloclastites and lava lobes followed by brecciated pumice and glass resulting from explosive activity and fragments of obsidian and stony rhyolite related to brecciated lobes (Furnes et al., 1980; Mathews, 1947; Cas and Wright, 1987). The Torfajökull volcanic complex, Iceland's largest rhyolite center is dominated by rhyolite erupted in subglacial and subaerial environments, with minor basaltic hyaloclastites and fluvioglacial sediments (Tuffen et al., 2001). Subglacial volcanism is distinguished by the following features: 1) dominance of breccias, with evidence for magma-water interaction (perlitised obsidian, blocky ash shards, fines-rich veins, matrix vesicles); 2) no evidence for the existence of paleotopography which could have confined a non-glacial lake (Smellie and Skilling, 1994, Smellie and Hole, 1997); 3) columnar jointing suggesting that many lava bodies in the sequence chilled against steeply inclined, sub-planar surfaces such as ice walls (Lescinsky and Sisson, 1998); 4) faceted clasts and a mud matrix consistent with a subglacial derivation (Tuffen et al., 2001); and topographic features like flat-topped flows.

Glacial deposits are typically unsorted, angular, chemically immature and rarely contain clays. Glaciomarine deposits are commonly dominated by till sheets that form near the ice-grounding line when ice reaches a lake or sea and starts to melt, releasing glacial debris into the water. Till sheets are also associated with turbidites, submarine debris flows, and storm deposits (Eyles et al., 1985; Lonne, 1995; Wang and Hesse, 1996). Till sheet-debris flow facies associations can be difficult to distinguish from non-glacial submarine debris flows, or if there is significant volcanic debris, from

volcanic lahars, a mass of flowing volcanic debris intimately mixed with water (Jerram and Petford, 2011). Additionally lahars can entrain non-volcanic clasts and occur subaqueously, subaerially, or subglacially when subglacial eruptions cause the ice to melt and generate high water content (Cas and Wright, 1987; Jerram and Petford, 2011). Finally, large clasts can be transported long distances in icebergs and as the icebergs melt, the clasts fall to the sea floor and typically land in muds, becoming dropstones. Dropstones are associated with laminated mud (or other, shallower water deposits) (Thomas and Connell, 1985; Postma et al., 1988).

Diamictite unit of Member A. The diamictite unit in member A occurs near the base of the volcanics, between beds of explosive volcanic rocks. Outsized volcanic clasts, especially if they are pumice clasts, could be emplaced directly through airfall from a volcanic source, but this is an unlikely explanation for the polymict clasts we observed. In this case, the outsized clasts do not appear to be related to graded beds nor show evidence of imbrication, and some of the clasts are not locally sourced. The pale mature quartzite clasts could be from the Frog quartzite below, but the dark quartzite and the carbonate clasts have an uncertain origin. As many of the clasts display some amount of rounding, that seems to argue against exotic clasts of unknown source having purely a magmatic source, such as lithic clasts or wall rock derived from the magma conduit. We suggest that the diamictite of member A is possibly a subglacial till sheet or lahar. However, we cannot rule out a marine debris flow interpretation, as direct indicators of glacial sedimentation such as glacial faceting and striating of clasts were not documented in this diamictite unit. As the diamictite bed is within the stack of subaqueous volcanics, it is likely that the diamictite was deposited synchronously with local volcanism and that the dates on the volcanic rocks also provide ages for the formation of the associated diamictite units.

Diamictite and exotic clasts in Member E. Potential indicators of a glacial influence include exotic clasts such as the rounded granite clast near the base of Section A1419, as well as laminated siltstone and carbonate clasts. However, the dominant clast and matrix lithologies are volcanic and ho-

mogeneous, which suggests that any potential glacial influence was overwhelmed by the volcanic influence. Near the top of member E, the thinly laminated volcanic beds could be indicative of airfall ashes and tuffs, ground or ash-cloud surge deposits, or epiclastic reworking of volcanically derived sediment. Additionally, within these units, diamictites with bed penetrating dropstones that deform laminations suggest a glaciogenic origin. However, in volcanic settings, dropstones of country rock or volcanic rocks can form as near vent ballistic blocks and bombs, particularly in phreatomagmatic eruptions (Cas and Wright, 1987). We neither observed bread-crust textures characteristic of volcanic bombs nor faceted or striated clasts to distinguish between these two depositional settings. Taken together, we suggest the volcanic facies preserved at Gataga Mountain are similar to those described from sub-ice settings in Iceland and Antartica (for example Furnes et al., 1980; Mathews, 1947; Cas and Wright, 1987; Tuffen et al., 2001; Smellie and Skilling 1994, Smellie and Hole 1997) and are broadly consistent with eruption in a sub-ice to subaqueous setting below an ice shelf.

Iron formation

The return of iron formation to the sedimentary record is a distinctive characteristic of the Sturtian glaciation (Macdonald et al., 2010b; Cox et al., 2013) and has been previously documented in several other basal glaciogenic units of the Windermere Supergroup (Klein and Beukes, 1993, Halverson et al., 2011; Macdonald et al., 2010a; Cox et al., 2013; 2015; Baldwin et al., 2016). Neoproterozoic iron formation has classically been linked to Snowball Earth and the idea that ice cover would restrict ocean-atmosphere O_2 exchange, leading to bottom-water stagnation (Kirschvink, 1992; Klein and Beukes, 1993). However, recent syn-Snowball ocean circulation models suggest that ocean mixing is just as vigorous during a Snowball glaciation as it is during ice-free times (Ashkenazy et al., 2013). Moreover, the classic model would predict that the iron formation should form during deglaciation when the ocean and atmosphere mixed and oxygenated runoff provided and oxidant to drive insoluble Fe-oxide precipitation; however, iron formations are not restricted to the top of glacial deposits

but instead tend to be associated with glaciation, localized in semi-restricted rift basins (Macdonald et al., 2013b; Cox et al., 2013). The stratigraphy and geochronology at Gataga Mountain suggest that iron formation was deposited early in the Sturtian glaciation. The association with the Gataga Volcanics is consistent with a volcanic, hydrothermal iron source (Cox et al., 2013; 2015) and the role of local restriction in rift basins providing protection from eddy mixing (Ashkenazy et al., 2013).

Matulka group

The ooid grainstone and laminated siltstone and sandstone of the Matulka group were deposited during non-glacial conditions. Ferri et al. (1999) suggested that the clastic units of the Matulka group could be correlated with coarse clastic rocks further north, and the rapid changes in facies of the associated units were due to block faulting related to extensional tectonism, consistent with syn-sedimentary alkalic volcanism. We propose that the ooid grainstone was deposited in an agitated carbonate bank or shoal. A high-energy subtidal depositional setting associated with tidal sand bars and/or a migrating barrier complex is needed to generate the ooids, and, in section A1419, the large rip up clasts of carbonate suggest storm or wave activity. The overlying finely laminated graded beds of the maroon-green siltstone display no evidence for storm or wave activity and could indicate an overall deepening of the basin. Finally, near the top, the renewed carbonate deposition and immature sandstone suggest a shallowing of the basin along with new proximal detrital input.

Unconformities

My stratigraphic data, map relationships, and age model imply two unconformities in the sequence. The first, between the Frog quartzite and the Gataga volcanics, is suggested by the sharp contact and the dramatic change in environment. For the Gataga Volcanics, the depositional environment dramatically changes from the shallow shoreface environment with desiccation cracks of the Frog quartzite to the deeper water epiclastic volcanic deposits, basalt flows as well as the laminated silt-

stones and glacially influenced diamictite of the basal Gataga Volcanics. This major change in depositional environments along with the sharp contact between the two suggests that there may be an uncertain amount of time missing.

Second, there is likely an unconformity with significant time missing between the Gataga Volcanics and the Matulka group. The map relations and the truncation of member F of the Gataga volcanics into carbonate of the Matulka group suggest an angular unconformity. The lack of similarity in the volcanic geochemistry between the Gataga Volcanics and the Matulka group volcanics further indicates that the Gataga Volcanics are distinct from the Matulka group and the Matulka group likely does not conformably overly the volcanics. We propose that the rift related volcanics of the Gataga Volcanics and the Matulka volcanics represent two separate rift-related volcanic events.

3.5.4 Regional Correlations

Regional equivalents of the Gataga Volcanics include the broadly distributed massive diamictite and stratified glacial deposits with coarse-grained ice-rafted debris of the Rapitan Group in the Ogilvie Mountains (Eagle Creek formation) (figs. 10 and 11), and the Mackenzie, and Wernecke Mountains (Mount Berg, Sayunei and Shezal) (fig. 11). In the Ogilvie Mountains, a glaciogenic origin for the Rapitan Group is confirmed by the presence of faceted and striated clasts, bed-penetrating dropstones, common outsized and exotic clasts and glacial push structures in the Eagle Creek Formation (Macdonald et al., 2011; Macdonald et al., 2010a; Strauss et al., 2014b). In the Mackenzie and Wernecke Mountains, the Rapitan Group depositional environment has been interpreted as a glacially influenced marine setting, based on the presence of lonestones, striated clasts, and till pellets in otherwise fine- to medium-grained turbiditic rocks (Young, 1976; Eisbacher, 1981; 1985). Additionally, the Rapitan Group contains jasper-hematite iron formation that can be as much as 100 m thick (Eisbacher, 1981; Yeo, 1981; Baldwin et al., 2016).

In the Ogilvie Mountains, the Eagle Creek Formation is underlain by the Mount Harper Vol-

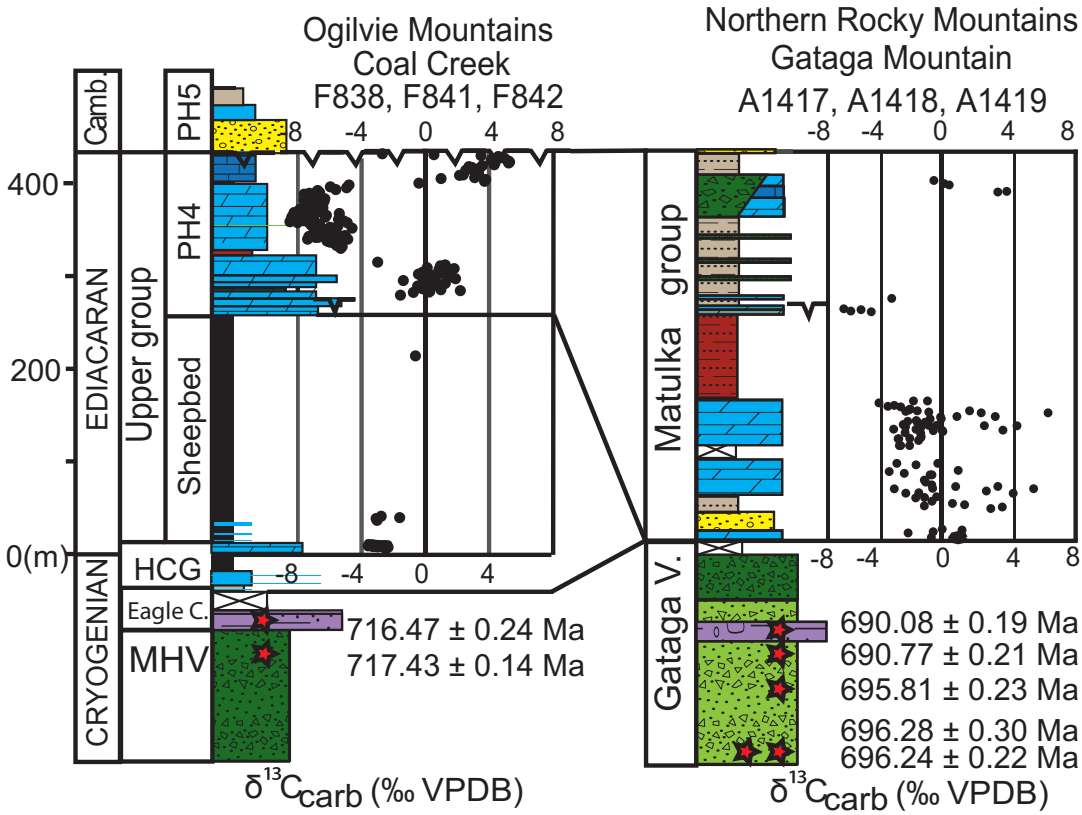


Figure 3.10: Composite chemostratigraphy and regional correlations of the Gataga Volcanics with strata in the Coal Creek inlier in northwestern Canada (Macdonald et al., 2013b). See figure 2 for lithology key.

canics. A rhyolite dome near the top of the volcanics was dated with CA-ID-TIMS U-Pb zircon at 717.43 ± 0.14 Ma and a tuff within the overlying diamictite was dated at 716.47 ± 0.24 Ma (Macdonald et al., 2010a). Although we broadly correlate the Gataga Volcanics with the Sturtian glaciation, the presence of 707 Ma detrital zircon near the base of member A suggests that much of the early stage of glaciation is missing and that the Gataga Volcanics are not strictly correlative with the Mt. Harper Volcanics. This is also consistent with an unconformity at the base of the Gataga volcanics.

Farther south, near the British Columbia-Yukon border, Neoproterozoic strata outcrops near Toobally Lake and Pool Creek. At Toobally Lake, there are outcrops of the massive, orange weathering, mud matrix-supported glacial diamictite of the Toobally Formation as well as overlying alkali basalt tuffs and breccia (Pigage and Macnaughton, 2004; Pigage, 2006; Pigage, 2009). Samples were analyzed with laser ablation inductively coupled plasma mass spectrometry (LA-ICPMS), and two young zircons were isolated from the one sample from the Toobally Formation (653.1 ± 2.9 Ma, 649.0 ± 2.9 Ma with 1σ error, Pigage, 2009). However, these ages should be viewed critically since only two young zircon grains were isolated and U-Pb microbeam techniques are not always as precise and accurate as needed. Typical dates from U-Pb microbeam techniques such as LA-ICPMS have 2σ uncertainties that are about an order of magnitude larger than for ID-TIMS (Condon and Bowring, 2011), and although the dates from the two techniques usually overlap, in some cases the standard deviation of spot analysis date on a single zircon will not encompass the ID-TIMS date on that zircon (Schoene, 2014).

In the Pool Creek area, outcrops of pale quartz-rich sandstone and green argillite with volcanic clasts are exposed and appear to be intruded by the Pool Creek Syenite (Allen et al., 2001; Pigage, 2006; Pigage, 2009; MacNaughton et al., 2014). Some samples were analyzed with LA-ICPMS, but only one young zircon with large error was obtained from the argillite unit (654 ± 25 Ma with 1σ error- Pigage, 2009). Zircon fractions isolated from the Pool Creek Syenite underwent ID-TIMS (without chemical abrasion) and displayed very strange U-Th-Pb systematics, with very low U con-

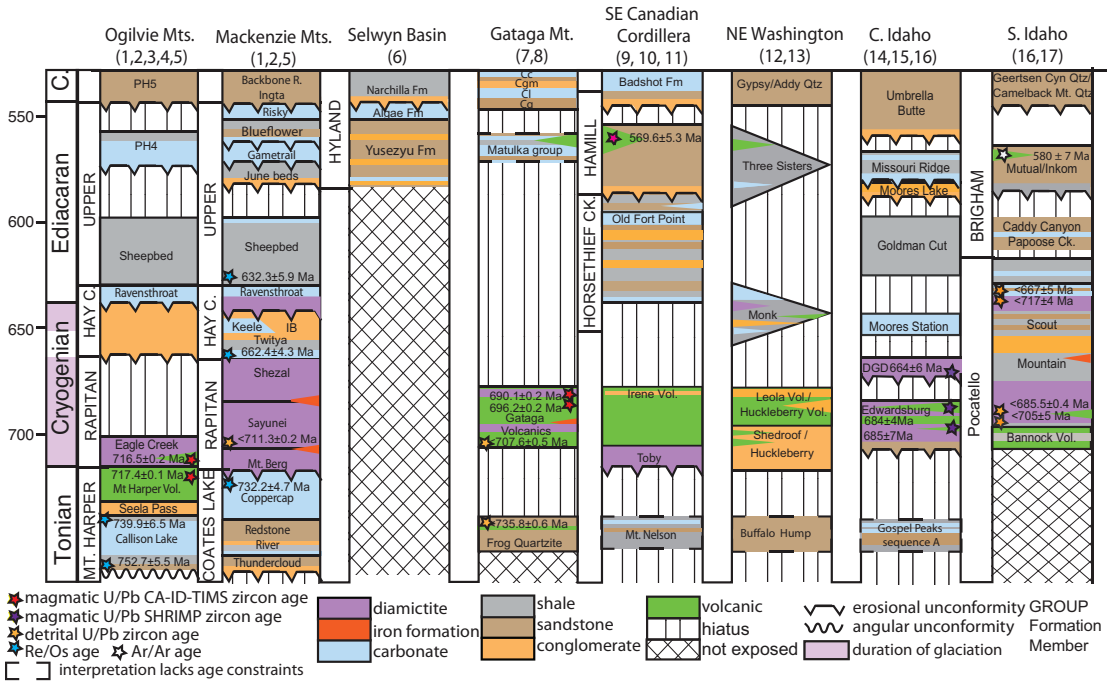


Figure 3.11: Correlation chart of key Windermere Supergroup successions on the western margin of Laurentia. Schematic stratigraphy and age constraints are modified from: (1) Macdonald et al., 2010a; (2) Macdonald et al., 2013b; (3) Strauss et al., 2014a; (4) Strauss et al., 2015; (5) Rooney et al., 2014 and 2015; (6) Moynihan, 2014; (7) This study; (8) Ferri et al., 1999; (9) Warren, 1997; (10) Kendall et al., 2004; (11) Devlin, 1989; (12) Brown et al., 1994; (13) Miller, 1994; (14) Lund et al., 2003; (15) Lund et al., 2010; (16) Fanning and Link, 2004; (17) Keeley et al. (2013). Also highlighted are potential durations for the Sturtian (717-662 Ma) and Marinoan (655-635 Ma) Snowball Earth glaciations. Dashed boxes highlight interpretations that lack supporting geochronological data.

tents and very high Th contents (Pigage and Mortensen, 2004). In addition to the atypical U and Th concentrations, most of the zircon fraction analyses were scattered along the concordia rather than on it, likely reflecting the effects of post-crystallization Pb-loss (Pigage and Mortensen, 2004). The resulting U-Pb isotopic dating of zircon fractions from the different intrusive phases resulted in a cluster of ages of 640-650 Ma for the Pool Creek Syenite and associated dykes (Pigage and Mortensen, 2004). The Pool Creek Syenite is not known to intrude the Toobally Formation.

In general, the work on the Neoproterozoic strata in the Toobally Lake and Pool Creek area suffers from imprecise geochronology and poor exposure that limits conclusive interpretations of the stratigraphic relationships and regional correlations. The Toobally diamictite was suggested to be Marinoan in age as the preferred depositional age was 650 Ma based on the detrital zircon LA-ICPMS ages (Pigage, 2009). Furthermore, the Toobally Formation was previously correlated with the Stelfox member of the Ice Brook Formation in the Mackenzie Mountains and with the Vreeland Formation to the south (see discussion below) based the stratigraphic position of the Toobally Formation beneath lower Cambrian strata and on the presence of lithological similarities. One such similarity was a parallel laminated dolostone, at least 20m thick and low in the Toobally succession, with similarities to Marinoan cap carbonates (Pigage and MacNaughton, 2004). This dolostone was interpreted to be an olistolith as its bedding was dramatically different from the regional dip of the Toobally Formation and folding was unlikely to cause the difference (Pigage and MacNaughton, 2004). No similar cap carbonate was observed to overlie the Toobally Formation (Pigage and MacNaughton, 2004; Pigage, 2009). It was argued that the absence of a cap carbonate might indicate non-deposition or erosion above the Toobally Formation (Pigage and MacNaughton, 2004). However, considering the uncertainty in the lithological correlations and in the LA-ICPMS ages, it is also possible that the Toobally diamictite and overlying volcanics are correlative with the Gataga Volcanics.

To the south in the central Rocky Mountains, correlatives of the Gataga Mountain sequence

may be non-exposed, or could potentially correlate with the Vreeland Formation, which has previously been assigned a Marinoan age (Smith et al., 2011; McMechan, 2000; McMechan, 2015). Vreeland formation was originally suggested to be correlative with the Sturtian glacial deposits (Slind and Perkins, 1966), the revision was due to cap carbonate features, mapping relations, and its stratigraphic height in the Windermere succession combined with pre-existing age constraints. The Vreeland formation is overlain by a limestone cap carbonate and laminated dolomite olistoliths with negative $\delta^{13}C_{carb}$ values that were correlated with Marinoan cap dolomites (McMechan 2000). However, in some cases, such as in the Ogilvie Mountains, strata between the Sturtian glacial deposits and Marinoan cap carbonate is only a few tens of meters thick (Macdonald et al., 2010a) or absent (Macdonald et al., 2013a). The current mapping relationships of the Vreeland formation suggests laterally continuous facies and stratigraphic continuity, while the Rapitan shows evidence of syn-sedimentary tectonism (Eisbacher 1981), which has led authors to suggest that the Vreeland post-dates major tectonic-activity at the base of the Windermere. Despite these lines of evidence for a Marinoan age for the diamictite, we want to point out that in some places the Vreeland formation has been documented as demonstrating rapid facies into grits and argillites of the lower part of the McKale formation, which might be more consistent with a Sturtian age (McMechan, 1990).

Finally, as the Vreeland Formation lacks any geochronological constraints, the key argument for its being Marinoan is that it is well above the base of the Windermere succession. This assertion was based on the observation that it was underlain by at least 568 meters and interfingers with 150 meters of siltstone, argillite and calcareous siltstone of the Paksumo formation near Paksumo Pass and in the Deserters Range by unnamed succession of chloritic wacke, quartzite, pelite and minor limestone (as well as minor amphibolite), non-conformably overlying the 728+9/-7 Ma Deserters Gneiss (U-Pb zircon Evenchick, 1988). Because previous estimates of the age of the basal Windermere were 770 Ma, authors assumed that the Vreeland was much older than the Toby and Rapitan Diamictites, and thus must correspond to the younger glacial interval, not the older. With the updated age

constraints (eg. Macdonald et al., 2010; Strauss et al., 2014; Rooney et al., 2015), this argument may be less persuasive than it was previously. Finally, we want to point out that the Vreeland diamictite expands to over a kilometer in thickness, and Sturtian-age diamictites are commonly thick in the Cordillera whereas Marinoan diamictites are often thin or absent (for example Macdonald et al., 2013a; Eisbacher, 1978). Consequently, we suggest that Vreeland Formation may be correlative with the Gataga Volcanics, the Rapitan Group and the Sturtian glaciation, however, we acknowledge that this goes against several lines of evidence that suggest that the Vreeland may in fact be younger.

In southern British Columbia, we correlate the Gataga Volcanics with the undated glaciogenic Toby Formation and the localized rift-related mafic volcanic rocks of the Irene Formation (fig. 11). The Toby Formation is gradationally overlain by mafic basalt flows, basalt breccia, and pillow basalts of the Irene Volcanics (Brown et al. 1994; Warren, 1997). The pillows are observed to have chilled margins and minor intrapillow micrite. There are also mafic tuff, tuff breccia and hyaloclastic. At the top of the Irene Volcanics occurs a 100 m thick conglomerate (Brown et al. 1994). In Washington State, these units are likely correlative with the Huckleberry Formation, the Shedroof Conglomerate and Leola Volcanics (Miller, 1994).

Further south, we correlate the Gataga Volcanics with the Edwardsburg Formation and the Bannock Volcanic Member of the Pocatello Formation of southeastern Idaho (Lund et al., 2003; Fanning and Link, 2004; Keeley et al., 2012). Although both the Edwardsburg and Pocatello formations include poorly sorted, matrix-supported diamictites, a glacial origin for the Edwardsburg Formation has not been established. The Edwardsburg Formation has been dated by SHRIMP methods on zircon to 685.6 ± 7 Ma (Lund et al., 2003). A glacial origin has been demonstrated for the Scout Mountain Member of the Pocatello Formation, and epiclastic deposits at Oxford Mountain have been dated with CA-IDTIMS at 685.5 ± 0.4 Ma, providing a maximum depositional age constraint for the upper portion of the glacial succession (Keeley et al., 2012).

We attempted to constrain the age of the Matulka group and associated volcanic rocks using the

carbon isotope chemostratigraphy, but this was hindered by the lack of definitive trends, the dominance of scatter and highly altered nature of the carbonates. Based on the data from the less recrystallized carbonates (A1417), we compared the Matulka group with strata in the Coal Creek inlier, Ogilvie Mountains (fig. 10), which also overlie volcanic rocks (Macdonald et al., 2010; 2013b). Using this comparison we suggest that the Matulka group could be correlative with the PH4 in the Coal Creek inlier, both displaying broadly similar stratigraphy and correlative carbon isotope trends, with negative excursions in the middle of the section, and at the top, swinging to positive values around +4‰ and then back towards 0‰. In the Mackenzie Mountains the Sheepbed Formation, which underlies PH4 in the Coal Creek inlier, has been dated to 632.3 $\pm$ 5.9 Ma (Re-Os from Rooney et al., 2015), while strata correlated with PH4 have been suggested to be ca. 570 Ma due to preserved Ediacaran biota (Macdonald et al., 2013b). Thus, we suggest that the Matulka group may be younger than 630 Ma, and likely close to ca. 570 Ma. This is also consistent with the suggested unconformity between the Matulka group and the underlying Gataga Volcanics.

In addition to the strata exposed in the Ogilvie Mountains, the Ediacaran-Cambrian Hyland Group is exposed in the Selwyn Basin in the southern Yukon, where there is a similar sequence of carbonate followed by maroon mudstone and additional carbonate and siliciclastic strata (fig. 11). The Hyland Group consists of the Yusezyu, Algae, and Narchilla formations (Colpron, 2012). The Yusezyu Formation is dominated by brownish-grey shale, sandstone and grit (pebbly sandstone), becoming calcareous near top of formation (Colpron, 2012). The basal Algae formation includes 250-350 m thick of pale to dark grey, thinly to medium-bedded cliff-forming limestone and dolostone with ooids, intraclasts, cross beds and minor chert. There is an irregular erosional surface between it and the overlying Cambrian Narchilla Formation. The Narchilla Formation is an almost 1 km thick deformed sequence of dominantly fine-grained clastic rocks. In some localities, the Narchilla Formation has been divided into two members, one dominated by grey siltstone and shale, and one dominated by maroon and green argillite with a distinct contact between them (Cecile, 2000). In

other localities, the Narchilla Formation is observed to have a highly variable basal siliciclastic to conglomeratic-grit member overlain by a thin-bedded bioturbated green, mauve or maroon mudstone, siltstone, and shale, with some sandstone-rich intervals (Moynihan, 2014). Lithological correlations would suggest that the basal Matulka group could be correlative with the Algae Formation, and the Maroon-siliciclastic member is correlative with the Narchilla Formation, suggesting that the Matulka group could be as young as Cambrian.

Further south, the Matulka group may correlate with the Hamill Group in the SE Canadian Cordillera (Devlin, 1989; Warren, 1990; Colpron et al., 2002), the Three Sisters Formation in northeast Washington (Miller, 1994), and the Missouri Ridge and Mutual/Inkom formations in Idaho (Lund et al., 2003; Christie-Blick 1997; Link et al., 1993). Most of these units include carbonates and siliciclastics, as well as volcanic deposits in two cases (fig. 11). My suggested correlation of the Matulka group with later Ediacaran age strata is influenced by the known existence of Hamill Group volcanics already dated to later Ediacaran time.

3.5.5 Rift History

Although my new data do not resolve uncertainties related to the paleogeography and identity of the conjugate continent, or the geometry of rifting along the western margin of Laurentia, it does bear on the timing and number of rift events. As rifting is connected to alkalic igneous rocks and coarse sedimentation, more data on those sequences assists in understanding those connections. Several authors favor discrete rift events rather than protracted rifting, such as Colpron et al. (2002) who suggested that there were two stages for the rifting leading to continent separation, with the first stage of rifting at 750 Ma to 700 Ma and a second stage of rifting at 600-570 Ma. My data, along with recent geochronology from Yukon and Idaho suggest that most of the rift-related magmatism occurred between 716-660 Ma (Macdonald et al., 2010a; Keeley et al., 2012). This appears to be distinct from the ca. 775 Ma magmatism associated with the Gunbarrel LIP (Harlan et al., 2003; Mil-

ton et al., 2014) and the subsequent 775-717 Ma subsidence in the ChUMP basins and equivalents in Canada.

Our new ages for the Gataga Volcanics suggest a <707 Ma maximum depositional age for the basal Gataga Volcanics and include 696-690 Ma magmatic ages for upper felsic Gataga Volcanics. Furthermore, the volcanic and zircon geochemistry suggest anorogenic rift type volcanism.

When considering this rift stage and the Gataga data in relation to other sections along the margin (fig. 11), rift related volcanism in the northern Coal Creek inlier of the Yukon occurred predominantly prior to ca. 717 Ma, perhaps triggered by the Franklin LIP. We suggest that the Gataga volcanism is part of a pulse of ca. 710-685 Ma magmatism further south along the western margin. In central Idaho, the mixed diamictite and volcanics of the Edwardsburg have a basal 685±7 Ma magmatic age (SHRIMP U/Pb zircon), and an upper 684±4 Ma magmatic age (SHRIMP U/Pb zircon) (Lund et al., 2003). Also, in southern Idaho, within the lower Scout Mountain member of the Pocatello formation, zircon from reworked tuffs have been dated to <685.5 ± 0.4 Ma (detrital CA-IDTIMS U/Pb zircon; Keeley et al., 2012), and <705 ±5 Ma (detrital SHRIMP U/Pb zircon; Keeley et al., 2012). Although these deposits are not primary, the zircon provenance does appear to be proximal (Keeley et al., 2012). In addition, near the top there is a 717 ±4 Ma (SHRIMP U/Pb zircon) age on a porphyritic silicic clast (Fanning and Link, 2004) has been used to suggest protracted volcanism in that area spanned 30 Myr. There may be an additional pulse of younger magmatism that is hinted at in overlying units, with a 664±6 Ma magmatic age (SHRIMP U/Pb zircon; Lund et al., 2010) on a tuff within an upper diamictite in Central Idaho, and in southern Idaho, a <667±5 detrital age (SHRIMP U/Pb zircon concordia; Fanning and Link, 2004) from a reworked tuff within an upper sandstone.

Geochemically distinct volcanism in the non-glacial Matulka group is likely related to a younger episode of rifting. We propose that the Matulka group is broadly correlative with unit PH4 in the Yukon, and with the Hamill-Gog Group in southern British Columbia, which contains volcanics

dated with U-Pb TIMS on zircon at 569.6 ± 5.3 Ma (Colpron et al., 2002). Additionally, in the Gataga area, the volcanics in the Matulka group are overlain by a Cambrian conglomerate unit (Cgm) that is potentially rift related, which suggests that extension may have been active from the Ediacaran to earliest middle Cambrian.

3.5.6 Cryogenian Glaciation

Existing geochronological constraints on the Sturtian glaciation from the Rapitan Group in the Ogilvie Mountains demonstrate that it started by ca. 716 Ma (Macdonald et al., 2010a). If the Sturtian glaciation lasted >55 million years (Rooney et al., 2014; 2015), then the diamictite units within the Gataga Volcanics likely were deposited during the Sturtian glaciation. The volcanic stratigraphy of the Gataga Volcanics is consistent with eruption in sub-glacial conditions, with evidence for ca. 690 Ma glaciation in the Gataga area including cosmopolitan clasts, diamictite, and dropstones. The detrital age from the Frog quartzite gives a maximum age constraint of <735 Ma on the onset of the glaciation in the area. Additionally we provide a maximum age constraint at the base of Member A of <707 Ma, about 10 meters below the basal diamictite, but above the contact between the Frog quartzite and the Gataga Volcanics.

Near the border of Yukon and the Northwest Territories, a detrital zircon CA-ID-TIMS U-Pb date of 711.34 ± 0.24 Ma was reported from the Sayunei Formation and used to argue that onset of the Sturtian glaciation was not synchronous on the Laurentian margin (Baldwin et al., 2016). However, the sample was collected at the top of the Sayunei Formation from a cross-bedded hematitic siltstone beneath a thin iron formation, just below the transition from the Sayunei to the Shezal Formation (Baldwin et al., 2016). In the measured section from which they collected this sample from, there is about 200 m of Sayunei Formation below the sample, but the base of the section was not exposed. Typically, the Sayunei Formation is several hundred meters thick and sits above an unconformity of unknown duration, likely related in part to glacio-eustatic sea level fall and in part

to syn-depositional faulting (Eisbacher, 1981; 1983). Thus, the 711.33 ± 0.25 Ma date is a maximum age constraint for the top of the Sayunei Formation and base of Shezal Formation, and is consistent with synchronous onset of the Sturtian glaciation by ca. 716.5 Ma. Similarly, for the Gataga Volcanics, we suggest that there is an unconformity with an uncertain amount of time missing at the base, and the only maximum constraint we have on the onset of glaciation is the <735 Ma detrital zircon constraint from the top of the non-glacial Frog Quartzite.

3.6 Conclusions

Here we report new ages for the Gataga Volcanics with a <707 Ma maximum depositional age for the basal Gataga Volcanics and 696-690 Ma eruptive ages for upper felsic Gataga Volcanics. Evidence for ca. 690 Ma glaciation includes cosmopolitan clasts, diamictite, and dropstones suggestive of sub-glacial volcanism during the Sturtian Snowball Earth glaciation. Finally, the correlation of the Matulka with the Upper group in the Yukon indicates that there could be significant time missing between the Gataga Volcanics and the Matulka group, and that there are thus two episodes of extension, basin formation, and magmatism recorded at Gataga Mountain. The first episode includes the Gataga Volcanics and associated volcanism, and is part of southward propagating extension along the western margin of Laurentia. This volcanism is tentatively syn-glacial in the Gataga area. A second occurrence of geochemically distinct anorogenic/rift-related volcanic rocks occurs in the non-glacial Matulka group, which we correlate with ca. 570 Ma volcanism and basin formation along the margin.

4

Paleomagnetism of the Chuar Group and evaluation of the 780-720 Ma Laurentian apparent polar wander path: implications for the makeup and breakup of Rodinia

4.1 Abstract

During the Neoproterozoic Era (1000-541 Ma) the Earth experienced global glaciations, the diversification of crown group eukaryotes, and potentially a second great oxidation event, all of which are

A version of this chapter is being prepared for publication: Eyster, A. E, Weiss, B. P., Karlstrom, K. E., Kremers, J., Macdonald, F.A. *in prep for EPSL, AJS or GSAB*

commonly associated with the breakup of the supercontinent Rodinia. However, both the makeup of Rodinia and the timing of breakup remain poorly constrained. Current paleomagnetic reconstructions depict the breakup of the Cordilleran western margin of Laurentia at ca. 780-750 Ma. Meanwhile, geological data from the Cordillera suggest that rift-related volcanism occurred predominantly between 720-680 Ma and at ca. 570 Ma, and that the eventual development of the passive margin did not occur until the Precambrian-Cambrian boundary at ca. 540 Ma. Here I report new paleomagnetic data from the 780-729 Ma Chuar Group of the Grand Canyon Supergroup, and re-evaluate paleogeographic models for the makeup and breakup of Rodinia along the Cordilleran margin of Laurentia. The new poles are preserved in hematite and magnetite, and the primary nature of this paleomagnetic direction is supported by five of the seven Van der Voo (1990) reliability criteria. In addition to this primary direction, pervasive mid to high temperature overprints carried by hematite were identified. I incorporated these updated paleomagnetic poles with recent geochronological data and existing paleomagnetic data to present a new and revised ca. 780-720 Ma Laurentian Apparent Polar Wander Path. Having examined the 780-720 Ma paleomagnetic database of other cratons, I present reconstructions for 780 Ma, 750 Ma and 720 Ma, and conclude that the dataset is most consistent with a modified AUSMEX configuration at both 780 Ma and 750 Ma (as well as 1070 Ma). Moreover, I do not find a good match for a rifted conjugate margin on any major craton. I conclude that there may not have been a conjugate margin for the Cordilleran western Laurentia and that instead 780-720 Ma tectonism was associated with right-lateral strike slip motion along the present day Mexico margin and associated minor extension on the Cordilleran margin. On the northern Laurentian margin, rifting was initiated by the Franklin LIP at ca. 720 Ma, with magmatism and extension propagating south down the margin (in present day coordinates). This scenario does not necessitate the separation of a major craton from the Cordilleran margin of Laurentia during the Neoproterozoic and suggests that instead the rift-drift transition near the Precambrian-Cambrian boundary may have been the result of the rifting of a ribbon continent with

Laurentian affinity.

4.2 Introduction

The identification of the supercontinent Pangea and the associated concept of the changing surface configuration of the continents dramatically changed our understanding of the Earth and its dynamics. Now the theory of plate tectonics includes detailed reconstructions of plate speeds and configurations over the past 200 million years, spanning the tenure of Pangea. Paleogeographic reconstructions of earlier eras are more uncertain. Multiple authors have proposed temporal cyclicity to supercontinent amalgamation and breakup continuing back into the Proterozoic (Li et al., 2006; Zhong et al., 2007; Nance et al., 2014; Murphy et al., 2009), yet beyond the Pangea, the supercontinent cycle remains hypothetical. Tectonics and continental configurations associated with supercontinent cycles may drive climate and evolutionary change on geologic timescales. For example, the breakup of supercontinent Rodinia has been implicated in the initiation of Snowball Earth (Li et al., 2008; Kirschvink et al., 1992; Godderis et al., 2004). The existence and timing of supercontinents throughout Earth's history may influence many other aspects of the long-term Earth system, from the core to the atmosphere (Reddy and Evans, 2009, Nance et al., 2013). To investigate this supercontinent cycle and its connection to the rest of the Earth system, first the timing and configuration of each potential supercontinent must be resolved. The most recent supercontinent, Pangea, is the best understood. The timing and configurations of earlier supercontinents, Gondwana, and especially Rodinia, are less well constrained.

There is general agreement that Earth's continental crust assembled to form the supercontinent Rodinia in the late Mesoproterozoic and early Neoproterozoic. Rodinia is thought to have been produced by collisional events of broadly Grenvillian (late Mesoproterozoic) age, and to have been relatively long-lived (ca. 1100-750 Ma) (McMenamin and McMenamin, 1990; Hoffman, 1991). A

plethora of different reconstructions, many of them with a strong focus on paleomagnetic data, have been published and most conclude that crustal blocks rifted apart from western/Cordilleran Laurentia by 750 Ma (Meert and Torsvik, 2003; Cawood, 2005; Li et al., 2008; Sears and Price, 1978; Moores, 1991; Hoffman, 1991; Dalziel, 1997; Sears and Price, 2003; Pisarevsky et al., 2003; Li et al., 2008; Evans, 2009; Fu et al., 2015; Merdith et al., 2017). Despite over 25 years of work on Neoproterozoic paleogeography, there is still little agreement on the composition of Rodinia and the timing of its demise. Despite the differences, these models all have Laurentia forming the core of Rodinia because Laurentia was surrounded by Cambrian passive margins suggested to have formed during the supercontinent's breakup in the late Neoproterozoic (Bond et at. 1984; Hoffman et al., 1991).

The age of rifting predicted from paleogeographic models is very different than the age predicted from geological work on Cordilleran Laurentia. The rift history of the Cordillera is recorded in the Windermere Supergroup of the U.S. and Canadian Cordillera (Fig 2A; Ross 1991; Link et al. 1993). The Windermere Supergroup is commonly divided into three main stratigraphic ensembles: 1) narrow fault-bounded extensional basins referred to as the ChUMP basins (Dehler et al., 2007; Dehler et al., 2017; Macdonald, et al., 2013; Strauss, et al., 2014; Smith, 2015), 2) Cryogenian siliciclastic and volcanic successions often interbedded with glacial diamictites that have been interpreted as representing rift basins, and 3) a more widespread succession of Ediacaran carbonate and siliciclastic strata, composed largely of turbidites, that are widely interpreted to be related to subsidence and the initiation of passive margin sedimentation (Stewart, 1972; Ross, 1991; Jefferson and Parish, 1989; Eisbacher, 1979; Colpron et al., 2002; Macdonald et al., 2013b).

Although evidence for ca. 780 Ma volcanism is present in the form of sills and dikes and basalts associated with the Gunbarrel event (Harlan et al., 2003; Milton et al., 2017), these volcanics are very local along the margin. The ChUMP basins themselves display similarities to cratonic basins and lack abundant volcanics (Dehler et al., 2007; Dehler et al., 2010). It is suggested that these basins could have been connected during eustatic highs, making an epeiric sea called the "ChUMP seaway"

(Dehler et al., 2010; 2017). At the same time to the north, there is evidence for some transpressional faulting (e.g. Eisbacher, 1978; Thorkelson et al., 2001) and fault-influenced deposition of carbonate platforms (Strauss et al., 2014).

The most abundant volcanism in the lower Windermere Group did not occur until ca. 720 Ma, with the eruption of the Franklin LIP near centered on northern Canada. 720-660 Ma volcanic rocks with rift-related geochemical signatures are also found in the central and southern Canadian Cordillera and in Washington, Idaho, and Death Valley (Miller, 1985; Miller, 1994; Brown, 1995; Keeley et al., 2012; Lund et al., 2010). This volcanism has been dated at 717 Ma in the Yukon (Macdonald et al., 2010), 690 Ma in northern British Columbia (Eyster et al., *accepted*) and ca. 685 Ma in Idaho (Keeley et al., 2012; Lund et al., 2010).

However, subsidence analysis of Neoproterozoic and Cambrian strata (Bond and Kominz, 1984) shows that the rift-drift transition and development of the passive margin did not occur until the Precambrian-Cambrian boundary (now 541 Ma). Thus basal Windermere magmatism is too old to be tied to the thermal subsidence and development of the Paleozoic passive margin. This discrepancy in ages could suggest multiple rift events or protracted rifting (Prave et al., 1999; Colpron et al. 2001). Indeed, a third episode of Late Ediacaran rift-related volcanism has also been identified in British Columbia (Colpron et al. 2001).

Recent age constraints on the Chuar group in the Grand Canyon place that stratigraphy in the time from 782 Ma-729 Ma (Dehler et al., 2017; Rooney et al., submitted) and thus provide the high resolution window for this period that is required in order to obtain a geochonologically calibrated Apparent Polar Wander Path (APWP) and to test the various hypotheses for the conjugate rift margin. Here, I present new Laurentian paleomagnetic data from the Chuar Group. I progress by evaluating the Laurentian APWP from 780-720 Ma, and then compare those poles with those of Australia, Tarim, and South China as all three have been suggested to be the conjugate margin of Laurentia during Rodinia.

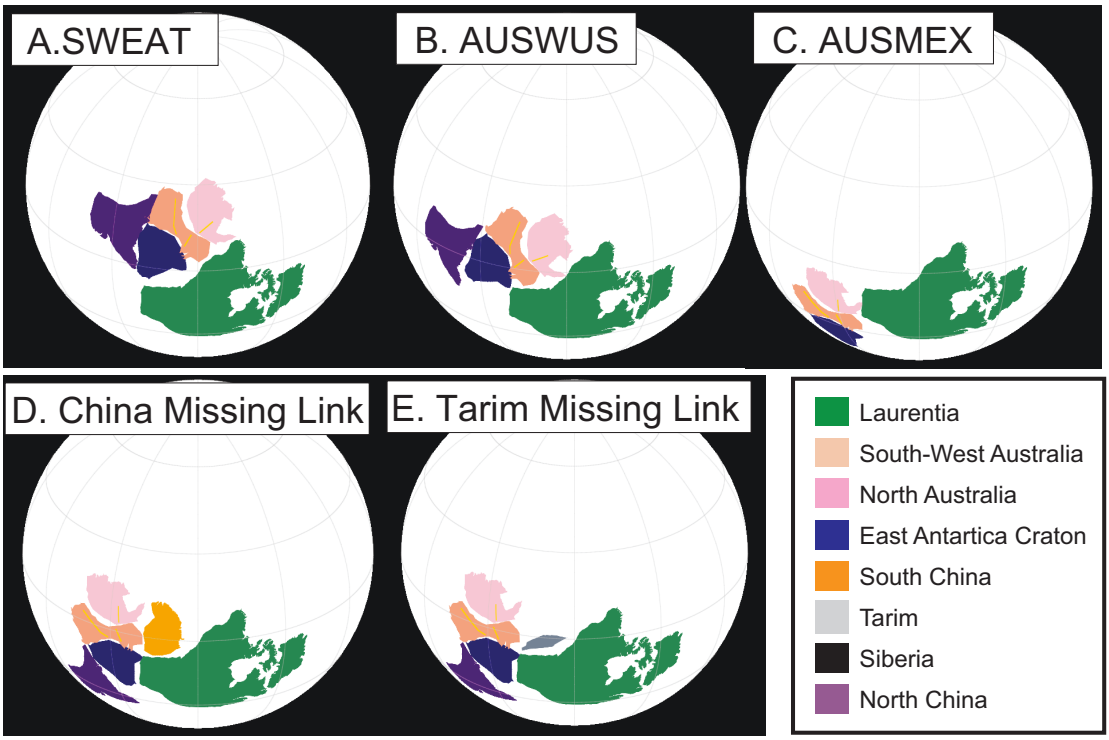


Figure 4.1: Rodinia reconstructions for the Western Laurentia margin. A. SWEAT (after Hoffman, 1991; Moores, 1991; and Daizal 1991). B. AUSWUS (after Karlstrom et al., 1999). C. AUSMEX (after Wingate and Giddings, 2004). D. Missing Link China (After Li et al., 2008). E. Missing Link Tarim (After Wen et al., 2016).

4.2.1 Previous Rodinia Reconstructions

Early models suggested a Southwest US-East Antarctic (SWEAT) connection based on orogenic piercing points (Moores, 1991) (Fig. 1A) – specifically, connecting the Grenville orogen to East Antarctica (Dronning Maud Land) and into India and Australia, and connecting the Wopmay orogen of northwest Canada to eastern Australia and into Antarctica (Moores, 1991). In northwest Canada, stratigraphic, metallogenetic, and paleomagnetic data supported the suggestion that northwestern Laurentia and southern Australia were originally connected, but began to rift apart as early as 1200 Ma, and finally began to develop two opposing passive continental margins by about 750 Ma (Young, 1992). In particular, this explained the two cratons similar rift history: Late Pro-

terozoic rifting and Early Cambrian carbonate platform development. Hoffman (1991) expanded on this by suggesting that the rifting centered on Laurentia was followed by fan-like collapse and eventual amalgamation of Gondwana. At the time, paleomagnetic results from Laurentia and Australia seemed to support this scenario, though the dataset was sparse (Powell et al., 1993). Additionally, Daziel (1991) created a Precambrian reconstruction that aligned the Grenville front with a comparable tectonic boundary in East Antarctica truncated along the Weddell Sea margin.

As an alternative, the Australia-SouthWest United States (AUSWUS) model (Fig. 1B) was proposed based on aligning linear rift-transform segments between ancestral Australia and western Laurentia (Brookfield, 1993). It was elaborated by Karlstrom et al. (1999), who showed that the AUSWUS reconstruction was corroborated by similarities in the composition and tectonic setting of Paleoproterozoic-Neoproterozoic rocks between western U.S. and Australia. Specifically, the presence of juvenile arc assemblages (Yavapai in Laurentia and Arunta in Australia), and quartz arenite–rhyolite sequences (Mazatzal in Laurentia and Reynolds-Musgrave in Australia; Dirks and Wilson, 1990). Finally, both continents contained broadly correlative ore-deposits and, importantly, the southwestern U.S. contained distinctive suites of 1.22-1.07 Ga zircons that required a western source (Ross et al., 1992).

A third hypothesis, the Australia-Mexico (AUSMEX) reconstruction (Fig. 1C) was inspired by paleomagnetic data from the 1.07 Ma Bangemall sills in Australia (Wingate and Giddings, 2004). In addition to satisfying paleomagnetic constraints, this configuration was suggested to align late Mesoproterozoic orogenic belts in northeast Australia and southernmost Laurentia (Wingate and Giddings, 2004)—specifically, juxtaposing the high-grade metamorphic and magmatic rocks of the Australian Cape River Province with the southern continuation of the Grenville Province of Laurentia (Rivers, 1997).

The Missing Link model (Fig. 1D) initially modified the SWEAT model and suggested that South China was located between Australia–East Antarctica and Laurentia, serving as the "missing-link"

between the two continents (Li et al., 1995). This model resolved some discontinuities in crustal provinces of Australia-East Antarctica and Laurentia, provided a western source region to generate the late Mesoproterozoic detrital grains in the Belt Basin. This model also explained similarities in the Neoproterozoic stratigraphy of South China, southeastern Australia and western Laurentia, and between Cathaysian South China and southern Laurentia. More recently, the Missing Link model has been modified to use the AUSWUS or AUSMEX models for the reconstruction of Australia (Li et al., 2008).

However, there are some recent challenges to this model, in the form of new geochronology and better understanding of the Ediacaran-Paleozoic position of South China (Wen et al., 2016). New geochronologic data on the assembly of Yangtze and Cathaysia (Sibao or Jiangnan orogen), suggests that orogeny occurred after the Grenville orogeny (Zhao et al., 2011; Wang et al., 2014). Ediacaran work suggests that South China likely was adjacent to NW Australia in the early Paleozoic, and that would require a complicated path of South China from the missing link position around northern Australia (Li et al., 2013; Cawood et al. 2013). Most recently, some authors have suggested that Tarim may be a more viable missing link (Fig 1E; Wen et al., 2016). This was suggested in part due to the well-developed Neoproterozoic glacio-rift strata on both continents, as well as similar Paleoproterozoic intrusions (Wen et al., 2016).

4.3 Geologic Overview

Exposed along the Colorado River in the Grand Canyon, the Grand Canyon Supergroup is made up of the older Mesoproterozoic Unkar Group (ca. 1255–1100 Ma) and the Neoproterozoic Chuar Group (Fig. 2A, B; ca. 780–727 Ma; Dehler et al., 2017; Rooney et al., submitted). The focus of this study is the strata of the Chuar Group and overlying Sixtymile Formation that outcrops in Chuar Valley, AZ. The underlying Cardenas basalt and associated sills and dikes within the Unkar Group

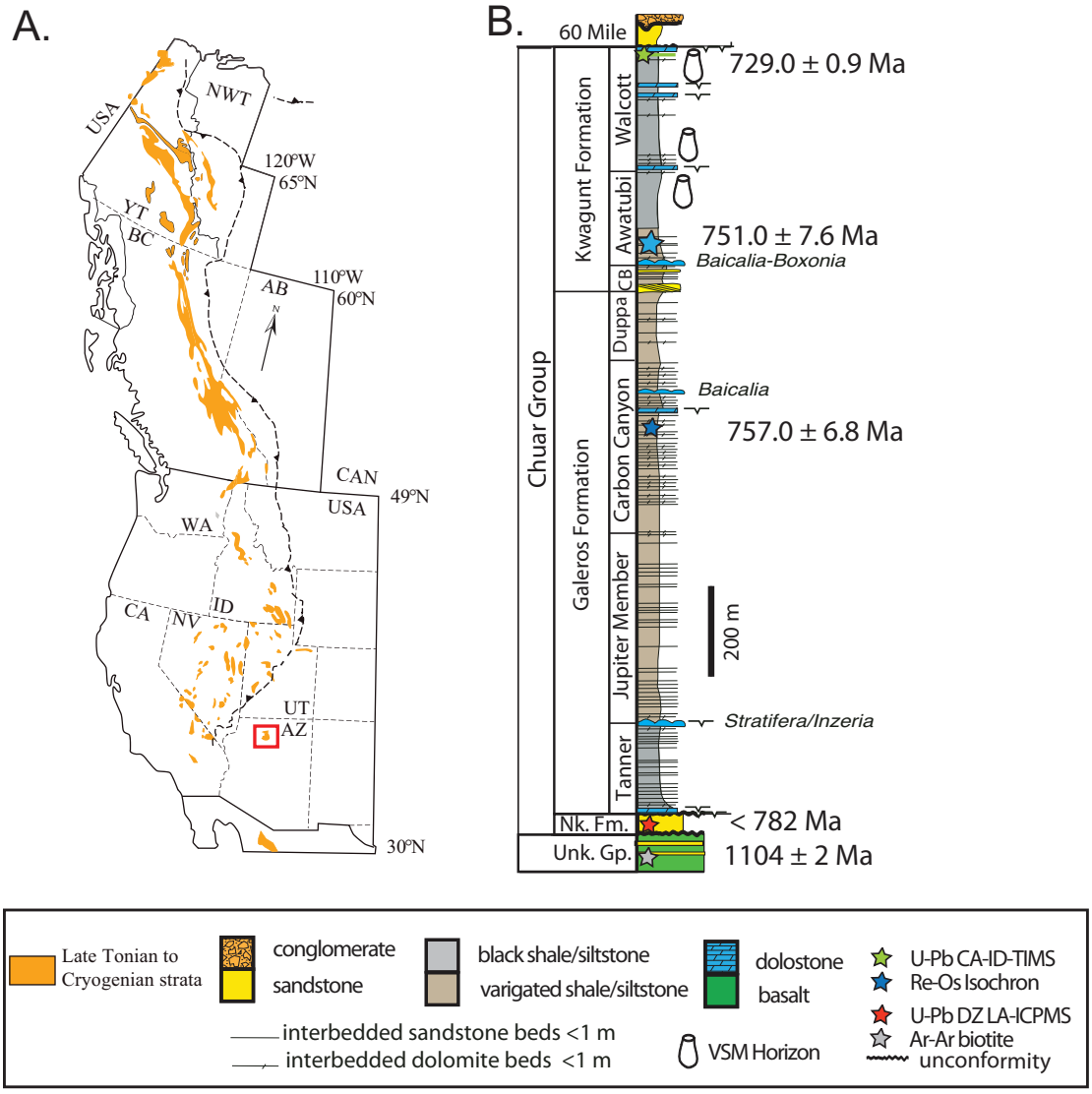


Figure 4.2: A. Map of western North America with Neoproterozoic inliers (After Lund et al., 2010). Red box highlights location of the Grand Canyon and the Neoproterozoic Chuar group. B Composite stratigraphic column of the Grand Canyon stratigraphy along with updated age constraints from Rooney et al., submitted and Dehler et al., 2017. Stratigraphic column after Karlstrom et al., 2000, Dehler et al., 2001.

were initially dated to 1070±70 Ma (Rb-Sr whole-rock; Elston and McKee, 1982), but subsequently refined to 1103±10 Ma (Ar-Ar contact metamorphic biotite from sill associated with Cardenas basalt; Timmons et al., 2005; and reanalyzed by Bright et al., 2014). These volcanics are thought to be the extrusive expression of the southwestern North American diabase province (Hammond, 1990; Howard, 1991; Harlan et al., 1993). Although precise U-Pb ages have not been obtained directly from the Cardenas basalt, the associated diabase intrusions have been dated with U-Pb thermal ionization mass spectrometry (TIMS) on at 1080±2 Ma, 1080±3 Ma, 1088±3 Ma, and 1094±2 Ma (Bright et al., 2014).

Overlying an unconformity above the Cardenas basalt is the basal unit of the Chuar Group, the Nankoweap Formation. The Chuar Group is divided into the Nankoweap, the Galeros, and the Kwagunt formations (Fig. 2B). The Nankoweap Formation is 100-150 m thick and consists of two informal members, the lower red member, which is dominated by hematite-cemented sandstone and mudstone, and the upper white member, which is composed of siltstone and thin-bedded, fine-grained red bed sandstones (Elston and Scott, 1973). Due to unconformities both above and below, it was previously unclear whether the Nankoweap formed at the end of Mesoproterozoic basin formation or the start of Neoproterozoic basin formation, but a new U-Pb detrital zircon age of 782 Ma ($n = 14$) provides a maximum depositional age constraint (Dehler et al., 2017). This age, along with similar detrital zircon populations in the overlying strata has led to the inclusion of the Nankoweap Formation with the Chuar Group (Dehler et al., 2017). The overlying Galeros and Kwagunt formations consist of 1600 m of shale with interbedded m-scale sandstone and dolomite marker beds (Dehler et al., 2001). Unconformably above the Kwagunt is the Sixtymile Formation comprised of sandstone and intraformational conglomerate, originally thought to be Neoproterozoic in age, until recent detrital zircon data demonstrated that it was Cambrian in age (Karlstrom et al., GSA Fall meeting 2016).

The Galeros Formation is divided into the Tanner, Jupiter, Carbon Canyon, and Duppa Mem-

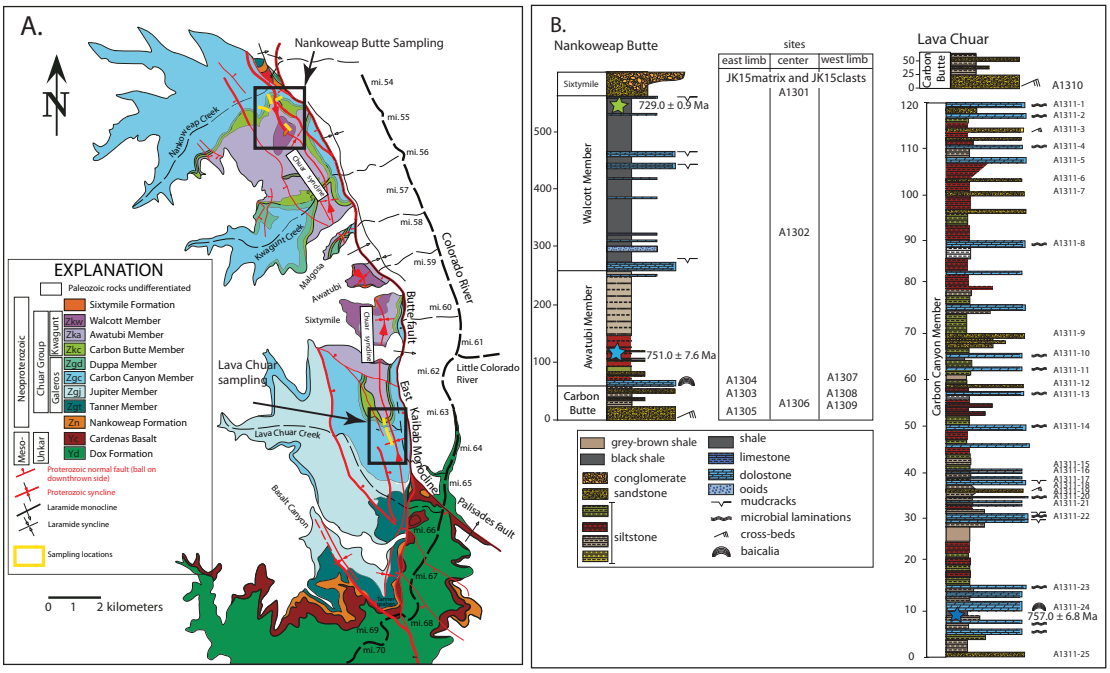


Figure 4.3: A. Map of the Chuar Valley (Modified from Karlstrom et al., 2000). Boxes highlight the sampling locations of Nankoweap Butte and Carbon Canyon. B. Stratigraphic sampling sites.

bers and the Kwagunt Formation is divided into the Carbon Butte, Awatabi, and Walcott Members (Fig 2B; Ford and Breed, 1973). Both the Tanner and Jupiter members are dominated by fine-grained siliciclastic rocks that have unique dolomite marker units at the base, the Tanner Dolomite and the *Stratifera/Inzeria* stromatolite unit (Ford and Breed, 1973). The overlying Carbon Canyon is characterized by alternations of varicolored mudstone with mudcracks, orange dolostone, pale carbonate stromatolite units, and thin sandstone beds (Dehler et al., 2001). The upper member of the Galeros is the Duppa Member, which is dominated by recessive sandstones and siltstones. The Kwagunt Formation conformably overlies the Galeros Formation and includes the sandstone dominated Carbon Butte Member, variegated shale and *Boxonia* stromatolites of the Awatabi Member, and dolostone and black shale of the Walcott Member (Dehler et al., 2001). The cyclicity within the Chuar is suggested to reflect glacioeustatic fluctuations during the climatic transition into the Sturtian Snowball Earth (Dehler et al., 2001).

Of particular focus for this study were several key marker beds within the Carbon Butte and Awatabi members, particularly, the basal red sandstone marker bed of the Carbon Butte Member, the white sandstone marker bed at the top of the Carbon Butte Member, and the *Boxonia* stromatolite marker bed at the base of the Awatabi Member (Fig. 4J). These distinctive marker beds allowed very clear comparisons of paleomagnetic data across the Chuar Syncline. The basal red sandstone marker bed (Fig. 4A,B) is a 4-11 m thick, resistant, ridge forming quartzarenite to subarkosic sandstone that marks the base of the Carbon Butte Member (Dehler et al., 2001). The very base is marked by horizontally bedded strata with symmetric ripples, this is followed by large (1-2 m) low-angle-inclined cross-beds along with large-scale trough cross-beds. The upper portions of this unit is marked by horizontally bedded strata. The large low angle cross-beds have been interpreted as tidally produced epsilon cross-beds on a shallow marine shelf, and the trough cross-bedded sandstone superimposed on the low angle cross-beds has been suggested to reflect migration of dunes within a tidal channel (Dehler et al., 2001). However, it is also possible that these could alternatively

be interpreted as dunes within the shore-face of an associated barrier bar-a complex of sand waves formed from wave influences in the shallow to intertidal lacustrine setting (Dehler et al., 2001). The white sandstone marker unit (Fig. 4C,D) is at the top of the Carbon Butte Member is 1-2 m thick with 3-10 cm thick beds. It is a very mature quartz arenite that displays prominent ripples. This unit has also been documented as having bipolar cross-bedding (Dehler et al., 2001). It marks a moderate to high-energy environment, and the bipolar crossbeds have been suggested to reflect a shallow subtidal to intertidal marine setting (Dehler et al., 2001). The basal *Boxonia* stromatolite (Fig. 4E,F) bed marks the base of the Awatabi Member. Along with the *Boxonia* stromatolites, this unit laterally displays stratiform to domal microbial buildups with cm-scale laminae that are interpreted to have formed in a lower energy shallow water environment.

Tectonically, the deposition of the Galeros and Kwagunt seems to be tied to the north-trending Chuar Syncline (Fig. 4I) and tectonic movement on the parallel Butte Fault (Fig. 3A). Intraformational faults are found throughout the Chuar Group strata, including the basal Tanner Member and middle Carbon Canyon and Carbon Butte Members, suggesting that faulting was occurring throughout Chuar Group deposition. Thickness changes perpendicular to the fault and the Chuar Syncline axis indicate growth strata related to fault movement, indicating that activity along the Butte fault was syndepositional with the Chuar Group (Timmons et al, 2001). The deposition of the Sixtymile Formation was originally tied to the daylighting of the Butte Fault, but given the updated Sixtymile Formation age constraints, that hypothesis may no longer be correct. The Butte Fault has been suggested to be related to early rifting of Rodinia, however, as the ChUMP basin sequences involve local rifting and subsidence, it may be likely that they are related to local intercontinental subsidence rather than active rifting.

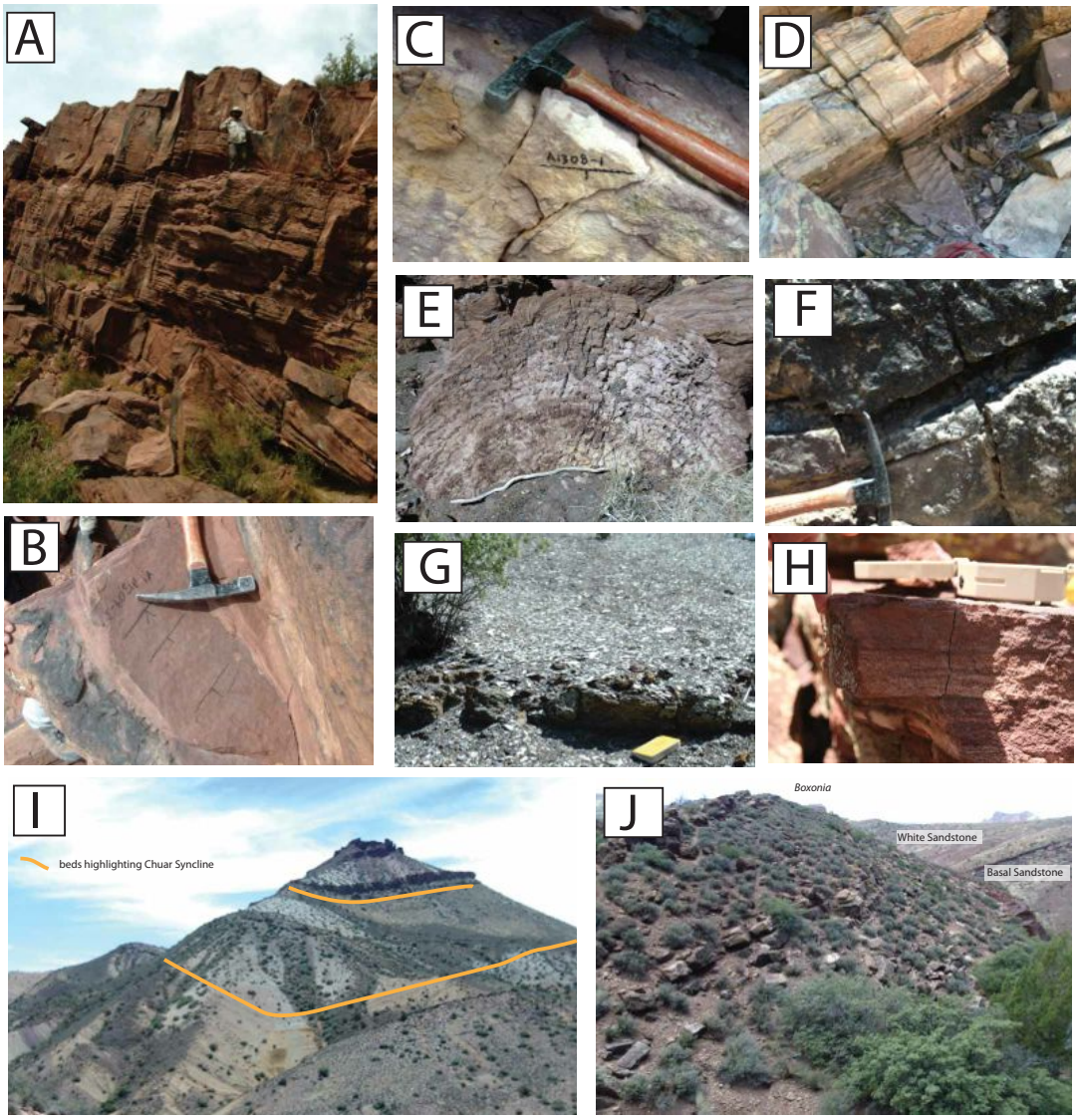


Figure 4.4: Field Photos. A,B. Carbon Butte basal sandstone. C, D. Carbon Butte white sandstone unit. E. F. Awatabi *Boxonia* unit. G. Walcott Member example non-carbonate outcrop (A1302). H. Sixtymile formation basal sandstone (A1301). I. Nankoweap Butte with Chuar Syncline. J. Important marker beds of Carbon Butte and Awatabi.

4.4 Methods

Paleomagnetic samples were collected via hand-sampling with orientations measured by a combination of Brunton and sun compass. The orientations of bedding were measured to correct for tilting. Sampling was concentrated at two main localities: Nankoweap Butte and Lava Chuar (Fig. 3A, Table 1). At Lava Chuar, sampling was focused on the Sixtymile Formation and the Awatabi and Carbon Butte Members of the Kwagunt Formation. From the Sixtymile Formation samples were collected from both clasts and matrix (Fig. 4G). Samples were collected from three prominent marker beds from the Awatabi and Carbon Butte Members from both limbs of the Chuar Syncline. The Walcott Member is dominated by slope forming shale and diagenetically altered minor dolomite that were deemed unfit targets for paleomagnetic studies. As a result, only one bed was sampled from the Walcott Member (Fig. 4H). At Lava Chuar, sampling focused on the Carbon Butte basal sandstone and a section of the Carbon Canyon Member, starting 120 m below the contact between the Carbon Canyon Member and the Duppa Member and continuing up to the contact.

Back in the laboratory, individual samples were drilled and cut to specimens 2.5 cm in diameter and 2 cm long. Magnetization measurements were made with a 2G Enterprises 755 Superconducting Rock Magnetometer (SRM) in the Massachusetts Institute of Technology Paleomagnetism Laboratory using an automated sample handling system (Kirschvink et al., 2008). This instrument has a sensitivity of 10^{-9} Am^2 and is located in a magnetically shielded room (DC field $<$150 nT). The natural remanent magnetism (NRM) was measured for all specimens. Then, the specimens were immersed in a liquid nitrogen bath to preferentially remove the magnetization carried by multidomain magnetite and hematite grains. This procedure was followed by AF demagnetization up to 15 mT, and finally thermal demagnetization on all the specimens. The thermal demagnetization was conducted using an ASC Scientific Thermal Demagnetizer with peak DC fields inside $<$10 nT. Specimens were thermally demagnetized in steps of 2.5-50 °C until completely demagnetized.

TABLE 1. SAMPLING LOCATIONS

Lat (°N)	Lon (°W)	Site	Location	Formation	Member	Rock unit
36.264	111.882	A1301 JK15matrix JK15clasts	Nankoweap Butte	Sixtymile Fm.		Matrix Matrix clasts
36.268	111.885	A1302	Nankoweap Butte	Kwagunt Fm.	Walcott	
36.268	111.886	A1303	Nankoweap Butte -East limb of syncline	Kwagunt Fm.	Carbon Butte	White sandstone
36.268	111.886	A1304	Nankoweap Butte-East limb of syncline	Kwagunt Fm.	Awatabi	Boxonia
36.274	111.886	A1305	Nankoweap Butte East limb of syncline	Kwagunt Fm.	Carbon Butte	Basal Sandstone
36.276	111.890	A1306	Nankoweap Butte-Center of syncline	Kwagunt Fm.	Carbon Butte	Basal Sandstone
36.274	111.890	A1307	Nankoweap Butte- West limb of syncline	Kwagunt Fm.	Awatabi	Boxonia
36.274	111.890	A1308	Nankoweap Butte- West limb of syncline	Kwagunt Fm.	Carbon Butte	White sandstone
36.274	111.891	A1309	Nankoweap Butte- West limb of syncline	Kwagunt Fm.	Carbon Butte	Basal Sandstone
36.167	111.839	A1310	Carbon Butte-center of syncline	Kwagunt Fm.	Carbon Butte	Basal Sandstone
start: 36.166 end: 36.162	start: 111.840 end: 111.838	A1311-1:25	Carbon Butte	Galeros Fm	Carbon Canyon	

Because lightning strikes can cause remagnetization, care was taken in the field to use both a sun compass and a Brunton to identify locations that may have experienced strong remagnetization. Most of the specimens from sites yielded resolvable components of magnetization. Magnetic components were determined using principal component analysis of both best-fitting lines and great circles (Kirschvink, 1980). When analyzing the data, a maximum angle of deviation (MAD) cutoff of 15° was applied, following the recommendation of Butler (1992), but in most cases the MAD angle was $<10°$. Specimen analysis was completed using the PaleoMag OS X program (Jones, 2002). Fisher statistics were used to calculate mean directions and plots and analysis were done using the PmagPy cookbook code, methods discussed in Tauxe et al. (2010).

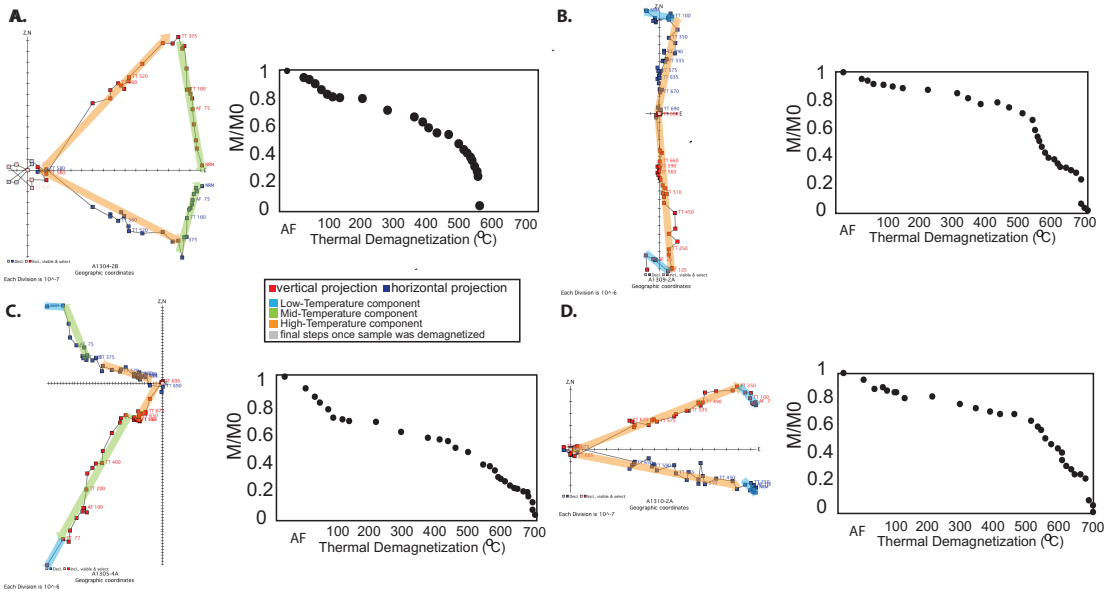


Figure 4.5: A. Representative orthogonal projection diagrams showing the demagnetization of sample A1304-2B that carries MT component and a shallow HT component carried by magnetite. B. Representative orthogonal projection diagrams showing the demagnetization of sample A1309-2A that carries a steep direction carried by hematite. C. Representative orthogonal projection diagrams showing the demagnetization of sample A1305-4A that carries a MT component as well as a shallow reversed HT component carried by hematite. D. Representative orthogonal projection diagrams showing the demagnetization of sample A1310-2A that carries a shallow HT component carried by hematite. The representative orthogonal projections are shown using in situ (geographic) coordinates. The corresponding M/M0 plots are shown to the right of each orthogonal projection.

4.5 Results

The magnetizations were classified based on unblocking temperatures and directionality into a dispersed low temperature component, steep mid-temperature (MT) and high-temperature (HT-shallow and HTs-steep) component directions (Fig. 5). Site means were taken for component directions (Fig. 6). The sites that did not yield useful data include those with very noisy sample demagnetization (A1308-white sandstone) and those with α_{95}>25° (A1306). The Tauxe and Watson (1994) fold test was applied and uncertainty was quantified by utilizing bootstrapped data sets and repetition of the fold test for various percentages of unfolding.

The low temperature component was removed during thermal demagnetization upon AF de-

TABLE 2. MID-TEMPERATURE COMPONENT DIRECTIONS

Site	MT demag. temp. (°C)	D/I (in situ) (°)	D/I (tilt corrected) (°)	α_{95} (°)	k	n/N
A1302	**400**	**302.4/59.2**	**287.5/58.3**	**14.6**	**30.3**	**4/4**
A1304	**350-400**	**7.2/ 61.2**	**278.5/ 69.6**	**8.1**	**98.5**	**4/4**
A1307	**350-400**	**336.6 / 71.5**	**152.3/ 83.1**	**18.8**	**14.01**	**5/6**
A1305	350-650 (1 sample with 650)	349.5/55.6	291.6/49.5	21.1	11.2	5/8
JK15m	**310-450**	**8.3/ 69.3**	**5.2/ 56.8**	**17.14**	**35.2**	**3/8**
JK15C	350-560	31.7/ 61.5	23.9/ 58.4	22.73	17.3	4/19
A1311	**200-400**	**2.7/ 63.2**	**7.7/ 51.3**	**7.23**	**29.0**	**15/33**
Stringent Site Mean†		**345.0/67.2 α_{95} =12.71 k=37.15**	**332.6/72.0 α_{95} =24.58 k=10.64**	**Fail fold test: unfolding: 8% range: -10– 50%**		**5 sites**

D and I—mean declination and inclination
k—Fisher's (1953) precision parameter
α_{95}—radius of confidence circle for the mean direction
n—number of samples used
N—total number of stratigraphic horizons or samples collected
†mean calculated for sites/sections with $\alpha_{95}<20$

magnetization or heating to 100°C. This component was highly scattered and will not be discussed further. The MT component direction was resolved in two sites with $\alpha_{95}<25°$ and five sites with $\alpha_{95}<20°$ (Table 2 and Fig. 5,6). This component is demagnetized upon heating to 200-560°C. In different samples, this unblocking temperature overlaps with some of the HT unblocking temperatures.

The HT directions from sites were generally observed to fall into three locations, one with steep positive inclinations to the north (HTs), and two with shallow inclinations, one with positive to the west, and one with negative to the east (Table 3, and Fig. 5, 6). The steep direction appeared to be very similar to the MT component direction, just with higher unblocking temperatures (up to 690°C). Both shallow HT directions had unblocking temperatures ranging from 565°C and 685°C, indicating hematite, as well as likely magnetite as the ferromagnetic carrier. Among all the samples, those that required great circle fits to the origin (such as dominated at sites A1302, A1307) were demagnetized much earlier than 565°C, starting at 400°C.

TABLE 3. HT-TEMPERATURE COMPONENT DIRECTIONS

Site	HT demag. temp. (°C)	D/I (in situ) (°)	D/I (tilt corrected) (°)	α_{95} (°)	k	n/N
Shallow directions						
60mile-matrix **A1301**	**650-700**	**281.0/13.7**	**281.4/11.2**	**16.67**	**14.07**	**6+2C/8**
Walcott						
A1302§	**450+**	**12.9/-20.8**	**13.7/-12.2**	**7.0**	**208**	**3C**
Awatabi-Boxonia						
A1304	**560-660**	**122.4/ -47.4**	**96.2/ -26.6**	**15.2**	**48.1**	**3+1C/4**
A1307	**375-560**	**103.4/-19.3**	**93.4/-32.8**	**17.7**	**49.5**	**1+3C/8**
Awatabi Mean†		***111.32/-33.70 α_{95} =76.7 k=12.8***	***94.82/-29.71 α_{95} =14.60 k=294.79***	***tilt α_{95}<< in situ α_{95}***		***2 sites***
Carbon Butte						
A1303-white ss	**635-680**	**108.5/ -32.4**	**92.34/ -15.9**	**7.72**	**86.30**	**5+1C/7**
A1305-Basal ss# (top 2.3 m)	***650-680***	***286.3/57.4***	***263.8/23.8***	***12.4***	***41.94***	***4/8***
A1310-Basal ss (bottom 0.45 m)	**650-665**	**100.2/-17.4**	**104.2/-21.9**	**11.70**	**51.40**	**4+1C/5**
Carbon Butte Mean†		***104.4/ -35.5 α_{95} =32.60 k=15.39***	***93.47/-20.74 α_{95} =15.89 k=61.27***	***Indeterminate unfolding: 88% range:-9 – 109%***		***3 sites***
Carbon Canyon A1311-8,11,20	475-490	274.3/33	278.9/26.3	27.8	13.85	3/33
Awatabi + Carbon Butte Mean†		***107.21/-34.89 α_{95} =18.17 k=18.67***	***94.00/ -24.35 α_{95} =8.68 k=78.60***	***Pass fold test unfolding: 83% range: 44 – 109%***		***5 sites 23 samples***
Sixtymile Fm						
**Jk15clasts*	605-680	37.1/42.0	35.0/38.3	53.8	1.4	16/19
JK15clasts with steep PDF direction	630-685	10.6/60.4	7.7/57.6	7.36	68.22	7/19
Steep direction						
A1301- *Sixtymile Fm*	**570-660**	**8.6/66.4**	**3.4/64.5**	**17.56**	**21.26**	**4/8**
A1309- *Carbon Butte*	**605-675**	**7.5/51.2**	**50.2/60.2**	**15.6**	**20**	**5/6**
A1311- *Carbon Canyon*	**565-690**	**357/65.6**	**2.7/54.8**	**14.64**	**22.59**	**5/33**
HT steep Mean†		***4.8/61.16 α_{95} =13.8 k=80.47***	***18.17/61.7 α_{95} =21.93 k=32.6***	***Fail fold test unfolding: 32% range: -8– 35%***		***3 sites***

D and I—mean declination and inclination
k—Fisher's (1953) precision parameter
α_{95}—radius of confidence circle for the mean direction
n—number of samples used, C indicates sample with great circle fit
N—total number of stratigraphic horizons or samples collected
§great circle pole demagnetization approaches up in the southeast quadrant
#reversed for calculations of means
†mean calculated for sites/sections with α_{95}<20
*R=1.42, R_o=6.45, thus randomness cannot be rejected

TABLE 4. MEMBER DATA FROM WEIL ET Al., 2004

Member	D/I (in situ) (°)	D/I (tilt corrected) (°)	α_{95} (°)	k	n/N
Walcott:					
JG60-18	290/54	303/29	18	27	7/7
JG60-6	299/50	290/30	13	28	7/7
Walcott Mean†	***294.70/52.09 α_{95} =14.92 k=281.93***	***296.37/29.88 α_{95} =24.31 k=107.65***	***tilt α_{95} >> in situ α_{95}***		***2 sites 14 samples***
Awatabi:					
JG-53-2	*107/-31*	*98/-13*	*11*	*76*	*6/7*
Carbon Butte					
#AW-13-4	272/3	272/23	9	39	8/8
AW-12-10	*88/−25*	*94/−34*	*12*	*65*	*6/8*
AW-12-11	*103/−13*	*108/−28*	*16*	*258*	*6/8*
****AW-12-13***	***85/−28***	***83/−36***	***21***	***20***	***7/8***
AW-12-14A	*92/−20*	*97/−39*	*12*	*60*	*6/8*
AW-12-14B	*97/−19*	*103/−37*	*12*	*39*	*8/8*
Carbon Butte Mean†	***94.48/-16.08 α_{95} =9.57 k=64.89***	***98.66/-32.65 α_{95} =8.49 k=82.05***	***Indeterminate Unfolding: 79% range: -10 – 109%***		***5 sites 32 samples***
Awatabi + Carbon Butte Mean†	***96.38/-18.63 α_{95} =9.86 k=47.10***	***98.53/-29.38 α_{95} =9.44 k=51.31***	***Indeterminate Unfolding: 54% range: -10 – 109%***		***6 sites 38 samples***
Carbon Canyon					
AW-12-8	260/60	256/17	13	27	6/8
AW-12-9	256/48	254/−11	9	90	7/8
AW-12-15	277/31	285/35	15	24	7/8
AW-12-19	299/−8	296/1	16	16	7/7
AW-12-20	284/5	285/7	7	53	6/7
AW-13-1	264/6	264/−5	11	31	7/7
AW-13-2	264/18	259/10	15	16	7/7
AW-13-3	254/26	245/22	14	21	7/8
AW-13-6	241/−20	247/−5	12	31	7/8
AW-13-7	260/−19	263/2	17	22	6/7
AW-13-8	267/−2	267/10	14	24	7/7
AW-13-9	252/−29	259/−7	15	27	6/7
AW-13-10	264/−6	263/13	14	25	7/7
AW-13-11	263/−30	269/−5	19	13	7/8
Carbon Canyon mean	***265.14/5.34 α_{95} =16.14 k=7.03***	***264.93/6.11 α_{95} =9.65 k=17.93***	***Pass fold test unfolding: 98.5% range: 71 – 109%***		***14 sites 94 samples***
Jupiter					
AW-12-22	268/−11	266/−5	16	20	8/8
AW-12-23	270/3	272/5	6	112	8/8
PDF					
Carbon Butte					
T-52-1[b]	5/64	313.26/68.78	8	56	8/8
T-65-1[b]	4/54	21.64/44.07	11	50	5/8
T-65-2[b]	5/53	21.86/42.92	7	107	6/8
JG-60-2[b]	0/61	325.62/44.00	6	122	6/8
JG-60-3[b]	5/55	319.23/34.68	8	151	6/8
JG-53-4[b]	13/57	320.21/ 63.65	10	51	6/8
JG-53-5[b]	345/63	295.92/54.84	10	30	9/9
AW-13-5[b]	6/51	36.16/60.33	7.8	61	8/8
AW-12-12[b]	11/68	35.25/50.65	9	61	8/8

D and I—mean declination and inclination
k—Fisher's (1953) precision parameter
α_{95}—radius of confidence circle for the mean direction
n/N—number of samples used/total number of samples
#reversed for calculations of means
*discarded from subsequent analysis because α_{95} <20 °
†mean calculated for sites with α_{95}<20

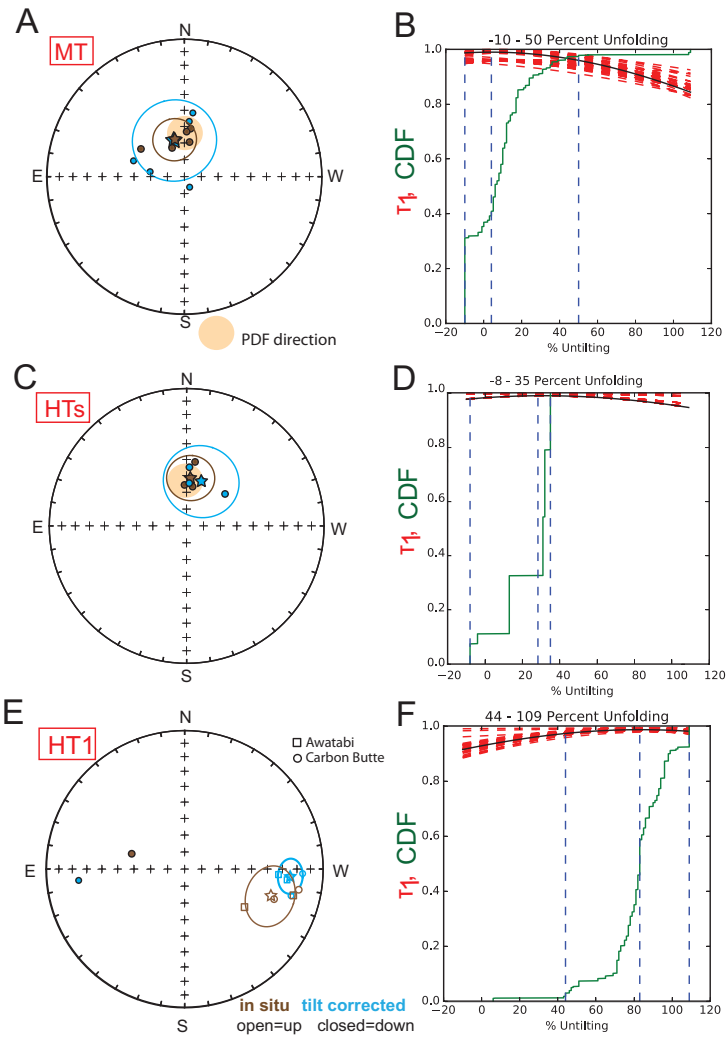


Figure 4.6: Equal area component site mean results and results from the Tauxe and Watson (1994) fold test. A,B. Sixtymile Formation, Walcott member, Awatabi member, Carbon Canyon member mid temperature component directions. C,D. Carbon Canyon, Carbon Butte, Awatabi and Sixtymile Formation Steep high temperature origin trending component directions. E,F. Awatabi and Carbon Butte member high temperature origin trending component directions. Note that site A1305 has high stability HT directions reversed from the rest. For the plots of the site-mean directions the negative directions represented by open symbols and positive directions represented by closed symbols. The geographic/in-situ directions are plotted in brown and the tilt corrected directions are plotted in blue. The mean component directions are plotted with stars and with the circle of α_{95} indicated. The direction of the present day field (PDF) is indicated in light orange. For the Tauxe and Watson (1994) fold tests, the black curves indicate maximum eigenvalue (τ_1) as a function of untilting. The red dashed curves are a sampling of the first 50 bootstrapped results. The green line is the cumulative distribution of the percent untilting required to maximize τ_1 for all the bootstrapped data sets. The dashed vertical lines are 95% confidence bounds on the % untilting that yield the most clustered result (maximum τ_1). If the 95% confidence bounds include 0, then a pre-tilt magnetization is indicated. If the 95% confidence bounds include 100, then a post-tilt magnetization is indicated. If the 95% confidence bounds exclude both 0 and 100, syn-tilt magnetization is possible.

4.5.1 Results and Fold tests by Member

Carbon Canyon Member

The Carbon Canyon section was dominated by the HTs direction and yielded only three stratigraphic sampling heights with shallow directions. These sampling heights were all along the syncline axis and involved only 1-2 samples and were stratigraphically dispersed so the stratigraphic secular variation of the Carbon Canyon Member could not be properly analyzed and a fold test could not be applied. The three sampling heights with resolvable shallow to intermediate components were all normal polarity and trended to the west.

Carbon Butte Member

Resolvable HT component directions were obtained from three sites of the Carbon Canyon Member (Table 3, Fig. 6). These sites included the basal sandstone and the white sandstone. One site (A1305-from the very top of the Carbon Butte basal red sandstone) displays a reversed shallow direction from the others. When the reversal test is applied (Fig. 7C), it passes the Watson's V test ($V_{Watson's} = 2.1 < V_{critical} = 10.5$), and the test of McFadden and McElhinny (1990) results in an angle between means of 15.2°, which is less than the critical angle of 60.9°. However, because of the few number of sites that test itself is indeterminate. The Tauxe and Watson (1994) fold test resulted in maximum tau_1 at 88% unfolding, however, was indeterminate as the range of bootstrapped sites included both 0 and 100% unfolding.

Awatabi Member

For the Awatabi Member, two sites displayed HT directions, both of the same polarity, reversed and to the east. These were both from the same bed (the *Boxonia* stromatolite marker bed) but were on opposing limbs of the Chuar Syncline. Demagnetization behavior included steep directions (MT or

HTs) recovered from all the samples with resolvable directions, followed by linear or great circle decay towards the origin. As there were only two sites, the Tauxe and Watson (1994) fold test could not be applied, but the large improvement in the α_{95}upon tilt correcting suggests that it is pre-folding (see Table 3. tilt corrected α_{95}=14.60<< in situ α_{95}=76.7)

Walcott Member

From the Walcott Member, HT directions were obtained from one site (A1302) (Table 2,3), which displayed steep directions demagnetized around 450°C, followed by directions that followed a great circle towards the east and up.

Sixtymile Formation

From the Sixtymile Formation, resolvable directions were obtained from one basal matrix site (A1301), and from clasts and matrix samples of the upper conglomeratic units (JK15clasts and JK15matrix). Samples from A1301 displayed HTs directions that were demagnetized upon heating to 570-660°C. All of the samples displayed trends towards shallow directions that were isolated upon heating to 650-700°C. Great circle fits were required for two of the samples, while the rest could be fit with lines trending towards the origin (Fig. 7A). For JK15matrix, three of the samples displayed a coherent steep MT direction similar to the other overprints. For JK15clasts, 16 samples displayed resolvable high-coercivity directions, with 9 of the samples with directions similar to HTs (Fig. 7B). The value of the resultant vector (R) is 5.4, less than the critical value (R_o) of 6.456 at the 95% confidence level, thus suggesting that a random distribution cannot be rejected at the 95% confidence level (Watson, 1956). The samples with the HTs direction included clasts with no lower temperature component, or with a lower temperature component removed at or below 300°C. Of the clasts, there were 4 samples with MT directions close to HTs, and, of these, only two displayed higher coercivity linear components, one with a HTs direction, and one pointing shallowly up to the east. There were no

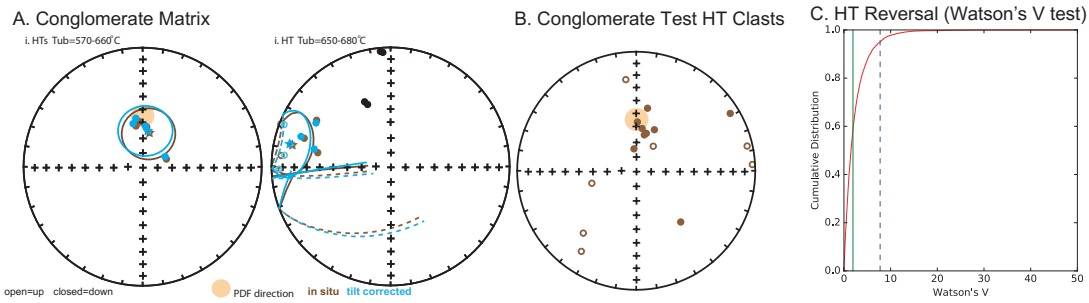


Figure 4.7: Results from field tests. A. Conglomerate Matrix i) HTs component directions. ii) HT origin trending component directions. B. Conglomerate clasts HT origin trending directions. The geographic/in-situ directions are plotted in brown and the tilt corrected directions are plotted in blue. The direction of the present day field (PDF) is indicated in light orange. The mean component directions are plotted with stars and with the circle of α_{95} indicated. C. Isolated site reversal test of Watson.

systematic differences observed between the various samples. This inconclusive conglomerate test suggests that the HTs overprint is pervasive, however, in certain cases, small demagnetization step sizes allow it to be identified and a primary magnetization to be isolated.

4.5.2 Combined directions and fold tests

The Tauxe and Watson (1994) fold test was then applied to the MT and HTs directions for all sites, and the HT directions combined from the Carbon Butte and basal Awatabi members (Fig. 6). The MT direction is a post-tilting direction, as the maximum τ_1 occurred at 8% untilting and the 95% confidence interval spanned -10% to 50% unfolding. HTs direction was also post-folding, it failed the Tauxe and Watson (1994) fold test as the maximum tau_1 occurred at 32% unfolding and the 95% confidence bounds are -8 to 35% unfolding. The Awatabi and Carbon Butte member HT directions were combined for subsequent analysis, as there was nothing to suggest that the basal Awatabi was substantially younger than the Carbon Butte. Combined, these directions pass the Tauxe and Watson (1994) fold test as the maximum tau_1 occurs at 83% unfolding and the 95% confidence bounds are from 44-109% unfolding, suggesting that the magnetization was acquired pre-folding. In tilt corrected coordinates, the reversal test (for the isolated reversed section) results in an observed angle

between the mean directions of 13.3° and a critical angle calculated for the two sets of observations at which the null hypothesis of a common mean direction would be rejected with 95% confidence of 26.7°. However, again, due to the limited number of observations, the high value of the critical angle places the reversal test in the "indeterminate" classification of McFadden and McElhinny (1990). Due to vector demagnetization revealing multiple components, the fold test, and the presence of reversals, I suggest that the shallow HT direction is a primary direction carried by hematite, as well as possibly by magnetite. It is found in five sites (23 samples) in both the Awatabi and Carbon Butte members.

Pervasive overprinting (HTs and MT) was identified throughout the Chuar Group, especially in the Carbon Canyon and Carbon Butte members and in the Sixtymile Formations. This steep direction (HTs) failed the fold test and was very similar to the present day field. For many samples it followed a decay to the origin, unblocking between 565-690°C. The MT direction was very similar to the HTs, but instead unblocked between 310-560°C, and was normally followed by a higher temperature component with a different direction. This was identified in the Walcott, Awatabi, and Carbon Canyon members with site means $\alpha_{95}<20°$, and in the Carbon Butte Member and Sixtymile Formation with site meand $\alpha_{95}>20°$. In certain cases, especially notable for site A1302 of the Walcott Member and the A1307 of the Awatabi *Boxonia* stromatolites, the prominent MT direction was dominantly followed by great circles to the origin. In such cases, if larger demagnetization step sizes had been applied instead, the origin trending demagnetization could have been misidentified and a steeper component could have been interpreted as decaying to the origin.

With regards to reversal frequency, the few directions obtained from the Carbon Canyon were all normal. Conversely, the basal-middle beds of the Carbon Butte basal sandstone marker bed were reversed, while the top 2.3 meters displayed normal directions. At the top of the Carbon Butte, the white sandstone marker bed displayed reversed directions, as did the overlying units. This suggests that at least two reversals were captured in the stratigraphy of the Kwagunt Formation.

4.6 Discussion

4.6.1 Comparison of with previous work

The Chuar Group has been the focus of several paleomagnetic studies but much of the initial work was never published in peer-reviewed journals, instead only summarized in abstracts or review papers with no published demagnetization or sample data (Elston, 1989; Elston, 1986; Link et al., 1993). The only previous demagnetization and sample data from the Chuar Group is from a study conducted by Weil et al. (2004). The study by Weil et al. (2004) focused on samples from the Kwagunt and Galeros formations (Table 5), and included thermal demagnetization. From the Galeros formation, the Jupiter and Carbon Canyon members were sampled and resolvable shallow to intermediate directions were obtained with unblocking temperatures of 630-680°C (indicative of hematite). As there were only two sites from the Jupiter member, they were combined with the sites from the Carbon Canyon member, and combined these directions passed the fold test (Weil et al., 2004). From the Kwagunt formation, samples were collected from the Carbon Butte, Awatabi, and Walcott members. Most of the Kwagunt samples had discrete low inclination, E-W trending directions with unblocking temperatures between 650 and 680°C (as expected for hematite) (Weil et al., 2004). For some samples, there was also a north-directed, moderate-steep positive inclination magnetization overprint removed upon heating to 300°C and interpreted as a recent overprint (Weil et al., 2004). However, for nine sites from the Carbon Butte Member this component displayed unblocking temperatures up to 680°C (Weil et al., 2004). For the combined Kwagunt members, a fold test was applied (Tauxe, 1998), resulting in maximum clustering at 80% unfolding and was interpreted to support a primary magnetization acquired at the time of, or soon after, deposition (Weil et al., 2004).

However, when the data is reanalyzed and within-member fold tests are applied, none of the Kwagunt members pass (Table 5). The Walcott member sites appear more dispersed when tilt cor-

rected, and the Carbon Butte member sites result in an indeterminate fold test, which is also the case when the single Awatabi site is combined with the Carbon Butte sites (Table 5). These indeterminate results are also mirrored by the negligible difference between the geographic and tilt corrected site mean circles of 95% confidence (α_{95}; Table 5). This is likely because the resolvable directions came from sites on only one limb of the Chuar Syncline.

This can be compared to the results presented in this study, where the combined basal Awatabi-Carbon Butte sites do pass the bootstrapped fold test, and the within-member site means for the Awatabi and Carbon Butte have much smaller α_{95} when tilt corrected (Table 4). In general, the Carbon Butte and Awatabi site mean directions from this study were similar to the results from Weil et al. (2004) with respect to polarity and declination, however, the Walcott directions appear different from the one site isolated in this study (Fig. 8A).

Walcott Direction

The Walcott directions from this study were carried only by great circle fits, moving from the steep MT direction and approaching reversed directions similar to the Awatabi/Carbon Butte directions. The Walcott directions of Weil et al. (2004) display normal polarity directions with declinations $\sim$30 degrees north of the E-W axis, and one site had an α_{95} =18° (Fig. 8A). As mentioned earlier, the Walcott site mean directions of Weil et al. (2004) are more tightly clustered in their in-situ coordinates (*in-situ* α_{95}*=14.92*$<<$ *tilt* α_{95} *=24.31*), although that observation may be biased by the fact that both those sites are on the same limb of the Chuar Syncline. When the tilt-corrected Walcott sites were compared with the other Awatabi and Carbon Butte Members sites combined, the Watson's V test for a common mean resulted in failure with $V_{critical}$of 9.4 $<$ $V_{Watson's}$ of 9.5 (Fig. 8Aiii). In addition, when examining the Walcott directions, it almost appears that the two sites lie along a great circle between the steep MT and HTs directions and the normal Awatabi/Carbon Butte HT directions (Fig 8A).

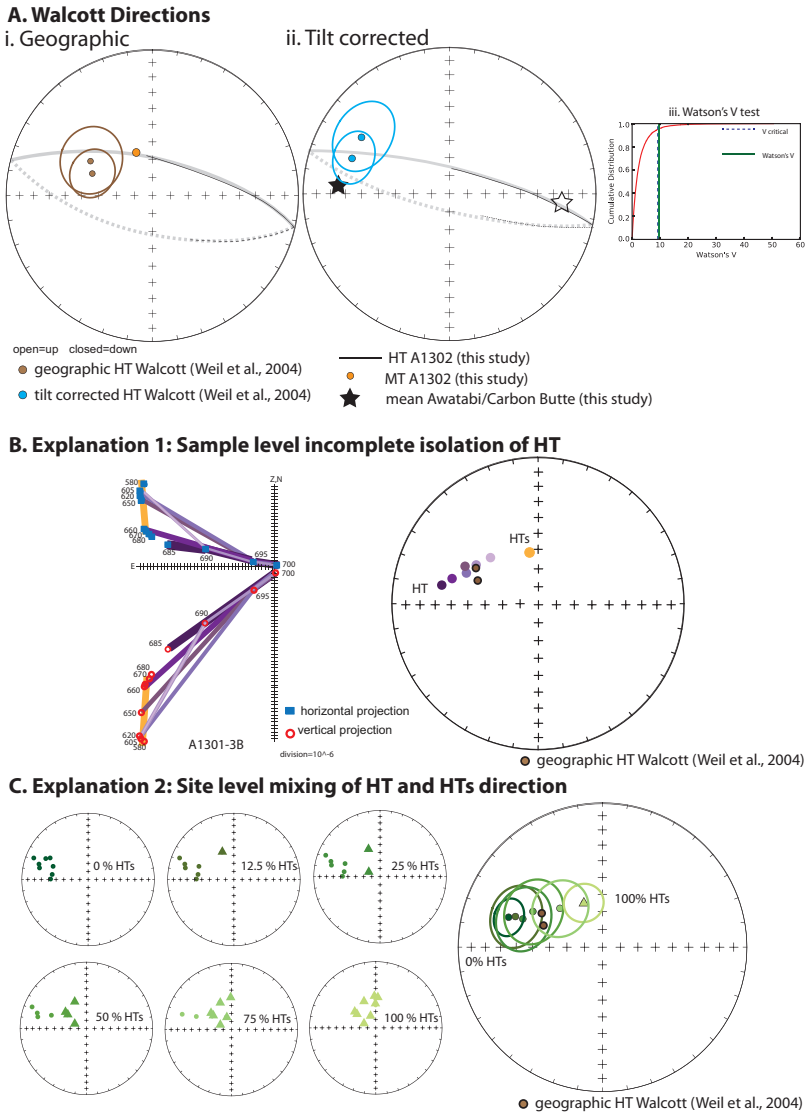


Figure 4.8: Ai, ii. geographic and tilt corrected equal area plot of the Walcott sites. The geographic/in-situ directions are plotted in brown and the tilt corrected directions are plotted in blue. The MT Walcott direction and HT great circle direction from this study are also indicated. The direction of the present day field (PDF) is indicated in light orange. The mean normal and reversed Awatabi and Carbon Butte directions are plotted with stars. iii. Watson's V test comparing the tilt corrected Walcott directions with those from the underlying Awatabi and Carbon Butte members. B. Explanation 1 for Walcott directions: sample level incomplete isolation of HT. C. Explanation 2 for Walcott directions: site level mixing of HT and HTs directions.

TABLE 5. POTENTIAL EXPLANATION FOR WALCOTT SITE MEANS

	D (°)	I (°)	MAD/ α_{95} (°)	n_{steps} or $n_{samples}$	k
Explanation 1: Temperature steps used in line fits					
HT: 685, 690, 695, 700	281.5	34.4	1.5	4	
2: 660, 695, 700	285.9	39.5	0.9	3	
3: 650, 695, 700	297.2	43.2	1.9	3	
4: 620,695, 700	291.7	48.9	6.6	3	
5: 580, 605, 690, 700	302.4	48.5	6.8	4	
6: 580, 605, 690,	314.0	53.2	2.7	3	
MT:	351.1	61.3	4.6	29	
Explanation 2: Mixing between HT and HTs					
HTs	Kappa: 27, N: 8, Mean Dec: 351, Mean Inc: 6				
	336.8	52.7			
	292.1	75.1			
	310.1	56.7			
	304.3	61.4			
	358.9	49.9			
	336.4	73.0			
	3.4	52.2			
	359.7	62.3			
HT	Kappa: 27, N: 8, Mean Dec: 281.5, Mean Inc: 34.3				
	296.3	29.5			
	299.6	34.5			
	278.0	44.5			
	270.7	42.8			
	291.6	12.9			
	283.4	25.6			
	290.6	43.0			
	287.4	23.4			
Site means					
0% HTs	287.67	32.34	9.45	8	35.33
12.5% HTs	290.72	36.11	15.99	8	17.32
25% HTs	289.49	41.15	16.75	8	11.89
50% HTs	297.14	45.00	17.4	8	11.88
75% HTs	312.38	57.25	15.95	8	13.01
100% HTs	336.98	62.69	10.99	8	26.36

Although I was not able to reproduce the Walcott data, and no published demagnetization data was shown for the Walcott directions of Weil et al. (2004), based on examination of other samples and directions, two explanations for the interpretation of the Walcott data of Weil et al. (2004) are offered. Bearing in mind that the HTs and MT directions were pervasive among the upper units of the Kwagunt formation, I suggest that the steep overprint directions may bias the Walcott samples, either by 1) allowing incomplete isolation of the primary HT direction, or 2) resulting in mixing of HT and HTs directions within a site (Fig. 8B, C). First, the anomalous Walcott directions may be due to sample level incomplete isolation of the HT direction (Fig. 8B). This is demonstrated by reanalyzing demagnetization data for sample A1301-3B, which includes a steep magnetization until 660°C, followed by a shallow demagnetization until 700°C. Depending on the chosen demagnetization temperature steps, the apparent origin trending direction can range along a great circle between the primary direction (HT) and the overprint direction (HTs) (Fig. 8B, Table 5). Thus, if the demagnetization steps are not small enough, it is possible to obtain a line fit that does not reflect the actual origin trending direction. Especially in cases where samples required a great circle fit to the origin, incomplete isolation or recognition of the origin trending direction could bias site means. This is especially applicable to the Walcott directions, for in this study the Walcott samples had a steep MT overprint and only great circle fits to the origin. Furthermore, it is not unusual for Proterozoic paleomagnetic poles to appear steep due to mixing with a recent steep overprint. This is found for the Borden dikes of the Franklin Large Igneous Province where steep magnetizations are suggested to result from the superposition of a Cretaceous-Tertiary aged chemical remanent magnetization on normal and reversed primary Franklin components (Pehrsson and Buchan 1999). Similarly, some of the steep Grenville poles are suggested to be contaminated by a steeper recent overprint (Brett and Dunlop, 2012). In such cases, when there is partial or complete overprinting by a steep-down (occasionally steep up) magnetization, one might expect magnetization directions for stable sites to be "streaked" along a great circle between the primary directions and the steep younger overprint

direction both at the site and the specimen level. When there is such a pronounced overprint, larger demagnetization step sizes can potentially lead to misidentification of the origin trending demagnetization and false interpretation of the primary direction.

Alternatively, at the site level, there could be incorrect identification of HTs overprints as primary and hence mixing of HT and HTs directions. This may also explain the larger within-site scatter (α_{95} =18°) reported for one of the Walcott sites. This effect is demonstrated by using the HT and HTs directions of sample A1301-3B and generating sets of Fisher distributed data (Table 5; Fig 8C; Kappa: 27, N: 8 distribution similar Walcott sites of Weil et al., 2004). Using these generated datasets, site means were calculated while increasing the percentage of HTs directions mixed in with the primary HT directions. When 50-75% of the samples had HTs directions instead of HT directions, the generated site mean directions overlapped with the Walcott directions, with similar α_{95}, but with smaller *k* than the reported Walcott directions.

The final option is that the Walcott directions are indeed very different from the underlying units. Whatever the case, I suggest that the current paleomagnetic data from the Walcott member should not be combined with the Carbon Butte and Awatabi Members into a Laurentian 750 Ma pole. This is especially true as the Carbon Butte and basal Awatabi are as much as 20 Myr older than the Walcott.

4.6.2 Inclination Flattening

The remanence of sedimentary rocks can be susceptible to inclination flattening (aka inclination shallowing) during initial depositional processes and later compaction. This inclination flattening can bias the resulting paleolatitudes to lower latitudes and the magnitude of this effect can depend on various physical properties such as grain size, grain-size distribution, and grain shape (Tauxe and Kent, 1984). The inclination correction (or flattening) factor, *f*, is defined as $\tan(I_D)/\tan(I_F)$, where I_D is the inclination of the measured remanence and I_F is the original inclination of the ancient

TABLE 6. PALEOMAGNETIC DIRECTIONS AND POLES

Direction	N*	In situ directions			Tilt corrected directions			Fold Test	†Paleomagnetic Poles†			
		Declination/ Inclination (°)	k	α_{95} (°)	Declination/ Inclination (°)	k	α_{95} (°)	Pass/Fail/Synfold/Ind: unfolding (range)	Latitude/ Longitude (°N/°E)	A_{95} (°)	N	K
MT Sixtymile, Carbon Butte+ Carbon Canyon	5	345.0/67.2	37.15	12.71	332.6/72.0	10.64	24.58	Fail: 8% (-10– 50%)	§73.38/219.23	19.9	5	15.6
HT Steep Sixtymile,Carbon Butte+ Carbon Canyon	3	4.8/61.16	80.47	13.8	18.17/61.7	32.6	21.93	Fail: 32% (-8 – 35%)	§82.46/274.56	16.13	3	59.44
HT Sixtymile $n_{samples}$=8, α_{95}=16.67, k=14.07	1	281.0/13.7	NA	NA	281.4/11.2	NA	NA	NA	§10.0/157.2 #12.5/155.9	NA	1	NA
HT Awatabi	2	111.32/-33.70	12.8	76.7	94.82/-29.71	294.79	14.60	Indeterminate: 84% N=2	§29.11/161.81 #13.16/168.4 ##15.71/171.19	59.55 10.20 10.42	2	19.75 600.87 576.24
HT Carbon Butte	3	104.4/ -35.5	15.39	32.60	93.47/-20.74	61.27	15.89	Indeterminate: 88% (-9 – 109%)	§23.97/167.87 #9.10/164.82 ##11.21/167.83	24.23 15.81 15.84	2	26.93 61.82 61.59
HT Awatabi +Carbon Butte	5	107.21/-34.89	18.17	18.67	94.00/ -24.35	78.60	8.68	Pass: 83% (44 – 109%)	#10.73/166.25 ##13.02/169.17	7.61 7.67	5	101.9 100.40
HT Awatabi +Carbon Butte (this study) +Carbon Butte (Weil et al., 2004)	10	100.29/-25.46	19.81	11.12	96.14/-28.50	68.12	5.89	Synfolding: 75% (48 - 91%)	††14.2/166.4 #13.96/167.12 ##12.65/166.10	4.11 4.94 5.06	10	139.0 96.50 91.88
HT Walcott	2	294.7/52.1	14.9	14.9	296.4/29.9	107.7	24.3	Indeterminate: -10% N=2	§37.1/174.7	18.5	2	185.0
HT Carbon Canyon (reanalyzed from Weil et al., 2004)	14	265.14/5.35	7.7	16.14	264.93/6.11	17.92	9.65	Pass: 98.5 (71 – 109%)	#2.08/163.69 ##1.47/164.58	7.98 8.51	14	25.74 22.79

*N—number of sites
†Poles calculated as means from site mean poles for site location 36.30N, 248.10E with HT directions from sites A1305 and AW-13-4 (both Carbon Butte) reversed
§Calculated from the in situ direction
#Calculated from the tilt corrected direction
##Calculated from the tilt corrected direction using the maximum If calculated using f=0.738 for sandstones or f=0.8 for carbonates
††Calculated from the synfolding direction at 75% unfolding is: dec/inc=96.95/-27.98, a95=4.97, k=95.25

field. For large datasets, f can be inferred by the elongation-inclination (E-I) method (Tauxe and Kent, 1984). Some studies have identified inclination flattening by comparing the inclinations of sandstones vs. mudstones (Evans et al., 2000). As they are different lithologies, mudstones are expected to be more affected by compaction and thus inclination flattening than sandstones. Thus if the inclinations vary by lithology, then it can be expected that some sort of inclination flattening may have taken place (Evans et al., 2000). Alternatively, the anisotropy caused by flattening has been estimated using intensive laboratory measurements. These have focused on measuring the anisotropy of the magnetic susceptibility, isothermal remanance (AIR method), of anhysteretic remanence (AAR), or of the thermoremanent magnetization (ATR method) (Jackson et al., 199; Schmidt and Williams, 2013). These laboratory experiments can be complicated by the coercivity of hematite and samples with mixed carriers of both magnetite and hematite (Kodama and Dekkers, 2004; Schmidt et al., 2009). Results from all laboratory estimates are consistent with those from the E–I method (Kent and Tauxe, 2005; Tan et al., 2007; Tauxe et al., 2008; Tan and Kodama, 2002;

Schmidt and Williams 2013). Although in general, the E-I method results in the greatest magnitude of inclination flattening (Tauxe and Kent, 2005).

An in-depth study compared inclination flattening in the late Cryogenian Australian Elatina Formation arenites, the Ediacaran argillaceous Brachina and Wonoka Formations, and the carbonate Nuccaleena Formation (Schmidt and Williams, 2013). They compared multiple methods and confirmed that the arenites tended to experience less flattening than argillites, with the arenites having f =0.738 and the argillites f=0.35–0.38, while carbonates had f = 0.8.

Since not enough samples were collected to apply the E-I method, the corrections of Schmidt and Williams (2013) were applied to the samples in this study (Table 6). Additionally, corrections were applied to the data of Weil et al. (2004) based on his sample descriptions (Table 6).

4.6.3 Proposed New Paleomagnetic Poles

With these datasets, I propose two new Laurentian poles for 750 Ma (Table 6). Both are combined from directions of the Awatabi and Carbon Butte. One is from this study, and the other combines the Awatabi and Carbon Butte results from the Weil et al. (2004) study. The combined Carbon Butte and Awatabi (CB+A) direction from this study passes the fold test with maximum tau_1 occurs at 83% unfolding and 95% confidence bounds are from 44-109% unfolding. The sites were then corrected for inclination flattening. When combined with the directions of Weil et al. (2004), the Tauxe and Watson (1994) fold test resulted in designation of syn-folding, with maximum tau_1 at 75% and the range of 48 – 91% unfolding.

To obtain an appropriate paleomagnetic pole to associate with the 757 Ma Re-Os age in the Carbon Canyon member, the Jupiter member sites were omitted and only the Carbon Canyon member sites were used to calculate a ca. 757 Ma pole for the presented reconstructions (Table 6). This pole passes the fold test, with maximum tau_1 at 98.5% unfolding, and a range of 71-109%.

Of minor additional note, the virtual paleomagnetic pole obtained from the HT directions of

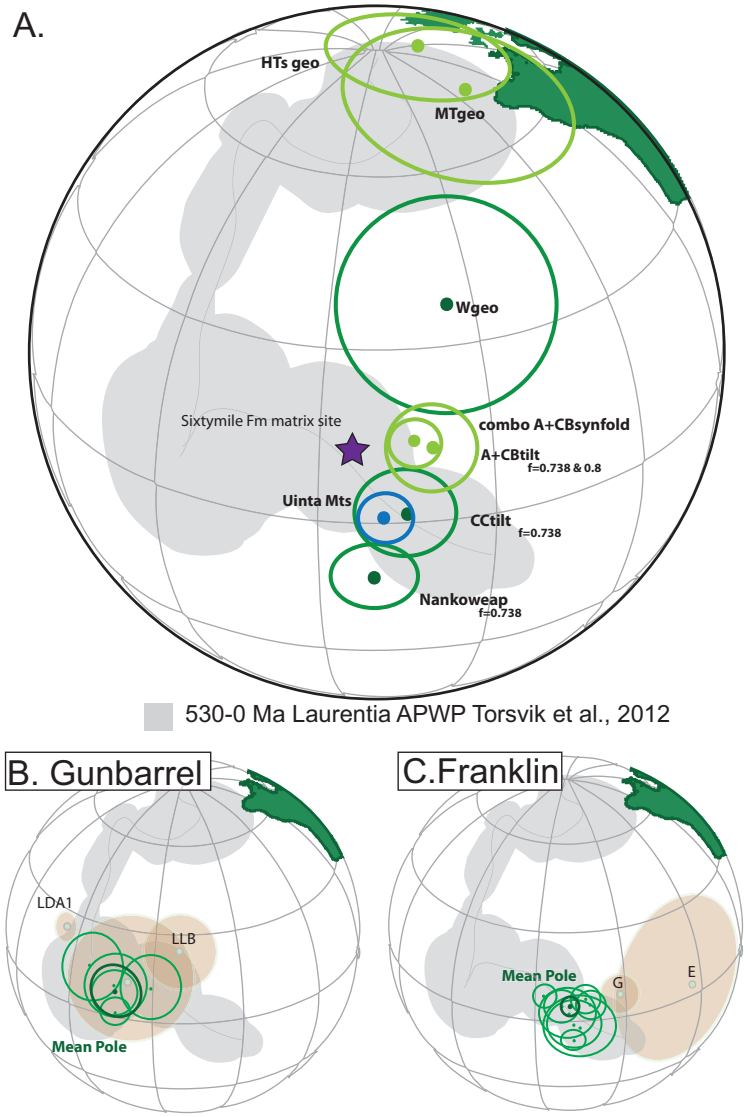


Figure 4.9: A. Paleomagnetic Poles from the Chuar. In light green are the new poles from this study, and in darker green are reanalyzed poles from Weil et al. (2004). HTs geo is the high temperature steep direction in geographic coordinates. MTgeo is the mid-temperature direction. Wgeo is the Walcott pole in geographic coordinates (Weil et al., 2004). A+CB tilt is the flattening corrected combined Carbon Butte and Awatabi pole from this study only. Combo A+CBtilt is the pole from synfolding Awatabi and Carbon Butte directions combined from this study and Weil et al., 2004. CCtilt is the flattening corrected Carbon Canyon mean pole from Weil et al., 2004. The Nankoweap f=0.738 is the flattening corrected Nankoweap pole from Weil et al., 2003. In grey is the 530 Ma to present Laurentian APWP from Torsvik et al. (2012). In blue is the Uinta Mountain pole (Weil et al., 2006), which may be correlative with any of the members of the Chuar group. The purple star indicates the paleomagnetic VGP direction from the single Sixtymile site with resolvable high coercivity primary directions. B. Paleomagnetic poles from the Gunbarrel Event. S= tsezotene Sill, LDA1 and LLB are Little Dal poles. In dark green is the mean Gunbarrel pole calculated in this study. C. Paleomagnetic poles from the Franklin LIP. G is the Greenland pole, E is the Ellesemere pole. In dark green is the mean Franklin pole calculated by Denyesyn et al., 2009.

the one Sixtymile matrix site (A1301) does not bear similarity to the Walcott direction of Weil et al., 2004, but instead is similar to Cambrian Laurentian directions of ca. 500 Ma (Torsvik et al., 2012) (Table 6; Fig. 9).

4.6.4 Interpretation of the shallow directions

Several lines of evidence suggest that the Awatabi and Carbon Butte direction (HT CB+A) is primary. The HT direction is carried by hematite (and possibly magnetite or low temperature unblocking hematite), passes a fold test (or is synfolding). In addition the presence of a reversed unit adds weight to the conclusion that HT is primary. Specifically, the primary nature of this direction is supported by a well-determined rock age and documentation in five sites (this study direction: 5 sites, 23 samples, α_{95}=8.68o, $<$ 16o, and k=78.60 $>$ 10; combined pole: 10 sites, 58 samples α_{95}=5.89o $<$ 16o, and k=68.12 $>$ 10). Additionally, adequate demagnetization with vector subtraction has been applied, but the paleomagnetic poles do have resemblance to younger paleomagnetic poles. When considering the key pole criteria of Buchan (2014), HT is related to a robust age and the primary remanence is properly isolated. Despite the fact that the fold test from this study just establishes the relative timing of magnetization, it still suggests magnetization close to the age of deposition, as this folding is essentially syndepositional. Thickness changes perpendicular to the Butte fault and the Chuar Syncline axis indicate growth strata related to fault movement and syndepositional growth of the Chuar syncline (Timmons et al, 2001).

4.6.5 Interpretation of the steep directions

For the HTs direction, unblocking temperatures suggest that hematite is the main magnetic carrier. As high temperatures were needed to thermally demagnetize this component (680°C for many samples), a very high metamorphic temperature, inconsistent with the observed low degree of metamorphism, would have been required order to have a thermoviscous origin; therefore, this result is

interpreted as a chemical remanent magnetization (CRM). CRM is acquired as a magnetic mineral nucleates and grows through a critical volume at which its magnetic direction becomes stable with respect to thermal fluctuations (Stokking and Tauxe, 1990). This can occur during mineral alteration (e.g., oxidation of magnetite to hematite) or mineral precipitation (grain growth or crystallization), which may accompany weathering, diagenesis, or low-grade metamorphism (Stokking and Tauxe, 1990). CRM remagnetization overprints via secondary precipitation/growth of hematite or conversion to hematite are generally a result of large-scale fluid flow during orogenesis (Miller and Kent, 1988), pronounced hydrothermal events (Witte and Kent, 1991), hydrothermal systems circulating in permeable rocks below basalts (Wynne et al., 1998), or migration of fluids along fractures and unconformities during uplift-enhanced surface meteoric fluid circulation (Geissman and Harlan, 2002; Preeden et al., 2009). As this direction is very similar to the present day field direction, it is likely a recent overprint and could be related to the Laramide orogeny or to the 400-550 ka Uinkaret volcanic field (Crow et al., 2008; Hamblin, 1970).

4.6.6 Rotation of the Colorado Plateau

When considering paleomagnetic data, it is important to ensure that the regions are tectonically coherent and have not been complicated by larger regional block rotations. It is suggested that the Laramide orogeny involved a clockwise rotation of about 2-4 degrees of the Colorado Plateau relative to the continental interior (Hamilton, 1988). As the Grand Canyon is located at the very southwest margin of the Colorado plateau, its putative rotation may need to be corrected. Some suggest that the angle of rotation was moderate (5°, Bryan and Gordon, 1990), but more recent paleomagnetic studies have suggested that this clockwise rotation may have been as large as 13.5° to 15° to account for differences in declination of Mesozoic paleomagnetic poles (Kent and Witte, 1993; Steiner and Lucas, 2000; Kent et al., 2012). Luckily, the underlying Cardenas basalt and associated Unkar Group Intrusions can be used to understand the magnitude of the Colorado Plateau rotation in

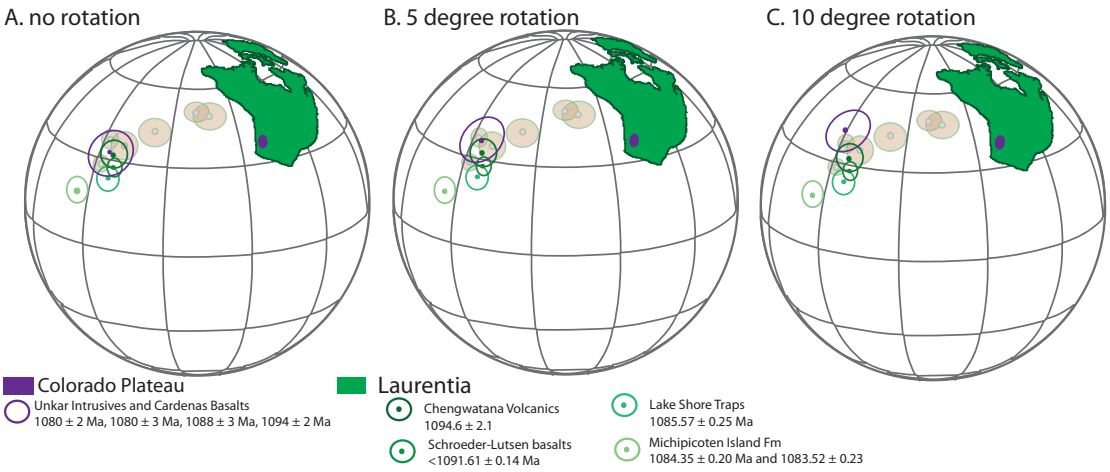


Figure 4.10: Testing the block rotation of the Colorado plateau by comparing the paleomagnetic poles from the ca. 1094-1080 Ma Grand Canyon Unkar intrusives and Cardenas basalt to the 1095 Ma-1083 Ma portions of the midcontinent rift Logan Loop. A, B, C, Colorado plateau rotated 0, 5, 10 degrees relative to North America using an euler pole of 34.6°N 254.6°E (Hamilton, 1988).

the Grand Canyon area. A normal polarity paleomagnetic pole was obtained from Cardenas basalt and Unkar Intrusions (32°N, 185°E, dp = 6.8°/dm = 9.3°; n=3 flows, 13 intrusions; Weil et al., 2003). This direction was interpreted to be primary based on a partial contact test of the (Weil et al., 2003). As these units are ca. 1100 Ma that suggests comparison with paleomagnetic results from the Mesoproterozoic (1.1 Ga) Midcontinent Rift (MCR). The U-Pb baddeleyite ages (1080±2 Ma, 1080±3 Ma, 1088±3 Ma, and 1094±2 Ma) obtained by Bright et al. (2014) were used to compare the Unkar Intrusives and Cardenas basalt with the MCR volcanics (Fig. 10. Table. 10).

Early paleomagnetic studies of the MCR, suggested that there might be asymmetric reversals preserved in the volcanics. However, a high-resolution study of paleomagnetic data that spanned three geomagnetic field reversals from a well-described series of basalt flows at Mamainse Point showed that each reversal was in fact symmetric and the previously documented reversal asymmetry was an artifact of the rapid motion of North America during this time (Swanson Hysell, et al., 2009). Now the Keweenaw volcanics and associated Logan Loop is one of the best constrained geochrono-

logic and paleomagnetic parts of the Precambrian Laurentian APWP. Given the age constraints, the Chengwatana Volcanics (1094.6±2.1 Pb-Pb Zartman et al., 1997), Schroeder-Lutsen Basalts (<1091.61±0.14 Ma chemical abrasion-isotope dilution-thermal ionization mass spectrometry [CA-ID-TIMS] Fairchild et al., 2017), the Lake Shore Traps (1085.57±0.25 Ma CA-ID-TIMS Fairchild et al., 2017), and the Michipicoten Island Formation (1084.35±0.20 Ma and 1083.52±0.23 CA-ID-TIMS Fairchild et al., 2017) are of particular relevance for this study.

The suggested rotation of the Colorado plateau with a pole at 34.6°N 254.6°E (Hamilton, 1988) was applied for three different cases: rotations of 0°, 5°, and 10° of the Colorado plateau and associated pole (Fig. 10). In the unrotated state, the Cardenas-Unkar Intrusive pole lies coincident with the Chengwatana Volcanics. When the Colorado plateau is rotated greater than 15 degrees, the $A_{95}$of the Cardenas-Unkar Intrusive pole no longer overlaps with any of the Keweenawan volcanics. The uncertain age constraints on the Cardenas-Unkar Intrusive pole hinders a robust comparison, however, the data suggests that the Colorado plateau has rotated less than 15°, most likely less than 5°, and is most similar to the Keweenawan poles in its unrotated state. Thus corrections for large-scale tectonic block rotations were not applied.

4.7 Interpretations of Directions and Comparison to the Laurentian Apparent Polar Wander Path

Three paleomagnetic poles were distinguished in this study: a mid-temperature (MT), and two high-temperature poles (HT and HTs), These poles are plotted (Fig. 9A) along with the Laurentian apparent polar wander path (APWP) from 510 Ma to the present (Torsvik et al., 2012). The other main poles constraining the Laurentian APW path are those from the ca. 775 Ma Gunbarrel event (Fig. 9B), from the <780 Ma Nankoweap Formation (Fig. 9A), the ca. 750 Ma Uinta Mountain Group (Fig. 9A), and those from ca. 720 Ma Franklin event (Fig. 9C).

4.7.1 Gunbarrel event

The Gunbarrel Event (Table 7; Fig. 9B) is marked by ca. 775 Ma mafic dikes and sheets, in three widely separated areas of Cordilleran North America (the Canadian Shield, the Mackenzie Mountains in the northern Cordillera, and the Wyoming Province) that may mark a giant radiating dyke swarm (Park et al., 1995, Ernst et al., 2003). The magmatism has been attributed to mantle-plume activity or upwelling asthenosphere leading to crustal extension accompanying initial breakup of the supercontinent Rodinia and development of the proto-Pacific Ocean (Harlan et al., 2003; Ernst and Buchan, 2002).

In the Wyoming province, the Wyoming dikes include the Tobacco Root dikes, the Mount Moran dike and the Christmas Lake dike. For the Tobacco Root dikes, hornblende concentrates from the Group B dikes yield Ar-Ar ages of 778–772 Ma, whereas biotite from a baked contact zone yielded a plateau date of 788 Ma (Harlan et al., 2008). Hornblende from the Christmas Lake dike yielded Ar-Ar plateau date of 774 Ma (Harlan et al., 1997). For the Mount Moran dike, Ar-Ar results from a hornblende-pyroxene concentrate were discordant and contained excess Ar, which led Harlan et al. (1997) to suggest a ca. 780 age.

In northwestern Canada, zircon separated from the Concajou Canyon gabbroic sill of the Tsezotene intrusive suite yielded a weighted mean Pb-Pb TIMS date of 779.5±2.3 Ma (Harlan et al., 2003). Paleomagnetism of the Tsezotene intrusive suite was investigated by Park et al. (1981; 1989), which was found to contain both normal and reversed magnetizations. These authors argued that the sill was large enough to cool slowly and capture secular variation with both normal and reversed magnetizations (Park et al., 1981). Towards the interior of Laurentia, the Hottah dikes were dated with TIMS Pb-Pb on baddeleyite 780±1 (Harlan et al., 2003) and yielded a paleomagnetic pole with large A_{95} studied by Park et al. (1995). The Little Dal Basalts have recently been redated using CA-ID-TIMS U-Pb on zircon to 774.93±0.54 Ma (Milton et al., 2017). The Little Dal Basalts have been

geochemically linked to the ca. 780 Ma Gunbarrel magmatic event (Dudas and Lustwerk, 1997). Morris and Aitken (1982) undertook a paleomagnetic study of the Little Dal Basalts at a locality near Keele River, and Park and Jefferson (1991) reanalyzed their data. The original study found two poles that could be primary (LD-A and LD-L). But as LD-L was more abundant in the lower, less altered parts of the basalt sections, it was interpreted as primary. However, LD-L is about 20° away from the rest of the Gunbarrel poles. Park and Jefferson (1991) discuss the possibility that tectonic rotations may have complicated the interpretations of those poles. In addition, a larger tilt correction moves the LD-L direction closer to that expected from the Gunbarrel direction. Due to possible tectonic complications, the results from the Little Dal Basalt were not included in the calculated mean Gunbarrel pole.

4.7.2 Nankoweap Formation

Paleomagnetism of the Nankoweap Formation was investigated by Weil et al. (2003), who collected sandstone samples from eight sites. The demagnetization showed that almost all samples displayed a single vector component with a minor secondary component. The in-situ secondary component was subparallel to the Earth's present-day field (PDF). This secondary component was normally removed by 200°C and was interpreted as a viscous overprint. A fold test was applied to the combined seven sites with resolvable directions, and the parametric bootstrap fold test was applied which gave a maximum clustering at 80% unfolding and a 95% confidence interval that includes 100% unfolding (Weil et al., 2003). This direction was corrected for sandstone inclination flattening using f=0.738 (Table 7,8,9).

4.7.3 Uinta Mountain Group (UMG)

A paleomagnetic study was undertaken by Weil et al. (2006), that obtained paleomagnetic data from the Eastern Uinta Mountains (Home Mountain Canyon: N=3; Bull Canyon: N=10; Sparks-

Talamantes Creek: N=9 localities) as well as from the north-central Uintas (Sheep Creek Canyon: N=23; Browne Lake: N=1; Carter Creek: N=5; Dowd Springs: N=5; and Flaming Gorge Reservoir dam: N=16). Sampling was focused on hematite-cemented medium to fine-grained sandstone and siltstone. The strata exposed in the western Uinta Mountains are characteristically different than those in the eastern Uinta Mountains, and it is still uncertain how the eastern and western Uinta Mountain Group strata correlate. The western Uinta Mountain Group is composed of quartzose and arkosic sandstone and interbedded mudstone, much of which is hematite- cemented, whereas the eastern section consists of conglomerate, sandstone and mudstone, and hematite-cemented red sandstone (Hansen, 1965). Although no specific stratigraphic information was given on the paleomagnetic sampling localities, most of the sites were in the north-central Uintas (Weil et al., 2006). More recent work has still kept the eastern portions as undifferentiated, but Dehler et al. (2005) has suggested two potential correlations for the strata near Sheep Creek (the focused main paleomagnetic sampling locality). First that exposed strata may be the upper-middle part of the Uinta Mountain Group thrust above the Red Pine Shale, or secondly, that the it is correlative with the Red Pine Shale to the west, representing a facies change (Dehler et al., 2005; 2007). These have different interpretations for the APWP. If the relationship is a thrust contact, the Uinta Mountain Group strata there may be correlated with the lower members of the Chuar Group, and the pole should range in age from <782 to 751 Ma. Alternatively, if the Uinta Mountain pole is dominated by the Red Pine Shale, correlative with the Walcott member, then the Uinta Mountain Group pole should be assigned an age between 751-729 Ma. The 717 Ma Franklin pole (potentially similar to the pole expected for the top of the Walcott) and the Carbon Canyon+Jupiter poles are very similar; thus, those paleomagnetic poles cannot be used to better determine the stratigraphic height of the Uinta Mountain Group pole. The stratigraphic and temporal resolution for the Uinta Mountain Group paleomagnetic pole is not high enough to warrant its use in the presented paleomagnetic reconstructions.

TABLE 7. 780-720 MA LAURENTIAN PALEOMAGNETIC POLES

Pole	Unit/Fm	Age (Ma)	Type of Age and Reference	Paleomagnetic Pole			Paleomagnetic Reference	NOTES
				Lat.	Long.	A95 (dp,dm)		
Cambrian Sixtymile Fm	Sixtymile Fm			-3.9	142.4	6.3	Elston et al., 2002.	In text "Data presented and discussed by Link et al., 1993" but no data reported
Franklin individual studies	Coronation–Baffin intrusions	723+4/-2	U-Pb baddeleyite upper intercept (Heaman et al. (1992)	8.0	167.0	5.0	Fahrig et al. 1971	Age from 10 analyses (6 sites):Coronation sill, Quadyuk Island (Bathhurst inlet) Cumberland dike (NE Baffin)
	Coronation sills	723+4/-2	See above Heaman	–1.0	163.0	9.0	Robertson and Baragar 1972	
	S Baffin dikes			6.3	168.2	4.8	Fahrig and Schwarz 1973	
	NW Baffin dikes	716+4/-5	Weighted average of U-Pb baddeleyite fractions (Pehrsson & Buchan, 1999	9.2	153.3	3.8	Christie and Fahrig 1983	Age from one dike
	Miscellaneous dikes	undated		3.0	161.3	9.2	Park 1974	
	Natkusiak lavas and sills (Victoria)	716.33±0.54	U-Pb (n=5 single baddeleyite) Gabbroic sills and dikes from Victoria Island Macdonald et al., 2010)	–7.0	163.0	4.0	Palmer and Hayatsu 1975	Previously pub. ages: 718±2 upper intercept of 1 baddeleyite 3 zircon fractions from 2 sills, 723+12/-2 from 5 baddelyite fractions from 3 victoria island sills (Heaman et al 1992)
	Natkusiak upper lavas (Victoria)	undated		6.0	159.0	5.7	Palmer et al. 1983	The eruption age not directly dated
	Brock Inlier sills (Lasard River)	708±4	Associated dikes (Ernst et al 2004)	–2.0	165.0	12.0	Park 1981	
	Thule Greenland	712±2 721±4	U-Pb baddeleyite fractions	8.8	178.5 8	7.28	Denyszyn et al. 2009	Anomalous. Resolved by early Cenozoic block rotations around the Nares Strait region.
	Ellesmere	721±2 716 ± 1 713 ± 3 713 ± 2	U-Pb baddeleyite fractions younger ages from (Denyszyn, Halls and Davis, 2009)	4.08	206.8 8	30.28	Denyszyn et al. 2009	anomalous SW directed remanence from concentrated sampling of secular variation or pyrrhotite chemical remagnetization during Ellesmerian Orogeny (Denyszyn, Halls and Davis, 2009)
Franklin Mean poles	Victoria/Baffin Int. & Ext.			5.0	163.0	5.0	Park (1994)	
	Mainland/Baffin intrusives			5.8	165.8	3.8	Fahrig and Schwarz 1973	
	Victoria/ Baffin. Int. & Ext.			8.0	163	4.0	Buchan et al. 2000	
	***Victoria/ Mainland/BaffinInt. & Ext.**	**716.33±0.54**	**(Macdonald et al., 2010)**	**6.7**	**162.1**	**3.0**	**Denyszyn et al. 2009**	**Site-filtered by Denyszyn et al., 2009 from previous studies**
	Victoria/ Mainland/Baffin/Greenland . Int. & Ext.			8.4	163.8	2.8	Denyszyn et al. 2009	Site-filtered previous studies combined with variably rotated data from Greenland and Ellesmere
Kwagunt	***Carbon Butte+Awatabi**	**751.0± 7.6**	**Re-Os in Awatabi Mb. (Rooney et al., submitted)**	**13.02**	**169.17**	**7.67**	**This Study**	Tilt corrected pole is corrected for flattening using *f*=0.8 for carbonates and *f*=0.738 for sandstones
	***COMBO Carbon Butte+Awatabi**	**751.0± 7.6**	**Re-Os in Awatabi Mb. (Rooney et al., submitted)**	**14.2**	**166.4**	**4.11**	**This Study**	**Results from this study combined with results for Carbon Butte member from Weil et al. (2004). Pole is synfolding at 75% (48-91%).**
	Kwagunt	ca. 750-736		18	166	7.0	Weil et al. 2004	Pole was used with 740 Ma age
	Kwagunt			1.9	162.4	5.6	Elston et al., 2002	See above comment for Elston 2002
Galeros	***Carbon Canyon**	**757.0 ± 6.8**	**Re-Os in middle of Carbon Canyon Member (Rooney et al., submitted)**	**1.47**	**164.6**	**8.51**	**Reanalyzed Weil et al. (2004).**	**Tilt corrected pole is corrected for flattening using *f*=0.738 for sandstones**
	Galeros	ca. 800		-1.9	163	6.95	Weil et al. 2004	
	Galeros			-12.2	163.0	1.7	Elston et al., 2002	See above comment for Elston 2002
Uinta Mountain Gp	Uinta Mountain Gp	ca. 800-750		0.8	161.3	3.3	Weil, et al. 2006	Plotted for comparison purposes. Unclear stratigraphic context, likely correlative with the Chuar poles that do have geochronologic constraints.
Nankoweap	***Nankoweap**	**< 782 Ma**	**detrital zircons (n = 14) Dehler et al., 2017**	**-11.7**	**159.4**	**7**	**Reanalyzed Weil et al., 2003**	Tilt corrected pole is corrected for flattening using *f*=0.738 for sandstones
	Nankoweap	**900**		**-10**	**163**	**7**	**Weil et al., 2003**	**pole was used with 900 Ma age**
	Nankoweap	900		12.5	174.4	(4.5,7.7)	Elston and Scott (1973)	small number of samples and sites
	Nankoweap upper			-8.0	161.1	2.4	Elston et al., 2002	See above comment for Elston 2002
	Nankoweap lower			7.4	178.1	2.5	Elston et al., 2002	See above comment for Elston 2002
Gunbarrel Event	Wyoming dike mean	ca. 780		13.0	131.0	4.0	Harlan et al. (1997)	
	Tobacco Root-B dike	775 ± 3	hbl Ar-Ar	14.6	127.0	11.6	Harlan, S.S. et al. 2008	
	Christmas Lake dike	774 ± 4	hbl Ar-Ar	7.4	137.0	8.3	Harlan, S.S. et al.1997	
	Mount Moran dike	775 ± 10	discordant Ar-Ar on hbl-px	11.6	148.9	10.2	Harlan, S.S. et al.1997	
	Tsezotene sills	779.5±2.3	U-Pb Concajou Canyon Harlan et al 2003	1.6	137.8	5.0	Park et al. (1981; 1989);	
	Little Dal Basalts	774.93±0.54	U-Pb CA-IDTIMS Milton et al 2017	24	115	7	LLA1/LD-L: Morris & Aitken (1982)	Anomalous. Potentially due to local tectonic rotations Alternatively due to a Paleozoic overprinting event.
	Little Dal Basalts	774.93±0.54	U-Pb CA-IDTIMS Milton et al 2017	11	137	11	LLA2: Park and Jefferson 1991	No published demagnetization data.
	Hottah Sheet	780±1	Harlan et al 2003	13	141	22	Park et al 1995	
	***Gunbarrel Mean**	**774.93±0.54**	**U-Pb CA-IDTIMS Milton et al., 2017**	**8.8**	**137.7**	**11.9**	**This study (K=60.44)**	**Tobacco Root-B, Christmas Lake, Mount Moran dikes, Tsezotene sills**

4.7.4 Franklin Large Igneous Province (LIP)

The ca. 720 Ma Franklin Large Igneous Province (LIP) includes sills, dikes, and volcanic rocks in northern and northwestern Canada and northwestern Greenland. The most obvious signature of the Franklin LIP is the radiating Franklin dyke swarm that converges towards the northern margin of Canada. U-Pb zircon and baddeleyite ages from the Franklin LIP rocks span from ca. 730-710 Ma, however, this large spread may be due in part to imprecise multigrain techniques. The most precise, single grain chemical abrasion-ion dilution-thermal ion mass spectrometry (CA-ID-TIMS) on zircon and baddeleyite associated with the Franklin LIP yielded an age of 716.33 ± 0.54 (Macdonald et al., 2010).

Paleomagnetic data from the Franklin LIP provide robust Neoproterozoic constraints for Laurentia and an important tie point for Neoproterozoic paleogeography (Table 7; Fig. 9C). Many studies have collected and analyzed Franklin aged paleomagnetic samples from northwest Canada. These studies span six key regions: the Canadian Mainland, Victoria Island, Baffin Island, Devon Island, Ellesmere Island and northern Greenland. On the Canadian Mainland, the dated Coronation Sills (Robertson and Baragar, 1972) and Lasard River intrusions of the Brock inlier have been sampled for paleomagnetism (Park, 1981). These sites span enough time to average out secular variation, as both normal and reverse directions were found over a wide area. The Coronation Sills are dominated by reverse polarity directions, while the likely younger Lasard River intrusions contain both polarities (Robertson and Baragar, 1972, Park, 1981, Ernst et al., 2001, Heaman et al., 1992). On Victoria Island, the Natkusiak basalts and associated intrusives were the focus of two studies. The initial study of the Natkusiak basalts revealed only reversed magnetization directions (Palmer and Hayatsu, 1975). A later study of about 740 m of the Natkusiak flows revealed a double reversal, although the lower reverse direction was badly contaminated by a downward steep overprint (Palmer et al., 1983). As the dikes in the area were observed to both feed and cut sills and flows, dikes were interpreted to

be active throughout the duration of the Franklin LIP (Palmer et al., 1983). Sills were dominantly sampled from the associated intrusives, with Pb-Pb TIMS multi-grain baddeleyite and zircon dates ranging from 718±2 Ma to 723+12/-2 Ma (Heaman et al., 1992), and were almost all reversed in magnetization, with only one displaying a normal direction (Palmer and Hayatsu, 1975; Palmer et al., 1983). To the east, the Baffin Island dikes have been intensively sampled all across the island and have been split into several groups: the Franklin dikes, the Borden dikes and the Strathcona Sound dikes. The northwest trending Franklin dikes dominate Baffin Island and have been the focus of multiple paleomagnetic studies distinguishing both normal and reverse polarities (Christie and Fahrig, 1983, Fahrig et al., 1971; Fahrig and Schwarz, 1973). Initially, the northwest trending Borden dikes (on the Borden Peninsula) were thought to be part of a much older event, due to an older ca. 950 Ma age, cross-cutting relationships and a steep paleomagnetic direction (Christie and Fahrig, 1983). Revaluation of the dikes by Pehrsson and Buchan (1999) updated the date to Franklin times (ca. 720 Ma), and suggested that the steep magnetizations resulted from the superposition of a Cretaceous–Tertiary aged chemical remanent magnetization on normal and reversed primary Franklin components. As the Strathcona Sound dike swarm is tangential to and cross-cuts the main Franklin dikes, it represents a slightly younger event (Christie and Fahrig, 1983). Despite its younger age, the Strathcona Sound dikes have a similar paleomagnetic direction to the rest of the Franklin dikes (Christie and Fahrig, 1983). The mean paleomagnetic directions from Mainland Canada, Victoria Island and Baffin Island have some overlap at the 95% confidence level (Fig. 9C), but this is not the case for paleomagnetic poles from Ellesmere Island, Devon Island and Greenland. Interpretation of the Devon Island dikes and Ellesmere Island dikes is complicated by the presence of a possible Ellesmere microplate that includes Devon and Ellsemere Islands and may have moved relative to the rest of North America during early Cenozoic motions (Denyszyn et al., 2009). The Devon Island dikes display directions generally shallow and down to the west, with one dike shallow up to the east (reversed) (Denyszyn et al., 2009). On Ellesmere Island, three dikes were sampled for paleomagnetic

study; two of them had anomalous directions, one of which yielded a U-Pb TIMS multi-grain fraction baddeleyite age of 721+/-2 Ma (Denyszyn et al., 2009). The anomalous SW directed remanence is suggested to be caused by rotation of an Ellesmere microplate, unintentional concentrated sampling of secular variation or by pyrrhotite chemical remagnetization during Ellesmerian Orogeny (Denyszyn, Halls and Davis, 2009). Across the Nares Strait, Franklin aged dikes and sills were sampled from the northern Thule area of Greenland, where the resulting anomalous paleomagnetic directions were of both normal and reversed (Denyszyn et al., 2009).

There is longstanding discussion regarding the amount of tectonic movement along the Nares Strait and the original location of Greenland. Although it is acknowledged that seafloor spreading in the Labrador Sea resulted in tectonic motions and rotations, the magnitude of possible strike slip motions is debated, and the tectonic rotations of the other Arctic islands is still undecided (Roest and Srivastava, 1989; Torsvik et al., 2001a). Across the Nares Strait, the similarities in the Paleozoic geology of Ellesmere Island and northwest Greenland suggest that no more than 70 km of offset occurred (Denyszyn et al., 2009). However, the main dike concentrations on both sides of the Nares Strait (on Devon Island and near Thule on Greenland) are offset by 200 km, suggesting large sinistral motion (Denyszyn et al., 2009). Denyszyn et al. (2009) suggested that the differences in the Ellesmere Island, Devon Island and Greenland paleomagnetic data from the regions to the west was best resolved by early Cenozoic block rotations around the Nares Strait region. Their data supports a 20° rotation between Mainland Canada and an Ellesmere microcontinent (that includes at least Ellesmere and Devon islands), along with a 14° rotation of Greenland (Denyszyn et al., 2009). The magnitude and direction of the Greenland rotation agree with that needed to close the Labrador Sea (Roest and Srivastava, 1989). However, problematic overlap of Devon Island over Baffin island and differences between paleomagnetic data from Greenland, Ellesmere and Devon islands suggest an extinct plate boundary that separated the combined Devon and Ellesmere islands from Greenland and accommodated addition movements between them (Denyszyn et al., 2009). As

Lancaster Sound (between Devon and Baffin islands) is filled with thick Cenozoic sediments in a westward narrowing basin, it is possible that this area may have accommodated movement of the Devon-Ellesemere microcontinent (Denyszyn et al., 2009). The microcontinent rotation is also consistent with a ~25° difference between Permian poles from Ellesmere Island and North America (Torsvik et al., 2001a). This rotation is also in agreement with the restoration by Rowley and Lottes (1988) where Ellesmere is displaced from North America, helping to explain extension in the Arctic Oceans. In addition to tectonic motions of Greenland, Ellesmere and Devon Islands, Baffin Island may have moved relative to North America along faults in the Hudson Strait during the opening of the Labrador Sea (Pinet et al., 2013). As this motion is not thought to be very large, it is unlikely to change the Baffin pole position too drastically.

The unadjusted paleomagnetic data from Ellesmere Island, Devon Island and Greenland all act to pull the paleomagnetic pole of the Franklin LIP to the west. As mentioned earlier, these sites may have been biased by an anomalous field or tectonic motions and rotations, the extent to which is still undecided. Thus, when piecing together Neoproterozoic paleogeography, a more cautious calculation of the Franklin mean pole includes only sites from regions unaffected by these issues. Importantly, using the adjusted/rotated mean pole of Denyszyn et al. (2009), the mean pole from Canada of Denyszyn et al. (2009), or the mean pole of Buchan et al. (2000), yield almost indistinguishable results. In the subsequent reconstructions, I have used the mean pole from Canada of Denyszyn et al. (2009).

4.8 Neoproterozoic Paleogeography

With a more robust 780-720 Ma Laurentian APW path, I can compare the Laurentian dataset with paleomagnetic and geochronologic data from other cratons (Table 8), and explore the paleogeographic implications for Rodinia. In particular, below I evaluate the SWEAT, AUSWUS, AUS-

TABLE 8. CRATON PALEOMAGNETIC POLES

Craton	Unit/Fm	Age (Ma)	Type of Age+ Reference if different	Paleomagnetic Pole Lat.	Long.	A95 (dp, dm)	Paleomagnetic Reference	NOTE
Laurentia	***Franklin LIP Victoria/ Mainland/Baffin Int. & Ext.**	**716.33±0.54**	**Macdonald et al., 2010**	**6.7**	**162.1**	**3.0**	**Denyszyn et al. 2009**	**Site-filtered by Denyszyn et al., 2009 from previous studies**
	***Carbon Butte+Awatabi**	**751.0± 7.6**	**Re-Os in Awatabi Mb. (Rooney et al., submitted)**	**13.0 2**	**169.17**	**7.67**	**This Study**	**Tilt corrected pole corrected for flattening using *f*=0.8 for carbonates and *f*=0.738 for sandstones**
	***COMBO Carbon Butte+Awatabi**	**751.0± 7.6**	**Re-Os in Awatabi Mb. (Rooney et al., submitted)**	**14.2**	**166.4**	**4.11**	**This Study**	**Results combined with Carbon Butte Mb. results from Weil et al. 2004. Pole is synfolding at 75% (48-91%).**
	***Carbon Canyon**	**757.0 ± 6.8**	**Re-Os in middle of Carbon Canyon Mb. (Rooney et al., submitted)**	**1.47**	**164.6**	**8.51**	**Reanalyzed Weil et al. 2004**	**Tilt corrected pole corrected for flattening using *f*=0.738 for sandstones**
	***Nankoweap**	**< 782**	**detrital zircons (*n* = 14) Dehler et al., 2017**	**-11.7**	**159.4**	**7**	**Reanalyzed Weil et al., 2003**	**Tilt corrected pole corrected for flattening using *f*=0.738 for sandstones**
	***Gunbarrel Mean**	**774.93±0.54**	**U-Pb CA-IDTIMS (Milton et al., 2014)**	**8.8**	**137.7**	**11.9**	**This study**	**Tobacco Root-B, Christmas Lake, and Mount Moran dikes, Tsezotene sills**
Southern Australia	Walsh cap dolomite	750-700	Maloof et al., 2006 suggested ca. 720	-21.5	282.4	12.2	Li, 2000	Likely age from Rooney et al., 2015: 662 Ma (Sturtian cap or 632 Ma (Marinoan cap)
	***Mundine Well dikes**	**755±3**	**Pb-Pb weighted mean zircon SHRIMP**	**45.3**	**135.4**	**4.1**	**Wingate and Giddings, 2000**	
	Kanpa Fm	760-720	correlations	74.0	128.8	(7.7, 14.8)	Pisarevsky 2007	Close to some Middle Devonian Australian poles. Preliminary result because it is based on six samples.
	***Hussar Fm**	**800-760**	**correlations**	**62.2**	**85.8**	**10.3 (7.3, 14.6)**	**Pisarevsky 2007**	
	Browne Fm	830-800	correlations	44.5	141.7	(5.1, 9.0)	Pisarevsky 2007	
Northern Australia	Bitter Springs Fm. Johnny's Creek Member	780-660	Uncertain age, constrained by fold test to be pre-Paleozoic	15.8	83.0	13.5	Swanson Hysell, et al., 2012.	
	Wooltana volcanics	827± 6?		-62.0	142.0	16.0	McWilliams & McElhinny 1980; Preiss, 2000	Very uncertain age constraints: McWilliams & McElhinny 1980 , M. Idnurm, unpublished 1997
	Yilgarn B dikes		Originally thought to be 750–700 Ma	77.9	162.0	28.1	Giddings 1976	younger (possibly Mesozoic) overprint (Halls and Wingate, 2001)
S. China	Liantuo sediments	748±12	SHRIMP U-Pb (Ma et al. 1984)	4.0	161.0	13	Evans et al. 2000	Unpublished age from the pmag locality is ~778 Ma. Macdonald et al., personal comm. But cited as" Basal Liantuo Fm" (eg. Buchan 2013). Paleomagnetic data spans the upper part of the formation
	Liantuo	720±15	SIMS U-Pb (Lan et al 2015)	12.7	157.4	5.2	Jing et al., 2015	
	***Liantuo average**	**720±15**	**SIMS U-Pb (Lan et al 2015)**	**13.2**	**155.2**	**5.27**	**Jing et al., 2015**	
	UWA site 1		Basal unit of the upper Liantuo	11.7	159.0	10.7	Evans et al. 2000	No reversals, N<25 samples and no field test
N. China	Mean poles	ca. 700	Mean of several undated poles	-42.9	107.0	5.7	Zhang et al. 2006	Mean of poles from chinese paper published in the 1980s
	Nanfen		Unclear geologic context, ca. 925 Ma in age based on recent correlations (Fu 2015)	-16.5	121	11.1	Zhang et al. 2006	800–780 Ma age suggested by Li et al., 2008. No demag available.
Tarim	***Beiyixi (Baiyisi)**	**755±15 732.0±8**	**755: SHRIMP zircon U-Pb. 732: SHRIMP zircon U-Pb Xu et al. (2005)**	**17.7**	**194.2**	**4.2**	**Huang et al. 2005**	**This age probably suffers from inheritance. Volcanics overlie the Sturtian age Baiyisi diamictites**
	***Qiaoenbrak Formation**	**<717 Ma**	**Sturtian age**	**-6.3**	**17.5**	**9.1**	**Wen et al. 2013**	**<730 Ma**
	Aksu dykes	807±12		214	271	11.0	Chen et al. 2004	Likely overprint: similar to Mid Paleozoic APWP (Wen et al. 2016)
India	***Malani igneous suite**	**771±5**	**U-Pb zircon SIMS (Gregory et al. 2009)**	**69.4**	**75.7**	**6.5**	**Meert et al. 2013**	**LA-ICP-MS Pb-Pb discordant zircon: 752 ± 18 Ma.(Meert et al. 2013)**
	Malani igneous suite	771±5	U-Pb zircon SIMS (Gregory et al. 2009)	67.8	72.5	8.8	Gregory et al. 2009	
	Malani igneous suite	771-751: 751±3,771±2	U-Pb zircon Tucker unpublished	68.0	88.0	8	Torsvik et al. 2001	Pre. Res. 108
	Mahe dikes	750.2±2.5	U-Pb zircon Takamaka dolerite	80.0	79.0	11	Torsvik et al. 2001	Pre. Res. 110
Congo	***Mbozi gabbro**	**743±30 748±6 <755±25**	**743: K-Ar (Brock 1968), 755: K-Ar bt Syenite intrusions (Cahen & Snelling, 1966; 748: U-Pb zircon (Mbede et al. 2004)**	**46.0**	**325.0**	**9**	**Meert et al. 1995**	**755 Ma age recalculated in Evans 2000, Mbede et al age is unpublished except for conference proceedings**
	Luakela Volcanics	765±5	U-Pb zircon SHRIMP (Key et al., 2001)	40	302	14	Wingate et al., 2010	
	Gagwe Lavas	795±7	Ar-Ar (Deblond et al. 2001)	25	93	10	Meert et al. 1995	May actually be an overprint (Wingate et al., 2010)
Siberia	***Kitoi (Sayan) dikes**	**743 ± 47 758 ± 4**	**743: Sm–Nd. 758: Ar-Ar (Sklyarov et al. 2003)**	**1.1**	**22.4**	**7.4**	**Pisarevsky et al. 2013**	**Likely correlative with Franklin LIP, suggesting 720 Ma age. Pole is also presented as:-0.4°N, 201.8°E, A95=6.1°**

***pole used in reconstruction**
'A_{95}' is radius of the circle of confidence about the mean pole and is usually calculated with Fisher statistics on site mean poles.
When site mean poles are not available A_{95} is estimated as the square root of dp × dm, where dp and dm are the semi-axes of the 95% ellipse of confidence about the mean pole (Khramov, 1987, p. 97).

MEX, and South China and Tarim missing link configurations of Rodinia. I start by reviewing the existing data for continental cratons, with a focus on published paleomagnetic poles in the 780-720 Ma interval.

4.8.1 Australia

Rift basins in Australia are interpreted to represent two episodes of extension, one ca. 700-650 Ma the second ca. 600 Ma, with extension suggested to be off the present day eastern margin (Preiss et al., 1978; Walter et al., 1995; Preiss, 2000 Greene, 2010). Some have suggested that rifting was associated with ca. 825-750 Ma mafic dikes and volcanism (Wingate and Giddings, 2000; Li et al., 1999;

TABLE 9. SELECT SEDIMENTARY POLES CORRECTED FOR INCLINATION FLATTENING

Formation	flattening	Site mean direction			Paleomagnetic Pole		
		D	I	a_{95}	Paleolatitude	Paleolongitude	$^{\dagger}A_{95}$ (dm,dp)
#Nankoweap							
	f=0	259.8	-4.1	7.1	-10	163	4.94 (3.5, 7.0)
	f=0.7380 (sandstones)	259.8	-5.55	7.1	-9.9	161.9	4.94 (3.5, 7.0)
*Hussar Formation							
	f=0	163.3	4.6	14.6	62.2	85.8	10.32 (7.3, 14.6)
	f=0.35 (mudstones)	163.3	12.95	14.6	65.6	80.1	10.32 (7.3, 14.6)

#Nankoweap Formation is located 36.3^{0}N, 248.1^{0}E

*m. Lancer 1 is located at $25^{0}02'44.5''$S, $123^{0}45'20.1''$E

†When site mean poles are not available A95 ≈√(dp x dm), where dp and dm are the semi-axes of the 95% ellipse of confidence about the mean pole (Khramov, 1987)

Ernst et al., 2008). Focus on the southern Georgina Basin has suggested that the Neoproterozoic continental margin of Australia consisted of northwest striking rift segments offset by northeast striking transform faults (Greene, 2010); however, this interpretation is not unique and focuses on sedimentation that post-dates 780-720 tectonism.

Browne Formations /Hussar/ Kanpa

Paleomagnetic studies of the Kanpa, Hussar, and Browne formations in the Central Officer Basin of Central Australia have been studied by Pisarevsky et al. (2007). Red mudstone, siltstone and sandstone from the Browne Formation yielded single polarity remanances (Pisarevsky et al., 2007). The Browne Formation is correlated with the Bitter Springs Formation in the Amadeaus basin and the upper Callanna Group in the Adelaide rift complex (Grey et al., 2005). Although the Browne Formation has no direct geochronological constraints, the upper Callanna Group has been dated at 802±10 Ma (Rook Tuff U–Pb (Fanning et al., 1986) and the Bitter Springs isotope excursion has a maximum constraint from a tuff dated at 811.5±0.25 Ma (U-Pb CA-ID-TIMS zircon Fifteenmile

Group, Yukon, Canada; Macdonald et al., 2010). Thus the Browne Formation pole could be used for ca. 810 Ma reconstructions.

The Hussar Formation overlies the Browne Formation with a sharp contact that may represent a minor erosional hiatus. The lower half of the Hussar Formation consists of mudstone, with minor interbedded sandstone, dolostone and evaporite, whereas the upper part of the unit is dominantly sandstone, with minor interbedded mudstone and dolostone. The Kanpa Formation overlies the Hussar Formation with a sharp conformable contact. Kanpa Formation consists mainly of mudstone, claystone and sandstone in the lower beds, followed by stromatolitic dolostone, sandstone and mudstone. The Kanpa Formation also contains grey shale beds with carbonaceous disks tentatively identified as megascopic alga Chuaria, possible ash beds, and the Keene Basalt (Grey et al., 2005). From the Hussar Formation, most sandstone samples are magnetically unstable, and only 17 samples (mostly mudstones) yielded a stable remanence carried by magnetite and hematite. Two polarities are present, with directions oriented upwards to the north and downwards to the south. As the Hussar Formation pole had not been corrected for inclination flattening, a flattening correction of $f = 0.35$ was applied to the direction carried in the Hussar mudstone samples (Table 9). The Kanpa pole was based on only six samples and was considered a preliminary result, especially due to similarities with Middle Devonian Australian poles. The Hussar and Kanpa Formations are correlated with the Burra Group in the Adelaide rift complex, with basal constraints of 777 ± 7 Ma (U–Pb sensitive high mass-resolution ion microprobe [SHRIMP] zircon Boucaut Volcanics; Preiss and Cowley, 1999). The Hussar pole does bear similarity to the later Devonian Retreat batholith pole (Anderson et al., 2004), but as the Hussar Formation also displays normal and reversed directions it was not likely an overprint direction and can be used in ca. 780 reconstructions.

Mundine Dike Swarm Pole

An extensive swarm of dolerite dikes, the Mundine Dike Swarm, intrude into Archean and Proterozoic rocks of the Pilbara Craton of Western Australia. Most of the dikes are less than 30 meters wide and are fine- to medium-grained, although some are wider, coarse-grained, and have individual strike lengths of over 200 km (Wingate and Giddings, 2000). A joint geochronologic and paleomagnetic study obtained Pb-Pb zircon data and a paleomagnetic pole that placed Australia at low latitudes.

Zircons grains were isolated from the center of a medium- to coarse-grained 25-meter wide quartz dolerite dike (Wingate and Giddings, 2000). From the various SHRIMP analyses the Pb-Pb ages all agreed within error, but when considering $^{206}Pb/^{238}U$ ratios, two analyses were slightly normally discordant and more than half were strongly reversely discordant (Wingate and Giddings, 2000). This suggested unsupported radiogenic Pb (Mattinson et al., 1996), or enhanced sputtering of Pb relative to U, due to radiation-induced microstructural changes (McLaren et al., 1994). Thus the reported age is from a weighted mean Pb-Pb age of 755 ± 3 Ma. The paleomagnetic study obtained a positive baked contact test to indicate that the magnetization from the Mundine Dike Swarm was from emplacement and cooling at 755 Ma (Wingate and Giddings, 2000). This paleomagnetic data for eight dikes was combined with the previous results for six Northampton dikes to obtain the paleomagnetic pole for Australia at 750 Ma (Wingate and Giddings, 2000). Given its age and the paleomagnetic sample data, this pole was include in the presented reconstructions.

Walsh Tillite Cap

The Wash Tillite is a glacial diamictite exposed in eastern Kimberley, northwestern Australia. Initially, researchers suggested that the Wash Tillite might be correlative with the Sturtian deposits (Dow and Gemuts, 1969; Plumb and Gemuts, 1976). However, more recent work has suggested that the Wash Tillite should be correlative with the younger Marinoan glacial deposits (Plumb,

1981; Grey and Corkeron, 1998; Coats and Preiss, 1980). A paleomagnetic study sampled the cap carbonate overlying the Wash Tillite (the Wash Tillite Cap-WTC) and obtained a direction from six sites that passed a fold test (Li, 2000). As the resulting paleomagnetic pole was 58° away from the Elatina Formation pole expected for the Marinoan glaciation, this led to the suggestion that the Walsh Tillite was Sturtian (ca. 770-750 Ma) rather than Marinoan in age, and the WTC pole was introduced as a ca. 750 tie point for Australia in reconstructions (Maloof et al., 2006; Li et al., 2008; Zhang et al., 2006; Li and Evans, 2011). When incorporated into paleogeographic reconstructions, it was used to argue for the break-up of Rodinia by 750 Ma. However, the dismissal of the geological correlations in favor an arbitrary 750 Ma age is puzzling, and given recent geochronological calibrations on Snowball Earth glaciations, the likely age for the WTC pole is either 662 Ma (if a Sturtian cap), or more likely 632 Ma (a Marinoan cap) (Rooney et al., 2015). With these revised age constraints, this paleomagnetic pole was not used in the presented reconstructions.

Yilgarn Dikes

The paleomagnetic pole from the Yilgarn B dikes of Western Australia was initially thought to be robust and used as a tie point for all 1050-700 Ma reconstructions (Giddings, 1976). This pole was one of the original paleomagnetic constraints for the SWEAT hypothesis (Powell et al., 1993). However, a paleomagnetic study resampled the same rocks from which a positive baked contact test was reported, but obtained a negative baked contact test (Halls and Wingate, 2001). This was combined with petrographic and rock magnetic data to suggest that that pole was a secondary overprint likely Mesozoic in age (Halls and Wingate, 2001). Thus, this pole was not used in the presented reconstructions.

4.8.2 South China

South China comprises the Yangtze and Cathaysia blocks (Grabau, 1924). The Yangtze block has a late Archean–Paleoproterozoic core and younger orogenic belts (Wang et al., 1995), while the Cathaysia block has pre–1.4 Ga continental crust (Jahn et al., 1990; Li et al., 1992; Shui, 1987; Zhou et al., 1993; Li, 1994). There are well-developed Neoproterozoic rift systems in South China, that have helped served as a geologic basis for proposed connections to Australia and Laurentia (Wang, 1985; Xing, 1989; Qiao, 1989a, 1989b; Dong and Liu, 1991; Li, 1991; Li et al., 1995).

Liantuo Formation

Exposed in the Hubei province and the lower Three Gorges of the Yangtze River, the arkosic to argillitic Liantuo Formation contains interbedded volcanic ash horizons, and is laterally equivalent to the Tonian Banxi Group. Unconformably overlying the Liantuo Formation is the Marinoan Nantuo Formation (Wang et al., 1981; Liao, 1981; Condon et al., 2005). These units have been suggested to reflect continent rifting and passive-margin development, similar in style and age to those found in Australia and western Laurentia. This observation helped place it as a missing link between Australia and Laurentia (Li et al., 1995; Li et al., 1996 ; Li et al., 2008). However, other work suggests that South China is surrounded by a 970-750 Ma arc, explaining the abundant ash interbeds within the Banxi Group and Liantuo formation (Cawood et al., 2013). Consistent with this alternative interpretation, some have placed it near the northwest Australian shelf (Kirschvink, 1992; Cawood et al., 2013).

Two important paleomagnetic studies have focused on the Liantuo Formation, both focusing on the upper part of the formation (Evans et al., 2000; Jing et al., 2015). The Liantuo Formation has been the focus of several geochronology studies. The lower Liantuo was dated with SHRIMP U–Pb zircon age of 779 ± 12 Ma (20 zircon analyses) from a reworked tuff sample within the lower

Liantuo Formation (Du et al. 2013). The upper Liantuo has been dated to 748 ± 12 Ma (SHRIMP U–Pb from 23 zircon analyses Ma et al., 1984). More recently a SHRIMP U–Pb zircon age of 724 ± 12 Ma was reported from the same locality (2 zircon analyses; Gao and Zhang (2009). These radiometric dates suggest that the depositional age of the top Liantuo Formation should postdate ca. 725 Ma. New, as of yet unpublished, ages from the paleomagnetism sites of Jing et al. (2015) and Evans et al., 2000 suggest the age is ca. 778 Ma. In the presented reconstructions, South China is constrained using the Liantuo paleomagnetic pole in both the ca. 750 and ca. 720 Ma time windows. Regardless of the correct age of the Liantuo pole, South China is at mid latitudes and is placed adjacent to the western margin of Australia, not the eastern, as this configuration is consistent with the later Ediacaran paleomagnetic data that suggests that the South China block was located to the northwest of Northern Australia (Jing et al., 2015)

4.8.3 North China

The North China Block has an Archean to Paleoproterozoic basement, and Meso-Neoproterozoic to sedimentary basins (e.g. Wang and Qiao, 1984). Some reconstructions place North China near Siberia (Li et al., 1996), while others have suggested that North China was alongside western Laurentia (Wang et al., 1997). Unfortunately, there is sparse paleomagnetic data for North China, and the Nanfen Pole has been used to suggest that North China was connected to Laurentia and near Siberia until 700 Ma (Zhang et al., 2006). Unfortunately, the sample and demagnetization data from the Nanfen pole has not been published in peer-reviewed literature (Lin, 1984) and the age of the Nanfen Formation is unknown. Newer work correlates the Nanfen Formation with the lower part of the ca. 890-925 Ma Huaibei Group (e.g. Xiao et al., 2014). Thus, this paleomagnetic pole was not incorporated into the presented reconstructions. The newer correlations suggest that there are no Cryogenian-Ediacaran basins that could be tie points to the margin of Laurentia. As Mesoproterozoic work has suggested that North China was near Siberia (Zhang et al., 2006; Fu et al., 2015),

North China is tenuously placed close to Laurentia and Siberia but this reconstruction lacks constraints.

4.8.4 Tarim

Tarim's basement is composed of Proterozoic schist of the Aksu Group that is intruded by a series of unmetamorphosed northwest-trending mafic dikes. The overlying sedimentary sequences consist of the Cryogenian Baiysi, Qiaoenbrak and Yuermeinak Formations, and the Ediacaran Sugetbrak and Chigebrak Formations (Gao et al., 1985; 1993; Turner, 2010; Zhu et al., 2011; Xu et al., 2013; Wen et al., 2015). Both the Qiaoenbrak and Yuermeinak Formations are dominated by sandstone, siltstone and conglomerate, and contain diamictites interpreted to record multiple Cryogenian glaciations (Gao et al., 1985; Gao and Qian, 1985; Wen et al., 2015). Marinoan-age cap dolostone was recently documented above the glacial deposits of the younger Yuermeinak Formation (Wen et al., 2015). It is suggested that Tarim was adjacent to northwest Australia (Li et al., 1996; Li et al., 2008), next to Laurentia as a missing link alternative (Wen et al., 2015), or near North China (Wang et al., 2015).

Baiyisi Formation

Baiyisi Formation is likely correlative with Sturtian glaciation and includes a sequence of siliciclastics, diamictite, a lower volcanic unit, shale and then a final second volcanic unit (Wen et al., 2015; 2016). From the basal volcanics, a SHRIMP U-Pb age analysis gives a weighted mean age of 755±15 Ma (Xu et al., 2005). Recent SHRIMP zircon U−Pb geochronologic data from the volcanic rocks above the Baiyisi diamictites were dated to 725±10 Ma, while those below were dated to 740±7 Ma, respectively (Xu et al., 2009). These analyses display a wide spread of dates and suggesting that they include inherited grains, which would bias the weighted mean to an older age. A paleomagnetic study was conducted on the basalts of the second volcanic unit (Huang et al., 2005). As these basalts

are overlying the Sturtian Baiyisi diamictites and have been dated to 725±10 Ma, the Baiyisi volcanics pole is likely syn- to post-Sturtian in age, and is thus incorporated into the ca. 720 reconstruction.

Qiaoenbrak Formation

The Sturtian correlative Qiaoenbrak Formation has also been the focus of a paleomagnetic study, and its pole is very similar the Baiyisi pole but includes a negative soft-sediment fold test and a positive conglomerate test. The negative soft-sediment fold test and the positive conglomerate tests suggest that the CRMs likely represent the post-depositional remanent magnetizations. As a result this paleomagnetic pole is not corrected for inclination flattening. This pole is included in the presented ca. 720 reconstruction of Tarim.

4.8.5 North Australia

North Australia is suggested to have been close to West Australia during the Neoproterozoic, but experienced a later relative rotation (Schmidt et al., 2006; Li and Evans, 2011).

Johnny's Creek Member (Bitter Springs Formation)

The Bitter Springs Formation is exposed in the Amadeus Basin of north-central Australia. Within the Bitter Springs Formation, the paleomagnetism of the Johnny's Creek Member was investigated by Swanson Hysell et al. (2012). From the siltstones of Johnny's Creek Member a high-temperature component carried by hematite was isolated. This component direction passed a regional fold test, which suggested that the magnetization was acquired prior to Paleozoic folding, thus it was interpreted as a primary/early diagenetic magnetization (Swanson Hysell et al., 2012). The region has experienced extensive overprinting events, so it is possible that the Johnny's Creek Member magnetization is not primary (Swanson Hysell et al., 2012). Alternatively, the magnetization is primary

and hence constrains the motion of northern Australia relative to southern Australia. Towards this, Swanson Hysell et al. (2012) compared the pole to the Mundine Wells dike pole from southern Australia. This comparison, incorporating the proposed relative rotation of Li and Evans (2011), was found to bring the Johnny's Creek member pole into better agreement with the Mundine Wells dike pole (Swanson Hysell et al., 2012), thus supporting the relative rotation hypothesis between southern and northern Australia.

4.8.6 Congo

Congo is placed aside from Laurentia; broadly following published reconstructions (e.g. Hoffman, 1991; Merdith et al., 2017, Li et al., 2008). This configuration is supported during the 775-720 Ma window by paleomagnetic data from both the Mbozi complex and the Luakela volcanics.

Mbozi Complex

Situated in southern Tanzania, the Mbozi complex covers over 300 km^2 and is dominated by gabbros and pyroxenites. These layered mafic units were subsequently intruded by dolerites and finally syenite dikes (Brock, 1968). Early work obtained a K-Ar bulk rock age of 743±30 Ma (Brock, 1968) and a K-Ar age of 755±25 Ma on biotite separated from the intruding syenites (Cahen & Snelling, 1966). This 755 Ma age was reported in Evans (2000) where it was recalculated using the updated decay constants from Dalrymple (1979). These dates have been superseded by a U-Pb zircon age of 748±6 Ma (Mbede et al. 2004). Unfortunately, that age is unpublished except for in conference proceedings. A paleomagnetic study of 10 sites was undertaken by Meert et al. (1995). Thermal and AF demagnetization revealed two components, including one interpreted as primary from 64 samples (Meert et al. 1995). This paleomagnetic pole was supported by 5 of the 7 van der Voo criteria, but lacked field tests and presence of reversals (Meert et al. 1995). The Mbozi pole was used to constrain the Congo's position at 750 Ma in the presented reconstructions.

Luakela volcanics

The Zambian Luakela volcanics include unmetamorphosed and undeformed basaltic to andesitic flows. Zircons from two samples of basaltic andesite from the Luakela volcanics yielded SHRIMP U-Pb zircon ages of 765±5 and 763±6 Ma (Key et al., 2001). Paleomagnetic analysis isolated multiple components from 65 samples (9 sites), including one component carried mainly by single-domain magnetite and interpreted to be primary (Wingate et al., 2010). This interpretation was supported by the presence of reversed directions (Wingate et al., 2010).

4.8.7 India

The earliest proposed models of Rodinia suggested that East Gondwanaland (India-Australia-Antarctica) remained intact during the tenure of the supercontinent (Hoffman, 1991). However, evolving paleomagnetic data suggests that this may not have been the case (Torsvik et al., 2001b, 2001c; Gregory et al., 2009; Meert et al., 2013).

Malani igneous suite

The extensive felsic Malani igneous suite in northwest India includes an initial phase of felsic extrusives over 3 km thick, followed by intrusion of granite plutons. The final stage includes crosscutting rhyolitic dikes (Mukherjee, 1966; Bhushan, 1985). The unmetamorphosed igneous suite was folded prior to the deposition of overlying sediments (Mukherjee, 1966; Bhushan, 1985).

U-Pb zircon ages of 751±3 and 771±2 Ma were reported in the paleomagnetic study of Torsvik et al. (2001b) as personal communication from R. D. Tucker. Subsequently, a U-Pb secondary ion mass spectrometry (SIMS) 771±5 Ma (MSWD = 1.5) age was obtained from 14 concordant analyses on 10 zircon crystals from a rhyolitic tuff (Gregory et al., 2009). More recently, LA-ICP-MS discordant analyses on zircon from a mafic dike resulted in U-Pb dates ranging between 700 to 727 Ma

(weighted mean U-Pb ca. 704 Ma, Pb-Pb 752±18 Ma) (Meert et al., 2013).

Several studies have examined the Malani igneous suite, from which a grand mean pole has been reported (Torsvik et al., 2001b, Gregory et al., 2009; Meert et al. 2013). The primary nature of the pole is supported by baked contact tests and a statistically positive fold test (Torsvik et al., 2001b; Gregory et al., 2009; Meert et al., 2013). This data suggests that India was at intermediate latitudes and likely not part of East Gondwana.

Mahe intrusives- Seychelles

Although a continental fragment, the Seychelles has been placed adjacent to India until around 65 Ma (Plummer and Belle, 1995; Torsvik et al., 1998). The Mahe intrusives of the Seychelles include granite intrusions as well as basaltic and dolerite dikes. TIMs work was conducted on zircon from the Takamaka dolerite dyke, resulting in a U-Pb age of 750.2±2.5 (Torsvik et al., 2001). Following AF and thermal demagnetization, paleomagnetic results from 7 dikes suggested that a primary direction was carried by magnetite or titanium-poor titanomagnetite (Torsvik et al., 2001c). This direction was supported by 4 of the 7 van der Voo criteria (lack of tectonic coherence with the India craton and no field tests or reversals) (Torsvik et al., 2001c). The Seychelles was then restored relative to India and the Malani intrusive suite (Euler pole: Latitude=25.8°, Longitude=330° and rotation angle=28°) (Torsvik et al., 2001c). However, as this restoration relied on paleomagnetism and the assumed coeval nature of the Malani intrusive suite and the Mahe Intrusives rather than a geologic basis, only the Malani intrusive suite pole was used to constrain India in the reconstructions presented here.

4.8.8 Siberia

Paleomagnetic data from dikes proposed to be ca. 760 Ma (Kitoi Dykes), and recent work using LIP piercing points are considered as constraints for Siberia (Pisarevsky et al. 2013; Ernst et al., 2016). Past

reconstructions have used geological considerations as well as sparse paleomagnetic constraints, and have usually placed Siberia adjacent to northern Laurentia in a wide variety of orientations (Hoffman 1991; Condie et al., 1994; Rainbird et al., 1998; Evans and Mitchell, 2011), or as the conjugate margin to western Laurentia (Sears and Price 2003). Alternatively, others have agreed that Siberia was near the northern Laurentian margin, but argue for a large gap between Siberia and northern Laurentia (Pisarevsky et al., 2008; 2014).

Within the Irkutsk peninsula, by the Kitoy river (or Kitoi river) the Sharizhalgai uplift includes two generations of dikes (Paleoproterozoic and Neoproterozoic in age). Of particular interest for the reconstructions presented here are the northwest trending "Kitoi" dikes (Pisarevsky et al., 2013), also referred to as the Nersa complex dikes (Gladkochub, 2010) or the Sayan dikes (Ernst et al., 2016). These tholeiitic gabbro dolerites dikes trend N-NE and range from 7 km to potentially 15 km in length, all dipping to the southwest (Sklyarov et al., 2003).

These units have been dated to 743±47 Ma with Sm-Nd on pyroxene, plagioclases and whole rock) Sklyarov et al. (2003), as well as 758±4 Ma Ar-Ar from plagioclase (Gladkochub, 2006). Despite these ca. 700–800 Ma ages, the convergence of these dikes with the NE trending Baikal dikes, suggests that they may be part of a radiating dike swarm correlated with the Franklin and Irkutsk LIPs (see discussion below), and thus ca. 720 Ma (Ernst et al., 2016). As the existing ages involve the less robust Ar-Ar and Sm–Nd methods, it was thought that future geochronology studies using U-Pb on zircon could result in substantially younger ages (Gladkochub et al., 2006). A CRM was isolated from 10 sites by Pisarevsky et al. (2013) and interpreted as primary due a partial contact test that found scattered remanence of the unbaked host rocks.

Importantly, recent geochronological work has identified robust age matches between southern Siberia and northern Laurentia that suggests that they were adjacent from 1875-720 Ma (Ernst et al., 2016). In particular, it was shown that the Franklin LIP in Laurentia was likely a correlative event with the Irkutsk LIP in Siberia. The Irkutsk LIP of southern Siberia includes the Dovyren intrusive

massif (724±3 Ma, U–Pb baddeleyite; Ernst et al., 2016), volcanic rocks associated with the Inyaptuk Formation (729±14 Ma; Ariskin et al., 2013), Upper Kingash intrusions (726±18 Ma, U–Pb, Ernst et al., 2016), Tartai intrusion (713±6 Ma, U–Pb SHRIMP Polyakov, 2013), as well as the poorly dated Sayan (see discussion above) and Baikal dikes (Ernst et al., 2016). Thus pre-720 Ma, Siberia is placed to the north of Laurentia in a configuration without overlap, similar to those presented in Ernst et al. (2016) and Pisarevsky et al. (2013).

4.8.9 Antarctica, Baltica, Amazonia, Kalahari, Rio de La Plata, Sao Francisco, West Africa

There is no paleomagnetic data for Antarctica, Baltica, Amazonia, Kalahari, Rio de La Plata, Sao Francisco, and West Africa during the 780-720 Ma period, other published configurations were examined before these cratons were incorporated into the reconstructions presented here (Hoffman, 1991; Li et al., 2008; Evans, 2009; Li and Evans, 2011, Li et al., 2013; Merdith et al., 2017).

Antarctica is placed in connection to Australia in its Gondwana configuration (Harley, 2013). The original SWEAT model suggested that eastern Antarctica was connected in its Gondwana configuration with Australia and India, and lay adjacent to the southwestern United States. Subsequent work has identified features related to a Pinjarra Orogen suggesting that eastern Antarctica should be split into an eastern Antarctic craton and the Mawson craton, the latter suggested to be connected to Australia as a single craton post 1200 Ma (Fitzsimons, 2003a, b; Cawood and Buchan 2007; Cawood & Korsch 2008; White et al. 1999). This treatment of the Mawson craton was incorporated into the presented reconstructions.

For Baltica, the Sveconorwegian Orogen is a geologic tie point to the Laurentian Grenville Orogen, and thus most reconstructions place Baltica adjacent to the northeastern margin of Laurentia, although the exact configuration is uncertain (Hoffman, 1991; Bogdanova et al., 2008; Evans, 2009). Similarly, the Amazonian Rondonia-Sunsas orogenic belt may be correlative with the Grenville

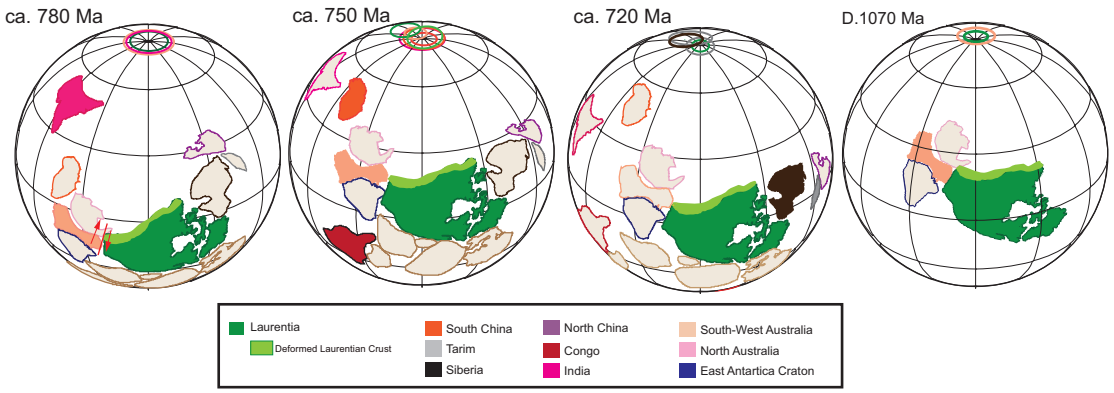


Figure 4.11: Paleogeographic reconstructions. Brightly colored continents are those with paleomagnetic data within 10 Ma of the reconstructed time. Continents with colored outlines lack paleomagnetic data within 10 Ma to support any reconstruction for that time. A. 780 Ma, B. 750 Ma, C. 720 Ma, D. 1070 Ma reconstruction with only Laurentia, Australia and associated cratons. Paleomagnetic poles are from the Australian Bangemall sills (1070 Ma U-Pb) and the Laurentian Nonesuch Shale (1087 Ma Re-Os).

Orogen, suggesting that Amazonia also be placed adjacent to the Laurentian eastern margin (Hoffman, 1991; Loewy et al., 2003; Davidson, 2008; Li et al., 2008). Further south, the Grenville aged Namaqua-Natal orogenic of the Kalahari Craton was suggested as a tie point to southeast Laurentia (see Hoffman, 1991; Li et al., 2008). There are also proposed connections between Kalahari, Rio de la Plata and Laurentia, so Rio de la Plata is placed adjacent to the eastern margin of Laurentia between Kalahari and Amazonia (Li et al., 2008; Evans, 2009). Another smaller craton, Sao Francisco is placed farther from Laurentia's margin, but adjacent to the Congo (Li et al., 2008; Evans, 2009).

In considering West Africa, there are very few constraints, either geological or paleomagnetic. The craton lacks Grenville aged metamorphism and so it was either part of a larger craton such as Amazonia, or not part of the supercontinent (Trompette, 1997; Merdith et al., 2017). Recent reconstructions were followed by placing West Africa near Amazonia (Merdith et al., 2017).

4.9 Paleogeographic reconstructions ca. 780, 750 and 720 Ma

Paleomagnetic and geochronologic data was compiled (Table 8) and reconstructions were created for three time windows: ca. 780, 750 Ma and 720 Ma (Fig. 11). Uncertainties were highlighted by filling in the continents for which there is paleomagnetic data within 10 Ma of the reconstructed time. Continents with only colored outlines lack paleomagnetic data within 10 Ma to support any reconstruction for that time. For the ca. 780 Ma reconstruction, there are only paleomagnetic poles for India (Malani Intrusives), Australia (inclination Flattened Hussar Pole) and Laurentia (Gunbarrel event). For the ca. 750 Ma reconstruction, there are poles for Congo (Mbozi Complex), Australia (Mundine Wells Dike Swarm), Laurentia (Carbon Canyon pole and Awatabi+Carbon Butte pole), as well as South China (Liantuo). For Laurentia the Awatabi+Carbon Butte pole, the Carbon Canyon pole (reanalyzed from Weil et al., 2004) and the Nankoweap pole (Weil et al. 2003) are displayed. The 755 Ma Mundine Wells Dike pole is plotted halfway between the ca. 751 Ma Awatabi+Carbon Butte pole and the ca. 757 Ma Carbon Canyon pole. Finally, for the ca. 720 Ma reconstruction, there are three continents with paleomagnetic poles within 10 Ma, Laurentia with its Franklin pole, Siberia with the Kitoi-Sayan dike pole, and Tarim with the Baiyisi volcanics pole and Qiaoenbrak Formation pole.

With regards to these reconstructions, an AUSMEX configuration is permissible for each of the time windows, with paleomagnetic data supporting the configuration at 780 and 750 Ma. Between these two times, the paleomagnetic data suggests some right lateral motion between Laurentia and Australia (Fig. 11A). As suggested previously, the SWEAT and AUSWUS configurations are untenable given the paleomagnetic data and thus Australia cannot be the conjugate rifted margin for Laurentia. South China is an unlikely candidate for the conjugate margin of Laurentia, as by 750 Ma it would have needed to have already rifted away, and both geologic data and Ediacaran paleomagnetic data suggest a position near western Australia (Kirschvink, 1992; Cawood et al., 2013; Jing et al.,

2015). Tarim has also been suggested as a candidate for the rifted margin but, as shown here, comparison of the ca. 720 Ma paleomagnetic data suggests that Tarim and Laurentia are at similar latitudes and would overlap if placed at the same longitude, making that reconstruction untenable. Thus I suggest that it should be instead placed near Siberia and North China.

With regards to the other cratons, paleomagnetic and geologic considerations forbid Siberia as the conjugate margin to western Laurentia. Furthermore, Congo and India both have paleolatitude constraints that prohibit their connections to western Laurentia (Meert et al. 1995; Torsvik et al., 2001b, 2001c; Gregory et al., 2009; Meert et al., 2013). Due to the similarities between Sao Francisco and Congo, the former is also an unlikely candidate for the western margin (Li et al., 2008). Geologic tie points suggest that Antarctica is likely attached to Australia and is not the conjugate margin for Laurentia (Fitzsimons, 2003a, b; Cawood and Buchan 2007; Cawood and Korsch 2008; White et al. 1999). Similarly, geological tie points for Baltica and Amazonia, Kalahari, and Rio de la Plata, suggest they were on or near the eastern margin of Laurentia and thus cannot be conjugates for the western margin (Bogdanova et al., 2008; Loewy et al., 2003; Davidson, 2008; Li et al., 2008).

These reconstructions of the western margin of Laurentia suggest two scenarios for the identity of the conjugate craton: either (a) there was a craton with currently unexplored connections to Laurentia (such as West Africa), or (b) western Laurentia did not have a conjugate craton and instead the final rift event involved a ribbon continent (Fig. 12). I propose that between 780-750 Ma, southern crustal extension may have been triggered by dextral strike-slip motion between Laurentia and Australia along the southwestern Laurentian promontory. This resulted in initial extensional to transtensional basins along southwestern Laurentia (Fig. 12A). This was followed by ca. 720 Ma rifting of Siberia on the northern margin, triggered by the Franklin LIP (Fig 12B). Finally, there was progression of rift volcanism south along the margin ca. 720-660 Ma (Fig. 12C; Macdonald et al., 2010; Rooney et al., 2014 and 2015; Lund et al., 2003; Lund et al., 2010; Condon and Bowring, 2011; Keeley et al., 2013).

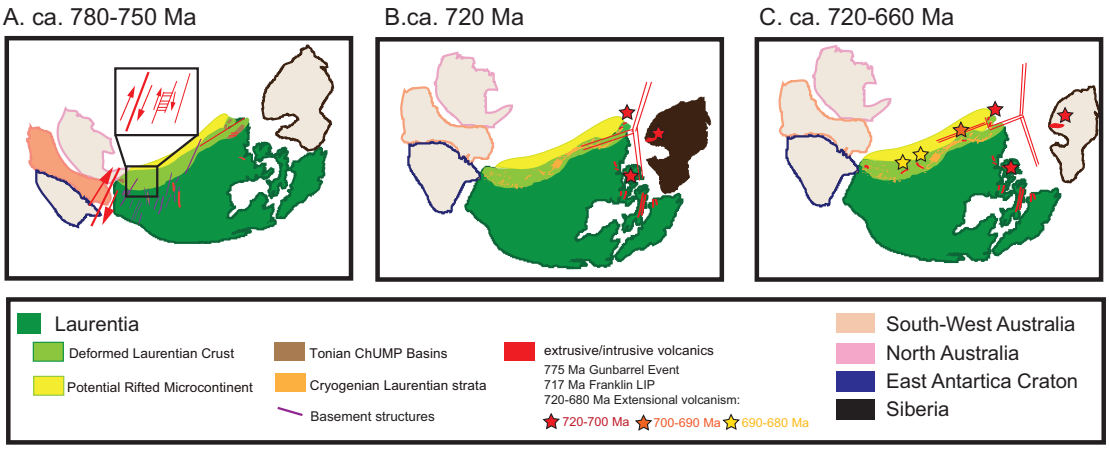


Figure 4.12: ca. 780-660 Ma tectonic interpretations. A. 780-750 Ma strike-slip motion between Australia and Laurentia. Basement structures are highlighted. B. 720 Ma eruption of the Franklin LIP that initiated the rifting of Siberia from the northern margin. C. 720-660 Ma rift magmatism that propagated south down the margin.

This model is consistent with inferences of Precambrian structures (Marshak et al., 2000; Timmons et al., 2001; Marshak et al., 2017). These structures, although more recently involved in the uplift related to the Paleozoic Ancestral Rockies event or the Mesozoic-Cenozoic Laramide event, are interpreted to reflect Proterozoic extensional fault systems (Marshak et al., 2000; Timmons et al., 2001; Marshak et al., 2017). They have been divided based on orientation into northwest-trending structures and north-trending structures (Marshak et al., 2000). The northwest-trending structures appear to be continental in scale and include the Texas- Mogollon- Walker lineament, the Lewis and Clark–Oklahoma–Alabama lineament, Mojave- Sonora mega shear, and Uncompahgre uplift, (Marshak and Paulsen, 1996; Marshak et al., 2000; Timmons et al., 2001; Whitmeyer and Karlstrom 2007). These structures are inferred to be late Mesoproterozoic in age due to the similarity of orientations to those displayed by the Mesoproterozoic Unkar Group, and thus interpreted to represent Grenville aged northeast directed continental extension (Timmons et al., 2001). The north-trending structures are inferred from steep reactivated (Laramide) structures, including the Defiance monocline, Grand Hogback, Grand Wash fault, Hurricane monocline, Front Range and Rio Grande rift

(Marshak, et al., 2000). The orientation of these structures bear similarity to the Butte Fault and Chuar Syncline, leading to the suggestion that these structures were established ca. 750 Ma and related to the deposition of the Neoproterozoic ChUMP basins (Timmons et al., 2001). Alternatively, the north trending structures may be related to the northwest-trending features established in the late Mesoproterozoic to Neoproterozoic (Marshak and Paulsen, 1996; Karlstrom and Humphreys, 1998).

My proposed strike slip motion between Australia and North America may parallel these northwest trending structures. Typically strike slip tectonics can include minor extensional basins in the form of extensional duplexes (Woodcock and Fischer, 1986). In this scenario, the older basement northwest trending structures could help accommodate my proposed strike slip motion, while the north trending features such as the Butte fault that lie between the northwest trending structures and could be associated extensional duplexes within a dextral strike slip system. If the early ca. 750 Ma ChUMP basin formation in southern Laurentia are associated with strike-slip motions rather than pure rifting, it would explain the presence of the narrow basins, the puzzling absence of a late Neoproterozoic passive margin sequence with broad subsidence and voluminous volcanism typically associated with the rift extensional basins. This absence indicates that stretching factors were low from 750 to 600 Ma, which is consistent with this model of narrow transtensional basins rather than a true rift.

The eventual rift event that triggered the rift-drift transition may have involved the rifting of a ribbon continent with Laurentia affinity. The eventual rifted continental fragment may have continued to disintegrate, or alternatively could have re-accreted later to Laurentia as a Cordilleran ribbon continent (Johnston et al., 2008; Hildebrand et al., 2009), but not necessarily with the outlines envisioned in Hildebrand's Rubia. In this model, the final rifting of Laurentia may be comparable to that of the Artic Ocean, where the Gakkel Ridge separates the continental Lomonosov Ridge from the Barents shelf of Europe (Sweeney et al., 1982; Rowley and Lottes, 1988). Some suggest that

the Lomonsov Ridge block was sheared from Eurasia in the late Cretaceous along a trans-Arctic left lateral offset, and later this weakness was utilized when the North Atlantic rift propagated into the Arctic in the Early Tertiary (Sweeney et al., 1982). The continental nature of the Lomonosov Ridge is supported by its crustal thickness of 22-30 km and the existence of fragments of Upper Permian zircon-bearing rocks (Grantz et al., 1998; Grantz, et al., 2001; Shipilov 2008). It is suggested that the Lomonosov microcontinent existed as an independent microplate for 10–15 Ma (Shipilov, 3008). This type of rifting, rifting without a conjugate craton margin, may have been important in the Neoproterozoic rifting of Laurentia.

This reconstruction may have very different implications for the connections between supercontinent rifting and Tonian TPW, and supercontinents and mantle plumes. Previous reconstructions have suggested rapid TPW during the period 780-750 Ma related to the occurrence of a high-latitude superplume (Evans, 1998, 2003; Li et al., 2003; Li et al., 2008). In the presented reconstruction there is a slight clockwise rotation of Laurentia between 780-750 Ma, but there is no evidence for large-scale TPW movement and a resulting rotation of Laurentia as previously suggested. Furthermore, previous work suggested that large supercontinents are associated with thermal insulation that may elevate the temperature of the upper mantle (e.g., Anderson, 1982; Gurnis, 1988), and may drive thermal upwelling and breakup. Other suggest that instead thermal insulation is ineffective, and circum-supercontinent subduction zones and mantle avalanches drive upwelling and superplumes (e.g., Kellogg et al., 1999). This type of phenomenon is suggested to explain the dual superplumes under Africa and Pacific (e.g., Zhao, 2001; Courtillot et al., 2003; Anderson, 1982). Without conjugate cratons on its western margin, Laurentia is no longer at the center of an insulated and subduction bound supercontinent. Thus, the location of the suggested plume-related Gunbarrel Event no longer is consistent with the older plume-supercontinent hypothesis.

TABLE 10. MESOPROTEROZOIC PALEOMAGNETIC POLES

Pole	Age (Ma)	Type and Age Reference	Paleomagnetic Pole				Paleomagnetic Reference
			Latitude	Longitude	A_{95}	N	
North Shore Volcanic Group (upper SW sequence)	1098.4 ± 1.9, 1096.6 ± 1.7	Pb-Pb weighted mean, Davis and Green, 1997	35.8	182.1	3.1	47	Tauxe and Kodama, 2009; mean calculated in Fairchild et al., 2017
Portage Lake Volcanics	1096.2 ± 1.8	U-Pb concordia intercept, Davis and Paces, 1990	27.1	182.0	2.2	97	Books, 1972; Hnat et al., 2006
Chengwatana Volcanics	1094.6 ± 2.1	Pb-Pb zircon, weighted mean, Zartman et al., 1997	30.9	186.1	4.9	8	Kean, et al. 1997
Schroeder-Lutsen basalts	<1091.61 ± 0.14	CA-ID-TIMS Fairchild et al., 2017	27.1	187.8	3.0	50	Tauxe and Kodama, 2009; Fairchild et al., 2017;
Lake Shore Traps	1085.57 ± 0.25	CA-ID-TIMS Fairchild et al., 2017	23.1	186.4	4.0	31	Kulakov et al., 2013
Michipicoten Island Fm	1084.35 ± 0.20, 1083.52 ± 0.23	CA-ID-TIMS Fairchild et al., 2017	17	174.7	4.4	23	Palmer and Davis, 1987; Fairchild et al., 2017
Nonesuch Formation	1078 ± 24	Re-Os Cumming et al., 2010	7.3	174.7	3.0	29	Henry et al., 1977; Symons et al., 2013
Bangemall Sills	1071±8, 1067±14, 1068±22, Mean: 1070 ± 6	U-Pb SHRIMP Baddeleyite/ zircon Wingate and Giddings, 2004	33.8	95.0	8.3	11	Wingate and Giddings, 2004
Cardenas Basalts-Unkar Intrusives	1080 ± 2,1080 ± 3 1088 ± 3,1094 ± 2	U-Pb baddeleyite Bright et al. 2014 on correlative units	32.0	185.0	9.6	16	Weil et al., 2003

4.9.1 Remark on the longevity of AUSMEX

The possible configuration for Australia and Laurentia ca. 1070 Ma is also displayed (Fig. 11D), based on the Australian Mesoproterozoic Bangemall sills and the more recently dated Laurentia Nonesuch Formation (Wingate et al. 2004; Cumming et al., 2010). Exposed in the Mesoproterozoic Bangemall basin, the dolerite Bangemall sills intrude into unmetamorphosed, fine-grained carbonate and siliciclastic marine sedimentary rocks known as the Bangemall Supergroup (Muhling and Brakel, 1985; Martin et al., 1999). The southern parts of the basin were subsequently folded as part of the Edmund Fold Belt (Muhling and Brakel, 1985). Geochronology work on baddeleyite and zircon yielded ages of 1071±8, 1067±14 and 1068±22 Ma, which were combined to yield a mean age of 1070±6 Ma, regarded as the intrusion age (Wingate and Giddings, 2004). The paleomagnetic direction from the Bangemall Sills has been tilt corrected and is supported by a partial baked contact test, in that the baked rocks had overprint, but no stable direction was obtained from the unbaked host rocks (Wingate and Giddings, 2004).

This Bangemall pole is compared with paleomagnetic data from the Laurentian midcontinent rift. Overlying Keweenawan volcanics previously discussed are siliciclastics of the Oronto Group that are suggested to be post-rift fluvial/lacustrine sediments, related to broad crustal subsidence

(Ojakangas et al., 2001). The basal Copper Harbor Formation is dominated by red-brown conglomerates with some basal volcanics, and sandstones deposited in alluvial fans. The overlying Nonesuch Formation consists of gray-to-black siltstones, shales and very fine sandstone deposited in anoxic water. Recent work has been done using Re-Os geochronology to obtain an age of 1078±24 Ma for the Nonesuch Formation (Cumming et al., 2010). Thus the new age constraints allow a slightly more refined comparison between Laurentia and Australia ca. 1070 Ma than initially investigated by Wingate and Giddings (2004), but it still supports a ca. 1070 Ma AUSMEX configuration for Australia and Laurentia.

4.10 Conclusions

New paleomagnetic poles preserved in hematite and magnetite from Awatabi and Carbon Butte members of the Kwagunt Formation are interpreted as primary and pass five of the seven Van der Voo (1990) reliability criteria. In addition, the results of this study are combined with those reported in Weil et al., (2004), resulting in a combined mean pole from the Awatabi and Carbon Butte members. Pervasive steep overprints were identified, both a mid-temperature component direction demagnetized between 200-560°C and a high temperature component direction demagnetized up to 680°C. These overprints are found in the Carbon Canyon Member of the Galeros, the Carbon Butte, the Awatabi and the Walcott members of the Kwagunt, as well as the Sixtymile Formation. Previously, a steep component was only documented the Carbon Butte Member, and I have shown the widespread nature of these overprints, supported by a partial conglomerate test. Previously reported poles from the Walcott Member were not replicated, and I suggest that these directions were biased and streaked by the pervasive overprint.

I have incorporated the new combined Awatabi and Carbon Butte paleomagnetic pole with existing paleomagnetic data and recent geochronological data to present a new revised ca. 780-720

Ma Laurentian APWP. Having examined the 780-720 Ma database of other cratons, I present reconstructions for 780, 750, and 720 Ma, and conclude that there is evidence for an AUSMEX configuration at both 780 and 750 Ma (as well as 1070 Ma). I suggest that there may not have been a major craton as a conjugate margin for western Laurentia, and that instead ca. 780-750 Ma southern crustal extension was triggered by strike slip motion along the southwestern Laurentian promontory. Furthermore, post ca. 720 Ma, northern crustal extension may have been triggered by the Franklin LIP and then propagated down the continental margin. I propose that the eventual Ediacaran rift event associated with the rift-drift transition may have involved a ribbon continent of Laurentian affinity.

A

Supplementary Information, figures and Tables for Chapter 2

A.1 Sample Analysis

If a specimen component fit had a MAD>15, it was discarded from subsequent analysis. For samples with multiple specimens with the same component I used Fisher statistics to find an average component direction for the sample. The data was discarded if the associated CSD>20. In some cases, if there were two specimens, one that seemed very different from all the other samples, and the other that was similar, then I would examine that specimen that was an outlier and exclude it from the mean if it seemed anomalous (unblocking temperatures, etc)

Finally, as this dataset was particularly noisy, some component directions did not always display desired precision. This was particularly apparent for the LT and HT components. For the LT com-

SUPPLEMENTARY TABLE S1. SAMPLE LOCATION DATA				
Site/ Section	MHV member	type	Latitude (^{o}N)	Longitude (^{o}E)
A1117	dike	site	64.73438	-139.76778
A1118	sill	site	64.73637	-139.76372
A1119	dike feeder	site	64.73637	-139.76372
A1120	dike	site	64.68373	-139.86320
A1121	dike	site	64.68373	-139.86320
A1122	Seela Pass Fm.	5.6 m section	64.68060	-139.96107
A1123	Member A	49.0 m section	64.68060	-139.96107
A1125	Member A	21.9 m section	64.76650	-140.11252
A1126	Eagle Creek fm. (with basalt clasts)	conglomerate test/ 22 m section	64.76176	-140.12360
A1127	dike	site	64.76179	-140.12360
A1128	Member B	191.5 m section	64.70884	-140.04704
A1129	Eagle Creek fm. (with basalt clasts)	conglomerate test	64.70535	-140.04903
A1201	Member D-younger intrusion	site	64.66237	-140.01630
A1202	Member D- younger intrusion	site	64.66253	-140.00642
A1203	Member D	1.3 m section	64.66323	-140.00482
A1204	Member C	3 m section	64.28337	-140.82295
A1206	Member B	site	64.65967	-140.00342
A1207	Member D	site	64.28337	-140.82295
A1209	Member B and Eagle Creek fm.	273.0 m section	64.67632	-139.86698
A1210	Member A	55.4 m section	64.68047	-140.86070

SUPPLEMENTARY TABLE S2. LOW-TEMPERATURE COMPONENT MEAN DIRECTIONS WITH α_{95}<20°						
Site/Section	LT demag. temp.	D/I (in situ) (^{o})	D/I (tilt corrected) (^{o})	α_{95} (°)	k	n/n_c
Approach 1						
A1128	100 °C	50.4/79.7	209.0/82	19.8	2.9	27/59
A1210	150°C (LN-250°C)	51.8/84.4	212.2/55.3	9.8	20.6	12/22
MHV Mean Direction		**54.0/80.9 α_{95} =5.8 k=1886.5 CSD=1.86**	**209.2/69.7 α_{95} =56.6 k=21.6 CSD=17.42**			**2 sections 39 samples**
Approach 2						
A1210	150°C (LN-250°C)	44.7/83.9	213.2/56.1	10.3	20.4	11flows 12/22
MHV Mean Direction		**44.7/83.9 α_{95} =10.3 k=20.4**	**213.2/56.1 α_{95} =10.3 k=20.4**			**11 flows 1 section 12 samples**
Approach 3						
N.D.						

D and I—mean declination and inclination
k—Fisher's (1953) precision parameter
α_{95}—radius of confidence circle for the mean direction
n—number of samples used
n_c—total number of samples collected

SUPPLEMENTARY TABLE S3. MID-TEMPERATURE COMPONENT DIRECTIONS α_{95}<20°						
Site/ Section	MT demag. temp. (°C)	**D/I (in situ) (°)**	**D/I (tilt corrected) (°)**	α_{95} (°)	k	n/n_c
Approach 1						
A1123	425 (300-500)	145.4/-81.5	50.3/-51.5	7.3	28.6	15/17
A1125	450 (375-515)	67.2/-88.0	62.4/-36.1	5.0	128.2	7/11
A1126	450 (350-475)	225.6/-86.2	14.5/-54.8	9.3	31.7	8/10
A1128	475(200-530)	160.6/-84.0	60.2/-74.1	4.1	24.5	52/59
A1203	450(415-475)	196.6/-78.8	190.8/-70.9	4.8	135.7	6/7
A1204	425 (450-530)	167.4/-64.7	218.1/-75.5	14.9	27.3	5/8
A1209	425 (425-560)	145.0/-82.8	35.8/-45.6	8.9	19.4	15/21
A1210	475 (400-545)	120.1/-81.4	48.1/-48.5	2.8	155.9	19/22
MHV Mean Direction		**161.7/-82.1 α_{95} =5.9 k=89.6**	**49.1/-65.4 α_{95} =20.1 k=9.5**			**8 sections 128 samples**
Approach 2						
A1123	425 (300-500)	147.5/-82.2	49.1/-51.7	7.6	28.4	14 flows 15/17
A1125	450 (375-515)	67.2/-88.0	62.4/-36.1	5.0	128.2	7 flows 7/11
A1126	450 (350-475)	225.6/-86.2	14.5/-54.8	9.3	31.7	8/10
A1128	475(200-530)	176.4/-84.7	58.9/-77.9	6.5	40.9	13 flows 45/59
A1203	450(415-475)	196.7/-78.8	190.8/-70.9	8.6	845	2 flows 6/7
A1204	425 (450-530)	171.5/-63.2	217.9/-73.5	49.4 CSD=15.4	27.7	2 flows 5/8
A1209	425 (425-560)	145.6/-83.8	34.5/-45.2	9.2	19.5	14 flow 15/21
A1210	475 (400-545)	118.5/-81.3	48.1/-48.3	3.3	160.0	14 flows 19/22
MHV Mean Direction		**164.4/82.3 α_{95} =6.3 k=79.4**	**48.4/-66.0 α_{95} =20.6 k=8.2**			**1 site 7 sections 74 stratigraphic horizons 121 samples**
Approach 3						
A1128 Flow 1	475(200-530)	87.2/-66.2	134.2/-73.0	6.9	316.8	3/3
A1128 Flow 2	475(200-530)	207.1/-79.6	58.4/-81.8	12.2	102	3/4
A1128 Flow 2	475(200-530)	169.9/-73.1	102.6/-75.1	11.3	24.8	8/9
A1128 Flow 3	475(200-530)	213.4/-89.5	41.3/-72.5	4.9	55.7	16/18
A1203 Flow 1	450(415-475)	189.1/-80.2	186.4/-72.1	10	150.9	3/3
A1203 Flow 2	450(415-475)	202.6/-77.3	194.8/-69.6	12.7	94.8	3/4
A1204 Flow 1	425 (450-530)	148.3/-69.0	220/-84.4	12.2	102.4	3/6
A1210 Flow 1	475 (400-545)	124.2/-82.2	47.1/-49.2	12.3	101.8	3/4

ponents, I choose to exclude some LT component directions from the site/section means if they were very shallow or appeared to be drastically anomalous (60 degrees away) from many of the other samples from the site/section. For the HT components, the main difference was that some components were upper hemisphere and some were lower hemisphere directions. In my analysis I split up the means into a lower hemisphere and upper hemisphere means. I then used the cutoff of N>3 and a95<20 for each mean. It was in this way that the HT1 and HT2 clusters became apparent and isolated.

SUPPLEMENTARY TABLE S4. HIGH-TEMPERATURE HT2 COMPONENT DIRECTIONS WITH α_{95}<20°						
Site/ Section	**HT2 demag. temp. (°C)**	**D/I (in situ)(°)**	**D/I (tilt corrected) (°)**	**α_{95}(°)**	**k**	**n/n_c**
Approach 1						
A1123	565 (555-575)	51.6/-51.4	46.4/-11.7	18.6	7.0	11/17
A1128	570 (350-585)	37.5/-48.9	38.3/-30.9	16.8	30.7	4/59
A1209	680 (655-680)	61.7/-59.1	44.6/-15.6	14.36	74.7	4/21
A1210	595 (545-645)	58.6/-40.5	52.7/-2.8	10.1	14.2	16/22
MHV Mean Direction		**52.2/-50.3 α_{95} =11.7 k=62.3**	**45.8/-15.3 α_{95} =14.9 k=39.0**			**4 sections 35 samples**
Approach 2						
A1123	565 (555-575)	50.0/-51.4	45.3/-11.5	18.8	6.8	11flows 11/17
A1128	570 (350-685)	45.0/-46.2	44.1/-28.2	52.3 CSD= 16	25.0	2flows 4/59
A1209	680 (655-680)	61.7/-59.1	44.6/-15.6	14.36	74.7	4flows 4/21
A1210	595 (545-645)	60.18/-40.3	54.0/-3.1	12.2	15.1	11 flows 13/22
MHV Mean Direction		**54.0/-49.5 α_{95} =10.9 k=72.3**	**47.1/-14.6 α_{95} =13.0 k=50.6**			**4 sections 28 flows 32 samples**
Approach 3						
A1128 Flow 1	575	29.3/-51.1	32.2/-33.4	16.9	30.65	3/3
MHV Mean Direction		**N. D.**	**N.D**			

D and I— D and I—mean declination and inclination
k—Fisher's (1953) precision parameter
α_{95}—radius of confidence circle for the mean direction
n—number of samples used
n_c —total number of stratigraphic horizons or samples collected

SUPPLEMENTARY TABLE S5.
HIGH-TEMPERATURE HT1 COMPONENT DIRECTIONS WITH α_{95}<20°

Site/ Section	HT1 demag. temp.(°C)	D/I (in situ)(°)	D/I (tilt corrected)(°)	α_{95}(°)	k	n/n_c
Approach 1						
A1126 matrix	560 (545-585)	349.1/80.9	209.1/59.0	16.4	57.7	4[#]/5
A1126 clasts*	555 (530-585)	72.3/43.0	116.4/52.9	114.5	1.1	5/5
A1128	575 (400-630)	168.5/60.3	185.0/47.5	4.9	31.2	28/59
A1203	560-580	179.1/34.8	178.7/42.8	10.5	33.9	7/7
A1207	575-585	5.3/-21.2	5.5/-29.2	13.3	18.3	9/9
A1209	575-685	170.9/74.9	196.7/29.8	12.35	13.3	12/21
MHV Mean Direction[†]		**179.1/58.1 α_{95} =31.3 k=6.9**	**190.0/42.1 α_{95} =14.3 k=29.5**			**1 site and 4 sections 60 samples**
Approach 2						
A1126 matrix	560 (545-585)	349.1/80.9	209.1/59.0	16.4	57.7	4 horizons 4/5 (2c)
A1126 clasts*	555 (530-585)	72.3/43.0	116.4/52.9	114.5	1.1	5/5
A1128	575 (400-630)	158.9/58.8	177.7/47.8	8.5	29.6	11 flows 28/59
A1203	560-580	179.5/35.0	179.2/43.0	13.1	367	2 flows 7/7
A1207	575-585	5.3/-21.2	5.5/-29.2	13.3	18.3	1 flow 9/9
A1209	575-585	149.4/79.5	195.8/36.2	14.8	11.6	10 flow 10/21
MHV Mean Direction[†]		**175.6/59.2 α_{95} =32.7 k=6.4**	**188.4/43.5 α_{95} =13.6 k=32.4**			**1 site and 4 sections 28 stratigraphic horizons/flows 58 samples**
Approach 3						
A1203 Flow 1	560-580	176.7/33.2	176.0/41.1	18.6	25.3	4/4
A1203 Flow 2	560-580	182.4/36.9	182.5/44.9	19.7	40.4	3/3
A1207	575-585	5.3/-21.2	5.5/-29.2	13.3	18.3	9/9
A1128 Flow 1	500-575	157.4/64.2	174.8/54.6	15.4	36.5	4/4
A1128 Flow 2	560-605	183.9/60.7	196.3/45.1	8.8	47.9	7/9
A1128 Flow 3	575-630	163.8/51.4	178.0/39.7	16.45	57.2	3/3
A1128 Flow 4	400-575	156.6/66.6	182.3/55.0	13.0	50.25	4/19
MHV Mean Direction[†]		**174.9/48.3 α_{95} =14.6 k=18.1**	**182.4/44.4 α_{95} =7.7 k=61.8**			**7 flows 34 samples**

D and I— D and I—mean declination and inclination
k—Fisher's (1953) precision parameter
α_{95}—radius of confidence circle for the mean direction
n—number of samples used
n_c —total number of stratigraphic horizons or samples collected
*Not used in mean direction
[†]Used reversed A1207 site mean direction in calculation
[#]2 of these samples are great circle fits

SUPPLEMENTARY TABLE S6. WATSON'S V STATISTIC TEST FOR THE APPROACH 1 MT POLE			
	Kent and Irving 2010 70 Ma pole	Besse and Courtillot, 2002 77.9 Ma pole	Torsvik et al., 2012 80 Ma Pole
MT pole Post-rotation	Watson's V: 1.0 Vcritical: 7.0 PASS	Watson's V: 1.5 Vcritical: 6.7 PASS	Watson's V: 0.9 Vcritical: 6.8 PASS
MT pole Pre-rotation	Watson's V: 7.8 Vcritical: 6.9 FAIL	Watson's V: 6.9 Vcritical: 6.7 FAIL	Watson's V: 8.6 Vcritical: 6.8 FAIL

SUPPLEMENTARY TABLE S7.

Rotation parameters for the reconstructions in Figures 7 and 8. Figure 7 only reconstructs Yukon block.

Craton/block/terrane	Euler Pole		Angle of Rotation (°)
	Latitude (°N)	Longitude (°E)	
	720 Ma		
Laurentia	-44.77	-14.89	133.98
Yukon block*	-66.81	45.17	54.99
Amazonia	1.47	52.28	110.1
Pampean/Rio de La Plata	2.77	52.94	135.76
Sao Francisco	9.65	54.38	129.51
Baltica	45.09	-143.91	177.44
Congo	16.74	85.88	126.21
West Africa	4.46	82.71	135.73
Kalahari	22.36	83.48	122.25
Australia	-11.67	-124.32	-89.35
North China	1.44	178.52	-127.11
India	67.52	70.38	35.07
Siberia	6.01	-18.79	59.41
Tarim	37.04	122.87	-133.4
	615 Ma		
Laurentia	-31.65	26.07	145.61
Yukon block*	0.0	0.0	101
Amazonia	15.85	56.36	143.78
Pampean/Rio de La Plata	15.92	52.13	144.2
Sao Francisco	11.72	54.46	137.73
Baltica	33.91	-132.86	175.83
Congo	17.73	83.46	133.94
West Africa	22.01	84.04	136.37
Kalahari	19.32	83.66	133.19
Australia	-2.47	-141.79	-76.98
North China	4.28	9.57	146.82
India	22.3	-58.21	-31.33
Siberia	12.44	-176.67	-109.38
Tarim	31.22	108.16	-139.28

* rotated relative to Laurentia

Figure S1. A1126 Conglomerate test
Eagle Creek Formation-Rapitan Group Equivalent

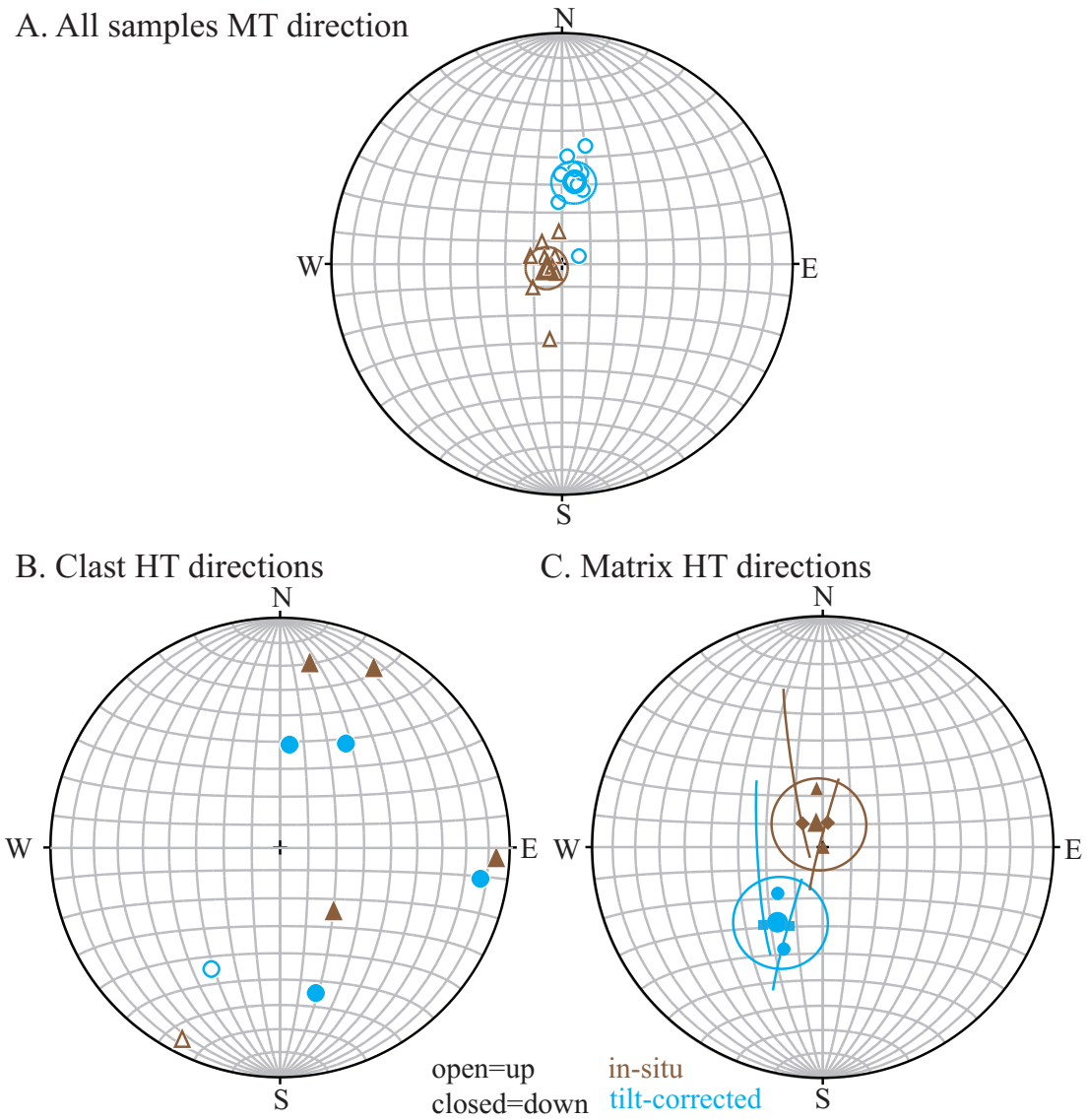


Figure A.1: MT, and HT clast and matrix results for conglomerate test A1126

Abbott, G., 1997, Geology of the Upper Hart River Area, Eastern Ogilvie Mountains, Yukon Territory (116A/10, 116A/11): Exploration and Geological Services Division, Yukon, Indian and Northern Affairs Canada, Bulletin, v. 9, 92 p.

Abbott, J. G., 1996, Implications of probable Late Proterozoic dextral strike-slip movement on the Snake River Fault, in Cook, F.A. and Erdmer, P., editors, Slave– Northern Cordillera Lithospheric Evolution (SNORCLE) Transect: Lithoprobe Report 50, p. 138-140.

Aitken, J. D., 1993, Tectonic evolutionnd basin history. In: Sedimentary Cover of the North American Craton in Canada. D.E. Stottand J.D. Aitken, (eds.): Geological Survey of Canada, Geology of Canada, no. 5, p. 483-504.

Aitken, J. D.,and Long, D. G. F., 1978, Mackenzie tectonicrc—Reflection of early basin configuration?: Geology, v. 6, p. 626-629.

Aitken, J.D., 1981, StratigraphyAnd sedimentology of the upper Proterozoic Little Dal Group, Mackenzie Mountains, Northwest Territories, in Campbell, F.H.A., editor, Proterozoic basins of Canada: Geological Survey of Canada Paper v. 81, p. 47-71.

Aitken, J.D., 1989, Uppermost Proterozoic formations in central Mackenzie Mountains, Northwest Territories: Geological Survey of Canada, Bulletin 368, 26 p.

Aitken, J.D., 1991a, The Ice Brook FormationAnd Post-Rapitan, Late Proterozoic glaciation, Mackenzie Mountains, Northwest Territories: Geological Survey of Canada Bulletin, v. 404, p. 1–43.

Aitken, J.D., 1991b, Two late Proterozoic glaciations, Mackenzie Mountains, northwestern Canada: Geology, v. 19, no. 5, p. 445–448.

Aitken, J.D.,And McMechan, M.E., 1992, Middle Proterozoic Assemblages, in Gabrielse, H.,And Yorath, C.J., editors, Geology of the Cordilleran Orogen in Canada: Geological Survey of Canada, Geology of Canada, no. 4, p. 97-124. (also Geological Society ofAmerica, The Geology of NorthAmerica, v. G-2).

Allen, C.M., Campbell, I.H., 2012, Identification and elimination of a matrix-induced systematic error in LA-ICP-MS $^{206}Pb/^{238}U$ dating of zircon: Chemical Geology 332-333, 157-165.

Allen, T.L., Pigage, L.C. and MacNaughton, R.B., 2001, Preliminary geology of the Pool Creek map area (95C/5), southeastern Yukon. In: Yukon Exploration and Geology 2000, D.S. Emond and L.H. Weston (eds.), Exploration and Geological Services Division, Yukon, Indian and Northern Affairs Canada, p. 53-72

Alt, J. C., 1999, Very low-grade hydrothermal metamorphism of basic igneous rocks, in Low-Grade Metamorphism, edited by M. Frey and D. Robinson, p. 169 - 201, Blackwell, Malden, Mass.

Alt, J. C., and D. A. H. Teagle, 2003, Hydrothermal alteration of upper oceanic crust formed at a fast-spreading ridge: Mineral, chemical and isotopic evidence from ODP Site 801, Chem. Geol., 201, 191-211.

Ariskin, A. A. et al. Geochronology of the Dovyren intrusive complex, Northwestern Baikal area, Russia, in the Neoproterozoic. Geochem. Int. 51, 859-875 (2013).

Armin, R.A. and Mayer, L., 1983, Subsidence analysis of the Cordilleran miogeocline: Implications for timing of late Proterozoic rifting and amount of extension: Geology, v. 11, no. 12, p.702-705.

Aspler, L. B., Pilkington, M.,And Miles, W. F., 2003, Interpretations of Precambrian basement based on recentAeromagnetic data, Mackenzie Valley, Northwest Territories: Geological Survey of Canada, Current Research 2003-C2, 11p.

Baldwin, G.J., Turner, E.C., and Kamber, B.S., 2016, Tectonic controls on distribution and stratigraphy of the Cryogenian Rapitan iron formation, northwestern Canada: Precambrian Research, v. 278, p. 303-322.

Balgord, E.A., Yonkee, W.A., Link, P.K. and Fanning, C.M., 2013, Stratigraphic, geochronologic, and geochemical record of the Cryogenian Perry Canyon Formation, northern Utah: Implications for Rodinia rifting and snowball Earth glaciation: Geological Society of America Bulletin, v. 125, no. 9-10, p.1442-1467.

Banerjee, S. K., 1971, New grain size limits for paleomagnetic stability in hematite. Nature Phys. Sci., v. 232, p. 15–16.

Besse, J., Courtillot, V., 2002, Apparent and True Polar Wander and the geometry of the geomagnetic field over the last 200 Myr. Journal of Geophysical Research, v. 107, no. B11 2300.

Bhushan, S.K., 1985, Malani volcanism in western Rajasthan. Indian Journal of Earth Sciences, v. 12, no. 1, p.58-71.

Bjerrum, C.J. and Canfield, D.E., 2004, New insights into the burial history of organic carbon on the early Earth: Geochemistry, Geophysics, Geosystems, v. 5, no. 8, p. 9.

Bogdanova, S.V., Bingen, B., Gorbatschev, R., Kheraskova, T.N., Kozlov, V.I., Puchkov, V.N. and Volozh, Y.A., 2008, The East European Craton (Baltica before and during the assembly of Rodinia. Precambrian Research, v. 160, no.1, p.23-45..

Bond, G.C., and Kominz, M.A., 1984, Construction of tectonic subsidence curves for the early Paleozoic miogeocline, southern Canadian Rocky Mountains: implications for subsidence mechanisms, age of breakup, and crustal thinning: Geological Society of America Bulletin, v. 95, no. 2, p. 155.

Bond, G.C., Christie-Blick, N., Kominz, M.A. and Devlin, W.J., 1985, An Early Cambrian rift to post-rift transition in the Cordillera of western North America: Nature, v. 315, no. 6022, p. 742-746.

Books,K. Magnetization of the lower most Keweenawan lava flows in the Lake Superior area, 1968, Geological Survey research 1968, chapter D. U.S. Geological Survey Professional Paper P 0600-D, 248–254

Bowring, S.A., Schoene, B., Crowley, J.L., Ramezani, J. and Condon, D.J., 2006, High-precision U-Pb zircon geochronology and the stratigraphic record: Progress and promise. Paleontological Society Papers, v. 12, p. 25.

Brady, P. V., and S. R. Gislason. 1997, Seafloor weathering controls on atmospheric CO2 and global climate: Geochim. Cosmochim. Acta, 61, 965-973.

Brett, J.S. and Dunlop, D.J., 2008. Earth and Planetary Science Letters, 266(1), p.125-139.

Bright, R.M., Amato, J.M., Denyszyn, S.W. and Ernst, R.E., 2014. U-Pb geochronology of 1.1 Ga diabase in the southwestern United States: Testing models for the origin of a post-Grenville large igneous province. Lithosphere, pp.L335-1.

Brock, A., 1968, Metasomatic and intrusive nepheline-bearing rocks from the Mbozi syenite-gabbro complex, southwestern Tanzania. Can. J. EarthSci., v. 5, p. 387-419.

Brookfield, M.E., 1993. Neoproterozoic Laurentia-Australia fit. Geology, 21(8), pp.683-686.

Brown, D. A., P. T. Doughty, and P. Stinson, 1994, Preliminary geology of the Creston map area, southeastern British Columbia (82F/2): Geological fieldwork 1995-1.

Brunstein, F.C. (Editor). 2002, Magnetic anomaly map of North America. US. Geological Survey, US. Department of the Interior, Denver, Colo., scale 1 : 10 000 000.

Bryan, P. and Gordon, R.G., 1990. Rotation of the Colorado Plateau: An updated analysis of paleomagnetic poles. Geophysical Research Letters, 17(10), pp.1501-1504.

Buchan, K. L., and Ernst, R. E., 2013, Diabase dyke swarms of Nunavut, Northwest Territories and Yukon, Canada: Geological Survey of Canada, Open File 7464, 24 p.

Buchan, K. L., Mertanen, S., Park, R. G., Pesonen, L. J., Elming, S. Å., Abrahamsen, N., and Bylund, G., 2000, Comparing the drift of Laurentia and Baltica in the Proterozoic: the importance of key palaeomagnetic poles: Tectonophysics, v. 319 no. 3, p. 167-198.

Buchan, K.L., 2014, Reprint of "Key paleomagnetic poles and their use in Proterozoic continent and supercontinent reconstructions: A review". Precambrian Research, v. 244, p. 5–22.

Buchan, K.L., and Ernst, R.E., 2004, Diabase dyke swarms and related units in Canada and adjacent regions: Geological Survey of Canada, Map 2022A (scale 1:5 000 000) with accompanying compilation, 39 p.

Buchan, K.L., Ernst, R.E.,Bleeker, W., Davis, W.J., Villeneuve, M., vanBreemen, O., Hamilton, M.A., and Sošderlund, U., 2010, Proterozoic magmatic events of the Slave craton, Wopmay orogen and environs: Geological Survey of Canada, Open File 5985, 25 p.

Butler, R. F., 1992, Paleomagnetism: Magnetic Domains to Geologic Terranes:Boston,Blackwell Scientific Publications, 238 p.

Calver, C.R., Crowley, J.L., Wingate, M.T.D., Evans, D.A.D., Raub, T.D. and Schmitz, M.D., 2013, Globally synchronous Marinoan deglaciation indicated by U-Pb geochronology of the Cottons Breccia, Tasmania, Australia: Geology, v. 41, no. 10, p.1127-1130.

Cahen, L. and Snelling, N.J., 1966, The geochronology of equatorial Africa. North-Holland Publishing Company.

Camp, V.E., Ross, M.E. and Hanson, W.E., 2003, Genesis of flood basalts and Basin and Range volcanic rocks from Steens Mountain to the Malheur River Gorge, Oregon: Geological Society of America Bulletin, v. 115, no. 1, p.105-128.

Cas, R.A.F. and Wright, J.V., 1987, Volcanic Successions, Modern and Ancient: A Geological Approach to Processes, Products and Successions, 528 p.
Cawood, P.A., 2005, Terra Australis Orogen: Rodinia breakup and development of the Pacific and Iapetus margins of Gondwana during the Neoproterozoic and Paleozoic: Earth-Science Reviews, v. 69, no. 3, p.249-279.

Cawood, P.A. and Buchan, C., 2007, Linking accretionary orogenesis with supercontinent assembly. Earth-Science Reviews, v. 82, no. 3, p.217-256.

Cawood, P.A. and Korsch, R.J., 2008, Assembling Australia: Proterozoic building of a continent. Precambrian Research, v. 166, no.1, p.1-35.

Cawood, P.A., Wang, Y., Xu, Y. and Zhao, G., 2013. Locating South China in Rodinia and Gondwana: A fragment of greater India lithosphere?. Geology, 41(8), pp.903-906.

Cecile, M. P., 1984, Evidence against large-scale strike-slip separation of Paleozoic strata along the Richardson-Hess fault system, northernCanadianCordillera: Geology, v. 12, no. 7, p. 403-407.

Cecile, M.P. and Norford, B.S., 2000, Geology of the northeastern Niddery Lake map area, east-central Yukon and adjacent Northwest Territories (No. 553): Geological Survey of Canada.

Cecile, M.P., Morrow, D.W., and Williams, G.K., 1997, Early Paleozoic (Cambrian to Early Devonian) tectonic framework,CanadianCordillera: Bulletin ofCanadian Petroleum: Geology, v. 45, no. 1, p. 54-74.

Christie-Blick, N., and Levy, M., 1989, Concepts of sequence stratigraphy, with examples from strata of late Proterozoic and Cambrian age in the western United States, in Christie-Blick, N., and Levy, M., eds., Late Proterozoic and Cambrian Tectonics, Sedimentation and Record of Metazoan Radiation in the Western United States (28th International Geological Congress FieldTrip Guidebook T331): Washington, D.C., American Geophysical Union, p. 23-37.

Christie-Blick, Nicholas, 1997, Neoproterozoic Sedimentation and Tectonics in West-Central Utah [Ph.D. Thesis]: Brigham Young University Geology Studies, 30 p.

Christie, K. W., and Fahrig, W. F., 1983, Paleomagnetism of the Borden dykes of Baffin Island and its bearing on the Grenville Loop: Canadian Journal of Earth Sciences, v. 20, no. 2, p. 275-289.

Cisowski, S., 1981, Interacting vs. non-interacting single domain behavior in natural and synthetic samples: Physics of Earth and Planetary Interiors, v. 26, p. 56–62.

Coats, R.P. and Preiss, W.V., 1980. Stratigraphic and geochronological reinterpretation of late Proterozoic glaciogenic sequences in the Kimberley region, Western Australia. Precambrian Research, 13(2-3), pp.181-208.

Colpron, M., 2012, Preliminary observations on the geology of the Rackla belt, Mount Ferrell map area (NTS 106C/3), central Yukon. In: Yukon Exploration and Geology 2011, K.E. MacFarlane and P.J. Sack (eds.), Yukon Geological Survey, p. 27-43.

Colpron, M., Logan, J., and Mortensen, J., 2002, U-Pb zircon age constraint for late Neoproterozoic rifting and initiation of the lower Paleozoic passive margin of western Laurentia: Canadian Journal of Earth Sciences, v. 39, no. 2, p. 133-143, doi: 10.1139/E01-069.

Condon, D., and Bowring, S.A., 2011, A user's guide to Neoproterozoic geochronology, in Arnaud,

E., Shields, G., and Halverson, G., eds.,The Geological Record of Neoproterozoic Glaciations: Geological Society of London Memoir, v. 36, no. 1, p. 135-149.

Condon, D., Zhu, M., Bowring, S., Wang, W., Yang, A. and Jin, Y., 2005, U-Pb ages from the Neoproterozoic Doushantuo Formation, China: Science, v. 308, no. 5718, p.95-98.

Condon, D.J., Schoene, B., McLean, N.M., Bowring, S.A., Parrish, R.R., 2015, Metrology and traceability of U-Pb isotope dilution geochronology (EARTHTIME Tracer Calibration Part I): Geochimica et Cosmochimica Acta, v. 164, p. 464-480. doi:10.1016/j.gca.2015.05.026

Cook, F.A., Hall, K.W., and Lynn,C.E., 2005, The edge of northwestern North America at 1.8 Ga. Canadian Journal of Earth Sciences, v. 42, no. 6, p. 983–997

Corsetti, F. A. and Kaufman, A. J., 2003, Stratigraphic investigations of carbon isotope anomalies and Neoproterozoic ice ages in Death Valley, California: Geological Society of America Bulletin, v. 115, no. 8, p. 916-932.

Cox, G. M., 2015, Linking tectonics, LIP Emplacement and EnvironmentalChange in theCryogenian, [Ph.D. Thesis]: McGill University, 301 p.

Cox, G.M., Halverson, G.P., Minarik, W.G., Le Heron, D.P., Macdonald, F.A., Bellefroid, E.J. and Strauss, J.V., 2013, Neoproterozoic iron formation: an evaluation of its temporal, environmental and tectonic significance: Chemical Geology, v. 362, p.232-249.

Cox, G.M., Halverson, G.P., Poirier, A., Le Heron, D., Strauss, J.V. and Stevenson, R., 2016, A model for Cryogenian iron formation: Earth and Planetary Science Letters, v. 433, p.280-292.

Cox, G.M., Roots, C.F., Halverson, G.P., Minarik, W.G., Macdonald, F.A., and Hubert-Theou, L., 2013, Mount Harper Volcanic Complex, Ogilvie Mountains: A far-flung occurrence of the Franklin Igneous Event?, in MacFarlane, K.E., Nordling, M.G., and Sack, P.J., editors, Yukon Exploration and Geology 2012: Yukon Geological Survey, p. 19-36.

Crawford, B. L., Betts, P. G., and Aillères, L., 2010, An aeromagnetic approach to revealing buried basement structures and their role in the Proterozoic evolution of the Wernecke Inlier, Yukon Territory,Canada: Tectonophysics, v. 490, no. 1, p. 28-46.

Crittenden, M.D., Christie-Blick, N. and Link, P.K., 1983, Evidence for two pulses of glaciation during the late Proterozoic in northern Utah and southeastern Idaho: Geological Society of America Bulletin, v. 94, no. 4, p.437-450.

Crow, R., Karlstrom, K.E., McIntosh, W., Peters, L. and Dunbar, N., 2008. History of Quater-

nary volcanism and lava dams in western Grand Canyon based on lidar analysis, 40Ar/39Ar dating, and field studies: Implications for flow stratigraphy, timing of volcanic events, and lava dams. Geosphere, 4(1), pp.183-206.

Dalrymple, G.B., 1979, Critical tables for conversion of K-Ar ages from old to new constants. Geology, v. 7, no.11, p.558-560.

Dalrymple, R.W. and Narbonne, G.M., 1996, Continental slope sedimentation in the Sheepbed Formation (Neoproterozoic, Windermere Supergroup), Mackenzie Mountains, NWT: Canadian Journal of Earth Sciences, 33(6), p.848-862.

Dalziel, I. W.D., 1997, Neoproterozoic- Paleozoic geography and tectonics: review, hypothesis, environmental speculation: Geological Society of America Bulletin, v. 109, no. 1, p. 16-42.

Dalziel, I.W., 1991. Pacific margins of Laurentia and East Antarctica-Australia as a conjugate rift pair: Evidence and implications for an Eocambrian supercontinent. Geology, 19(6), pp.598-601.

Davidson, A., 2008, Late Paleoproterozoic to mid-Neoproterozoic history of northern Laurentia: an overview of central Rodinia. Precambrian Research, v. 160, no.1, p.5-22.

Davydov, V. I., Crowley, J. L., Schmitz, M. D., and Poletaev, V. I., 2010, High-precision U-Pb zircon age calibration of the global Carboniferous time scale and Milankovitch-band cyclicity in the Donets Basin, eastern Ukraine: Geochemistry, Geophysics, Geosystems, 10.1029/2009GC002736.

Deenen, M.H., Langereis, C.G., van Hinsbergen,D.J. and Biggin, A.J., 2011, Geomagnetic secular variation and the statistics of palaeomagneticDirections: Geophysical Journal International, v. *186*, no. 2, p. 509-520.

Dehler, C., Gehrels, G., Porter, S., Heizler, M., Karlstrom, K., Cox, G., Crossey, L. and Timmons, M., 2017. Synthesis of the 780- 740 Ma Chuar, Uinta Mountain, and Pahrump (ChUMP) groups, western USA: Implications for Laurentia-wide cratonic marine basins. Geological Society of America Bulletin, pp.B31532-1.

Dehler, C.M., Elrick, M., Bloch, J.D., Crossey, L.J., Karlstrom, K.E. and Des Marais, D.J., 2005. High-resolution δ13C stratigraphy of the Chuar Group (ca. 770–742 Ma), Grand Canyon: Implications for mid-Neoproterozoic climate change. Geological Society of America Bulletin, 117(1-2), pp.32-45.

Dehler, C.M., Elrick, M., Karlstrom, K.E., Smith, G.A., Crossey, L.J. and Timmons, J.M., 2001. Neoproterozoic Chuar Group (~ 800-742Ma), Grand Canyon: a record of cyclic marine deposition during global cooling and supercontinent rifting. Sedimentary Geology, 141, pp.465-499.

Dehler, C.M., Fanning, C.M., Link, P.K., Kingsbury, E.M., and Rybczynski, D., 2010, Maximum depositional age and provenance of the Uinta Mountain Group and Big Cottonwood Formation, northern Utah: Paleogeography of rifting western Laurentia: Geological Society of America Bulletin, v. 122, no. 9-10, p. 1686-1699.

Dehler, C.M., Porter, S.M., De Grey, L.D., Sprinkel, D.A. and Brehm, A.N.D.Y., 2006. The Neoproterozoic Uinta Mountain Group revisited: A synthesis of recent work on the Red Pine Shale and related undivided clastic strata, northeastern Utah. SPECIAL PUBLICATION-SEPM, 86, p.151.

Delaney, G.D., 1981, The mid-Proterozoic Wernecke Supergroup, Wernecke Mountains, Yukon Territory, in Campbell, F.H.A., editor, Proterozoic Basins of Canada: Geological Survey of Canada Paper 81, p. 1-23.

Denyszyn, S. W., Halls, H. C.,and Davis, D. W. (2006). A paleomagnetic, geochemical and U-Pb geochronological comparison of the Thule (Greenland) and Devon Island (Canada) Dyke Swarms and its relevance to the Nares Strait problem. Polarforschung, 74(1-3), 63-75.

Denyszyn, S. W., Halls, H. C., Davis, D. W., and Evans, D. A., 2009a, Paleomagnetism and U-Pb geochronology of Franklin dykes in High Arctic Canada and Greenland: a revised age and paleomagnetic pole constraining block rotations in the Nares Strait region: Canadian Journal of Earth Sciences, v. 46, no. 9, p. 689-705.

Denyszyn, S.W.,Davis,D.W., and Halls, H.C., 2009b, Paleomagnetism and U–Pb geochronology of the Clarence HeadDykes, Arctic Canada: orthogonal emplacement of maficDykes in a large igneous province: Canadian Journal of Earth Sciences, v. 46, no. 3, p. 155–167.

Devlin, W.J., 1989, Stratigraphy and sedimentology of the Hamill Group in the northern Selkirk Mountains, British Columbia: evidence for latest Proterozoic - Early Cambrian extensional tectonism. Canadian Journal of Earth Sciences, 26: 515-533.

Diehl, J.F. and Haig, T.D., 1994. A paleomagnetic study of the lava flows within the Copper Harbor Conglomerate, Michigan: new results and implications. Canadian Journal of Earth Sciences, 31(2), pp.369-380.

Dirks, P.H. and Wilson, C.J., 1990. The geological evolution of the Reynolds Range, central Australia: evidence for three distinct structural-metamorphic cycles. Journal of Structural Geology, 12(5-6), pp.651-665.

Dunlop, D. J., and Buchan, K. L., 1977, Thermal remagnetization and the paleointensity record of metamorphic rocks: Physics of the Earth and Planetary Interiors, v. 13, no. 4, p. 325-331.

Dunlop,D. J., 2002,Theory and application of theDay plot (Mrs/Ms versus Hcr/Hc), 1. Theoretical curves and tests using titanomagnetite data: Journal of Geophysical Research, v.107, no. B3

Edwards, B., Russell, J. and Anderson, R., 2002, Subglacial, phonolitic volcanism at Hoodoo Mountain volcano, northern Canadian Cordillera: Bulletin of Volcanology, v. 64, no. 3-4, p.254-272.

Eickmann, B., Bach, W. and Peckmann, J., 2009, Authigenesis of Carbonate Minerals in Modern and Devonian Ocean-Floor Hard Rocks: The Journal of Geology, v. 117, no. 3, p.307-323.

Eisbacher, G. H., 1983, Devonian-Mississippian sinistral transcurrent faulting along the cratonic margin of western North America: A hypothesis: Geology, v. 11, no. 1, p. 7-10.

Eisbacher, G.H., 1978, Re-definition and Subdivision of the Rapitan Group, Mackenzie Mountains: Geological Survey of Canada, Paper 77-35.

Eisbacher, G.H., 1981, Sedimentary tectonics and glacial record in the Windermere Supergroup, Mackenzie Mountains, northwestern Canada: Geological Survey of Canada Paper 80-27, 40 p.

Eisbacher, G.H., 1985, Late Proterozoic rifting, glacial sedimentation, and sedimentary cycles in the light of Windermere deposition, western Canada: Palaeogeography, Palaeoclimatology, and Palaeoecology, v. 51, no. 1, p. 231–254

Elston, D.P. and Scott, G.R., 1973. Paleomagnetism of some Precambrian basaltic flows and red beds, eastern Grand Canyon, Arizona. Earth and Planetary Science Letters, 18(2), pp.253-265.

Elston, D.P., 1979. Late Precambrian Sixtymile formation and orogeny at top of the Grand Canyon Supergroup, northern Arizona (No. 1092). US Govt. Print. Off.,.

Elston, D.P., 1986, Magnetostratigraphy of Late Proterozoic Chuar Group and Sixtymile Formation, Grand Canyon Supergroup, northern Arizona; correlation with other Proterozoic strata of North America. Geol. Soc. Am. Abstr. Prog. v. 18, no.5 , 353.

Elston, D.P., 1989, Grand Canyon Supergroup, northern Arizona; stratigraphic summary and preliminary paleomagnetic correlations with parts of other North American Proterozoic successions. In: Jenney, J.P., Reynolds, S.J. no. Eds., Geologic Evolution of Arizona, Arizona Geological Society Digest, v. 17. p. 259–272.

Ernst, R. E., Buchan, K. L., Harris, B. A., Hanes, J. A., Milner, M. W., and La Prairie, L. F. (2004, May). Ar40-Ar39 Dating of the Lasard River Mafic Dykes, and Implications for the Focus of the 0.72 Ga Franklin Large Igneous Province of Northern Canada. In AGU Spring Meeting Abstracts (Vol. 1, p. 07).

Ernst, R.E,. M.A. Hamilton, U. Söderlund, J.A. Hanes, D.P. Gladkochub, A.V. Okrugin, T. Kolotilina, A.S. Mekhonoshin, W. Bleeker, A.N. LeCheminant, K.L. Buchan, K.R. Chamberlain, A.N. Didenko, 2016, Long-lived connection between southern Siberia and northern Laurentia in the Proterozoic: Nature Geoscience, (in press), doi: 10.1038/NGEO2700

Ernst, R.E., Wingate, M.T.D., Buchan, K.L. and Li, Z.X., 2008. Global record of 1600-700Ma Large Igneous Provinces (LIPs): implications for the reconstruction of the proposed Nuna (Columbia) and Rodinia supercontinents. Precambrian Research, 160(1), pp.159-178.

Evans, D. A. D. and Mitchell, R. N. Assembly and breakup of the core of Paleoproterozoic-Mesoproterozoic supercontinent Nuna. Geology 39, 443-446 (2011).

Evans, D. A.D., 2000, Stratigraphic, geochronological, and paleomagnetic constraints upon the Neoproterozoic climatic paradox: American Journal of Science, v. 300, no. 5, p. 347-433.

Evans, D.A., Li, Z.X., Kirschvink, J.L. and Wingate, M.T., 2000. A high-quality mid-Neoproterozoic paleomagnetic pole from South China, with implications for ice ages and the breakup configuration of Rodinia. Precambrian Research, 100(1),

Evans, D.A.D. and Raub, T.D., 2011, Neoproterozoic glacial palaeolatitudes: a global update: Geological Society, London, Memoirs, v. 36, no. 1, p. 93-112.

Evans, D.A.D., 2009, The palaeomagnetically viable, long-lived and all-inclusive Rodinia supercontinent reconstruction: Journal of the Geological Society of London, Special Publications, v. 327, no. 1, p. 371-404.

Evans, D.A.D., 2013, Reconstructing pre-Pangean supercontinents: Geological Society of America Bulletin, v. 125, no.11-12, p.1735-1751.

Evenchick, C.A., 1988, Stratigraphy, metamorphism, structure, and their tectonic implications in the Sifton and Deserters Ranges, Cassiar and northern Rocky mountains, northern British Columbia: Bulletin of the Geological Survey of Canada, Dep. of Energy, Mines and Resources.

Ewart,A., R.W. Schon,andB.W. Chappell, 1992, The Cretaceous volcanic-Plutonic province of the central Queensland (Australia) coast–A rift-related 'calc-alkaline' province, in The Second Hutton Symposium The Origin of Granites and Related RocksEdited by P.E.Brown and B.W.Chappell Special Papers of the Geological Society of America, v. 272, p. 327- 346

Eyles, C.H., Eyles, N. and Miall, A.D., 1985, Models of glaciomarine sedimentation and their application to the interpretation of ancient glacial sequences: Palaeogeography, Palaeoclimatology, Palaeoecology, v. 51, no. 1, p.15-84.

Eyster, A. E., Fu, R. F., Strauss, J. V., Weiss, B. P., Roots, C.F., Halverson, G.P., Evans, D.A.D., Macdonald, F.A., 2016. Paleomagnetic evidence for a large rotation of the Yukon Block relative to Laurentia: Implications for a low-latitude Sturtian Glaciation and the break-up of Rodinia: Geological Society of America Bulletin.

Fahrig, W. F., and Schwarz, E. J., 1973, Additional paleomagnetic data on the Baffin diabase dikes and a revised Franklin pole, Canadian Journal of Earth Sciences, v. 10, no. 4, p. 576-581.

Fahrig, W. F., Irving, E., and Jackson, G. D., 1971, Paleomagnetism of the Franklin diabases: Canadian Journal of Earth Sciences, v. 8, no. 4, p. 455-467.

Fahrig, W.F., Irving, E., and Jackson,G. D., 1971, Paleomagnetism of theFranklin diabases: Canadian Journal of Earth Sciences, v. 8, no. 4, p. 455-467.

Fairchild, L.M., Swanson-Hysell, N.L., Ramezani, J., Sprain, C.J. and Bowring, S.A., 2017, The end of Midcontinent Rift magmatism and the paleogeography of Laurentia. Lithosphere, p.L580-1.

Fan, W.M.,Guo,F., Wang, Y.J. and Lin,G., 2003, Late Mesozoic Calc-alkaline volcanism of post-orogenic extension in the northern Da Hinggan Mountains, northeastern China: Journal of volcanology andGeothermal research, v. 121, no. 1, p.115-135.

Fang, D.J., Zhu, Z.W., Guo, Y.B., 1983. Study on the paleomagnetism of Upper Precambrian in Northern Jiangsu and correlation between the Upper Precambrian strata in South and North China. Sci. Geol. Sin. 4, 324-336 (in Chinese with English abstract).

Fanning, C.M., and Link, P., 2004, U-Pb SHRIMP ages of Neoproterozoic (Sturtian) glaciogenic Pocatello Formation, southeastern Idaho: Geology, v. 32, no. 10, p. 881, doi:10.1130/G20609.1.

Ferri, F., Rees, C., Nelson, J., and Legun, A., 1999, Geology and Mineral Deposits of the Northern Kechika Trough between Gataga River and the 60th Parallel: Geological Survey Branch, Mineral Resources Division, British Columbia Ministry of Energy and Mines Bulletin 107, 122 p.

Fitzsimons, I.C.W., 2003a. Does the late Neoproterozoic Darling Fault zone of western Australia extend all the way to the Transantarctic Mountains? SGTSG Field Meeting, Kalbarri, p. 130.

Fitzsimons, I.C.W., 2003b. Proterozoic basement provinces of southern and southwestern Australia, and their correlation with Antarctica. In: Yoshida, M., Windley, B.F., Dasgupta, S. (Eds.), Proterozoic East Gondwana: supercontinent assembly and break-up. The Geological Society, London, pp. 93

Ford, T.D. and Breed, W.J., 1973. Late Precambrian Chuar Group, Grand Canyon, Arizona. Geo-

logical Society of America Bulletin, 84(4), pp.1243-1260.

Fritz, W. H., 1972, Lower Cambrian trilobitesFrom the Sekwi Formation type section, Mackenzie Mountains, northwestern Canada: Geological Survey of Canada, Bulletin, v. 212, 90 p.

Fu, X., Zhang, S., Li, H., Ding, J., Li, H., Yang, T., Wu, H., Yuan, H., and Lv, J., 2015, New paleomagnetic results from the Huaibei Group and Neoproterozoic mafic sills in the North China Craton and their paleogeographic implications: Precambrian Research, v. 269, p. 90-106.

Furlanetto,F., Thorkelson, D.J., Gibson, H.D., Marshall, D.D., Rainbird, R.H., Davis, W.J., Crowley, J.L. and Vervoort, J.D., 2013, Late Paleoproterozoic terrane accretion in northwestern Canada and the caseFor circum-Columbian orogenesis: Precambrian Research, v. 224, p. 512-528.

Furnes, H., Fridleifsson, I.B. and Atkins, F.B., 1980, Subglacial volcanics-on the formation of acid hyaloclastites: Journal of Volcanology and Geothermal Research, v. 8, no. 1, p.95-110.

Gabrielse, H., 1967, Tectonic evolution of the northern Canadian Cordillera: Canadian Journal of Earth Sciences, v. 4, no. 2, p. 271-298.

Gabrielse, H., 1972. Younger Precambrian of the Canadian Cordillera: American Journal of Science, v. 272, no. 6, p.521-536.

Gabrielse, H., and Campbell, R.B., 1992, Upper Proterozoic assemblages. In Geology of the Cordilleran Orogen in Canada. Edited by H. Gabrielse and C.J. Yorath: Geological Survey of Canada,Geology of Canada, No. 4, Chap. 6, p. 127–150. (Also Geological Society of America, The Geology of North America, Vol.G-2.)

Gans, P.B., Mahood,G.A. and Schermer, E., 1989. Synextensional magmatism in the Basin and Range Province; a case study from the easternGreat Basin.Geological Society of America Special Papers, 233, p. 1-53.

Gawthorpe, R. L., and Leeder, M. R., 2000, Tectono-sedimentary evolution of active extensional basins: Basin Research, v. 12, no. 3-4, p. 195-218.

Gee, J.S., and Kent, D.V., 2007, Source of oceanic magnetic anomalies and theGeomagnetic polarity time scale: Treatise onGeophysics, v. 5:Geomagnetism, p. 455-507.

Gehling, J.G., Narbonne,G.M., Anderson, M.A., 2000, The first named Ediacaran body fossil, Aspidella terranovica: Palaentology, v. 43, p. 427–456.

Geissman, J. W., and Harlan, S. S., 2002, Late Paleozoic remagnetization of Precambrian crystalline

rocks along the Precambrian/Carboniferous nonconformity, Rocky Mountains: a relationship among deformation, remagnetization, and fluid migration: Earth and Planetary Science Letters, v. 203, no. 3, p. 905-924.

Gernon, T.M., Hincks, T.K., Tyrrell, T., Rohling, E.J. and Palmer, M.R., 2016, Snowball Earth ocean chemistry driven by extensive ridge volcanism during Rodinia breakup: Nature Geoscience, v. 9, no. 3, p.242-248.

Giddings, J.W., 1976. Precambrian palaeomagnetism in Australia I: basic dykes and volcanics from the Yilgarn Block. Tectonophysics, 30(1-2), pp.91-108.

Gladkochub, D. P. et al. 2010, Proterozoic mafic magmatism in Siberian craton: an overview and implications for paleocontinental reconstruction. Precambr. Res. v. 183, p. 660–668.

Goddéris, Y., Donnadieu, Y., Nedelec, A., Dupre, B., Dessert, C.,Grard, A., Ramstein,G., and Francois, L. M., 2003, The Sturtian 'snowball' Glaciation: fire and ice: Earth and Planetary Science Letters, v. 211, no. 1, p. 1-12.

Goodfellow, W., Cecile, M., and Leybourne, M., 1995,Geochemistry, petrogenesis, and tectonic setting of Lower Paleozoic alkalic and potassic volcanic rocks, northern Canadian Cordilleran miogeocline: Canadian Journal of Earth Sciences, v. 32, no. 8, p. 1236–1254.

Grantz, A. V. L. Pease, D. A. Willard, et al., "Bedrock Cores from 89° North: Implications for the Geology Framework and Neogene Paleooceanography of Lomonosov Ridge and Tie to the Barents Shelf," Geol. Soc. Amer. Bull. 113 1271–1281 (2001)

Grantz, A. , D. L. Clarc, R. L. Philips, S. R. Srivastava, et al., Phanerozoic Stratigraphy of Northwind Ridge, Magnetic Anomalies in the Canada Basin, and the Geometry and Timing of Rifting in the Amerasia Basin, Arctic Ocean,- Geol. Soc. Amer. Bull. 110 (6), 801-820 (1998).

Greene, D. C. 2010, Neoproterozoic rifting in the southern Georgina Basin, central Australia: Implications for reconstructing Australia in Rodinia, Tectonics, 29, TC5010, doi:10.1029/2009TC002543.

Greenwood, H. J., Woodsworth,G. J., Reed, P. B.,Ghent, E. D., and Evenchick, C.A., 1991, Metamorphism, Chapter 16 inGeology of the Cordilleran Orogen in Canada, H.Gabrielse and C. J. Yorath (ed.):Geological Survey of Canada,Geology of Canada, no. 4, p. 533-570.

Gregory, L. C., Meert, J. G., Bingen, B., Pandit, M. K., and Torsvik, T. H., 2009, Paleomagnetism and geochronology of the Malani Igneous Suite, Northwest India: Implications for the configuration of Rodinia and the assembly of Gondwana: Precambrian Research, v. 170, n. 1–2, p. 13–26,

http:// dx.doi.org/10.1016/j.precamres.2008.11.004

Grey, K., Hocking, R.M., Stevens, M.K., Bagas, L., Carlsen, G.M., Irimies, F., Pirajno, F., Haines, P.W. and Apak, S.N., 2005. Lithostratigraphic nomenclature of the Officer Basin and correlative parts of the Paterson Orogen, Western Australia. Geological Survey of Western Australia Report, 93, p.89.

Guiraud, R., and Maurin, J. C., 1992, Early Cretaceous rifts of Western and Central Africa: an overview: Tectonophysics, v. 213, no. 1-2, p. 153-168.

Halgedahl, S.L. and Jarrard, R.D., 1987. Paleomagnetism of the Kuparuk River Formation from oriented drill core: Evidence for rotation of the Arctic Alaska plate: Society of economic paleontologists and mineralogists: Pacific Section Special Publications, v. 50, p. 581–620.

Halls, H. C. Michael T.D Wingate, Paleomagnetic pole from the Yilgarn B (YB) dykes of Western Australia: no longer relevant to Rodinia reconstructions, Earth and Planetary Science Letters, Volume 187, Issues 1-2, 30 April 2001, Pages 39-53, ISSN 0012-821X, http://doi.org/10.1016/S0012-821X(01)00279-5.

Halverson, G.P., Poitrasson, F., Hoffman, P.F., Nédélec, A., Montel, J.M. and Kirby, J., 2011, Fe isotope and trace element geochemistry of the Neoproterozoic syn-glacial Rapitan iron formation: Earth and Planetary Science Letters, v. 309, no. 1, p.100-112.

Hamblin, W.K., 1970. Late Cenozoic basalt flows of the western Grand Canyon.

Hamilton, W. 1988, Laramide crustal shortening, in Interaction of the Rocky Mountain Foreland and the Cordilleran Thrust Belt, Geol. Soc. Am. Mem., 171, 27-39.

Harlan, S.S., Geissman, J.W. and Snee, L.W., 1997.US Government Printing Office.

Harlan, S.S., Geissman, J.W., Snee, L.W., 2008. Paleomagnetism of Proterozoic maficdikes from the Tobacco Root Mountains, southwest Montana. PrecambrianResearch 163, 239-264.

Harlan, S.S., Heaman, L., LeCheminant, A.N. and Premo, W.R., 2003, Gunbarrel mafic magmatic event: A key 780 Ma time marker for Rodinia plate reconstructions: Geology, v. 31, no. 12, p.1053-1056.

Harley, S.L., Fitzsimons, I.C. and Zhao, Y., 2013, Antarctica and supercontinent evolution: historical perspectives, recent advances and unresolved issues. Geological Society, London, Special Publications, v. 383, no.1, p.1-34.

Hawkesworth, C., Turner, S., Gallagher, K., Hunter, A., Bradshaw, T. and Rogers, N., 1995, Calc-alkaline magmatism, lithospheric thinning and extension in the Basin and Range: Journal of Geophysical Research: Solid Earth, v. 100, no. B6, p.10271-10286.

Heaman, L., LeCheminant, A., and Rainbird, R., 1992, Nature and timing of Franklin igneous events, Canada: implications for a Late Proterozoic mantle plume and the break-up of Laurentia: Earth and Planetary Science Letters, v. 109, p. 117–131.

Hein, F.J. and McMechan, M.E., 1994, Proterozoic-Lower Cambrian strata of the western Canada sedimentary basin: Geological Atlas of the Western Canada Sedimentary Basin. Canadian Society of Petroleum Geologists and Alberta Research Council, GD Mossop and I. Shetsen (comps.), p.57-67.

Helmstaedt,H., Eisbacher, G.H., and McGregor,H., 1979, Copper mineralization near an intra-Rapitan unconformity, Nite copper prospect, Mackenzie Mountains, Northwest Territories, Canada: Canadian Journal of Earth Sciences, v. 16, no. 1, p. 50-59.

Hildebrand, R.S., 2009, Did westward subduction cause Cretaceous-Tertiary orogeny in the North American Cordillera?: Geological Society of America Special Papers, 457, p.1-71.

Hnat, J.S., Van der Pluijm, B.A. and Van der Voo, R., 2006. Primary curvature in the Mid-Continent Rift: Paleomagnetism of the Portage Lake Volcanics (northern Michigan, USA). Tectonophysics, 425(1), pp.71-82.

Hoffman, P.F., 1991, Did the breakout of Laurentia turn Gondwanaland inside-out: Science, v. 252, no. 5011, p.1409-1412.

Hoffman, P.F., and Schrag, D.P., 2002, The snowball EarthHypothesis: testing the limits of global change: Terra Nova, v. 14, no. 3, p. 129–155.

Hoffman, P.F., Kaufman, A.J.,Halverson, G.P., and Schrag, D.P., 1998, A Neoproterozoic snowball Earth: Science, v. 281, no. 5381, p. 1342–1346.

Irving, E., and Thorkelson, D. J., 1990, On determining paleohorizontal and latitudinal shifts: paleomagnetism of Spences Bridge Group, British Columbia: Journal of Geophysical Research: Solid Earth, 95(B12), p. 19213-19234.

Jackson, M., 1990, Diagenetic sources of stable remanence in remagnetized Paleozoic cratonic carbonates: A rock magnetic study.Journal of Geophysical Research: Solid Earth, v. 95, no. B3, p. 2753-2761.

Jackson,J., and Molnar, P., 1990, Active faulting and block rotations in the western Transverse

Ranges, California:Journal of Geophysical Research: Solid Earth (1978–2012), 95(B13), p. 22073-22087

Jaffey, A.H., Flynn, K.F., Glendenin, L.E., Bentley, W.C., and Essling, A.M., 1971, Precision measurements of half-lives and specific activities of 235U and 238U: Physical Review C, v. 4., p. 1889-1906.

James, N. P., Narbonne, G. M., and Kyser, T. K., 2001, Late Neoproterozoic cap carbonates: Mackenzie Mountains, northwestern Canada: precipitation and global glacial meltdown: CanadianJournal of Earth Sciences, v. 38, no. 8, p. 1229-1262.

Jefferson, C.W. and Parrish, R.R., 1989, Late Proterozoic stratigraphy, U-Pb zircon ages, and rift tectonics, Mackenzie Mountains, northwestern Canada: Canadian Journal of Earth Sciences, v. 26, no. 9, p.1784-1801.

Jeletsky,J.A., 1962, Pre-Cretaceous Richardson Mountains Trough – its place in the tectonic framework of Arctic Canada and its bearing on some geosynclinals concepts: Transactions of the Royal Society of Canada, v. 56, no. 3, p. 55-84.

Jerram, D. and Petford, N., 2011, The field description of igneous rocks (Vol. 40): John Wiley and Sons

Jing, X.Q., Yang, Z., Tong, Y. and Han, Z., 2015. A revised paleomagnetic pole from the mid Neoproterozoic Liantuo Formation in the Yangtze block and its paleogeographic implications. Precambrian Research, 268, pp.194-211.

Johnson, C.L. and Constable, C.G., 1995, The time-averaged geomagnetic field as recorded by lava flows over the past 5 Myr: GeophysicalJournal International, v. 122, no. 2, p. 489-519.

Johnston, S.T., 2008, The Cordilleran Ribbon Continent of North America: Annual Review of Earth and Planetary Sciences, v. 36, p. 495-530.

Jones, C., 2002, User-driven integrated software lives: "PaleoMag" paleomagnetics analysis on the Macintosh: Computers and Geosciences, v. 28, no. 10, p. 1145-1151, http://dx.doi.org/10.1016/S0098-3004(02)00032-8

Karlstrom, K.E., Bowring, S.A., Dehler, C.M., Knoll, A.H., Porter, S.M., Des Marais, D.J., Weil, A.B., Sharp, Z.D., Geissman, J.W., Elrick, M.B. and Timmons, J.M., 2000. Chuar Group of the Grand Canyon: Record of breakup of Rodinia, associated change in the global carbon cycle, and ecosystem expansion by 740 Ma. Geology, 28(7), pp.619-622.

Karlstrom, K.E., Williams, M.L., McLelland, J., Geissman, J.W. and Ahall, K.I., 1999. Refining Rodinia: geologic evidence for the Australia-Western US connection in the Proterozoic. publisher not identified.

Karlstrom, K.E. and Humphreys, E.D., 1998, Persistent influence of Proterozoic accretionary boundaries in the tectonic evolution of southwestern North America. Rocky Mountain Geology, v. 33 no. 2, p.161-179.

Kean, W.F., Williams, I., Chan, L., Feeney, J., 1997. Magnetism of the Keweenawan age Chengwatana lava flows, northwest Wisconsin. Geophysical Research Letters 24, 1523–1526.

Keeley, J.A., Link, P.K., Fanning, C.M. and Schmitz, M.D., 2012, Pre-to synglacial rift-related volcanism in the Neoproterozoic (Cryogenian) Pocatello Formation, SE Idaho: New SHRIMP and CA-ID-TIMS constraints: Lithosphere, p.L226-1.

Kendall, B.S., Creaser, R.A., Ross, G.M., and Selby, D., 2004, Constraints on the timing of Marinoan -Snowball Earth- glaciation by 187Re-187Os dating of a Neoproterozoic, post-glacial black shale in western Canada: Earth and Planetary Science Letters, v. 222, p. 729-740

Kent, D. V., and W. K. Witte (1993), Slow apparent polar wander for North America in the Late Triassic and large Colorado Plateau rotation, Tectonics, 12, 291-300, doi:10.1029/92TC01966.

Kent, D.V. and Irving, E., 2010. Influence of inclination error in sedimentary rocks on the Triassic and Jurassic apparent pole wander path for North America and implications for Cordilleran tectonics. Journal of Geophysical Research: Solid Earth, 115(B10).

Kent, D.V. and Tauxe, L., 2005. Corrected Late Triassic latitudes for continents adjacent to the North Atlantic. Science, 307(5707), pp.240-244.

Key, R. M., Liyungu, A. K., Njamu, F. M., Somwe, V., Banda, J., Mosley, P. N., and Armstrong, R. A., 2001, The western arm of the Lufilian Arc in Zambia and its potential for copper mineralisation: Journal of African Earth Sciences, v. 33, p. 503–528, doi:10.1016/S0899-5362(01)00098-7.

Kirschvink, J. L., 1980, The least-squares line and plane and the analysis of paleomagnetic data: Geophysical Journal of the Royal Astronomical Society, v. 62, no. 3, p. 699 –718

Kirschvink, J. L., 1992, Late Proterozoic low-latitude global glaciation: the Snowball Earth, in Schopf, J. W., and Klein, C., eds., The Proterozoic Biosphere: Cambridge, Cambridge University Press, p. 51-52.

Kirschvink, J. L., Ripperdan, R. L., and Evans, D. A., 1997, Evidence for a large-scale reorganization

of Early Cambrian continental masses by inertial interchange true polar wander: Science, v. 277, n. 5325, p. 541-545.

Kirschvink, J.L., Kopp, R.E., Raub, T.D., Baumgartner, C.T., and Holt, J.W., 2008, Rapid, precise, and high-sensitivity acquisition of paleomagnetic and rock-magnetic data: Development of a low-noise automatic sample changing system for superconducting rock magnetometers: Geochemistry, Geophysics, Geosystems, v. 9, Q05Y01, doi: 10.1029/2007GC001856.

Kirschvink,J. L., 1992, Late Proterozoic low-latitude global glaciation: the snowball earth, in Schopf,J. W., and Klein, C., eds., The Proterozoic Biosphere: Cambridge, Cambridge University Press, p. 51-52.

Klein, C. and Beukes, N.J., 1993, Sedimentology and geochemistry of the glaciogenic late Proterozoic Rapitan iron-formation in Canada: Economic Geology, v. 88, no. 3, p.542-565.

Kodama, K.P. and Dekkers, M.J., 2004. Magnetic anisotropy as an aid to identifying CRM and DRM in red sedimentary rocks. Studia Geophysica et Geodaetica, 48(4), pp.747-766.

Kruiver, P. P., Dekkers, M. J., and Heslop, D. 2001, Quantification of magnetic coercivity components by the analysis of acquisition curves of isothermal remanent magnetization: Earth and Planetary Science Letters, v. 189, no. 3, p. 269-276.

Lane,L.S., 1997, Canada Basin, Arctic Ocean: evidence against a rotational origin: Tectonics, v. 16, no. 3, p. 363-387.

Le Heron, D.P., Cox, G., Trundley, A., Collins, A.S., 2011, Two Cryogenian glacial successions compared: aspects of the Sturt and Elatina sediment record of South Australia: Precambrian Research, v. 186, p.147-168.

Le Hir, G., Donnadieu, Y., Goddéris, Y., Pierrehumbert, R.T., Halverson, G.P., Macouin, M., Nédélec, A. and Ramstein, G., 2009, The snowball Earth aftermath: Exploring the limits of continental weathering processes: Earth and Planetary Science Letters, v. 277, no. 3, p.453-463.

Le Hir, G., Goddéris, Y., Donnadieu, Y. and Ramstein, G., 2008, A geochemical modelling study of the evolution of the chemical composition of seawater linked to a" snowball" glaciation: Biogeosciences, v. 5, no. 1, p.253-267.

LeCheminant, A. N., and Heaman, L. M., 1989, Mackenzie igneous events, Canada: Middle Proterozoic hotspot magmatism associated with ocean opening: Earth and Planetary Science Letters, v. 96, no. 1, p. 38-48.

Lescinsky, D.T. and Sisson, T.W., 1998, Ridge-forming, ice-bounded lava flows at Mount Rainier, Washington: Geology, v. 26, no. 4, p.351-354.

Li, Z. X., Evans, D. A. D., and Zhang, S., 2004, A 90 spin on Rodinia: possible causalLinks between the Neoproterozoic supercontinent, superplume, true polar wander andLow-latitude glaciation: Earth and Planetary ScienceLetters, v. 220, no. 3, p. 409-421.

Li, Z.X. and Evans, D.A., 2011, Late Neoproterozoic 40 intraplate rotation within Australia allows for a tighter-fitting and longer-lasting Rodinia. Geology, v. 39, no. 1, p.39-42.

Li, Z. X., Evans, D. A., and Halverson, G. P., 2013, Neoproterozoic glaciations in a revised global palaeogeography from the breakup of Rodinia to the assembly of Gondwanaland: Sedimentary Geology, v. 294, p. 219-232.

Li, Z.-X., Bogdanova, S.V., Collins, A.S., Davidson, A., De Waele, B., Ernst, R.E., Fitzsimmons, I.C.W., Fuck, R.A., Gladkochub, D.P., Jacobs, J., Karlstrom, K.E., Lu, S., Natapov, L.M., Pease, V., Pisarevsky, S.A., Thrane, K., Vernikovsky, V., 2008, Assembly, configuration, and break-up history of Rodinia: A synthesis: Precambrian Research, v. 160, no. 1-2, p. 179-210, doi: 10.1016/j.precamres.2007.04.021.

Li, Z.X., Zhang, L. and Powell, C.M., 1996. Positions of the East Asian cratons in the Neoproterozoic supercontinent Rodinia. Australian Journal of Earth Sciences, 43(6), pp.593-604.

Lin, J.L., 1984. The Apparent Polar Wander paths for the North and South China Blocks. Ph.D. thesis, University of Calfifornes Santa Barbara, 248 pp.

Link, P., Christie-Blick, N., Devlin, W., Elston, D., Horodyski, R., Levy, M., Miller, J., Pearson, R., Prave, A., and Stewart, J., 1993, Middle and Late Proterozoic stratified rocks of the western U.S. Cordillera, Colorado Plateau, and Basin and Range Province: Boulder, Colorado, The Geological Society of America, The Geology of North America, v. 2, p. 463-595.

Link, P.K., Miller, J.M.G., and Christie-Blick, N., 1994, Glacial-marine facies in a continental rift environment: Neoproterozoic rocks of the western United States Cordillera, in Deynoux, M., and others, eds., International Geological Correlation Project 260: Earth‘s Glacial Record: Cambridge, UK, Cambridge University Press, p. 29-59.

Lister, G.S., Etheridge, M.A. and Symonds, P.A., 1986, Detachment faulting and the evolution of passive continental margins: Geology, v. 14, no. 3, p.246-250.

Loewy, S.L., Connelly, J.N., Dalziel, I.W. and Gower, C.F., 2003, Eastern Laurentia in Rodinia: constraints from whole-rock Pb and U/Pb geochronology. Tectonophysics, v. 375, no. 1, p.169-197.

Lønne, I., 1995, Sedimentary facies and depositional architecture of ice-contact glaciomarine systems: Sedimentary Geology, v. 98, no. 1, p.13-43.

Lund, K., 2008, Geometry of the Neoproterozoic and Paleozoic rift margin of western Laurentia: implications for mineral deposit settings: Geosphere, v. 4, no. 2, p. 429-444.

Lund, K., Aleinikoff, J., Evans, K., and Fanning, C., 2003, SHRIMP U-Pb geochronology of Neoproterozoic Windermere Supergroup, central Idaho: Implications for rifting of western Laurentia and synchroneity of Sturtian glacial deposits: Geological Society of America Bulletin, v. 115, no. 3, p. 349-372.

Lund, K., Aleinikoff, J., Evans, K., Dewitt, E., Unruh, D., 2010, SHRIMP U–Pb dating of recurrent Cryogenian and Late Cambrian–Early Ordovician alkalic Magmatism in central Idaho: Implications for Rodinian rift tectonics: Geological Society of America Bulletin, v. 122, p.430–453.

Macdonald, F. A., Strauss, J. V., Sperling, E. A., Halverson, G. P., Narbonne, G. M., Johnston, D. T., Kunzmann, M., Schrag, D. P., and Higgins, J. A., 2013b, The stratigraphic relationship between the Shuram carbon isotope excursion, the oxygenation of Neoproterozoic oceans, and the first appearance of the Ediacara biota and bilaterian trace fossils in northwestern Canada: Chemical Geology, v. 362, p. 250-272.

Macdonald, F.A. and Cohen, P.A., 2011, The Tatonduk inlier, Alaska-Yukon border: Geological Society, London, Memoirs, v. 36, no. 1, p.389-396.

Macdonald, F.A., Halverson, G.P., Strauss, J.V., Smith, E.F., Cox, G.M., Sperling, E.A., and Roots, C.F., 2012, Early Neoproterozoic basin formation in Yukon, Canada: Implications for theMake-up and break-up of Rodinia: Geoscience Canada, v. 39, p. 77-99.

Macdonald, F.A., Prave, A.R., Petterson, R., Smith, E.F., Pruss, S.B., Oates, K., Waechter, F., Trotzuk, D. and Fallick, A.E., 2013a, The Laurentian record of Neoproterozoic glaciation, tectonism, and eukaryotic evolution in Death Valley, California: Geological Society of America Bulletin, v. 125, no. 7-8, p.1203-1223.

Macdonald, F.A., Schmitz, M.D., Crowley, J.L., Roots, C.F., Jones, D.S., Maloof, A.C., Strauss, J.V., Cohen, P.A., Johnston, D.T., and Schrag, D.P., 2010a, Calibrating the Cryogenian: Science, v. 327, no. 5970, p. 1241-1243, doi: 10.1126/science.1183325.

Macdonald, F.A., Smith, E.F., Strauss, J.V., Cox, G.M, Halverson, G.P. and Roots, C.F., 2011, Neoproterozoic and early Paleozoic correlations in the western Ogilvie Mountains, Yukon, in MacFarlane, K.E., Weston, L.H., and Relf C., editors, Yukon Exploration and Geology 2010: Yukon Geological Survey, p. 161-182

Macdonald, F.A., Strauss, J.V., Rose, C.V., Dudás, F.. and Schrag, D.P., 2010b, Stratigraphy of the Port Nolloth Group of Namibia and South Africa and implications for the age of Neoproterozoic iron formations: American Journal of Science, v. 310, no.9, p.862-888.

MacNaughton, R. B., Narbonne, G.M., and Dalrymple, R. W., 2000, Neoproterozoic slope deposits,MackenzieMountains, northwestern Canada: implications for passive-margin development and Ediacaran faunal ecology: Canadian Journal of Earth Sciences, v. 37, no. 7, p. 997-1020.

MacNaughton, R. B., Roots, C. F., andMartel, E., 2008, Neoproterozoic-(?) Cambrian lithostratigraphy, northeast Sekwi Mountain Map area, Mackenzie Mountains, Northwest Territories: new data from Measured sections: Geological Survey of Canada, Current Research (Online) no. 2008-16, 17 p.

Mair, J. L., Hart, C. J., and Stephens, J. R., 2006, Deformation history of the northwestern Selwyn Basin, Yukon, Canada: Implications for orogen evolution and Mid-Cretaceous Magmatism: Geological Society of America Bulletin, v. 118 no. 3-4, p. 304-323.

Maloof, A. C., Halverson, G. P., Kirschvink, J. L., Schrag, D. P., Weiss, B. P., and Hoffman, P. F., 2006, Combined paleomagnetic, isotopic, and stratigraphic evidence for true polar wander from the Neoproterozoic Akademikerbreen Group, Svalbard, Norway: Geological Society of America Bulletin, v. 118 no. 9-10, p. 1099-1124.

Marshak, S. and Paulsen, T., 1996, Midcontinent US fault and fold zones: A legacy of Proterozoic intracratonic extensional tectonism?. Geology, v. 24, no. 2, p.151-154.

Marshak, S., Domrois, S., Abert, C., Larson, T., Pavlis, G., Hamburger, M., Yang, X., Gilbert, H. and Chen, C., 2017, The basement revealed: Tectonic insight from a digital elevation model of the Great Unconformity, USA cratonic platform. Geology, v. 45, no. 5, p.391-394.

Marshak, S., Karlstrom, K. and Timmons, J.M., 2000, Inversion of Proterozoic extensional faults: An explanation for the pattern of Laramide and Ancestral Rockies intracratonic deformation, United States. Geology, v. 28, no. 8, p.735-738.

Martel, E., Turner, E. C., and Fischer, B. J., 2011, Geology of the centralMackenzieMountains of the northern Canadian Cordillera, Sewki Mountain (105P),Mount Eduni (106A), and northwestern Wrigley Lake (95M)Map-areas, Northwest Territories, NWT Special Volume, Volume 1: Yellowknife, CA, NWT Geoscience Office, p. 423.

Mathews W.H., 1947, Tuyas, flat-topped volcanoes in northern British Columbia: American Journal of Science, v. 245, no. 9, p. 560-570.

Mattinson, J.M., 2005, Zircon U-Pb chemical abrasion ("CA-TIMS") method: combined annealing and multi-step partial dissolution analysis for improved precision and accuracy of zircon ages: Chemical Geology, v. 220, no. 1, p. 47-66.

Maurin, J.C. and Guiraud, R., 1990, Relationships between tectonics and sedimentation in the Barremo-Aptian intracontinental basins of Northern Cameroon, In: C.A. Kogbe and J. Lang (Editors), African Continental Phanerozoic Sediments: Journal of African Earth Sciences, v. 10, p. 331-340.

McDonough, M.R. and Parrish, R.R., 1991, Proterozoic gneisses of the Malton Complex, near Valemount, British Columbia: U-Pb ages and Nd isotopic signatures: Canadian Journal of Earth Sciences, v. 28, no. 8, p.1202-1216.

McDonough, W.F., Sun S.S., 1995, The composition of the Earth: Chemical Geology, v. 12, p. 223-253.

Mbede, E. I., Kampunzu, A. B. and Armstrong R. A. 2004, Neoproterozoic inheritance during Cenozoic rifting in the western and southwestern branches of the East African rift system: evidence from carbonatite and alkaline intrusions. Conference abstract, The East African Rift System: Development, Evolution and Resources, Addis Ababa, Ethiopia, June 20 - 24, 2004.

McElhinny,M.W. andMcFadden, P.L., 1997, Palaeosecular variation over the past 5 Myr based on a new generalized database: Geophysical Journal International, v. 131, no. 2, p.240-252.

McElhinny,M.W. andMerrill, R.T., 1975, Geomagnetic secular variation over the past 5 My: Reviews of Geophysics, v. 13 no. 5, p. 687-708.

McFadden, P.L. and McElhinny, M.W., 1990, Classification of the reversal test in palaeomagnetism: Geophysical Journal International, v. 103, no. 3, p. 725-729.

McLaren, A.C., Gerald, J.F. and Williams, I.S., 1994. The microstructure of zircon and its influence on the age determination from Pb/U isotopic ratios measured by ion microprobe. Geochimica et Cosmochimica Acta, 58(2), pp.993-1005.

McLean, N.M., Condon, D.J., Schoene, B., Bowring, S.A., 2015, Evaluating uncertainties in the calibration of isotopic reference materials and multi-element isotopic tracers (EARTHTIME Tracer Calibration Part II): Geochimica et Cosmochimica Acta, no. 164, p. 481-501. doi:10.1016/j.gca.2015.02.040.

McMechan, M.E., 1990, Upper Proterozoic to Middle Cambrian history of the Peace River Arch: evidence from the Rocky Mountains. Bulletin of Canadian Petroleum Geology, 38(1), p.36-44.

McMechan, M.E., 2000, Vreeland Diamictites-Neoproterozoic glaciogenic slope deposits, Rocky Mountains, northeast British Columbia: Bulletin of Canadian Petroleum Geology, v. 48, no. 3, p.246-261.

McMechan,M.E., Thompson, R.I., Cook, D.G., Gabrielse, H. and Yorath, C.J., 1992, Structural Styles: Foreland Belt: In: Geology of the Cordilleran Orogen in Canada, H. Gabrielse and C.J. Yorath (eds.), Geological Survey of Canada, Geology of Canada, no. 4, p. 634-650.

Meert, J.G., van der Voo, R. and Ayub, S., 1995, Paleomagnetic investigation of the Neoproterozoic Gagwe lavas and Mbozi complex, Tanzania and the assembly of Gondwana. Precambrian Research, v. 74, no. 4, p.225-244.

Meert, J.G. and Torsvik, T.H., 2003, The making and unmaking of a supercontinent: Rodinia revisited: Tectonophysics, v. 375, no. 1, p.261-288.

Meert, J.G., Pandit, M., Kamenov, G.D., 2013, Further geochronological and paleomagnetic constraints on Malani (and pre-Malani) magmatism in NW India. Tectonophysics v. 608, p. 1254-1267.
Merdith, A.S., Collins, A.S., Williams, S.E., Pisarevsky, S., Foden, J.F., Archibald, D., Blades, M.L., Alessio, B.L., Armistead, S., Plavsa, D. and Clark, C., 2017, A full-plate global reconstruction of the Neoproterozoic. Gondwana Research.

Miller, E.L., Soloviev, A., Kuzmichev, A., Gehrels, G., Toro, J. and Tuchkova,M., 2008, Jurassic and Cretaceous foreland basin deposits of the Russian Arctic: Separated by birth of theMakarov Basin?: Norwegian Journal of Geology, v. 88, p. 201-226.

Miller, F.K., 1994, The Windermere Group and late Proterozoic tectonics in northeastern Washington and northern Idaho, Regional geology of Washington: Washington Division of Geology and Earth Resources Bulletin, v. 80, p.1-19.

Miller, J. D., and Kent, D. V., 1988, Regional trends in the timing of Alleghanian remagnetization in the Appalachians: Geology, v. 16, no. 7, p. 588-591.

Miller, J.M., 1985, Glacial and syntectonic sedimentation: The upper Proterozoic Kingston Peak Formation, southern Panamint Range, eastern California: Geological Society of America Bulletin, v. 96, no. 12, p. 1537-1553.

Milton, J.E., Hickey, K.A., Gleeson, S.A. and Friedman, R.M., 2017. New U-Pb constraints on the age of the Little Dal Basalts and Gunbarrel-related volcanism in Rodinia. Precambrian Research.

Mitchell, R. N., Kilian, T.M., Raub, T. D., Evans, D. A., Bleeker, W., and Maloof, A. C., 2011, Sutton hotspot: Resolving Ediacaran-Cambrian Tectonics and true polar wander for Laurentia: Ameri-

can Journal of Science, v. 311, no. 8, p. 651-663.

Molina-Garza, R. S., J. W. Geissman, and R. Van der Voo (1995), Paleomagnetism of the Dockum Group (Upper Triassic), northwest Texas: Further evidence for the J1-cusp in the North America apparent polar wander path and implications for rate of Triassic apparent polar wander and Colorado plateau rotation, Tectonics, 14, 979 - 993, doi:10.1029/ 95TC01456.

Moores, E.M., 1991, Southwest US-East Antarctic (SWEAT) connection: a hypothesis: Geology, v. 19, no. 5, p. 425-428.

Morris, G.A., Larson, P.B. And Hooper, P.R., 2000, 'Subduction Style'Magmatism in a Non-subduction Setting: the Colville Igneous Complex, NE Washington State, USA: Journal of Petrology, v. 41, no. 1, p.43-67.

Morris, W. A., 1977, Paleolatitude of glaciogenic upper Precambrian Rapitan Group and the use of tillites as chronostratigraphicMarker horizons: Geology, v. 5, no. 2, p. 85-88.

Morrow, D. W., Cumming, G. L., and Aulstead, K. L., 1990, The Gas-Bearing Devonian Manetoe Facies, Yukon And Northwest Territories: Geological Survey of Canada, Bulletin 400, 54 p.

Morrow, D.W., 1999, Lower Paleozoic stratigraphy of northern Yukon Territory and northwestern District ofMackenzie: Geological Survey of Canada, Bulletin 538, 202 p.

Moynihan, D., 2014, Bedrock Geology of NTS 106B/04, Eastern Rackla Belt. *In:* Yukon Exploration and Geology 2013, K.E.MacFarlane,M.G. Nordling, and P.J. Sack (eds.), Yukon Geological Survey, p. 147-167.

Mukherjee, A., 1966, Tectonics of Late Precambrian ignimbrites in western Rajasthan n. India discussion. Geologie en Mijnbouw v. 45, p. 193–196.

Murphy, D.C., 1997, Geology of the McQuesten River region, northern McQuesten and Mayo Map areas, Yukon Territory (115P/14, 15, 16; 105M/13, 14): Exploration and Geological Services Division, Yukon Region, Indian and Northern Affairs Canada, Bulletin 6, 122 p.

Murphy, J.B., Nance, R.D. and Cawood, P.A., 2009. Contrasting modes of supercontinent formation and the conundrum of Pangea. Gondwana Research, 15(3), pp.408-420.

Mustard, P.S., 1991, Normal faulting and alluvial fan deposition, basal Windermere Tectonic Assemblage, Yukon, Canada: Geological Society of America Bulletin, v. 103, no. 10, p. 1346–1364.

Mustard, P.S., and Roots, C.F., 1997, Rift-related volcanism, sedimentation, and tectonic setting

of theMount Harper Group, Ogilvie Mountains, Yukon Territory: Geological Survey of Canada, Bulletin 492, 92 p.

Nance, R.D., Murphy, J.B. and Santosh, M., 2014. The supercontinent cycle: a retrospective essay. Gondwana Research, 25(1), pp.4-29.

Narbonne, G.M., 1994,New Ediacaran Fossils from the Mackenzie Mountains,Northwestern Canada: Journal of Paleontology, v. 68,No. 3, p. 411–416.

Narbonne, G.M., and Aitken, J.D., 1990, Ediacaran fossils from the Sekwi Brook area, Mackenzie Mountains,Northwest Canada: Palaentology, v. 33 ,No. 4, 945–980.

Narbonne, G.M., Gehling, J.G., 2003, Life after snowball: the oldest complex Ediacaran fossils: Geology, v. 31,N. 1, p. 27–30.

Narbonne, G.M., Xiao, S., Shields-Zhou, G., 2012, Ediacaran period. In: Gradstein, F., Ogg, J., Schmitz, M.D., G., O. (Eds.), Geologic Timescale 2012. Elsevier, Oxford, p. 427–449.

Nasdala, L., Lengauer, C.L., Hanchar, J.M., Kronz, A., Wirth, R., Blanc, P., Kennedy, A.K., Seydoux-Guillaume, A.M., 2002, Annealing radiation damage and the recovery of cathodoluminescence: Chemical Geology, v. 191, p. 121-140.

Norris, D. K., 1985, Eastern Cordilleran foldbelt of Northern Canada: its structural geometry and hydrocarbon potential: AAPG Bulletin, v. 69,No. 5, p. 788-808.

Norris, D.K., 1972, En echelon folding in theNorthern Cordillera of Canada: Bulletin of Canadian Petroleum Geology, v. 20,No. 3, p. 634-642

Norris, D.K., 1997, Geological setting. *In* The geology, mineral and hydrocarbon potential ofNorthern Yukon Territory andNorthwestern District of Mackenzie. Edited by D.K.Norris: Geological Survey of Canada, Bulletin 422, Chap. 3, p. 21–64.

Norris, D.K., and Dyke, L.D., 1997, Proterozoic. In The geology, mineral and hydrocarbon potential ofNorthern Yukon Territory andNorthwestern District of Mackenzie. Edited by D.K.Norris: Geological Survey of Canada, Bulletin 422, Chap. 4, p. 65–84.

O'Reilly, W., 1984, Rock and Mineral Magnetism: Glasgow, Blackie & Son Limited, 220p.

Ojakangas, R.W., Morey, G.B. and Green, J.C., 2001. The Mesoproterozoic midcontinent rift system, Lake Superior region, USA. Sedimentary Geology, 141, pp.421-442.

Ootes, L., Gleeson, S. A., Turner, E., Rasmussen, K., Gordey, S., Falck, H., and Pierce, K., 2013, Metallogenic Evolution of the Mackenzie and Eastern Selwyn Mountains of Canada's Northern Cordillera, Northwest Territories: A Compilation and Review: Geoscience Canada, v. 40, no. 1, p. 40-69

Palmer, H. 1970, Paleomagnetism and correlation of some Middle Keweenawan rocks, Lake Superior. Canadian Journal of Earth Science 7, 1410–1436

Palmer, H. C., and Hayatsu, A., 1975, Paleomagnetism and K-Ar dating of some Franklin lavas and diabases, Victoria Island: Canadian Journal of Earth Sciences, v. 12, no. 8, p. 1439-1447.

Palmer, H. C., Baragar, W. R. A., Fortier, M., and Foster, J. H., 1983, Paleomagnetism of Late Proterozoic rocks, Victoria Island, Northwest Territories, Canada: Canadian Journal of Earth Sciences, v. 20, no. 9, p. 1456-1469.

Park, J. C. Roots, and Brunet, N.,1992,Paleomagnetic evidence for rotation in the Neoproterozoic Mount Harper Volcanic Complex, Ogilvie Mountains, Yukon territory, Current Research,Part E: Geological Survey of Canada,Paper 92-1E,P. 1-10.

Park, J. K. Paleomagnetism of miscellaneous Franklin and Mackenzie diabases of the Canadian Shield and their adjacent country rocks, Can. J. Earth Sci. 11, 1012-1017, 1974.

Park, J. K., 1981, Paleomagnetism of basic intrusions from the Brock inlier, Northwest Territories, Canada: Canadian Journal of Earth Sciences, v. 18, no. 10, p. 1637-1641.

Park, J. K., 1997,Paleomagnetic evidence for low-latitude glaciation during deposition of the Neoproterozoic Rapitan Group, Mackenzie mountains, N.W.T., Canada: Canadian Journal of Earth Sciences, v. 34, no. 1,P. 34-49

Park, J.K. and Aitken, J.D., 1986. Journal of Geophysical Research: Solid Earth, 91(B5), pp.4955-4970.

Park, J.K. and Jefferson, C.W., 1991. Precambrian Research, 52(1), pp.1-35.

Park, J.K., 1995,Paleomagnetism of the late Neoproterozoic Blueflower and Risky formations of the northern Cordillera, Canada: Canadian Journal of Earth Sciences, v. 32,P. 718-729.

Park, K., K.L. Buchan and S.S. Gandhi, Paleomagnetism of 780 Ma Hottah gabbro sheets of the Wopmay Orogen, Northwest Territories, Canada, Cmr. Res., Geol. Surv. Can. Pap. 1995C, 195-200, 1995.

Passchier, S. and Erukanure, E., 2010, Palaeoenvironments and weathering regime of the Neoproterozoic Squantum "Tillite", Boston Basin: no evidence of a snowball Earth: Sedimentology, v. 57, no. 6, p.1526-1544.

Passchier, S., O'Brien, P.E., Damuth, J.E., Januszczack, N., Handwerger, D.A. and Whitehead, J.M., 2003, Pliocene- Pleistocene glaciomarine sedimentation in eastern Prydz Bay and development of the Prydz trough-mouth fan, ODP Sites 1166 and 1167, East Antarctica: Marine Geology, v. 199, p.179-305.

Pehrsson, S. J., and Buchan, K. L., 1999, Borden dykes of Baffin Island, Northwest Territories: a Franklin U-Pb baddeleyite age and a paleomagnetic reinterpretation: Canadian Journal of Earth Sciences, v. 36, no. 1, p. 65-73

Pigage, L.C. and MacNaughton, R.B., 2004. Reconnaissance geology of northern Toobally Lake (95D/8), southeast Yukon. In: Yukon Exploration and Geology 2003, D.S. Emond and L.L. Lewis (eds.), Yukon Geological Survey, p. 199-219.

Pigage, L.C. and Mortensen, J.K., 2004, Superimposed Neoproterozoic and early Tertiary alkaline magmatism in the La Biche River area, southeast Yukon Territory: Bulletin of Canadian Petroleum Geology, v. 52, no. 4, p.325-342.

Pigage, L.C., 2006, Stratigraphy summary for southeast Yukon (95D/8 and 95C/5). In: Yukon Exploration and Geology 2005, D.S. Emond, G.D. Bradshaw, L.L. Lewis and L.H. Weston (eds.), Yukon Geological Survey, p. 267-285.

Pigage, L.C., 2009, Bedrock geology of NTS 95C/5 (Pool Creek) and NTS 95D/8 map sheets, southeast Yukon: Yukon Geological Survey Bulletin 16, 1-150.

Pilkington, M., and Saltus, R. W., 2009, The Mackenzie River magnetic anomaly, Yukon and Northwest Territories, Canada—Evidence for Early Proterozoic magmatic arc crust at the edge of the North American craton: Tectonophysics, v. 478, no. 1,P. 78-86.

Pisarevsky, S. A., Elming, S.-Å., Pesonen, L. J.and Li, Z.-X. Mesoproterozoic paleogeography: supercontinent and beyond. Precambr. Res. 244, 207-225 (2014).

Pisarevsky, S. A., Natapov, L. M., Donskaya, T. V., Gladkochub, D. P.and Vernikovsky, V. A. Proterozoic Siberia: a promontory of Rodinia. Precambr. Res. 160, 66-76 (2008).

Pisarevsky, S. A., Wingate, M. T., Powell, C. M., Johnson, S., and Evans, D. A., 2003, Models of Rodinia assembly and fragmentation: Geological Society, London, Special Publications, v. 206, no. 1, p. 35-55.

Pisarevsky, S. A., Wingate, M. T.,Powell, C. M., Johnson, S., and Evans, D. A., 2003, Models of Rodinia assembly and fragmentation: Geological Society, London, SpecialPublications, v. 206, no. 1,P. 35-55.

Pisarevsky, S.A., Gladkochub, D.P., Konstantinov, K.M., Mazukabzov, A.M., Stanevich, A.M., Murphy, J.B., Tait, J.A., Donskaya, T.V. and Konstantinov, I.K., 2013,Paleomagnetism of Cryogenian Kitoi mafic dykes in South Siberia: implications for Neoproterozoic Paleogeography:Precambrian Research, v. 231,P. 372-382.

Pisarevsky, S.A., Wingate, M.T.D., Stevens, M.K. and Haines, P.W., 2007. Palaeomagnetic results from the Lancer 1 stratigraphic drillhole, Officer Basin, Western Australia, and implications for Rodinia reconstructions. Australian Journal of Earth Sciences, 54(4), pp.561-572.

Plummer, P.S. and Belle, E.R., 1995, Mesozoic tectono-stratigraphic evolution of the Seychelles microcontinent. Sedimentary Geology, v. 96 no.1-2, p.73-91.

Polyakov, G. V. et al. Ultramafic-mafic igneous complexes of the Precambrian East Siberian metallogenic province (southern framing of the Siberian craton): age, composition, origin, and ore potential. Russ. Geol. Geophys. 54, 1319-1331 (2013).

Porter, S. M. and Knoll, A. H., 2000, Testate amoebae in the Neoproterozoic Era: evidence from vase-shaped microfossils in the Chuar Group, Grand Canyon: Paleobiology, v. 26, p. 360-385.

Porter, S.M., Meisterfeld, R. and Knoll, A.H., 2003. Vase-shaped microfossils from the Neoproterozoic Chuar Group, Grand Canyon: a classification guided by modern testate amoebae. Journal of Paleontology, 77(3), pp.409-429.

Postma, G., Nemec, W. and Kleinspehn, K., 1988, Large floating clasts in turbidites: a mechanism for their emplacement: Sedimentary Geology, v. 58, p. 47-61.

Powell, C.McA., Li, Z.X., McElhinny, M.W., Meert, J.G., Park, J.K., 1993. Paleomagnetic constraints on timing of the Neoproterozoic breakup of Rodinia and the Cambrian formation of Gondwana. Geology 21, 889-892.

Powell, C.McA., Preiss, W.V., Gatehouse, C.G., Krapez, B., Li, Z.X., 1994. South Australian record of a Rodinian epicontinental basin and its mid-Neoproterozoic breakup (700 Ma) to form the palaeo-Pacific Ocean. Tectonophy- sics 237, 113-140.

Prave, A.R., 1999, Two diamictites, two cap carbonates, two δ 13C excursions, two rifts: the Neoproterozoic KingstonPeak Formation, Death Valley, California: Geology, v. 27, no. 4,P. 339-342.

Prave, A.R., Condon, D.J., Hoffmann, K.H., Tapster, S. and Fallick, A.E., 2016, Duration and nature of the end-Cryogenian (Marinoan) glaciation: Geology, v. 44, no.8, p.631-634.

Preeden, U., Mertanen, S., Elminen, T., and Plado, J., 2009, Secondary magnetizations in shear and fault zones in southern Finland: Tectonophysics, v. 479, no. 3,P. 203-213.

Preiss, W.V. and Cowley, W.M., 1999. Genetic stratigraphy and revised lithostratigraphic classification of the Burra Group in the Adelaide Geosyncline: MESA Journal, v. 14.

Pugh, D.C., 1983,Pre-Mesozoic geology in the subsurface ofPeel River map area, Yukon Territory and District of Mackenzie: Geological Survey of Canada, Memoir 401, 61P.

Pullaiah, G., Irving, E., Buchan, K. L., and Dunlop, D. J., 1975, Magnetization changes caused by burial and uplift: Earth andPlanetary Science Letters, v. 28, no. 2,P. 133-143.

Pyle, L. J., Narbonne, G. M., James, N.P., Dalrymple, R. W., and Kaufman, A. J., 2004, Integrated Ediacaran chronostratigraphy, Wernecke Mountains, northwestern Canada:Precambrian Research, v. 132, no. 1,P. 1-27.

Rainbird, R. H. et al. U-Pb geochronology of Riphean sandstone and gabbro from southeastern Siberia and its bearing on the Laurentia-Siberia connection. Earth Planet. Sci. Lett. 164, 409-420 (1998).

Rainbird, R.H., Cawood, P., Gehrels, G., 2012, The great Grenvillian sedimentation episode: record of supercontinent Rodinia's assembly. In: Busby, C., Azor, A. (Eds.), Tectonics of Sedimentary Basins: Recent Advances. Wiley, Ch, p. 29.

Rainbird,R.H., 1993, The sedimentaryRecord of mantlePlume uplift Preceeding eruption of the Neoproterozoic Natkusiak flood basalt: Journal of Geology, v. 101,P. 305–318.

Robertson, W. A., and Baragar, W. R. A., 1972, The petrology and paleomagnetism of the Coronation sills: Canadian Journal of Earth Sciences, v. 9, no. 2, p. 123-140.

Robertson, W. A., and Baragar, W.R. A., 1972, The petrology and paleomagnetism of the Coronation sills: Canadian Journal of Earth Sciences, v. 9, no. 2, p. 123-140.

Robyn, T.L., 1979, Miocene volcanism in eastern Oregon: An example of calc-alkaline volcanism unrelated to subduction: Journal of Volcanology and GeothermalResearch, v. 5, p. 149–161.

Roest, W. R.,and Srivastava, S. P. (1989). Sea-floor spreading in the Labrador Sea: a new reconstruction. Geology, 17(11), 1000-1003.

Rohr, K. M., Lane, L. S., and MacLean, B. C., 2011, Subsurface compressional structures and facies transitions imaged by seismicReflection data, eastern margin ofRichardson Trough, Peel Plateau, Yukon: Bulletin of Canadian Petroleum Geology, v. 59, no. 2, p. 131-146.

Rooney, A. D., Macdonald, F. A., Strauss, J. V., Dudás, F. Ö., Hallmann, C., and Selby, D., 2014,Re-Os geochronology and coupled Os-Sr isotope constraints on the Sturtian snowball Earth: Proceedings of the National Academy of Sciences, v. 111, no. 1, p. 51-56.

Rooney, A.D., Strauss, J.V., Brandon, A.D., and Macdonald, F.A., 2015, A Cryogenian chronology: Two long-lasting, synchronous Neoproterozoic glaciations: Geology, v. 43, no. 5, p. 459-462

Root, K. G., 1987, Geology of the Delphine Creek area, southeastern British Columbia: implications for the Proterozoic and Paleozoic development of the Cordilleran divergent margin [Ph.D. thesis]: University of Calgary, 446 p.

Roots, C.F., 1987,Regional tectonic setting and evolution of the Late Proterozoic Mount Harper volcanic complex, Ogilvie Mountains, Yukon, [Ph.D. thesis]: Carleton University, 180 p.

Ross, G.M., 1991, Tectonic setting of the Windermere Supergroup revisited: Geology, v. 19, no. 11, p.1125-1128.

Ross, G.M., Bloch, J.D., Krouse, H.R., 1995, Neoproterozoic strata of the southern Canadian Cordillera and the isotopic evolution of seawater sulfate: Precambrian Research, v. 78, p. 70-99.

Rowley, D. B.,and Lottes, A. L. (1988). Plate-kinematic reconstructions of the North Atlantic and Arctic: Late Jurassic to present. Tectonophysics, 155(1), 73-120.

Schlische, R.W., 1995, Geometry and origin of fault-related folds in extensional settings: AAPG bulletin, v. 79, no. 11, p.1661-1678.

Schlische, R.W., 2003, Progress in understanding the structural geology, basin evolution, and tectonic history of the eastern North American rift system: The Great Rift Valleys of Pangea in Eastern North America, v. 1, p. 21-64.

Schmidt, P.W. and Williams, G.E., 2013. Anisotropy of thermoremanent magnetisation of Cryogenian glaciogenic and Ediacaran red beds, South Australia: Neoproterozoic apparent or true polar wander?. Global and planetary change, 110, pp.289-301.

Schmidt, P.W., 2014. A review of Precambrian palaeomagnetism of Australia: Palaeogeography, supercontinents, glaciations and true polar wander. Gondwana Research, 25(3), pp.1164-1185.

Schmidt, Phillip W., George E. Williams, and Michael O. McWilliams. Palaeomagnetism and magnetic anisotropy of late Neoproterozoic strata, South Australia: Implications for the palaeolatitude of late Cryogenian glaciation, cap carbonate and the Ediacaran System. Precambrian Research 174, no. 1 (2009): 35-52.

Schmitz, M.D., Davydov, V.I., 2012, Quantitative radiometric and biostratigraphic calibration of the globalPennsylvanian - Early Permian time scale: Geological Society of America Bulletin, v. 124, no. 3-4, p. 549-577.

Schmitz, M.D.,Schoene, B., 2007, Derivation of isotope ratios, errors and error correlations for U-Pb geochronology using ^{205}Pb-^{235}U-(^{233}U)-spiked isotope dilution thermal ionization massSpectrometric data: Geochemistry, Geophysics, Geosystems 8, Q08006, doi:10.1029/2006GC00149.

Schoene, B., 2014, 4.10-U-Th-Pb Geochronology: Treatise on Geochemistry, Second Edition Elsevier, Oxford, p.341-378.

Schwab, D. L., Thorkelson, D. J., Mortensen, J. K., Creaser, R. A., and Abbott, J. G., 2004, The Bear River dykes (1265–1269 Ma): westward continuation of the Mackenzie dykeSwarm into Yukon, Canada: Precambrian Research, v. 133, no. 3, p. 175-186.

Sears, J. W., and Price, R. A., 1978, TheSiberian connection: a case for PrecambrianSeparation of the North American andSiberian cratons: Geology, v. 6, no. 5, p. 267-270.

Sears, J. W., and Price, R. A., 2003, Tightening the Siberian connection to western Laurentia: Geological Society of America Bulletin, v. 115, no. 8, p. 943-953.

Sears, J.W. and Price, R.A., 1978, The Siberian connection: a case for Precambrian separation of the North American and Siberian cratons: Geology, v. 6, no. 5, p.267-270.

Sears, J.W. and Price, R.A., 2003, Tightening the Siberian connection to western Laurentia: Geological Society of America Bulletin, v. 115, no. 8, p.943-953.

Sharp, I.R., Gawthorpe, R.L., Armstrong, B. and Underhill, J.R., 2000, Propagation history and passive rotation of mesoscale normal faults: implications for Synrift Stratigraphic development: Basin Research, v. 12, no. 3-4, p. 285-305.

Shephard, G.E., Müller, R.D. andSeton, M., 2013, The tectonic evolution of the ArcticSince Pangea breakup: Integrating constraints fromSurface geology and geophysics with mantleStructure: Earth-Science Reviews, v. 124, p.148-183.

Shipilov, E.V., 2008. Generations of spreading basins and stages of breakdown of Wegener's Pangea

in the geodynamic evolution of the Arctic Ocean. Geotectonics, 42(2), pp.105-124.

Skilling, I.P., 2009, Subglacial to emergent basaltic volcanism at Hlöðufell, south-west Iceland: a history of ice-confinement: Journal of Volcanology and Geothermal Research, v. 185, no. 4, p. 276-289.

Sklyarov, Eu V., D. P. Gladkochub, A. M. Mazukabzov, Yu V. Menshagin, T. Watanabe, and S. A. Pisarevsky. 2003, Neoproterozoic mafic dike swarms of the Sharyzhalgai metamorphic massif, southern Siberian craton." Precambrian Research, v. 122, no. 1, p. 359-376.

Slind, O.L. and Perkins, G.D. 1966, Lower Paleozoic and Proterozoic sediments of the Rocky Mountains between Jasper, Alberta and Pine River, British Columbia. Bulletin of Canadian Petroleum Geology, v. 14, p. 442- 468.

Smellie, J.L. and Hole, M.J., 1997, Products and processes in Pliocene-Recent, subaqueous to emergent volcanism in the Antarctic Peninsula: examples of englacial Surtseyan volcano construction: Bulletin of Volcanology, v. 58, no. 8, p.628-646.

Smellie, J.L. and Skilling, I.P., 1994, Products of subglacial volcanic eruptions under different ice thicknesses: two examples from Antarctica: Sedimentary Geology, v. 91, no. 1-4, p.115-129.

Smith, E.F., MacDonald, F.A., Crowley, J.L., Hodgin, E.B. and Schrag, D.P., 2016, Tectonostratigraphic evolution of the c. 780-730 Ma Beck Spring Dolomite: Basin Formation in the core of Rodinia: Geological Society, London, Special Publications, v. 424, no. 1, p.213-239.

Smith, E.I., Feuerbach, D.L., Naumann, T.R. and Mills, J.G., 1990, Mid-Miocene volcanic and plutonic rocks in the Lake Mead area of Nevada and Arizona; Production of intermediate igneous rocks in an extensional environment: GeologicalSociety of America Memoirs, v. 174, p. 169-194.

Smith, M.D., Arnaud, E., Arnott, R.W.C. and Ross, G.M., 2011, The record of Neoproterozoic glaciations in the Windermere Supergroup, southern Canadian Cordillera: Geological Society, London, Memoirs, v. 36, no. 1, p.413-424.

Spence, G.H., Le Heron, D.P. and Fairchild, I.J., 2016, Sedimentological perspectives on climatic, atmospheric and environmental change in the Neoproterozoic Era: Sedimentology, v. 63, no. 2, p.253-306.

Steiner, M. B. (2003), A cratonic Middle Jurassic paleopole: Callovian- Oxfordian stillstand (J-2 cusp), rotation of the Colorado Plateau, and Jurassic North American apparent polar wander, Tectonics, 22(3), 1020, doi:10.1029/2001TC001284.

Steiner, M. B., and S. G. Lucas (2000), Paleomagnetism of the Late Triassic Petrified Forest Formation, Chinle Group, western United States: Further evidence of "large" rotation of the Colorado Plateau, J. Geophys. Res., 105, 25,791-25,808, doi:10.1029/2000JB900093.

Stewart, J.N., 1972, Initial deposits of the Cordilleran geosyncline: evidence for a late Precambrian (850 m.y.) continental separation: Geological Society of America Bulletin, v.83, no. 5, p. 1345-1360.

Stokking, L. B., and Tauxe, L., 1990, Properties of chemical remanence inSynthetic hematite: testing theoretical predictions: Journal of Geophysical Research:Solid Earth (1978–2012), 95(B8), p. 12639-12652.

Strauss, J.V., Macdonald, F.A., Halverson, G.P., Tosca, N.J., Schrag, D.P., and Knoll, A.H., 2015, Stratigraphic evolution of the Neoproterozoic Callison Lake Formation: Linking the break-up of Rodinia to the Islay carbon isotope excursion: American Journal of Science, v. 315, p. 881-944.

Strauss, J.V., Rooney, A.D., Macdonald, F.A., Brandon, A.D., and Knoll, A.H., 2014, 740 Ma vase-shaped microfossils from Yukon, Canada: Implications for Neoproterozoic chronology and biostratigraphy: Geology, v. 42, no. 8, p. 659-662.

Strauss, J.V., Roots, C.F., Macdonald, F.A., Halverson, G.P., Eyster, A.E., and Colpron, M., 2014b. Geological map of the Coal Creek Inlier, Ogilvie Mountains (NTS 116B/10-15 and 116C/9,16) (1:100,000 scale), Yukon Geological Survey, Open File 2014-XX.

Swanson-Hysell, N.L., Maloof, A.C., Weiss, B.P. and Evans, D.A., 2009. Nature Geoscience, 2(10), pp.713-717.

Swanson-Hysell, N.L., Maloof, A.C., Kirschvink, J.L., Evans, D.A.D., Halverson, G.P., Hurtgen, M.T., 2012, Constraints on Neoproterozoic paleogeography and Paleozoic orogenesis from paleomagnetic records of the Bitter Springs Formation, Amadeus basin, central Australia. Amer. J. Sci. v. 312, p. 817-884.

Sweeney, J.F., Weber, J.R. and Blasco, S.M., 1982. Continental ridges in the Arctic Ocean: LOREX constraints. Tectonophysics, 89(1-3), pp.217-237.

Tan, X. and Kodama, K.P., 2002. Magnetic anisotropy and paleomagnetic inclination shallowing in red beds: Evidence from the Mississippian Mauch Chunk Formation, Pennsylvania. Journal of Geophysical Research: Solid Earth, 107(B11).

Tan, Xiaodong, Kenneth P. Kodama, Stuart Gilder, and Vincent Courtillot. Rock magnetic evidence for inclination shallowing in the Passaic Formation red beds from the Newark basin and a

systematic bias of the Late Triassic apparent polar wander path for North America. Earth and Planetary Science Letters 254, no. 3 (2007): 345-357.

Tauxe, L., 2005. Inclination flattening and the geocentric axial dipole hypothesis. Earth and Planetary Science Letters, 233(3), pp.247-261.

Tauxe, L., and Watson, G. S., 1994, The fold test: an eigen analysis approach. Earth and Planetary Science Letters, v. 122, no. 3, p. 331-341.

Tauxe, L., Butler, R. F., Van, der Voo, R., and Banerjee, S. K., 2010, Essentials of Paleomagnetism: Berkeley, University of California Press. 489p.

Tauxe, L., Kodama, K.P. and Kent, D.V., 2008. Testing corrections for paleomagnetic inclination error in sedimentary rocks: a comparative approach. Physics of the Earth and Planetary Interiors, 169(1), pp.152-165.

Tempelman-Kluit, D.J., 1970, Stratigraphy and structure of The 'Keno Hill Quartzite' in Tombstone River-Upper Klondyke River map areas, Yukon Territory (116B/7,B/8): Geological Survey of Canada, Bulletin 180, 103 p., 2 maps at 1:506 880 and 1:63 360 scale

Thomas, G.S.P. and Connell, R.J., 1985, Iceberg drop, dump and grounding structures from Pleistocene glacio-lacustrine sediments, Scotland: Journal of Sedimentary Petrology, v. 55, no. 2, p. 243-249.

Thompson, R.I., Roots, C.F., and Mustard, P.S., 1994, Geology of Dawson map area (116B, C, northeast of Tintina Trench): Geological Survey of Canada, Open File 2849.

Thorkelson, D. J., 2000, Geology and mineral occurrences of the Slats Creek, Fairchild Lake and -Dolores Creek- areas, Wernecke Mountains (106D/16, 106C/13, 106C/14), Yukon Territory. Exploration and Geological Services Division, Yukon, Indian and Northern Affairs Canada, Bulletin 10, 73p.

Thorkelson, D., Abbott, J., Mortensen, J., Creaser, R., Villeneuve, M., McNicoll, V., and Layer, P., 2005, Early and Middle Proterozoic evolution of Yukon, Canada: Canadian Journal of Earth Sciences, v. 42, no. 6, p. 1045–1071, doi: 10.1139/E05-075.

Timmons, J. Michael, Karl E. Karlstrom, Matthew T. Heizler, Samuel A. Bowring, George E. Gehrels, and Laura J. Crossey. Tectonic inferences from the ca. 1255-1100 Ma Unkar Group and Nankoweap Formation, Grand Canyon: Intracratonic deformation and basin formation during protracted Grenville orogenesis." Geological Society of America Bulletin 117, no. 11-12 (2005): 1573-1595.

Timmons, J.M., Karlstrom, K.E., Dehler, C.M., Geissman, J.W. and Heizler, M.T., 2001. Proterozoic multistage (ca. 1.1 and 0.8 Ga) extension recorded in the Grand Canyon Supergroup and establishment of northwest-and north-trending tectonic grains in the southwestern United States. Geological Society of America Bulletin, 113(2), pp.163-181.

Torsvik, T.H., Tucker, R.D., Ashwal, L.D., Eide, E.A., Rakotosolofo, N.A., de Wit, M.J., 1998, Late Cretaceous magmatism in Madagascar: palaeomagnetic evidence for a stationary Marion hotspot. Earth Planet. Sci. Lett. v. 164, p. 221 – 232.

Torsvik, T. H., Van der Voo, R., Meert, J. G., Mosar, J.,and Walderhaug, H. J., 2001a, Reconstructions of the continents around the North Atlantic at about the 60th parallel. Earth and Planetary Science Letters, 187(1), 55-69.

Torsvik, T.H., Carter, L.M., Ashwal, L.D., Bhushan, S.K., Pandit, M.K. and Jamtveit, B., 2001b, Rodinia refined or obscured: palaeomagnetism of the Malani igneous suite no. NW India . Precambrian Research, v. 108, no.3 , p. 319-333.

Torsvik, T.H., Ashwal, L.D., Tucker, R.D. and Eide, E.A., 2001c, Neoproterozoic geochronology and palaeogeography of the Seychelles microcontinent: the India link. Precambrian Research, v. 110, no.1, p. 47-59.

Torsvik, T.H., Van der Voo, R., Preeden, U., Mac Niocaill, C., Steinberger, B., Doubrovine, P., van Hinsbergen, D.J.J., Domeier, M., Gaina, C., Tohver, E., Meert, J.G., McCausland, P.J., and Cocks, L.R.M., 2012, Phanerozoic polar wander, palaeogeography and dynamics: Earth-Science Reviews, v. 114, no. 3, p. 325-368.

Trompette, R., 1997, Neoproterozoic ~ 600 Ma aggregation of Western Gondwana: a tentative scenario. Precambrian Research, v. 82, no.1-2 , p.101-112.
Tuffen, H., Gilbert, J. and McGarvie, D., 2001, Products of an effusive subglacial rhyolite eruption: Bláhnúkur, Torfajökull, Iceland: Bulletin of Volcanology, v. 63, no. 2-3, p.179-190.

Turner, E. C., 2011, Stratigraphy of The Mackenzie Mountains supergroup in The Wernecke Mountains, Yukon, *in* MacFarlane, K. E., Weston, L. H., and Relf, C., eds., Yukon Exploration and Geology 2010: Whitehorse, Yukon, Yukon Geological Survey, p. 207-231.

Turner, E.C., and Long, D.G.F., 2008, Basin architecture and syndepositional fault activity during deposition of The Neoproterozoic Mackenzie Mountains supergroup, Northwest Territories, Canada: Canadian Journal of Earth Sciences, v. 45, no. 10, p. 1159-1184.

Van der Voo, R., 1990, The reliability of paleomagnetic data: Tectonophysics, v. 184, no. 1, p. 1-9.

Veevers, J.J., Walter, M.R., Scheibner, E., 1997. Neoproterozoic tectonics of Australia-Antarctica and Laurentia and the 560 Ma birth of the Pacific Ocean reflect the 400 m.y. Pangean Supercycle. J. Geol. 107, 225-242.

Wallmann, K., 2001, Controls on the Cretaceous and Cenozoic evolution of seawater composition, atmospheric CO2 and climate: Geochim. Cosmochim. Acta, v. 65, p. 3005-3025.

Wang, D. and Hesse, R., 1996, Continental slope sedimentation adjacent to an ice-margin. II. Glaciomarine depositional facies on Labrador Slope and glacial cycles: Marine Geology, v. 135, no.1,p.65-96.

Warren, M.J., 1997, Tectonic significance of stratigraphic and structural contrasts between the Purcell anticlinorium and the Kootenay arc. Duncan Lake area, British Columbia [Ph. D. thesis]: Kingston, Ontario, Canada, Queen's University.

Watson, G. S., 1956, A test for randomness of directions: Geophysical Supplements to the Monthly Notices of the Royal Astronomical Society, v. 7, no. 4, p. 160-161.

Watson, G., 1983, Large sample theory of the Langevin distributions: Journal of Statistical Planning and Inference, v. 8, no. 3, p. 245–256.

Weil, A.B., Geissman, J.W. and Ashby, J.M., 2006. A new paleomagnetic pole for the Neoproterozoic Uinta Mountain Supergroup, central Rocky Mountain states, USA. Precambrian Research, 147(3), pp.234-259.

Weil, A.B., Geissman, J.W. and Van der Voo, R., 2004. Paleomagnetism of the Neoproterozoic Chuar Group, Grand Canyon Supergroup, Arizona: implications for Laurentia's Neoproterozoic APWP and Rodinia break-up. Precambrian Research, 129(1), pp.71-92.

Wen, B., Li, Y.X. and Zhu, W., 2013. Paleomagnetism of the Neoproterozoic diamictites of the Qiaoenbrak formation in the Aksu area, NW China: Constraints on the paleogeographic position of the Tarim Block. Precambrian Research, 226, pp.75-90.

Wendt, I. and Carl, C., 1991, The statistical distribution of the mean squared weighted deviation. Chemical Geology: Isotope Geoscience Section, v. 86, no. 4, p.275-285.
Werner R, Schmincke HU, Sigvaldason G., 1996, A new model for the evolution of table mountains: volcanological and petrological evidence from Herðubreið and Herðubreiðartogl volcanoes (Iceland): Geol Rundschau v. 85, p. 390-397.

Wernicke, B., 1985, Uniform-sense normal simple shear of the continental lithosphere: Canadian Journal of Earth Sciences, v. 22, no. 1, p.108-125.

White, R.W., Clarke, G.L. and Nelson, D.R., 1999, SHRIMP U-Pb zircon dating of Grenville-age events in the western part of the Musgrave Block, central Australia. Journal of Metamorphic Geology, v. 17, p.465-482.

Whitmeyer, S.J. and Karlstrom, K.E., 2007, Tectonic model for the Proterozoic growth of North America. Geosphere, v. 3, no. 4 , p.220-259.

Wingate, M.T. and Giddings, J.W., 2000. Age and palaeomagnetism of the Mundine Well dyke swarm, Western Australia: implications for an Australia-Laurentia connection at 755 Ma. Precambrian Research, 100(1), pp.335-357.

Wingate, M.T., Pisarevsky, S.A. and Evans, D.A., 2002. Rodinia connections between Australia and Laurentia: no SWEAT, no AUSWUS?. Terra Nova, 14(2), pp.121-128.

Wingate, M. T. D., Pisarevsky, S. A., and De Waele, B., 2010, Paleomagnetism of the 765 Ma Luakela volcanics in Northwest Zambia and implications for Neoproterozoic positions of the Congo Craton: American Journal of Science, v. 310, n. 10, p. 1333–1344, http://dx.doi.org/10.2475/10.2010.05

Witte,W. K., and Kent, D. V., 1991, Tectonic implications of a remagnetization event in the Newark Basin: Journal of Geophysical Research: Solid Earth (1978–2012), 96(B12), p. 19569-19582.

Wood, D.A., 1980, The application of a Th Hf Ta diagram to problems of tectonomagmatic classification and to establishing the nature of crustal contamination of basaltic lavas of the British Tertiary Volcanic Province: Earth and Planetary Science Letters, v. 50, no. 1, p.11-30.

Woodcock, N. H., and Fischer, M., 1986, Strike-slip duplexes: Journal of Structural Geology, v. 8, no. 7, p. 725-735.

Wynne, P. J., Enkin, R. J., Baker, J., Johnston, S. T., and Hart, C. J., 1998, The big flush: paleomagnetic signature of a 70 Ma regional hydrothermal event in displaced rocks of the northern Canadian Cordillera: Canadian Journal of Earth Sciences, v. 35, no. 6, p. 657-671.

Xu, B., P. Jian, H. F. Zheng, H. B. Zou, L. F. Zhang, and D. Y. Liu (2005), U-Pb zircon geochronology and geochemistry of Neoproterozoic volcanic rocks in the Tarim Block of northwest China: implications for the breakup of Rodinia supercontinent and Neoproterozoic glaciations, Precambrian Res., 136(2), 107-123

Yang, J., Cawood, P.A., Du, Y., Huang, H., Huang, H. and Tao, P., 2012, Large Igneous Province and magmatic arc sourced Permian-Triassic volcanogenic sediments in China: Sedimentary Geology, v. 261, p.120-131.

Yeo, G. M., 1984, The Rapitan Group: relevance to the global association of Late Proterozoic glaciation and iron-formation. [Ph. D. thesis]: University of Western Ontario, 599 p.

Yonkee, W. A., Dehler, C. D., Link, P. K., Balgord, E. A., Keeley, J. A., Hayes, D. S., Wells, M. L., Fanning, C. M., and Johnston, S.M., 2014, Tectono-stratigraphic framework of Neoproterozoic to Cambrian strata, west-central US: Protracted rifting, glaciation, and evolution of the North American Cordilleran margin: *Earth-Science Reviews*, v. 136, p. 59-95.

Yorath, C.J., 1992, Upper Jurassic to Paleogene assemblages. In: Geology of the Cordilleran Orogen in Canada, H. Gabrielse and C.D.Yorath (eds.),Geological Survey of Canada, Geology of Canada, no. 4, p. 331-371

Young, G.M., 1976, Iron-formation and glaciogenic rocks of the Rapitan Group, Northwest Territories, Canada: Precambrian Research, v. 3, no. 2, p.137-158.

Young, G.M., 1992. Late Proterozoic stratigraphy and the Canada-Australia connection. Geology, 20(3), pp.215-218.

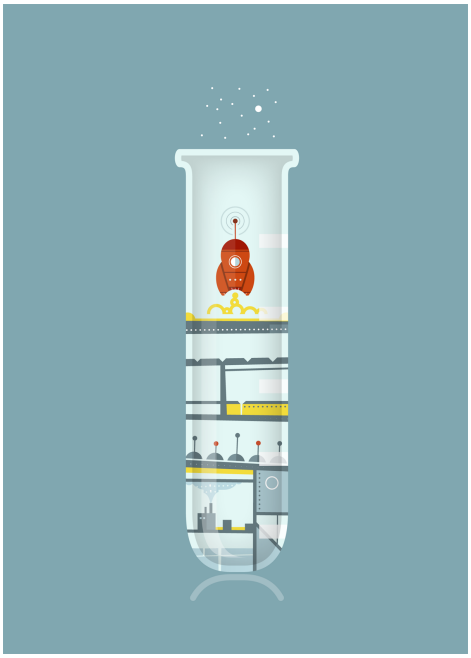
Young, G.M., 1995, Are Neoproterozoic glacial deposits preserved on the margins of Laurentia related to the fragmentation of two supercontinents?: Geology, v. 23, no. 2, p. 153–156.

Young, G.M., Jefferson, C.W., Delaney, G.D., and Yeo, G.M., 1979, Middle and Upper Proterozoic evolution of the northern Canadian Cordillera and Shield: Geology, v. 7, no. 3, p. 125– 128.

Woodcock, N.H. and Fischer, M., 1986, Strike-slip duplexes. Journal of structural geology, v. 8, no.7 , p.725-735.

Zhang, S., Jiang, G. and Han, Y., 2008, The age of the Nantuo Formation and Nantuo glaciation in South China: Terra Nova, v. 20, no. 4, p.289-294.

Zhong, S., Zhang, N., Li, Z.X. and Roberts, J.H., 2007. Supercontinent cycles, true polar wander, and very long-wavelength mantle convection. Earth and Planetary Science Letters, 261(3), pp.551-564.



This thesis was typeset using LaTeX, originally developed by Leslie Lamport and based on Donald Knuth's TeX. The body text is set in 11 point Egenolff-Berner Garamond, a revival of Claude Garamont's humanist typeface. The above illustration, *Science Experiment 02*, was created by Ben Schlitter and released under CC BY-NC-ND 3.0. A template that can be used to format a PhD dissertation with this look & feel has been released under the permissive AGPL license, and can be found online at github.com/suchow/Dissertate or from its lead author, Jordan Suchow, at suchow@post.harvard.edu.